STUDY ON SIZE EFFECT OF RC BEAM-COLUMN JOINTS WITH AND WITHOUT RETROFITTING UNDER CYCLIC LOADING

Thesis submitted

in partial fulfillment of the requirements

for the Degree of

DOCTOR OF PHILOSOPHY

By

Abdul Munim Choudhury

CIVIL ENGINEERING DEPARTMENT
INDIAN INSTITUTE OF TECHNOLOGY GUWAHATI
GUWAHATI-781039, INDIA
JUNE, 2010

CERTIFICATE

This is to certify that the thesis entitled ***"Study on size effect of beam-column joints with and without retrofitting under cyclic loading"*** *submitted by* ***Mr. Abdul Munim Choudhury,*** *Roll No. 06610408 to the Indian Institute of Technology Guwahati, for the award of the degree of Doctor of Philosophy in Civil Engineering is a record of bonafide research work carried out by him under our supervision and guidance. The thesis work, in our opinion, has reached the requisite standard fulfilling the requirement for the degree of Doctor of Philosophy.*

The results contained in this thesis have not been submitted in part or full to any other University or Institute for award of any degree or diploma.

(Dr. Anjan Dutta)
Professor
Department of Civil Engineering
Indian Institute of Technology Guwahati
Guwahati-781039, INDIA
Date:
Place: Guwahati

(Dr. Sajal Kanti Deb)
Professor
Department of Civil Engineer
Indian Institute of Technology Guwahati
Guwahati-781039, INDIA.
Date:
Place: Guwahati

STATEMENT

I do hereby declare that the matter embodied in this thesis is the result of investigations carried out by me in the Department of Civil Engineering, Indian Institute of Technology Guwahati, Assam, India.

In keeping with the general practice of reporting scientific observations, due acknowledgements have been made wherever the work described is based on the findings of others investigators.

Guwahati 781039

Date: (Abdul Munim Choudhury)

ACKNOWLEDGEMENT

This thesis is the result of the experimental investigation carried out at the department of Civil Engineering at Indian Institute of Technology, Guwahati, India. At the outset, I would like to express my deep sense of gratitude from the core of heart to my supervisors Dr. Sajal Kanti Deb and Dr. Anjan Dutta for initiating an interesting and innovative research topic and for their personal commitment, interesting discussion and valuable advice. I appreciate the opportunities I got to develop myself in a new area of structural engineering. They have been continuously encouraging throughout the work and contributed with valuable guidance and supervision. Such a huge experimental work was done for the first time in structural laboratory of IIT Guwahati, which demanded lot of new equipments to be purchased, fabrication of frames and mobilization of construction materials etc. My supervisors have taken lot of pains to manage the finance for all these materials and workmanship for casting the test specimens. They have never left me alone during the planning, organizing and conducting the tests. In every phase, I found them very close to share the agonies of failure and joys of success, not only in all these experimental works but also in my personal life during my stay in IIT Guwahti.

A substantial part of this thesis was based on experimental investigation. This would not have been possible without the support of technical staff of Structural Engineering Laboratory of IIT Guwahati. I express my gratitude to Mr. Arun Chandra Borsaikia, Scientific Officer, for his earnest effort to manage the masons and workers needed for casing of specimens, managing long steel bars for fixing the specimens to the strong floor and especially for operating the MTS servo hydraulic dynamic actuators during the testing. I express my thanks to Mr. Nripen Kalita, Bhuiya and Suresh for their continuous help and ideas for fixing and removing of the specimens during the course of the experiments.

I am also grateful to Mr. Gogoi, Mr. Mazumder, Mrs. Jhuri and Mr. Deepak; who are the office staffs of Civil Engineering Department for their help in various occasions.

I would also like to express my thanks to workshop staffs of Mechanical Engineering Department for helping me in fabrication of loading frames and many other works involving steel structures.

Thanks are also due to Prof. Sudip Talukder, Dr. K. D. Singh and Prof D. Chakravorty, who were the members of my doctoral committee and who contributed with valuable remarks and ideas to obtain the final results of this research work. I am also grateful to Dr. H. B. Kaushik, who has given me lot of ideas for the testing.

I would like to acknowledge the encouragement and enthusiasm which I received from Prof. Richard Scott of Durham University, U.K, who has been physically present during the testing of the first specimen. I am thankful to Dr. Alagurusundoro Murty of IIT, Madras, who has given me suggestion for casting of specimens by e-mail. I am grateful to Dr. S. S. Mahini of University of Sydney, Australia, who has given me suggestion regarding reference books and papers. I am grateful to Dr. M. Nabi of IIT Delhi, who has taken lot of pain for collecting and sending photocopy of some of the ACI journal, which were not available in IIT Guwahti.

I would like to thank the Director, National Institute of Technology, Silchar, India for deputing me to pursue the Ph.D. degree under Quality Improvement Program. I want to convey my thanks to Fosroc (India) Private limited for providing FRP material needed for retrofitting, TATA Steel for providing the reinforcement and STAR Cement for cement needed to cast the beam-column joint specimens.

Many of my friends and colleagues like Rama Rao, Srikanth, Raju, Sreeni, Marthong, Vizo, Monwar and Aminul, who helped me during the experimental work, I am gratefull

to all of them.

Finally, I express my thanks to my wife Sarhana, who has been looking with enormous patience after my family including education of the children during the days of my research duration. Few words of thanks are remaining for my children Tammy, Tanim and Tahsin, to whom I could not give enough company during this period. Indeed, I am grateful to my father in law, who helped me in several family affairs in this period. My heartfelt thanks are for my parents, by whose blessings I could complete this work successfully.

Abdul Munim Choudhury

IIT, Guwahati (India)

July , 2010.

CONTENTS

ABSTRACT

During some of the past devastating earthquakes, it was observed that beam-column joint acts as one of the weakest links in moment resisting framed structures. The behaviour of reinforced concrete frame structures in earthquakes all over the world has highlighted the consequences of poor performance of beam-column joints. It was observed that during earthquakes, the exterior joints had suffered more in comparison to the interior ones. The failure of the beam-column joints during earthquakes gave a new thrust in the research for improving seismic behaviour of beam-column joint. Further, 1980 onward lot of researches were also done on strengthening of seismic deficient beam-column joints, especially the exterior joints. Several conventional methods of retrofitting were tried. These methods had many difficulties and problems. However, these difficulties and problems were reduced considerably with the introduction of *Fibre-Reinforced Polymer* (FRP). Hence, recent research efforts have been focused on the use of FRP for retrofitting of beam-column joints.

Some of the researchers conducted tests on beam-column joint without varying the size of tested specimens. However, most of the investigators conducted tests on scaled down models. The results of scaled down models cannot be used directly for prototype implementation in actual field as the size of specimen plays an important role. Available theories of material behavior that predict size effects are receiving increasing attention in the technical literature. Concrete is a heterogeneous material, which is generally full of micro cracks. Upon loading, these micro cracks propagate and the accumulation of such micro cracks leads to failure of specimens. It is well established that the mathematical modeling of such behavior should be based on the theories of fracture mechanics. Material models based on fracture mechanics can predict a size effect, if geometrically similar specimens of different sizes are considered.

Literature survey shows that the experimental study of size effect was mainly done for basic RC structural elements. However, till today no study on size effect was reported for beam-column joint, which is a vital component of structural system and plays a very crucial role during earthquake. Hence, it is necessary to undertake study on size effect of structural behaviour of beam-column joints, particularly under cyclic loading. Further, very few researches were reported on size effect for retrofitted RC elements using FRP. Therefore, in the present research, experimental investigations were conducted for a detailed study on beam-column joints with three possible deficiencies to observe the change in various properties due to retrofitting under cyclic loading. With this motivation, the present research was initiated to study the size effect on RC beam-column joints with and without retrofitting.

As the objective of the work is to strengthen beam-column joints against future earthquakes, all the specimens were tested under cyclic loading in this study. Three common types of deficiencies in beam-column joints were identified and corresponding three types of retrofitted specimens were also considered in this study. The deficient joints were properly retrofitted using *Carbon Fiber Reinforced Polymer* (CFRP) and *Glass Fiber Reinforced Polymer* (GFRP). Thus, six types of specimens with three geometrically similar specimens in each category were considered. Therefore, eighteen specimens were tested covering three possible deficiencies consisting of control and retrofitted specimens of three different sizes. The retrofitted specimens were designed for enhanced load carrying capacity, ductility and stiffness. All the three dimensions of two third and one third scaled specimens were arrived at by geometrically scaling down the dimensions of full scaled specimen. The diameter of the reinforcing bars, development length, length of special confinement zone, cover of reinforcement etc. were also scaled down appropriately. All the constituent materials used for casting and retrofitting the specimens were tested for various properties as per relevant codes.

A constant axial load on the column was maintained by hydraulic jack during testing to simulate gravity loading. An "*A* frame" was fabricated to facilitate the application of the axial load. Roller supports and fixtures were fabricated for maintaining symmetrical boundary conditions at the ends of the columns. The cyclic load was applied by servo hydraulic dynamic actuators (MTS make). Nonlinear static analysis was carried out using the general purpose finite element software ANSYS 6.0 for getting prior information about the load at first crack, crack pattern, the load and deflection at yielding, ultimate load carrying capacity etc of all the specimens in order to appropriately plan the sequence of experimental investigation.

In the experimental investigations, displacement controlled load with a frequency of 0.025 Hz was applied. Amplitude of the displacement histories were scaled down for two-third and one-third models. The recorded data were used to draw hysteresis loop, envelope curve, variation of stiffness and energy dissipation with respect to drift angle. Comparisons were made between the test results of control and retrofitted specimens in term of all the above mentioned parameters and conclusions were drawn regarding the improvement in design parameters due to retrofitting.

The results obtained by testing the specimens were used to draw bi-logarithmic plots to explore the possible existence of size effect. It was observed that the bi-logarithmic plots for both control and retrofitted specimens follow closely the size effect law proposed by *Bažant* in all the cases studied. Further, it was observed that the size effect became more pronounced with increase in brittleness of specimens till failure. Based on experimental studies carried out for all the six categories of beam-column joints, some important conclusions were drawn regarding applicability of size effect to various parameters studied. The gain in ultimate strength, initial stiffness and cumulative energy dissipation for all specimens due to retrofitting corroborates the size effect principle. A parameter was introduced to compare the

energy dissipation of specimens per unit volume of joint (e_N) with different sizes of beam-column joints. This parameter was correlated with different drift angles for different sizes of the specimen and accordingly variation of e_N with drift angle for different sizes of specimens were plotted for both retrofitted as well as control specimen. The variation of stress with relative deflection were also correlated with size of the specimens.

It was concluded that the displacement ductility, the cumulative energy per unit volume of joint and variation of stresses with respect to relative deflection substantiate the existence of size effect.

LIST OF TABLES

LIST OF FIGURES

LIST OF SYMBOLS AND ABBREVIATIONS

B	Dimensionless constant used in Bazˇant's size effect law
C_b	Compressive force developed by compressive steel in beam
D	Depth of specimen
D_c	Diagonal compressive force developed due to concrete
D_s	Diagonal compressive force developed due to steel
D_0	A constant with the dimension of length used in Bazˇant's size effect law
E_{comp}	Modulus of elasticity of the cured FRP in fibre direction
E_f	Modulus of elasticity of fibres
e_N	Energy dissipation per unit volume of joint
E_m	Modulus of elasticity of the matrix
E_S	Modulus of elasticity of steel
E_T	Tangent modulus of elasticity of steel
E_x	Modulus of elasticity of FRP along X direction
E_y	Modulus of elasticity of FRP along Y direction
E_z	Modulus of elasticity of FRP along Z direction
$f_t^{/}$	Tensile strength of concrete material
G_{xy}	Rigidity modulus of FRP in XY plane
G_{yz}	Rigidity modulus of FRP in YZ plane
G_{zx}	Rigidity modulus of FRP in ZX plane
h_c	Depth of column in a beam-column joint
l_c	Distance between consecutive points of contraflexure in a column
M_R	The ratio of column-to-beam flexural capacity
T	Tensile force developed in a beam.

T_b	Tensile force developed by tensile steel in beam
V_{ch}	Shear contribution of concrete in strut mechanism
V_{col}	Shear force in Column
V_f	Volume fraction of fibres
V_{jh}	Shear force in the beam-column joint
V_m	Volume fraction of matrix
V_{sh}	Shear contribution of steel in truss mechanism
Z_b	Lever arm of beam in a beam-column join
α	Angle made by the diagonal force with horizontal angle
μ	Displacement ductility factor
μ_{xy}	Poission's ratio of FRP in XY plane
μ_{yz}	Poission's ratio of FRP in YZ plane
μ_{zx}	Poission's ratio of FRP in ZX plane
ϕ	Diameter of reinforcing bar
Δ	Displacement at any instant
Δ_u	Ultimate displacement
Δ_y	Displacement at yield
σ_{N_U}	Ultimate stress at failure used in bi-logarithmic plot

ABBREVIATIONS

ACI	American concrete institute
ASTM	American standard of testing materials
BWFLC	Beam weak in flexure large control
BWFMC	Beam weak in flexure medium control
BWFSC	Beam weak in flexure small control
BWFLR	Beam weak in flexure large retrofitted

BWFMR	Beam weak in flexure medium retrofitted
BWFSR	Beam weak in flexure small retrofitted
BWSLC	Beam weak in shear large control
BWSMC	Beam weak in shear medium control
BWSSC	Beam weak in shear small control
BWSLR	Beam weak in shear large retrofitted
BWSMR	Beam weak in shear medium retrofitted
BWSSR	Beam weak in shear small retrofitted
CWSLC	Column weak in shear large control
CWSMC	Column weak in shear medium control
CWSSC	Column weak in shear small control
CWSLR	Column weak in shear large retrofitted
CWSMR	Column weak in shear medium retrofitted
CWSSR	Column weak in shear small retrofitted
CFRP	Carbon fibre reinforced polymer
DMX	Maximum deflection found in the result of ANSYS
FRP	Fibre reinforced polymer
GFRP	Glass fibre reinforced polymer
HYSD	High yield steel deformed
IS	Indian standard
LVDT	Linear-variable differential transformer
MPa	Mega Pascal
MS	Mild steel
SMN	Maximum normal stress due to bending found in the result of ANSYS 6.0
WFT	Wet film thickness

CHAPTER 1

INTRODUCTION AND LITERATURE REVIEW

1.1 INTRODUCTION

During some of the past devastating earthquakes, it was established beyond doubt that beam-column joint acts as one of the weakest links in moment resisting framed RC structures. The behaviour of reinforced concrete frame structures as observed during earthquakes all over the world highlighted the consequences of poor performance of beam-column joints. Further, it was observed that during earthquakes, the exterior joints had suffered more in comparison to the interior ones. A typical case of beam-column joint failure is shown in Fig. 1.1. The failure of beam-column joints during past earthquakes opened a new research direction in the field of strengthening of beam-column joints for enhancing seismic safety. During the last few decades, lots of research was done on strengthening of seismic deficient external beam-column joints. Several methods of retrofitting such as construction of RC or steel jacket, attaching corrugated or plain steel plates were tried. These techniques were having many difficulties and problems like labour intensive, hard workmanship, requirement of

Fig. 1.1 Beam-Column joint failure in 2009 L'Aquila Earthquake [Dr Anna Brignola, University of Genoa]

increased dimension after strengthening, corrosion protection etc. However, with the introduction of Fibre-Reinforced Polymer (FRP), the above mentioned difficulties and associated problems could be addressed appropriately. Thus, recent research efforts have been focused on the use of FRP for retrofitting of beam-column joints. FRP has got many advantages. The main advantages of FRP composites are their high specific strength (i.e. strength to weight ratio) and high corrosion resistance. The former property leads to great ease in handling, reduced labour cost and less interruptions to existing services, while the later ensures durable performance.

Moreover, many researchers conducted tests on beam-column joints without varying the sizes of tested specimens. Some tests results are available for scaled models for a particular deficiency. These results cannot be used directly for prototype implementation in actual field because the size of specimen plays an important role for various properties. Available theories of material behavior that predict size effects are receiving increasing attention in the technical literature nowadays. It has been demonstrated that the size of the specimen plays an important role. However, in classical theories of solid mechanics, it is assumed that material properties such as the tensile or compressive strengths are not scale dependent. In engineering practice, such properties are generally measured on standard samples of the material and it is usually assumed applicable to structural elements whose size may differ from those of the test samples. Thus, the use of test results from standard specimen should be judiciously used in practice giving due consideration to the existence of size effect.

Concrete is a heterogeneous material, which is generally full of micro cracks. Upon loading, these micro cracks propagate and the accumulation of such micro cracks leads to a major crack and subsequently ends in failure. It is well established that the mathematical modeling of such behavior should be based on the principles of fracture mechanics. Material models based on fracture mechanics can predict a size effect, if geometrically similar specimens of different sizes are considered. It may also be noted that the story of size effect actually came

into existence as early as in 15th century, when Leonardo da Vinci first observed the size effect phenomena in chords of different lengths. Moreover, Gonnerman observed first the existence of size effect in 1925 in concrete during testing of concrete cylinders having different sizes.

1.2 BEAM-COLUMN JOINT

Beam-column joint may be defined as the portion of the column within the depth of the deepest beam [ACI 352R-02, 2002]. In a moment resisting frame, three types of joints can be identified viz. interior joint, exterior joint and corner joint, which is shown in Fig. 1.2. The severity of forces and demands during earthquake on the performance of these joints needs a better understanding of their behaviour. These forces develop complex mechanisms involving bond and shear within the joint. The joint region is subjected to horizontal and vertical shear forces whose magnitude is typically many times higher than in the adjacent beams and columns. The detailed discussion about some of the important features of joint behaviour has been given in the subsequent sub-section.

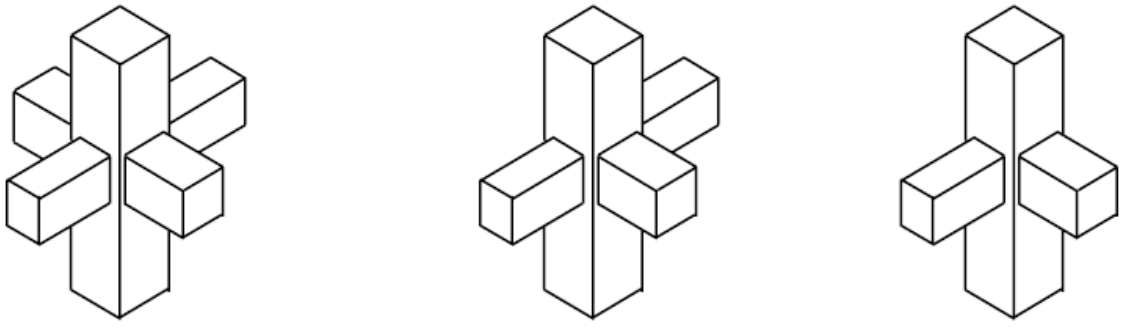

(a) Interior joint (b) Exterior joint (c) Corner joint

Fig. 1.2 Types of beam-column joints [Uma and Prasad, 2006]

1.2.1 Evaluation of Shear Strength of Beam-Column Joint

The joint shear strength is calculated by summing up the contribution of concrete and steel together. The total effective shear strength of the joint in the horizontal direction is given by

$$V_{jh} = V_{ch} + V_{sh} \tag{1.1}$$

In which, V_{ch} is the contribution from the concrete strut and V_{sh} is the contribution from the steel truss mechanism. The vertical and horizontal shear forces in the joint region develop diagonal compressive and tensile stresses within the joint core. The shear transfer mechanisms are very complex and hence, there exist different views between researchers with regard to design parameters of the joint. The model proposed by Paulay *et al.* (1978) considers that the total shear within the joint core is partly carried by a diagonal concrete strut (Fig. 1.3 a) and partly by an idealized truss, which consists of horizontal hoops, intermediate column bars and inclined concrete bars between diagonal cracks (Fig. 1.3 b). The strut mechanism is associated with a diagonal force (D_c) within the concrete strut developed by major diagonal concrete compression forces formed at the corners of the joint. A substantial portion of the total joint shear (horizontal and vertical) can be resisted by this mechanism. However, the strength of the strut mechanism is reduced by tensile strains perpendicular to the direction of the strut. In such situations, confinement of the joint core would help in improving the strength of the strut. The steel forces transferred through bond are introduced into concrete at the four boundaries of the joint core forming a compression field with diagonal cracks in the joint as shown in Fig. 1.3(b). These forces being in equilibrium generate a diagonal compression force D_s from all the concrete bars between the diagonal cracks. The mechanism associated is called truss mechanism which is supported by well distributed transverse reinforcement within the joint as shown in Fig. 1.3(b). The diagonal forces D_c and D_s are acting at an angle α with respect to the horizontal axis of the joint. The sum of horizontal components of these forces from both mechanisms gives

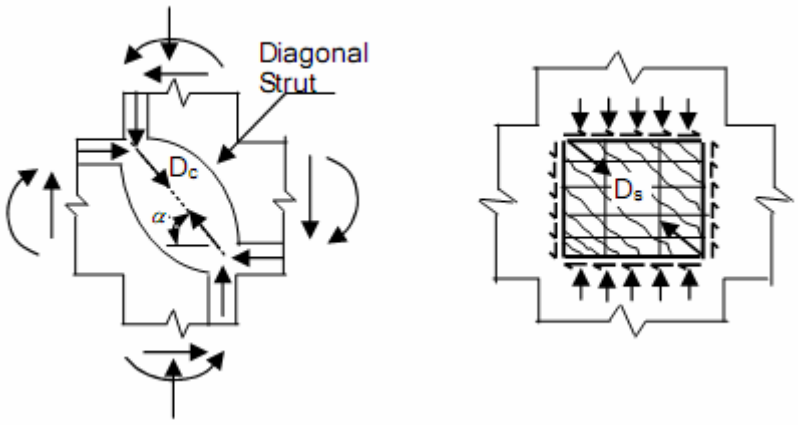

(a) Strut Mechanism (b) Truss Mechanism

Fig.1.3 Shear Resisting Mechanisms

an estimate of shear resistance in horizontal direction. Similarly, the sum of vertical components gives shear resistance in vertical direction. While designing beam-column joint, the compressive strength of the diagonal concrete strut is considered as the reliable source of strength. Many of the codes define nominal shear capacity of the joint based on strength of the strut. The nominal shear capacity is expressed in terms of allowable stress in concrete and effective joint area. In the first step of design, it is ensured that the shear force demand in the joint should be less than the nominal shear capacity. If this condition is not satisfied, then the dimensions of the joint are to be revised irrespective of the amount of reinforcement available within the joint.

1.2.2 Forces on Exterior Beam-Column Joint

In comparison to the interior joints, the exterior joints suffered more during past earthquakes and hence a discussion on force system acting on exterior joint is furnished. An exterior beam-column joint (Fig. 1.4) is considered with sub assemblage extending between the points of contraflexure. The shear force acting on the joint can be computed using equilibrium criteria. Fig. 1.4(a) shows the forces from the beam acting on the face of the joint. The bending moment and shear force distribution for the column is shown in

Fig. 1.4(b) and Fig.1.4(c) respectively. From Fig.1.4(b), it can be clearly observed that the nature of the bending moment above and below the joint changes and shows a steep gradient within the joint region. This causes large shear forces in the joint compared to that in the column. Fig. 1.4(c) indicates that the intensity of horizontal shear in the joint V_{jh} is typically

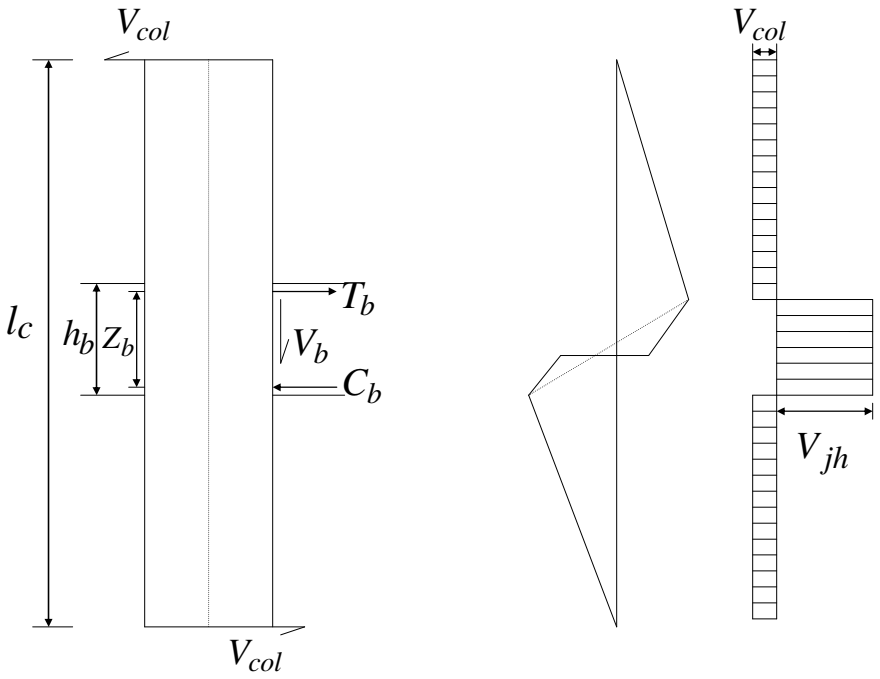

(a) Forces acting on column (b) Bending moments (c) Shear forces

Fig. 1.4 Free body diagram of an exterior beam-column joint [Paulay, 1989]

four to six times as large as across the column V_{col} [Paulay, 1989]. The horizontal shear force across the joint can be obtained based on equilibrium criteria. Assuming the beams to be symmetrically reinforced, tensile force T_b and a compressive force C_b is developed in the beam reinforcement. The vertical beam shear on the face of the joint is V_b.

Assuming $C_b = T_b$, the column shear V_{col} from the above forces is calculated based on equilibrium criteria as

$$V_{col} = \frac{T_b Z_b + V_b \frac{h_c}{2}}{l_c} \tag{1.2}$$

and the horizontal shear across the joint can be expressed as

$$V_{jh} = V_{col}\left(\frac{l_c}{Z_b} - 1\right) - V_b\left(\frac{h_c}{2Z_b}\right) \tag{1.3}$$

In the above equation, h_c is column depth and Z_b is the lever arm.

1.2.3 Simplified Approach for Evaluation of Shear

The above equations 1.2 and 1.3 are rigorous and involve various quantities to be evaluated. However, for engineering designs, a simpler approach is usually followed to arrive at a good estimate of the joint shear force, which is assumed to act on a horizontal plane passing through the joint. Fig.1.5 is a schematic representation of joint shear equilibrium in exterior joint. In an exterior Joint, the column shear, V_{col} can be expressed as

$$V_{col} = \frac{M_h}{l_c} \tag{1.4}$$

and the corresponding joint shear is

$$V_{jh} = T - V_{col} \tag{1.5}$$

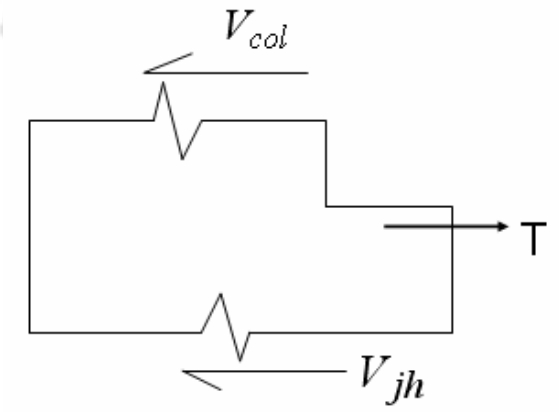

Fig.1.5 Joint Shear Equilibrium of an exterior joint

Under small lateral loads, inelastic deformations do not occur in the beam and column adjacent to a joint and the region would remain at elastic state even after a considerable number of displacement reversals. Under such circumstances, smaller amounts of joint shear reinforcement are generally enough. However, when the lateral loads are significant, plastic hinge is expected to develop in a section close to column face at the end of the beam.

1.2.4 Design of Shear Reinforcement

Presence of horizontal and vertical shear reinforcement within beam-column joint can develop truss mechanism in resisting shear. The design of shear reinforcement is governed by the minimum reinforcement area needed to support the truss mechanism and the maximum permissible area based on the highest stress developed at diagonal compression failure. Codes like IS 13920:1993 and ACI 352R-02 suggest expressions for horizontal reinforcement based on confinement of core concrete requirement to maintain the axial load carrying capacity of the column.

1.2.5 Strong Column-Weak Beam Principle

Designing beam column joint is considered to be a complex and challenging task for structural engineers, since the joint region is subjected to very high horizontal and vertical shear forces as compared to the adjacent beams and columns. If the joint is not designed properly, the possibility of plastic hinge formation in column increases substantially. This is dangerous for three reasons. First, the collapse mechanism associated with hinges in the columns has a lower ultimate load. Secondly, the energy absorption capacity of plastic hinges within the columns is normally less. It is evident from Fig. 1.6 that the area of the hysteresis loop in plastic hinge region of beam is higher than that in column. This indicates that the energy dissipated by plastic hinge in beam is higher. Third reason is chances of failure of column before the failure of beam increases leading to global failure, which may be

catastrophic. This may be reduced by employing the concept of strong column-weak beam principle. One of the factors to ensure a strong column-weak beam in a ductile moment resisting framed structure is restricting the value of M_R. It is defined as the ratio of column-to-beam flexural capacity and it is given by,

$$M_R = \frac{\sum M_C}{\sum M_B} \tag{1.6}$$

Where $\sum M_C$ is the sum of flexural capacities of the columns meeting at the joint under consideration and $\sum M_B$ is the sum of flexural capacities of beams at the same joint. The strong column-weak beam criteria is satisfied if M_R in eq. (1.6) is greater than 1.1 [Jain and Murty, 2006] or 1.2 as per American standard ACI 318 [2005] respectively.

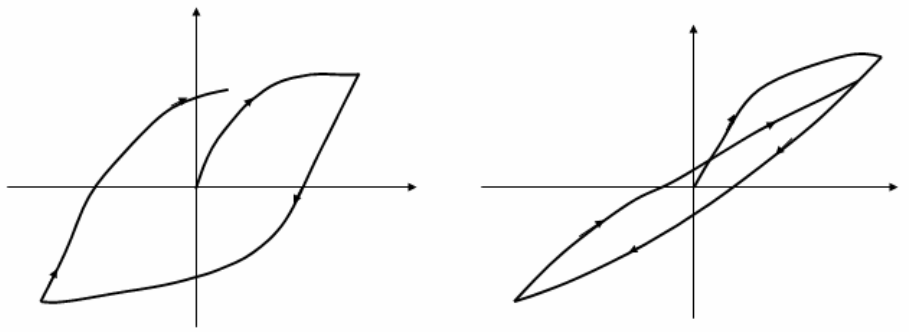

(a) Beam plastic hinge (b) Column plastic hinge

Fig. 1.6 Typical measured lateral-load displacement hysteresis loops for subassemblies of structural concrete [Paulay and Priestley, 1992]

1.2.6 Ductility of RC Structures

A designer must carefully select the design parameters to ensure adequate ductility in the joints. Any strengthening technique should ensure that it does not reduce the ductility from the original level. Rather, it should enhance the ductility of original structure if possible.

Ductility is basically the ability of a structure to accommodate deformations well beyond the

elastic limit. It is the capacity to dissipate energy through hysteretic behaviour and to sustain large deformations. For this reason, it is the most important characteristic required to be sought in the design of buildings located in earthquake prone regions. Ductility demand on a structure subjected to a severe lateral force can be estimated analytically by nonlinear time-history analysis. It can also be estimated experimentally by shaking table or pseudodynamic tests for a structure subjected to severe lateral loads. The displacement ductility factor μ is defined by the ratio of the total imposed displacement Δ at any instant to that at the onset of yield Δ_y. Using the idealised behaviour as shown in Fig. 1.7, the displacement ductility may be written as:

$$\mu = \Delta / \Delta_y \tag{1.7}$$

The ductility developed, when failure is imminent, is written as $\mu_u = \Delta_u / \Delta_y$.

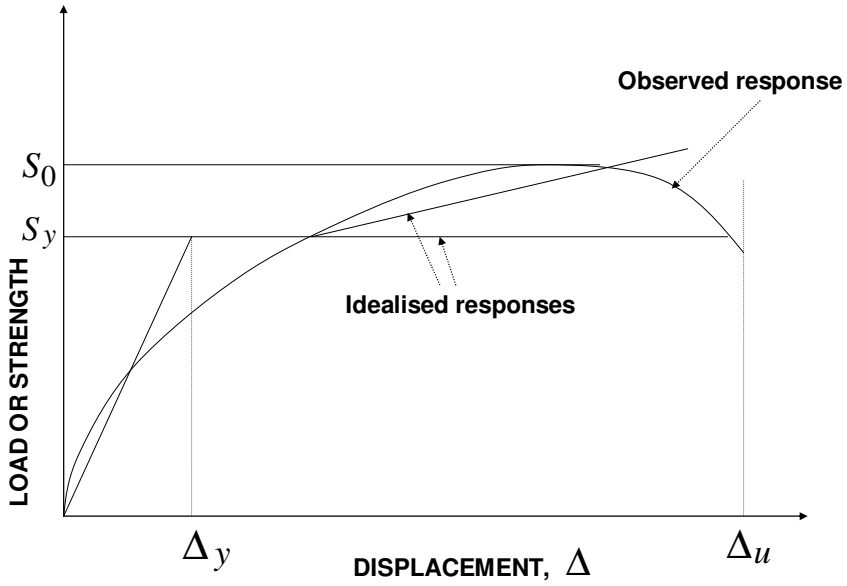

Fig. 1.7 Typical load-displacement relationship for a reinforced concrete ductile element [Paulay and Priestley, 1992]

1.3 RETROFITTING

The failure of many structures during recent earthquakes has emphasized the need for retrofitting in deficient structures. Most of the existing structures, especially which were constructed prior to 1970 are not adequately qualified to take the seismic load. Even, the structures which were designed and constructed following IS 1893: 1984 have been found seismically deficient as per the revised code IS 1893: Part 1:2002. It is often seen that retrofitting of building is generally more economical as compared to demolition and reconstruction even in the case of major structural damage. The purpose of seismic retrofitting is to provide adequate lateral strength by strategies that has been tested or proved to be effective during past earthquakes. There are two ways to retrofit an existing structure. The first approach is done by global modifications to the structural system, while the second is a member level approach of retrofitting, which is called local retrofitting. Local retrofitting deals with the increase of important properties at component level to fulfill the specific limit states. Classification of retrofitting of RC buildings as per Agarwal and Shrikhande [2007] is shown in Fig. 1.8. Generally global retrofitting strategies are applied when lateral load resisting system appears to be deficient in the entire structure. The basic objective of global retrofitting approach is to enhance the stiffness and strength of the overall structural system. Local retrofitting is generally used when the retrofit objectives are limited or direct treatment of the vulnerable components is needed.

1.3.1 Concrete Jacketing

Concrete jacketing is done by adding a thick layer of reinforced concrete of desired thickness in the form of a jacket with the existing structural element. This method is simple and economical as compared to steel and FRP jacketing. The jacketing enhances both ductility and strength. However, adequate dowelling of the existing concrete is required to facilitate composite deformation. Concrete jacketing increases the size of the structural element, which

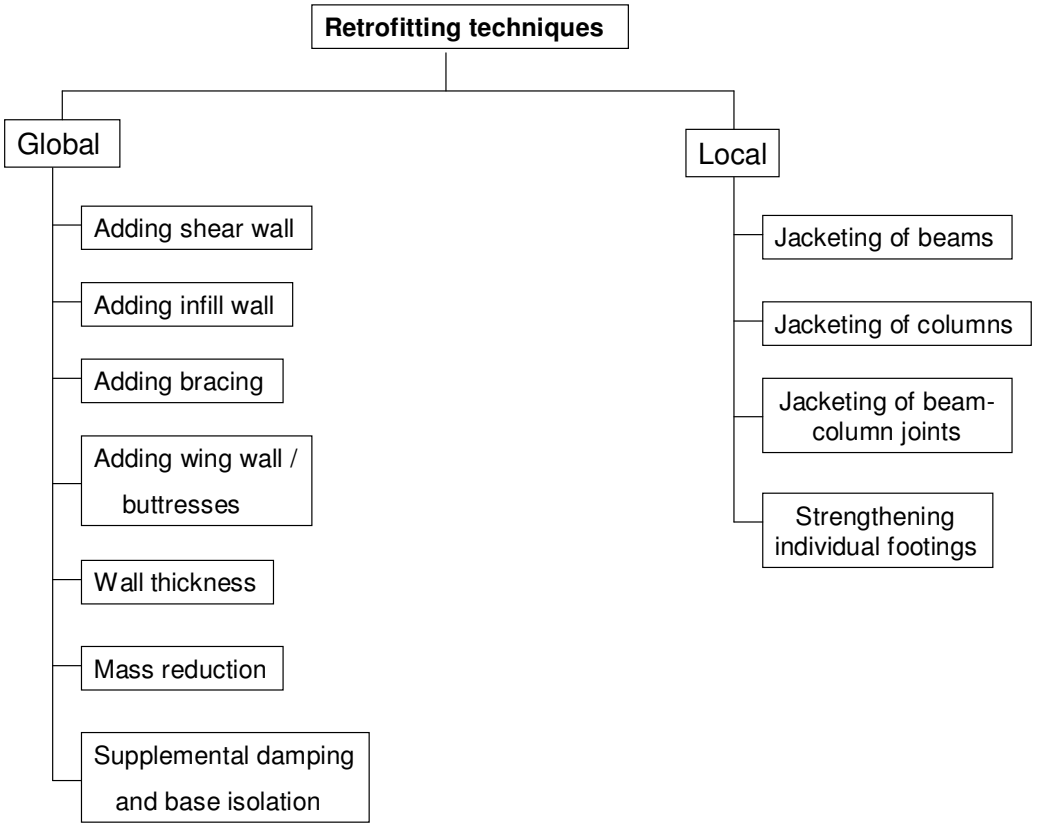

Fig. 1.8 Global and local methods of retrofitting [Agarwal and Shrikhande, 2007]

reduces the shear span ratio. There are some drawbacks in this traditional retrofit strategy like increase in weight of the member, more laborious, requires proper bonding between new and existing concrete, the effect of drying shrinkage induces tensile stress in the new concrete and involves drilling of holes in the slab or in the beam or in both at fairly close intervals. Drilling of holes in the structural members may lead to micro-cracking and weakness in the member.

1.3.2 Steel Jacketing

Steel jacketing involves bonding or anchoring the structural elements with steel plates and filling the gap with non-shrink grout, which increases the flexural strength, shear strength, ductility, stiffness and serviceability of the element. The bonded plates are prone to

premature debonding, which is a severe drawback of this technique. The other disadvantages of steel jacketing are difficulty in transportation, handling, installation of plates, poor resistance to corrosion, laborious and difficult to attain proper bond at remote locations.

1.3.3 Fibre Reinforced Polymer Composite Jacketing

Nowadays, the applications of FRP are gaining popularity in the civil engineering construction for their various advantages. The main advantages of FRP is its excellent corrosion resistance, fatigue resistance, high specific strength (i.e. strength to weight ratio), high specific stiffness, ease of transportation, handling, fixing with least interruption to the existing services and minimum increase in member size after retrofitting. FRP composites are both magnetically and electrically inert and suitable for strengthening structural elements where signal interference needs to be avoided. The natural period of vibration of the structures also remain unchanged of the structures retrofitted using FRP composites. The main drawback is that it is costlier than other conventional methods of retrofitting. The other disadvantages are its degradation of properties at high temperature, as in the case of outbreak of fire. A detailed discussion of FRP is given in the next section.

1.4 FIBRE REINFORCED POLYMER (FRP) COMPOSITE

Composite material signifies two or more materials combined together on a macroscopic scale to form a useful third material [Jones, 1999]. FRP composites are materials that contain two ingredients. These are the reinforcement and a continuous polymer, called the matrix. The common fibres are carbon, glass and aramid whilst epoxy and vinylster are common resins. Depending on the fibres used, FRP composites are classified as Glass-Fibre-Reinforced Polymer (GFRP) composites, Carbon-Fibre-Reinforced Polymer (CFRP) composites, Aramid-Fibre-Reinforced Polymer (AFRP) composites etc. The reinforcing

material is in the shape of fibres, which are typically stiffer and stronger than the matrix. The FRP composites are anisotropic materials, meaning that their properties are different in all directions.

Composite materials have a long history of usage. Their precise beginnings are unknown. For example, straw was used by the Isralelites to strengthen mud bricks. FRP composites are being used in other areas such as aerospace industry for many years and their superior properties are well established. In civil engineering, the FRP plate bonding technology was first investigated at the Swiss Federal Laboratory for Materials Testing and Research in 1984 [Meier *et al*. 1993]. Generally, two common methods of laying FRP composites are used for strengthening RC structures. The first one is wet lay up method, which is the most commonly used method. It involves the in situ application of resin to either a woven fabric or a unidirectional tow sheet. The second one is pre-fabrication of FRP composites in various forms, including pultrusion for plates for flexure in flexural strengthening and filament winding of shells in column strengthening.

In a composite material, the term *volume fraction of fibres*, V_f is defined as the ratio of volume of fibres to the total volume of composite material. Similarly, *volume fraction of matrix*, V_m is defined as the ratio of volume of matrix to the total volume of composite material. Typically, the volume fraction of fibres in FRPs is about 60%. Fibres are the principal stress bearing elements, while the resin protects fibres to transfer stresses among them. When the properties of the constituent materials (fibres, matrix) and their volume fraction are known, basic mechanical properties of FRP materials may be estimated. This may be achieved by applying the *rule of mixtures*, which can be expressed in mathematical form as follows (Jones 1999):

$$E_{comp} = E_f V_f + E_m V_m \tag{1.8}$$

where E_{comp} is the modulus of elasticity of the cured FRP in fibre direction, E_f is the modulus

of elasticity of fibres, E_m is the modulus of elasticity of the matrix.

1.5 HISTORICAL DEVELOPMENT OF SIZE EFFECT

The history of size effect stretches back to Leonardo da vinci [Bazˇant, 1999]. This was observed as early as in 15th century that "among chords of equal thickness, the longest one is having the least strength" implying increase proportionality. A major idea was given by Mariotte in 1686, where he observed that " a long rope and a short rope always support the same weight unless that in a long rope there may happen to be some faulty place in which it will break sooner than in a shorter." In other words, the longer the structure, the greater is the probability of encountering in it an element of low strength. This is the basic idea of statistical theory of size effect.

For two and half century, not much progress was achieved until the contribution of Griffith in the year 1921; the founder of fracture mechanics. He showed experimentally that the strength of a glass fibre could be raised from 42,300 psi to 491,000 psi when the diameter was decreased from 0.0042 in to 0.00013 in and concluded that "The weakness of isotropic solids……. is due to the presence of discontinuities or flaws……..". The effective strength of technical materials could be raised 10 to 20 times at least if these flaws could be eliminated.

The statistical theory of size effect came into existence from the time of Peirce, 1926. Peirce formulated the weakest link model; originated by Tippett in 1925. This was further refined by von Mises in 1936. The famous statistical theory was given by Weibull in 1939. He introduced what we call today Weibull distribution. Most of the subsequent research was done basically on refinement and applications of Weibull's theory.

Until about 1985, most of the mechanicians paid almost no attention to the study of deterministic size effect. Whenever a size effect was encountered, it was assumed to be

statistical and thus the field was neglected by mechanicians. This attitude however changed in 1980's and size effect gained its popularity in the study of concrete structures, composite structures etc. Bazant [1984] proposed the size effect law using the concept of fracture mechanics. Brief description of the law is provided in the subsequent section.

1.6 BAZANT'S SIZE EFFECT LAW

The assumption of classical theories is that the strength of geometrically similar structure is not dependant on size of the structure. This assumption is based on plasticity analysis. Concrete structures, which are quasibrittle in nature, however do not follow this trend. The size effect implies the dependence of strength of structure on its size. The strength is usually defined as nominal stress at peak load. The size effect involves the variation of nominal strength σ_{N_U} with size D. There are various possible correlation of the size effect, but the most widely accepted is the bi-logarithmic plot. In bi-logarithmic plot, $\log \sigma_{N_U}$ is plotted against log D. The simplest size effect law was proposed by Bazˇant [1984] covering various practical cases. The mathematical expression of this law is given here :

$$\sigma_{N_U} = \frac{Bf_t'}{\sqrt{1 + D/D_o}} \tag{1.9}$$

Where, f_t' is the tensile strength of the material, B is dimensionless constant, D_0 is a constant with the dimension of length. Fig. 1.9 shows the plot of this law. The strength theory based on yield or strength criteria predicts no size effect. This is represented by horizontal line in Fig 1.9. With help of linear elastic fracture mechanics it is established that the slope of the bi-logarithmic plot for brittle material is -1/2.

Further, it can be noted that for small specimen $D << D_0$, and hence Eq. 1.9 gets modified as

$$\sigma_{N_U} \simeq Bf_t' \tag{1.10}$$

whereas, for large specimen $D >> D_0$, and hence Eq. 1.9 yields

$$\sigma_{N_U} \propto D^{-1/2} \tag{1.11}$$

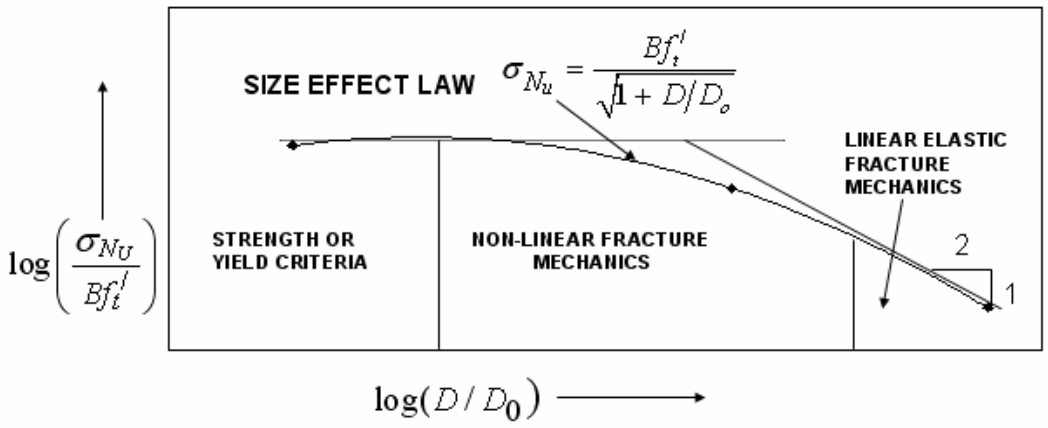

Fig 1.9 Plot of Bazˇant's size effect law

Bazˇant's size effect law has the advantage that it can be transformed into a linear regression plot as

$$Y = AX + C \tag{1.12}$$

In which,

$$X = D,\ Y = \left(f_t' / \sigma_{N_U} \right)^2,\ B = C^{-1/2} \text{ and } D_0 = C / A$$

Eq. 1.12 represents a straight line and the plot of this is the regression plot. A typical regression plot is shown in Fig. 1.10, in which $\left(f_t' / \sigma_{N_U} \right)^2$ is plotted in the Y axis and D is plotted in the X axis. A and C in Eq. 1.12 are the slope and intercept on Y axis of the regression plot. Once A and C become known, the coefficients B and D_0 can be easily determined using the expression given above.

Further, the existence of size effect may be attributed to the following factors [Bazˇant and Planas, 1998]:

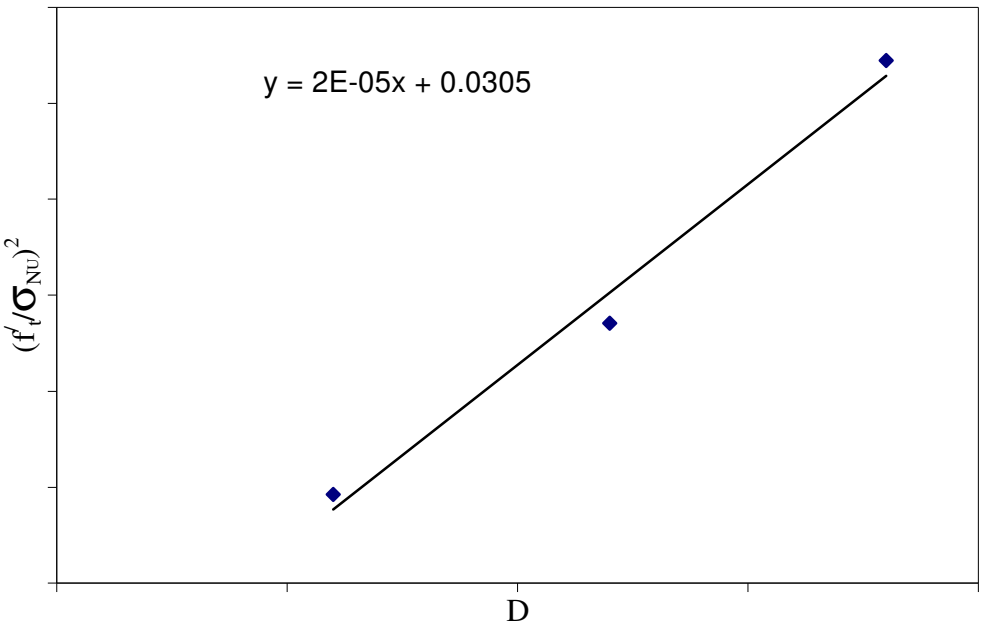

Fig. 1.10 Typical regression plot

1. Boundary layer effect (also known as wall effect): Concrete layer adjacent to the wall of the formwork has a smaller content of large aggregates and a large relative content of cement and mortar than the interior of the member.
2. Diffusion Phenomena (such as heat conduction or pore water transfer): Diffusion half times are proportional to the square of the size of the structure. Hence, for a thick member more time is needed for relaxation of stresses produced due to creep. Thus non-uniformity exists for a longer duration in a thick member leading to a reduction in strength in comparison to a small specimen.
3. Hydration Heat (or other phenomena associated with chemical reaction): This hydration heat produced in a concrete structure is proportional to the thickness. Thus for a thicker structure more heat is generated and subsequently a reduction in strength take place.
4. Statistical size effect: This is by the randomness of material strength and has traditionally been believed to explain most of the size effects in concrete structure this theory was supported by Weibull(1939).

5. Fracture mechanics size effect: This is the most important source of size effect in concrete structure. This occurs due to the release of stored energy of the structure into the fracture front. The fracture energy may be regarded as a material constant. For a smaller specimen work done per unit volume required is more than that of a bigger

   specimen to produce a fracture and hence a smaller specimen fails at higher unit strength.

6. Fractal nature of crack Surfaces: It is assumed that fractality plays a role in the formation of a new surface. However, this is not an authentic assumption.

The size effect can be observed if models of different scale are considered by maintaining geometric similarity i.e. when similitude criterions are strictly followed.

1.7 LITERATURE REVIEW

Large volumes of literatures related to experimental investigation on beam-column joint are available. A detailed survey has been carried out to identify the research objective. In this section, works carried out by the past researchers have been discussed and their important features have been highlighted with critical comments. Review presented in this section has been grouped into following six different categories:

i) Studies on RC beam-column joint

ii) Strengthening RC structures with concrete jacketing, steel jacketing and epoxy repairing

iii) Strengthening of RC beam and column with FRP

iv) Strengthening of RC beam-column joint with FRP

v) Size effect of composite coupons

vi) Size effect of concrete structural elements

1.7.1 Studies on RC Beam-Column Joint

In this section a literature review of studies on behaviour of RC beam-column joint is presented. The survey is presented in three subcategories, namely experimental, analytical and numerical studies.

1.7.1.1 Experimental Studies

The first experimental study on beam-column joint was conducted in the United States by Hanson and Connor [1967]. Seven exterior beam-column joints were tested under simulated cyclic earthquake loading. Performance of these specimens including moment capacities at first yield of reinforcements, ultimate moment and ductility of the assemblies, maximum beam deflection and anchorage bond stresses of beam reinforcements were reported. The authors concluded that properly designed cast-in-situ RC frames could resist severe earthquakes without loss of strength and moderate earthquakes without damage. These tests became the standard reference for subsequent investigations.

Megget and Park [1971] reported experimental investigation on the behaviour of exterior RC beam-column joints subjected to seismic loading with a low column axial load. Three specimens were designed using different methods, which were tested under the same cyclic loading in their investigation. The authors found that the joints of the specimens were not adequately reinforced against large shear stresses at inelastic loading conditions.

Scribner and Wight [1980] investigated the strength decay in RC beam-column joints under load reversals. Eight half-scale and six full-scale RC exterior beam-column subassemblies were tested in order to study the effect of intermediate longitudinal reinforcement on shear deterioration of flexural members subjected to repeated type of loading. Some specimen contained only vertical web reinforcement while some contained intermediate vertical reinforcement along with vertical web reinforcement. Specimens were tested under displacement-controlled cyclic loading. The authors concluded that severe loss of strength

and energy dissipation was observed for the members which were subjected to high shear stress. It was also concluded that the increase in size of vertical ties increased the energy dissipation capacity along with damage at a concentrated location, while longitudinal intermediate bars was capable of spreading the damage throughout the beam plastic hinge region.

Durrani and Wight [1985] reported results of an experimental investigation on the performance of an interior beam-column joint under earthquake-type loading, which had less joint reinforcement than recommended by ACI-ASCE Committee 352. They concluded that the joint shear stress had a pronounced effect on the behavior at large ductility levels and the joint hoop reinforcement. Some guidelines were suggested to simplify the design of joints.

Abdel-Fattah and Wight [1987] studied the relocating of plastic hinging zones for earthquake-resistant design of RC buildings. In their investigation, twelve full-size interior beam-column sub-assemblages were tested under cyclic loads. In addition to the main reinforcement in beam, intermediate longitudinal reinforcing bars were passed through the joint and were extended up to a specific length away from the column face in beam. The aim of the research was to relocate the potential beam plastic hinges away from the column face by the addition of these intermediate longitudinal bars. Three basic modes of failure including joint shear failure, localized beam hinging zone and distributed beam hinging were observed in their tests. The authors concluded that the performance of extra reinforcement in the joint could help in successfully relocating the plastic hinge away from the column face.

Ehsani and Alameddine [1991] investigated the behaviour of corner joints constructed with high-strength concrete. Twelve specimens were tested in their study in order to examine the recommendations of ACI-ASCE Committee 352 on the design of high-strength ductile moment resisting beam-column joints. The authors showed that the recommendations which were developed for normal strength concrete could not be applied to high-strength concrete

frame. They presented new requirements such as allowable joint shear stress and joint confinement for ductile design of RC beam-column joints.

Chutarat and Aboutaha [2003] investigated a solution for relocating potential beam plastic hinge zones by the use of headed bars in the exterior RC joints. Four large-scale beam-column subassemblies, with and without headed bars, were tested under quasi-static cyclic lateral loads/displacement in this investigation. The results showed that straight-headed bars could relocate beam potential plastic hinge regions very effectively.

Murty *et al.* [2003] tested twelve half-scale exterior beam-column joints under displacement-controlled cyclic loading to study the effectiveness of anchorages of longitudinal beam bars and the transverse reinforcement in the joint core. Four different reinforcement details for anchorage into the column for beam longitudinal bars were followed. The authors concluded that out of all the different joint reinforcement detailing investigated, the performance of the joint constructed following ACI standard hook was the best and it was easy to construct as well.

Joshi *et al.* [2005] tested four full scale exterior precast beam-column joint under cyclic loading in order to identify a suitable technique for connecting precast beam and column components. Following two different types connection techniques, precast and monolithic specimens were cast. Out of two types of detailing, one was done by the provisions of Indian standard code while the other was cast by using single U bar as top and bottom reinforcement of beam. The column was placed horizontally and beam was placed vertically in the test set up. The axial movement of the column was restrained by providing stiff supports fixed to the strong floor by steel studs. The ends of the column were supported on rollers equidistant from the beam centre. The authors concluded that the performance of the monolithic specimen with U bar detailing was better than all other types of joints used in their study.

Nie *et al.* [2008] tested six beam-column joints comprising of three interior and three corner joints for proposing a new connection system for concrete filled steel tube composite column

and RC beams. According to the new system, the column was encased by a steel tube. The tube was cut at the beam-column joint and the steel reinforcing bar in the RC beam was kept continuous at the floor level in which concrete was confined by multiple lateral hoops in the joint region. The specimens were tested under cyclic loading. The authors concluded that the new connection was capable of dissipating enough energy in addition to showing a good performance from ductility aspect.

The literature survey reveals that the test on beam-column joint was initiated as early as in 1967. Many tests were conducted using cyclic loading to simulate the effect of earthquake type of loading. Experimental studies were conducted on both exterior and interior beam-column joints on full scaled as well as scaled down specimens. Tests were conducted to explore the performance of different types of reinforcement in the connection of beam-column joints. Further, most of the researchers preferred to place the column in horizontal position and beam in vertical position for the ease in handling and placing of specimens in the test rig. In the experimental set up, the ends of the column were supported on rollers to simulate symmetrical boundary condition. However, it may be noted that no comparative study was carried out for the evaluation of performance of various types of deficient joints and also involving different sizes of specimen.

1.7.1.2 Analytical Studies

Among the analytical studies, Paulay *et al*. [1978] displayed a simple analytical model for representing the behaviour of interior beam-column RC joints under seismic loading. They assumed that the shear within the joint was resisted by the concrete strut and joint shear reinforcement acting together as a truss. They investigated the effects of reversed cyclic loading, in both the elastic and inelastic range of response. Discussion was made about the damaging effects of yield penetration into the joint and methods were suggested to minimise these effects.

Scarpas and Paulay [1981] proposed a new model for demonstrating the mechanisms of shear resistance in exterior beam-column joints. Their model was based on a verification of the applicability of the existing models of interior joint design to the design of exterior joints. The same mechanism (strut and tie model) as for interior joints was used in their new model, which was verified by experiments.

Paulay [1989] utilised simple laws of static to present the disposition of internal forces in ductile RC frame joints. He showed that due to shear force and resultant diagonal cracking in the joint core, significant orthogonal tensile forces were generated. Paulay established that the role of the joint shear reinforcement to sustain a diagonal compression field was more than to provide confinement of the concrete in a joint core.

Bakir and Boduroglu [2002] proposed a new design equation for predicting the joint shear strength of monotonically loaded exterior beam-column joints. Three different parameters including the beam longitudinal reinforcement ratio, influence of the joint aspect ratio and the amount of stirrup ratios were taken into account in their equation. The authors showed that the results of proposed design equation were more reliable than previously suggested ones.

He *et al.* [2008] proposed a constitutive model based on fracture energy for the analysis of reinforced concrete structures under cyclic loading. While modeling, emphasis was given on realistic hysteretic behavior of concrete incorporating strains, energy dissipation, damage and stiffness deterioration, crack closing opening and partial unloading/reloading. The proposed model was validated by using the measured data from experiments. The authors concluded that the model was capable of predicting the response of RC structures

under generalised cyclic loading.

The literature survey on analytical studies of beam-column joint indicates that models were developed for predicting the behaviour of RC beam-column joints under cyclic as well as

monotonic loading. Design equations were also developed and parametric studies were conducted for some identified design variables.

1.7.1.3 Numerical Studies

Studies on numerical investigation on the behaviour of RC joints were observed in literature from 1970's, when the non-linear finite element modeling was introduced. For example, Will *et al.* [1972] applied the finite element method in order to predict the behaviour of exterior RC beam-column joints tested at the University of Toronto. Plane stress rectangular elements were employed in order to model the concrete and steel reinforcements in their study and spring elements were used to simulate the interaction between the steel and concrete. The authors assumed that the concrete and steel had a linear elastic behaviour and that a linear bond-slip relationship exists. They compared the moment-rotation characteristics of the spandrel beam and stresses in the column longitudinal steel obtained from experimental tests with their predicted values obtained from the finite element analysis. The authors concluded that the proposed finite element analysis was able to predict the behaviour of the test specimens quite well, if the applied moments in the first cycle of loading were limited to about 80 percent of the yield moment of the critical sections.

Kwak and Fillippou [1990] made use of finite element analysis in order to study monotonically loaded reinforced concrete beam-column joints. Their model was capable of representing crushing and cracking of concrete. The authors proposed a new smeared finite element model based on an improved cracking criterion, which was derived from fracture mechanics principles. They also developed a new reinforcing steel model, which was embedded inside a concrete element and could account for the effect of bond-slip. Correlation studies between analytical and experimental results were performed. Several parametric studies were also conducted with the objective of checking the validity of

proposed models and identifying the significance of various parameters on the local and global response of reinforced concrete joints.

A numerical study on the behaviour of exterior beam-column joints using ANSYS was performed by Vollum [1998]. The influence of varying the element size, shear transfer coefficient for open cracks, modeling of reinforcement and load step and convergence criteria were investigated in this study. Concrete was modeled by a solid element (ANSYS Solid 65), which is an 8 noded brick element that employs William and Warnke [1975] model for the triaxial behaviour of concrete. The steel reinforcements were modeled by link elements that were connected to the nodes of the solid elements.

It is evident from literature that finite element analysis served as a very good tool for analysis of beam column joint. The general purpose finite element software ANSYS can be used to effectively model concrete using the available element library. Nonlinear analysis can be carried out to evaluate the performance of beam-column joint till failure.

1.7.2 Strengthening RC Structures with Concrete Jacketing, Steel Jacketing and Epoxy Repairing

Research on conventional methods of strengthening beam-column joints include concrete jacketing by encasing the existing column with a layer of RC concrete, steel jacketing by attaching flat or corrugated steel plates and epoxy repair by pressure injection. The available literature pertaining to strengthening/rehabilitation are discussed in the following sub-sections.

1.7.2.1 Strengthening with Concrete Jacketing

Corazao and Durrani [1989] tested five subassemblies of single beam-column connections and six multiple connection subassemblies, each consisting of two exterior and one interior connection with some including a floor slab for evaluating and improving methods of

repairing and strengthening beam-to-column connections, damaged by earthquakes. The specimens were repaired using techniques like replacement of damaged concrete, enlargement of section and addition of rolled steel elements. Epoxy injection and replacement of concrete techniques were successful in restoring strength of original specimens but was unsuccessful to restore the stiffness and energy absorption capacity. This was primarily due to difficulty faced in filling all the internal cracks. Specimens which were strengthened by reinforced concrete and steel encasement exhibited increased strength, stiffness and ductility with desirable mode of failure.

Alcocer and Jirsa [1993] performed experiments to study the suitability of jacketing of non-ductile frame elements as a rehabilitation technique. The need to drill holes through the beams for placing joint confinement reinforcement was eliminated. This was achieved by welding a steel cage around the joint. The cage was made by steel angles and flat bars. It was reported that the steel cage and the cornet ties confined the beam-column joint satisfactorily up to 4% drift. Important findings indicated that the shear strength of jacketed joints could be estimated using current recommendations for the design of beam-column joints in new construction. It was suggested that the current criteria on bar development should be met by longitudinal reinforcement in the jackets.

Hakuto *et al.*[2000] tested three one-way interior beam-column joints, which were without any joint reinforcement. The previously damaged specimens were strengthened by RC jacketing provided at the beams, columns and joints. The core of the joint strengthened by plain circular hoops, which was made up of two circular U-shaped ties. The undamaged specimens were retrofitted by providing column jacket only. The strengthening scheme changed the behaviour of the joint in ductile mode with formation of plastic hinges in beam, except for the specimen in which only column jacket was provided. The main drawback of the method was that the addition of joint core hoops was very much labour intensive.

1.7.2.2 Strengthening with Steel Jacketing

Ghobarah *et al.* [1997] and Biddah *et al.* [1997] proposed and evaluated an innovative seismic upgrading technique for existing reinforced concrete frame joints constructed prior to the 1970s using corrugated steel jacketing to provide high out of plane stiffness. The grouted corrugated steel jacket was provided with an intention for early lateral confining effect during the elastic phase of the reinforced concrete column, in addition to providing shear resistance for beam-column joint. The jacket was also anchored to the concrete by two steel angles and anchor bolts. Experimental results indicated that the corrugated steel jacket was an effective upgrading technique as it increased the joint shear strength and the energy dissipation capacity when subjected to high cyclic load levels. An analytical method was also proposed for the design of corrugated steel jackets by the authors.

Yen and Chien [2009] tested RC beam-column joints rehabilitated by steel plates to study the improvement of strength and stiffness. In the proposed rehabilitation scheme, steel plates were glued to both the lateral surfaces of beam and continued through the joint. The strengthened specimens showed a considerable improvement in the load-deflection curve. The authors also developed analytical model to predict the flexural strength of an RC beam web-bonded with steel plates. Further, two indices namely, the strength rehabilitation index (SRI) and ductility rehabilitation index (DRI) were proposed by the authors to estimate the decaying of strength and ductility of rehabilitated elements subjected to earthquake loading.

1.7.2.3 Repairing with Epoxy

French *et al.* [1990] conducted two test series in order to determine the effectiveness of epoxy techniques for repairing damaged joints. They pre-loaded two interior RC joints and then repaired one with pressure injection and the other by vacuum impregnation. Their repaired specimens were then subjected to the same load history as that was imposed on the original test specimens. The authors concluded that both techniques worked well in restoring

the strength, stiffness, energy-dissipation capacity and the bond. Authors recommended the vacuum impregnation technique due to its advantage in repairing of larger areas. The epoxy and resin injection techniques are usually employed when the damage level is low.

Beres *et al.*[1992] tested deficiently detailed, lightly reinforced interior beam-column joints. Methyl-methacrylate resin was used for repairing by vacuum injection. The failure of the specimens occurred by formation of extensive diagonal crack in the joint along with pullout of the embedded beam bottom bars. The repairing process was capable of restoring 75% of initial stiffness, 72% column shear capacity for the specimen tested by them. There was no change observed in the energy dissipation which was due to reduced rate of strength deterioration.

Filiatrault and Lebrun [1996] tested two one-way exterior beam-column joint, which were damaged by earthquake. One with non-seismic detailing conforming to the construction of fifties and sixties and other following seismic codal details were considered. The specimens were tested by the load history which was imposed on the original structure. The damaged specimens were repaired by epoxy pressure injection. The authors concluded that the repair procedure was effective in improving the strength, stiffness and energy dissipation.

Karayannis *et al.* [1998] tested eleven beam-column joint specimens after repairing only with epoxy injection. Their study was focused on effect of joint reinforcement arrangement on the efficiency of epoxy repair by pressure injection. Though the failure took place by beam hinging, yet the cracks were observed even in the first cycle itself. The authors reported the increase in load carrying capacity and energy dissipation was 8-40% and 53-139% respectively due to repairing.

Shash [2005] reported a case study where the cracks in reinforced beams of a single storey building were repaired by epoxy injection and the effectiveness of repairing was assessed by load test. The cracks were filled by injecting liquid epoxy resin. By performing the load test on the repaired beam the deflection noted was only 2.0 mm, which was less than the

allowable deflection of 6.4 mm (as per ACI 318). The author finally concluded that the repaired beam could safely carry the expected loads.

Issa and Debs [2007] tested fifteen concrete cubes for investigating the effectiveness of repairing cracks by using epoxy (Sikadur-52). Out of fifteen cubes cast, twelve cubes were cracked artificially. Six cracked cubes were tested without repairing and rest six were tested after repairing the cracks with epoxy by the method of gravity filling. Three virgin control cubes were also tested (without any crack). The comparison of compressive strength of the tested specimens revealed that the crack resulted the reduction in strength by 40.93% in comparison to control specimen. The repaired specimens also failed to regain the original strength and showed a reduction in strength by 8.23% in comparison to the control specimen.

The literature review on conventional retrofitting/rehabilitation technique indicates that these methods of strengthening beam-column joints (using concrete jacketing, steel jacketing and epoxy injection) can enhance many desirable properties like strength, stiffness, energy dissipation etc. These techniques may change the failure modes into most desirable ductile mode of failure including the formation of hinges in beam. In many cases, shear strength also get increased. However, there were some inherent drawbacks in adopting these methods. In epoxy injection technique, the gaining of original strength is doubtful as evidenced by many test results. Concrete jacketing is labour-intensive involving drilling through the beams, floor slabs and even in-place bending of the added joint transverse reinforcement. Steel jacketing is vulnerable to corrosion, difficult to handle for heavy weight and has objectionable aesthetics if corrugated steel sheets are used. Moreover, the functional aspects of the structures get hampered during the adoption of all these strengthening techniques.

1.7.3 Strengthening RC Beam and Column with FRP

With the introduction of Fibre-reinforced polymer (FRP), the difficulties and associated problems with conventional methods of retrofitting could be addressed appropriately. Thus, recent research efforts have been focused on the use of Fibre-reinforced polymer for retrofitting of beam-column joints, which has got many advantages as well. The main advantages of FRP composites are their high specific strength (i.e. strength to weight ratio) and high corrosion resistance. The former property leads to great ease in site handling, reduced labour cost and less interruptions to existing services, while the later ensures durable performance.

In civil engineering, the FRP plate bonding technology was first investigated at the Swiss Federal Laboratory for Materials Testing and Research [Mier *et al*. 1993], where tests in RC beams strengthened with CFRP plates started in 1984**.** A new direction of research on FRP strengthening of RC beams started around 1990 at the University of Arizona. Saadatmanesh and Eshani[1990] tested four beams under monotonic loads strengthened with epoxy-bonded GFRP plates and the results were compared with one control specimen. The authors concluded that GFRP plates could increase the flexural strength and stiffness of RC beams and the behaviour of retrofitted beams were very similar to beams retrofitted with steel plates. It was recommended that the epoxy should have sufficient stiffness and strength for transferring the shear stresses between concrete and composite plates.

Saadatmanesh and Ehsani [1991] reported the results of tests on a series of RC rectangular and T-beams strengthened by GFRP plates applied to their tension face. It was concluded again that the flexural strength of RC beams increased remarkably by the GFRP plates. In addition, it was showed that the epoxy bonded plates improved the cracking behaviour of the beams by reducing the crack width.

An *et al*. [1991] presented analytical models in order to predict the stresses and deformations

of strengthened beams. Their model was effective when the steel reinforcement ratio was low. The authors concluded that bonding composite to a concrete beam could increase its stiffness, yield moment and flexural strength.

Triantafillou and Plevris [1992] used the strain compatibility method, concepts of fracture mechanics and a simple model for the FRP peeling off de-bonding mechanism due to the developments of shear cracks. Their study focused on establishing a systematic analysis procedure for the flexural behaviour of FRP-strengthened RC members. Design curves for each dominated mechanism and graphs examining the effect of FRP sheets on the ductility and stiffness of strengthened components were presented. An experimental programme was also conducted in order to confirm the results of their analytical model.

Saadatmanesh and Malek [1998] presented design guidelines for flexural strengthening of RC beams with FRP plates applied to their tension face. Three failure modes including compression crushing of concrete, rupture of the plate, and local failure of concrete at the plate end due to stress concentration (de-bonding of the plate) were considered in their study.

Malek *et al.* [1998] presented a method for calculating shear and normal stress concentration at the cut-off point of RC beams strengthened with FRP plates. The effect of large flexural cracks along the beam was also investigated in their analytical model.

El-Mihilmy and Tedesco [2000] investigated the flexural behaviour of externally bonded FRP laminates in RC beams and presented a simple and direct analytical procedure to evaluate the ultimate flexural capacity of strengthened beams. Their procedure was based on the equilibrium equations and compatibility of strains which was applicable to RC rectangular sections. The limiting FRP reinforcement for ensuring ductile behaviour was established in their study. Design curves to facilitate implementation of the closed-form solutions were also presented.

Chaallal *et al.* [1998] proposed design guidelines for flexural and shear strengthening of RC beams. The flexural strengthening scheme was based on principle of compatibility and

equilibrium of forces. Further, design equations were developed for shear strengthening with four different pattern of FRP fixing. The four patterns considered were inclined stirrups, vertical stirrups, wings stirrups and U sheet stirrups of FRP jackets. Equations were proposed to find out the area of FRP needed for shear strengthening in all these cases.

A design approach based on providing fibre reinforcement to replace the inadequately anchored bottom steel reinforcement in the beam section was proposed by El-Amoury and Ghobarah [2002]. In their design process, FRP sheets were designed so that they develop the same design flexural moment as that of the original RC beam section. Equations were proposed for calculation of moment capacity of a strengthened specimen and the number of FRP layers needed to resist a design moment.

Arya *et al.* [2002] reviewed the design guidelines on flexural strengthening proposed in Technical Report 55, based on British design codes and standards. This review provided guidelines on selection of materials type and their properties, field application, workmanship and installation and long term monitoring. Equations were suggested for finding out flexural moment of beam sections strengthened with FRP and area of FRP section needed for a design moment. Finally, an illustrative example was given in details for design calculation of beam strengthened with FRP.

Teng et *al.* [2002] performed a comprehensive study of the existing research on the failure modes and typical behaviour of FRP-plated RC beams. These failure modes are classified into seven main categories, which are: (a) flexural failure by FRP rupture, (b) flexural failure by concrete crushing, (c) shear failure, (d) concrete cover separation, (e) plate-end interfacial debonding, (f) intermediate flexural crack induced interfacial debonding, and (g) intermediate flexural shear crack-induced interfacial debonding. Among them, failure modes (d) and (e) are referred to as plate end debonding failures and failure modes (f) and (g) are referred to as intermediate crack- induced interfacial debonding failures. For a given beam, a particular mode may be critical which depends on numerous parameters such as the amount

of internal flexural and shear reinforcement, the geometric and material properties of the FRP, the adhesive layer and the RC beam itself. The authors proposed expression for flexural and shear strengthening of RC elements. The flexural strengthening is based on compatibility and equilibrium of forces. The authors also proposed the equations for calculation of compressive strength of RC columns strengthened with FRP. The calculation covers various geometric shapes of the columns.

Anania *et al.* [2005] tested two series of half scaled beams to study the increase in flexural performance of RC beams strengthened with CFRP materials fixed by a newly developed anchorage system. Out of two series, one series of specimen was strengthened by CFRP, while the other one was left as control specimen. In their newly proposed anchorage system, at the intrados of the original beam, a joist of polyurethane was inserted, which was connected at its ends to two blocks. It was made of reoplastic mortar, whose function was to provide anchorage. A four point load test was conducted and continued up to ultimate load. The authors reported that flexural capacity of the Strengthened beam was found two times and ductility was found three times with respect to the original beam.

Anil [2006] tested six full scale T-beams to study the improvement in shear capacity due to strengthening with CFRP. Out of six specimens, two were treated as control and four as strengthened specimens. Beams were strengthened with inclined CFRP strips placed at a particular spacing. The specimens were tested under cyclic loading. The experimental result showed considerable enhancement in strength and ductility. The authors concluded that the failure mode and ductility of the specimens varied according to the CFRP strap with and its arrangement.

Singh [2008] tested six beams to evaluate the strength of various types of commercially available uni-axial CFRP stirrups. A design guideline was presented for estimating the shear strength of a concrete box beam prestressed using bonded and unbonded CFRP tendons and

reinforced with CFRP stirrups. The theoretical value of shear strength calculated by the developed equation matched with the experimental result within reasonable limit.

Gadve *et al.* [2009] tested seven cylindrical concrete specimens to study the effectiveness of FRP wraps in providing both active and passive protection to steel reinforcements in concrete that was already damaged by corrosion. Glass and carbon FRP sheets were wrapped on the specimens. Constant Anodic current was continued through the specimens for specified times. The experimental result showed that wrapping by FRP tremendously slowed down the rate of corrosion in addition to increase in pullout strength and decrease in mass loss. The authors reported that the cell voltages increased about 300% in the wrapped samples implying that the resistance to corrosion increased substantially due to the wrapping with FRP.

It is very clear from the literature that the strengthening with FRP enhances flexural strength, stiffness, ductility and even resistance to corrosion of RC structures to a considerable extent apart from improvement in many other behaviour. Design guidelines for strengthening of RC beams and columns with FRP were developed. Equations were proposed to calculate the ultimate capacity of RC beams and columns strengthened with FRP

1.7.4 Strengthening of Beam-Column Joint with FRP

FRP was used for both shear as well as flexural strengthening beam-column joint. A detailed literature survey of both the strengthening is given in the next subsections.

1.7.4.1 Shear Strengthening with FRP

Shear and anchorage failure at the beam-column joints occurred during the 1985 Mexico, 1986 San Salvador and 1989 Loma Prieta earthquake. This encouraged the researchers to investigate different strengthening techniques of moment resisting frame structures. The

literature for shear strengthening covers both experimental studies as well as theoretical studies.

The experimental studies by Pantelides et al. [1999] was performed by carrying out in situ tests using carbon fibre composite jackets for three columns and the cap beam of an existing concrete bridge pier, which was constructed in 1962. A horizontal quasi-static cyclic load was applied. It was found that the shear capacity of the cap beam and columns and the ductility of the pier were improved significantly.

Gergely *et al.* [2000] tested fourteen numbers of 1/3-scale T joints to study the improvement in shear capacity due to retrofitting by FRP. Four specimens were treated as control specimens, while the remaining were retrofitted by varying curing process, CFRP layout and surface preparation. The specimens were tested by placing column in horizontal position and beam in vertical position. The cyclic load applied was force controlled, each step having three cycles consisting of a push and a pull segment. The investigation showed significant shear capacity improvement, which was also supported by analysis. The authors concluded that surface preparation and FRP layout played a role in strengthening, while curing process did not play any important role in strengthening.

Ghobarah and Said [2002] tested four beam-column joints representing a typical joint built in accordance with pre-1970s codes. The joints were originally designed to fail in shear. Some joins were strengthened by unidirectional or bidirectional ($\pm 45^0$) glass fibe reinforced polymer (GFRP) sheets. Two specimens were tested as control specimens, which were further repaired and rehabilitated with U shaped GFRP sheet apart from providing mechanical anchorage with steel plates and threaded rods. The remaining virgin joints were retrofitted and tested. Four different strengthening techniques were used. During cyclic load test, a constant axial load was maintained on the column. Out of all the four strengthening techniques, the specimen in which fibres were properly extended and wrapped, the failure

was due to formation of beam plastic hinge without joint shear cracking. The scheme was unable to prevent expansion of joint concrete, which initiated delamination of FRP. The authors concluded that GFRP jacket increased the shear resistance of the joint along with enhancement in other desirable properties.

El-Amoury and Ghobarah [2002] modified the schemes of strengthening with GFRP by testing three specimens of beam-column joints with inadequate anchorage of bars at bottom of beam and without shear reinforcement. The control specimen was rehabilitated and tested. It showed about 100% increase in load carrying capacity with respect to the control specimen. The third specimen was an original specimen, which was retrofitted and tested. This specimen showed more than 100% increase in load carrying capacity with reference to control specimen. Rehabilitated and retrofitted specimens dissipated energy three times and six times respectively to that by specimen. The failure of rehabilitated specimen was due to debonding of composite sheets, while in retrofitted specimen the use of two U-shaped steel plates very efficiently eliminated debonding of GFRP and reduced the strength degradation. This specimen finally failed in joint shear.

Antonopoulos and Triantafillou [2003] tested eighteen exterior 2/3-scale beam-column joints for evaluating the contribution of FRP to the shear capacity of the joint. Most of the specimens were constructed without any stirrup for achieving joint shear failure. Out of eighteen specimens, two were tested as control specimens and the rest 16 were strengthened with different strategies of retrofitting. Except one, (where GFRP was used) all specimens were strengthened with different number of layers of CFRP strips on sides of columns and beams, some with L- shaped anchors comprising of steel angles, some with U-shaped CFRP sheets. Displacement-controlled loading was applied during the testing. Test results were interpreted in terms of gain in strength, stiffness and energy dissipation due to retrofitting. The percentage gain in strength due to retrofitting by CFRP varied from 15% to 85%,

increase in initial stiffness varied from 5% to 40% and enhancement in energy dissipation varied from 5.7% to 70.8%.

Mukherjee and Joshi [2005] conducted tests on two sets of scaled down RC beam-column joins to study the performance of FRP used for up gradation. One set of joints were cast with ductile adequate steel reinforcement following ductile joint reinforcement, while the other set were cast non-ductile joint reinforcement. Both sets of specimens were strengthened with different strategies. Some specimens were retrofitted with GFRP/CFRP sheets, some with GFRP/CFRP wraps, while some with CFRP plates and wraps. CFRP plates were used to improve bending stiffness. The control specimens were rehabilitated after testing, and their performance were also checked. A constant axial load was maintained during the application of displacement-controlled cyclic loading. There was considerable increase in initial stiffness, yield load, deflection at yield, ultimate deflection and energy dissipation for all the strengthened cases. The authors concluded that both GFRP and CFRP could be used for seismic retrofitting and rehabilitation.

Ghobarah and amoury [2005] tested six beam-column subassemblies representing pre-1970 code provision with non-ductile reinforcement detailing. The joints were subjected to quasi-static load that simulated seismic forces. The first three specimens had inadequate anchorage length of the bottom beam bars. Two of them were strengthened by using carbon-fiber-reinforced polymer sheets attached to the bottom face of the beam. The other three specimens had no steel ties available in the joint region, in addition to inadequate anchorage length of the beam bars. Two of the beam-column joints were strengthened by glass-fiber-reinforced polymer jackets. In addition, a well anchored steel reinforcement was added to the existing inadequately anchored bars with the help of threaded rods and steel ties. The authors reported that the rehabilitation techniques were effective in eliminating the brittle joint shear and steel bar bond-slip failure modes.

Mahini and Ronagh [2010] tested seven 1:2.2 scaled beam-column joint specimens retrofitted by web-bonding method under monotonic loading. The beams were wrapped with CFRP on both sides as well as around the back of the column for providing FRP anchorage. In the test set up adopted, the columns were supported at each end with specially designed supports that ensured free rotation without translation. The test result showed that web-bonding method was effective and capable of restoring or even upgrading strength. The authors also presented design graphs for selection of the type and the amount of FRP required for upgrading an existing joint to a specified moment capacity and curvature ductility.

It is evident that strengthening with FRP can improve the hysteretic response, joint shear capacity, ductility, energy dissipation etc. Placing GFRP along $\pm 45^0$ orientations in the joint region showed a good performance in shear strengthening. Most of the studied showed that the failure of FRP was by debonding of the composites from concrete, which has emphasized the need for thorough surface preparation of the concrete to make the bonding more effective. The loading cycles can be applied either displacement controlled or a combination of both force controlled and displacement controlled. Generally to estimate the yield displacement, in the first phase of loading, a force controlled loading is applied. Once the yield displacement becomes known, then displacement controlled loading is applied in the second phase. However, if a good estimation about yield displacement is available before hand, then directly from the beginning displacement controlled loading system can be adopted. Before applying the cyclic load, an axial load on the column was applied and was maintained constant during the testing. This application of this axial load in column was to simulate the gravity loading.

Tests were carried out for full-scaled and scaled down specimens by different researchers. Research was done to see the effect of curing process, FRP layout and surface preparation and conclusions were drawn. However, no research was reported to study the effect of the scale of the tested specimens.

Among the analytical studies in shear strengthening of beam-column joint, Pantazopoulou and Bonacci [1992] used stress equilibrium and strain compatibility to provide the shear strength of a joint with known geometry and reinforcement quantities. The mechanics of beam-column joints in laterally loaded frame structures was investigated in their model. Observations were drawn from a database of 86 beam-column joint tests compiled from published literature, and from the results of a simple mechanical model developed using equilibrium, kinematics, and material considerations. The study provided a detailed description of the parametric dependence of joint behaviour and diversity in experimental techniques used in various countries.

Antonopoulos and Triantafillou [2002] further extended the aforementioned model of Bonacci and Pantazopoulou [1995] to account for the effect of externally bonded FRP. Their model provided equations for stresses and strains at various stages of the response (before or after yielding of beam or column reinforcement) up to the ultimate capacity, defined by concrete crushing or fibre-reinforced polymer (FRP) failure due to fracture or de-bonding. Their model provided useful information on the shear capacity of FRP-strengthened joints in terms of the quantity and configuration of externally bonded reinforcement and may be used to design FRP patching for inadequately detailed beam-column joints. The authors analysed a series of case studies and compared the analytical model with existing test results. It was concluded that even low quantities of FRP materials provide significant enhancement of the shear capacity.

El-Amoury and Ghobarah [2002] proposed a design method for fibre jacketing in order to upgrade the shear capacity of existing beam-column joints in reinforced concrete moment resisting frames. They designed the fibre jacket to replace the missing transverse reinforcement at the joint core. In their methodology, the total joint shear force was calculated as the difference between the maximum force in the bottom steel considering 25% over-strength and the shear force in the column given by Park and Paulay (1975). They

arrived at the required area of the fibre in the joint based on the shear calculated as the difference between the total shear and the concrete shear resistance.

The literature survey on analytical studies of beam-column joint reveals that recommendations were proposed for enhancement of strength using FRP. Analytical models were developed to compute stresses and strains at various stages up to failure, which could be either due to fracture or de-bonding of FRP.

1.7.4.2 Flexural Strengthening

The experimental studies by Li et al. [1999] involved testing of three full scale interior beam-column joints under static loading. Two specimens were used as control and one was strengthened with hybrid FRP composite of E-glass, carbon cloth etc. Their results showed that retrofitting scheme enhanced the stiffness about 45%, and ultimate load carrying capacity about 30%.

Mosallam [2000] investigated the performance of glass epoxy and carbon-epoxy quasi-isotropic systems for retrofitting and repairing of beam-column joint. Six half-scale specimens, simulating interior beam-column joint were tested. Two were treated as control specimens and two as retrofitted specimens. The control specimens after failure were repaired by epoxy injection along with carbon-epoxy and E-glass-epoxy quasi-isotropic laminates. The specimens were tested by applying reversal loads to the top of column at the loading frequency of 0.25 Hz. It was found that the repaired specimen could be upgraded for attaining the ultimate load carrying capacity and displacement to a considerable extent. The retrofitted specimen showed an improvement in strength ranging from 10-44%. A slight increase in ductility and stiffness was also observed. The author concluded that the use of quasi-isotropic polymer laminates increased both the stiffness and the ultimate strength of the reinforced concrete moment-resistant frame. The author gave eight recommendations for

future research. Out of these, one was to see the effect by changing the specimen size and varying the beam and column cross sections.

Granata and Parvin [2001] conducted experiment to investigate the suitability of FRP fabric in the enhancement of moment capacity of exterior beam-column joints. Kelvar fibrer composite fabric were used for strengthening. Six scaled down specimens were tested to examine the effect of various thicknesses and configuration of FRP fabrics applied. Their study showed great improvement of flexural capacity of beam column joints and provided certain guidelines for the ascertaining appropriate FRP fabric thickness. The authors concluded that external FRP reinforcement was an effective way to increase the moment capacity of beam-column connections.

Li and Chua [2009] tested six interior full-scale beam-column joints, strengthened with CFRP and GFRP to study seismic behaviour of non-seismically detailed joints. Three specimens incorporating three different criteria were treated as control specimens, and three more as strengthened specimens. Observing the failure mode of the control specimens, the specimens to be strengthened were retrofitted with different strategies to overcome the specific deficiencies. Wet lay-up of FRP application was adopted. The strengthened specimens showed improvement in hysteretic response, stiffness and energy dissipation capacity. The authors concluded that the use of CFRP strips on strong column-weak beam was effective in flexural retrofitting.

The literature survey on experimental works on flexural strengthening reveals that externally bonded FRP composites can improve flexural capacity of the joint and can even shift the failure from the joint region leading to hinge formation in beam. It also considerably enhances the other desirable properties like stiffness, ductility, energy dissipation etc. Recommendation was forwarded to see the relative effect in enhancement of properties by changing the specimen size of retrofitted beam-column joints.

A parametric investigation into the application of FRP composite laminates to exterior beam-column joints in order to increase their flexural capacity under monotonic loads was carried out by Parvin and Granata [2000]. Nonlinear finite element analysis of three beam-column joints with laminates bonded to the tensile faces of the beam-end was carried out in their investigation. The authors modeled the concrete using ANSYS eight-noded solid element (solid65) that is specially designed for concrete material. They used a two noded link element (link8) for modeling the reinforcing steel and also an eight-node three-dimensional multi layer solid element (solid 45) for FRPs. The authors concluded that increase in laminate thickness or thickness of the wrap would provide reduction in the maximum stress, joint thickness or stress concentration at the edge of the laminate. They observed an increase in the moment capacity of up to 37% in their investigation.

Lakshmi *et al.* [2008] utilized ANSYS for the analysis of beam-column joints with different deficiencies subjected to cyclic excitation. The control as well as retrofitted specimens were simulated and reliable results were obtained in terms of gain in ultimate load carrying capacity for the retrofitted specimens. It was concluded that with the use of appropriate finite element and material model, the behaviour of RC and the retrofitted RC specimens could be very effectively simulated in ANSYS.

The survey indicates that nonlinear analysis of retrofitted beam-column joint could be very conveniently studied using ANSYS. Using appropriate element library, concrete, steel and FRP could be modeled. The use of FRP showed good enhancement in the load carrying capacity of RC beam-column joint.

1.7.5 Size Effect of Composites

In the available literature on size effect of composites, it is found that research was mainly done on tensile test, flexural test and compressive test of composite coupons made up of fibres and resins. This section gives a detailed literature survey on test of composites.

1.7.5.1 Tensile Test

Experiments on size effect on tensile strength started long back. Bullock [1974] compared tensile strength of carbon- epoxy taws and unidirectional laminate. The tensile strength of 25 mm long fibre with 70% volume fraction was measured as 1744 MPa with a Weibull modulus of 29. It was then compared with tensile strength of 6 ply laminated specimen of 70% volume fraction. It gave a strength of 1434 MPa supporting Weibull theory.

Hitchon and Philips [1978] compared tensile strength from straight coupons and hoop burst test on cylinders made with variety of carbon fibre/epoxy materials and different manufacturing methods. There was considerable variability in strengths and weibull moduli from the different tests. However, it was found that the smaller tensile coupon gave higher strength than the larger hoop burst specimens in a consistent manner and was in well agreement with weibull theory.

Jackson *et al.* [1992] conducted tests on composite coupons having four different laminate stacking sequences and having four different scaled sizes (1/4 ,½, ¾ and full scale). The test data proved that the tensile strength was dependant on specimen sizes. For all the four lay ups, the tensile strength and strain decreased with increase in specimen size.

Gurvich and Pipes [1995] reported a decrease in strength with increase in thickness for carbon fibre/epoxy specimens with correlated length and width.

Wisnom and Atkinson [1997] tested unidirectional Ciba E glass/913 epoxy preprag made specimens with different gauge lengths. Tapered specimen with plies dropped off internally near the ends was used to facilitate proper gripping. It was reported that the maximum tensile strain decreased with the increase in gauge length, which is strong evidence supporting size effect.

1.7.5.2 Flexural Test

A lot of test results are available in literature for flexural tests on specimens having different

sizes, out of which few are mentioned here. Wisnom [1991] reported flexural test on unidirectional XAS/913 carbon fibre/epoxy. Four point bending test was conducted on scaled specimens of 25, 50 and 100 ply thickness. A significant decrease in strength was observed by increasing the size of specimen. The tensile strain to failure decreased to about 8% for each doubling of specimen size, which corresponds to a weibull modulus of 25.

Jackson reported [1992] flexural tests on AS4/3502 carbon fibre/epoxy composite scaled beams. Tests were performed on unidirectional, angle ply, cross ply and quasi isotropic beams of eight different scaled sizes ranging from 1/6 scale to full scale. The 1/6 scale was corresponding to 8 ply thickness and full scale corresponding to 48 ply thickness. The author concluded that there was a significant scale effect on all the laminates tested. Small scaled beams failed at higher normalised load than and end displacement values than their full scale counterpart.

1.7.5.3 Compressive Test

Compressive tests of composites are very tedious even though a huge amount of research was undertaken. In compressive test, many problem arise like end loaded specimen tend to broom or split from the end and hence indirect loading by means of shear is often used. This leads to stress concentration and failure usually takes place where the specimen is gripped. High shear stress concentration may synergize the compressive stresses giving an incorrect result in finding compressive strength.

Componeschi [1993] investigated the compressive strength of carbon and glass fibre of 6.4-25.4 mm thick composite laminates, which were subjected to uniaxial compressive loading. Result of the experimental showed reductions in compressive strength of 27% and 23%for the larger carbon and glass specimens compared with the smaller ones.

Reeder [1995] investigated compressive strength of carbon fibre/epoxy with different gauge length. The thickness of laminates was 6.35 and 2.54 mm, with width as 25.4 mm and gauge

lengths varying from 4.8 to 254 mm. Short specimens failed prior to buckling and the corresponding strength increased with decrease in gage length.

Daniel and Hsiao [1999] tested three different sized specimens from 16 to 200 plies thick. The material used in their study was IM6G/3501-6 carbon epoxy composite of unidirectional and cross ply laminate. The longitudinal compressive strength showed a mild trend of decreasing values with increasing thickness.

Based on the documented research on size effect of composites it can be stated that mainly three types of tests viz. tensile test, flexural test and compressive tests were performed on composite coupons. Most of the researcher tried to correlate the results with weibull's theory. Wide ranges of specimens covering different laminate stacking sequences and different scaled sizes were tested. The important observations like decrease in strain and strength with increase in specimen size or thickness was observed supporting the existence of size effect in composites in most of the cases studied.

1.7.6 Size Effect of Concrete Structural Element

The experimental research on size effect of concrete structural elements may be traced long back in 1925. Gonnerman [Sabnis and Mirza, 1979] conducted the earliest study on size effect in concrete cylinder for investigating compressive strength with height/diameter ratio of 2. He varied the diameter of cylinder from 100 to 250 mm and examined the influence of age, cement aggregate ratio, relative consistency and aggregate fineness on compressive strength. One of the sample results is shown in Fig. 1.11**.** The figure shows that the compressive strength decreases with increase in diameter of the test-specimen, supporting the size effect. Mirza *et al.* [1972] tested more than 500 cylinders ranging from 25×50 mm to 150×300 mm at ages of 3, 7 and 14 days. It was shown that for various concrete mixes, 75 and 100 mm diameter cylinders exhibited strength increase of approximately 5 to 15% and

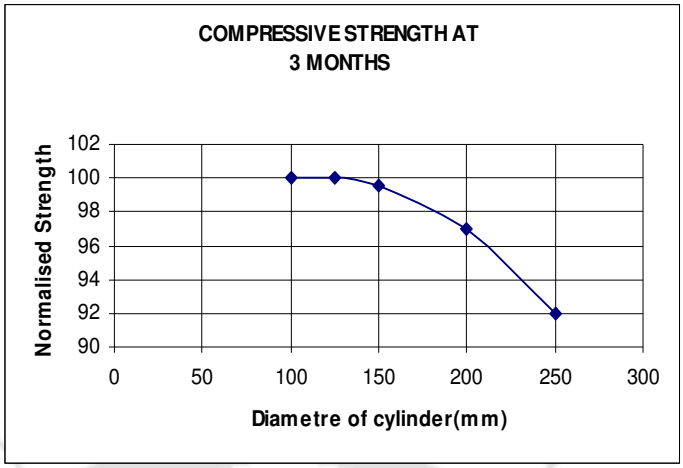

Fig. 1.11 A typical sample result of Gonnerman's test (1925)

for 50 mm diameter cylinders, strength increased up to 40% over the strength of 150 mm diameter cylinders.

In the last couple of decades, there have been numerous researches on size effect of specimens made of concrete. Bazˇant proposed the size effect law [1984] in line with the idea as proposed by Walsh [1972]. Walsh was apparently the first person to plot the test result as "$\log\sigma_{N_U}$ versus log D". However, he did not try to describe this plot mathematically or generalise it. Walsh's classical test was of limited range and included only one type of fracture specimen, which were not conclusive.

A stronger experimental verification was reported by Bazˇant and Pfeiffer [1986, 1987], which covers a broader size range and four different types of specimens. This research included test on mortar and test on concrete specimens. The results were plotted and found to satisfy the size effect law proposed by Bazˇant.

The result of the test performed by Jeng and Shah [1985] also support the size effect law proposed by Bazˇant, although a good fitting of the test data was not possible as the size range was very limited compared to the scatter obtained.

Sener *et al.* [1999] tested two groups of RC beams with splices located either in the mid span region with a uniform bending moment, or in one of the end regions with a uniform shear force. Beams of three different depths were considered, which were geometrically similar in all the three dimensions. The reinforcing bar diameters and cover thicknesses were also scaled in the same proportion. The results revealed the existence of a significant size effect, which was approximately described by the size effect law proposed by Bazˇant.

Sener *et al.* [2002] tested notched beams with and without steel fibres. Three different depths of beam were chosen and four point bending test were conducted. Nominal strength in all the cases were plotted in bi-logarithmic plot and the results followed Bazˇant's size effect law.

Rios and Riera [2004] proved the existence of size effect in geometrically similar reinforced concrete beams by Discrete Element Method (DME). The numerically simulated results were also validated using the experimentally observed data on similar specimen as obtained by earlier researchers.

Elfahal *et al.* [2004] reported size effect for concrete subjected to axial impact (cylindrical specimen). The experimentally observed results were further verified using the finite element software ABAQUS. The experimental as well as numerical results showed the existence of size effect.

Sener *et al.* [2004] tested a large number of geometrically similar columns with three different slenderness ratios. The failure strength σ_{N_U} was calculated from the failure load P found experimentally. Linear regression analysis was carried out to find characteristic depth D_0 and dimensionless parameter B. Finally, bi-logarithmic plotting of $\log(D/D_0)$ versus $\log(\sigma_{N_U}/Bf_t')$ was done and was found in agreement with Bazˇant's size effect law.

Bindiganavile and Banthia [2006] studied size effect of plain concrete beam under impact loading. Plain concrete of three different sizes were tested under three point impact load. The result of the impact test from their study as well as those from some of the previous studies

were fitted to Bazant's size effect law. Similarly, same data were plotted according to Multifractal scaling law. The plot of compressive strength followed both Bazant's size effect law and Multifractal scaling law.

Leung *et al.* [2007] conducted test on CFRP retrofitted beam (strengthened in shear) of three different sizes. A number of specimens with different retrofitting strategies were tested. It was observed that the retrofitted specimens with complete FRP wrapping did not show any size effect, whereas FRP-U stripped retrofitted specimen showed size effect in term of gain in strength. The result showed that the failure in the strengthened specimen with U configuration was due to debonding of FRP strips, while in the other strengthened case it was due to rupture of strips. The authors concluded that for the debonding failure, the bond capacity was directly proportional to the square root of the thickness and hence, with increase in thickness of FRP strips, the shear capacity was at a slower rate. In the second case of failure by debonding, the failure strength was directly proportional to thickness and hence with increase in size, there was increase in strength in same proportion leading to no size effect.

Coc and Sener [2009] tested geometrically similar columns of different sizes with different types of notches for both normal and high strength concrete to study the size effect. Three different slenderness ratios were covered in their study. Some specimens were having very shallow wide notch, some with deep and some with narrow notches. Axial loads were applied to the specimens till failure. Maximum ultimate stress was calculated and bi-logarithmic plot was drawn. The bi-logarithmic plots in all the cases followed Bazant's size effect law. The authors concluded that out of all three different types of notches, the specimens made with surface-notch showed more pronounced size effect than all other types of notches.

Summery of the literature on size effect of concrete structural elements made of concrete reveals that experimental research was initiated way back in 1925. Subsequently, lot of researches were done to correlate cylindrical and cube strength of concrete with size of the

tested specimens. However, recent researchers correlated the results of nominal strength found by testing specimens with the size effect law proposed by Bazˇant in most of the cases. In many cases, three sizes of geometrically similar specimens were considered for studying size effect in reinforced concrete elements. The reinforcing bar diameters and cover thicknesses were also scaled in the same proportion. Linear regression analysis using Bazˇant's size effect law was carried out for bi-logarithmic plotting. Size effect study was covered for reinforced structures under impact loading.

Further, the literature survey indicates that there were scanty research on size effect of retrofitted RC structures. Leung *et al*. [2007] conducted test on RC beams by retrofitting with CFRP. The enhancement in result was correlated with percentage gain only, without correlating to bi-logarithmic plot or any other well established law. More over, the test conducted was under monotonic loading only. Further, limited numerical study was done to investigate the existence of size effect, which was limited to RC beam only.

1.8 SCOPE AND OBJECTIVE OF THE PRESENT STUDY

Literature survey showed that although extensive experimental investigations were carried out to understand the behaviour of beam-column joints, yet no record could be found covering various deficiencies like beam-column joint with beam weak in flexure, beam weak in shear and column weak in shear altogether. Thus, a holistic approach was initiated to cover different deficient cases of beam-column joints so as to gather a comprehensive knowledge about the behaviour of these joints. These deficient beam-column joints were retrofitted with both GFRP and CFRP as per the requirements and a comparative study of enhancement in strength, displacement ductility, energy dissipation etc. due to strengthening was carried out to understand effectiveness of retrofitting in all the cases of deficient joints considered in the present study. Further, literature survey showed that the experimental study of size effect was primarily done for RC beams and columns. However, beam-column joint, which is a vital

structural element and plays a very crucial role during earthquake, did not somehow get any attention in the study of size effect. Thus, it was felt necessary to carry out studies on size effect of RC beam-column joint with and without retrofitting.

Further, it was observed from literature survey that large numbers of studies on size effect in pure composite materials were carried out in term of tension test, compression test and bending test. However, very limited research work was carried out in size effect of retrofitted RC structures using composites. The study carried by Leung *et al.* [2007] for beam under monotonic loading was observed to be the only reported work in the literature. However, the behaviour of beam-column joints subjected to cyclic loading have been studied in this experimental programme to assess the performance of the joint region during earthquakes. It may be noted that energy is dissipated by the hysteretic behaviour of the joint during the occurrence of an earthquake. Hence, energy dissipating capacity of a joint could be observed as very important property. Energy dissipating capacity of a joint was calculated in many experiments conducted by earlier researcher, but the size effect aspect of energy dissipation was not covered till date. Hence, the present study tried to correlate size of the joint specimen under test with the energy dissipation capacity of the joint. Similarly, among the limited number of numerical studies on beam-column joint carried out so far, no literature could be traced covering size effect of RC beam-column joints with and without retrofitting. Hence, numerical study was also undertaken in the present study considering different sizes using ANSYS 6.0. RC beam-column joints as well as retrofitted specimens were simulated, analysed and the findings were used for designing the experimental programme. To sum up, research was initiated with the following objectives:

- To carry out experimental study on size effect of various types of deficient RC external beam-column joint with and without retrofitting subjected to cyclic loading.

- To develop the experimental set-up needed for the testing of specimens of different sizes.
- To carry out tests for material characterization as per relevant codes.
- To carry out numerical study on RC beam-column joint with and without retrofitting for evaluation of yield displacement, ultimate load carrying capacity etc.
- To interpret the experimental findings for exploring the existence of size effect in term of various parameters like stress, stiffness, ductility, energy dissipation etc. for RC beam-column joint with and without retrofitting.
- To study the change in various properties of specimens due to retrofitting and to explore possibility of correlating these changes with size of the tested specimens.

1.9 ORGANIZATION OF THE THESIS

The thesis has been divided into eight chapters. Chapter 1 presents introduction, literature review, scope and objective of the present study**.** Chapter 2 covers material characterisation of various materials like coarse aggregates, fine aggregates, reinforcing steel and fibre reinforced polymer (FRP) used in the experiment. Chapter 3 provides a detailed description of the experimental procedure including selection of specimens, design and casting of specimens, retrofitting procedure etc. In Chapter 4, numerical analysis of all types of specimens, covering both RC and retrofitted RC beam-column joints using ANSYS 6.0 is presented. The numerical results have been used for designing the experimental programme. In Chapter 5, experimental study on beam-column joints with beam-weak in flexure RC specimens and corresponding retrofitted specimens have been covered. All the observations during testing and interpretation of results in terms of strength, ductility, stiffness degradation etc have been detailed. Effect of retrofitting in the performance of the joint has been also presented along the size effect of beam-column joint with and without retrofitting. In Chapter

6, experimental study on beam-column joints with beam-weak in shear RC specimens and corresponding retrofitted specimens have been covered with various observations during testing and interpretation of results etc. Similarly, Chapter 7 includes experimental study, observation and interpretation of result for RC beam column joints with column weak in shear as well as retrofitted beam-column joint. Chapter 8 presents the summary and general conclusion based on the entire experimental program and scope for future work.

1.10 CONCLUDING REMARKS

In general, the study of size effect goes back to 15th century with Leonardo da Vinci, the founder of this field. However, research efforts on size effect in civil engineering have been started in recent past and hence very limited research findings have been observed on size effect of RC and retrofitted RC structures. An extensive literature review has been presented in this chapter covering entire domain of experimental studies on RC beam-column joint including size effect of RC beam-column joint without and with retrofitting. For convenience, literatures have been grouped into six main divisions- (i) Studies on RC beam-column joint (ii) Strengthening RC structures with concrete jacketing, steel jacketing and epoxy repairing (iii) Strengthening of RC beam and column with FRP (iv) Strengthening of RC beam-column joint with FRP (v) Size effect of composite coupons (vi) Size effect of concrete structural elements. Based on detailed studies of literature and identifying various shortfall and inadequacies of earlier studies, finally the scope and objectives of the present study have been enumerated.

CHAPTER 2

CHARACTERIZATION OF MATERIALS

2.1 INTRODUCTION

This chapter discusses about the characterization of various materials used for construction and retrofitting of the beam-column joint specimens. The precision of the experimental work depends to a large extent on proper design of concrete mix as well as quality of casting of the specimens. The mix design was done as per provisions of relevant Indian standard codes. All the constituent materials such as cement, fine aggregates and coarse aggregates were tested prior to the design of concrete mix. To cover all the cases of beam-column joint specimens, six different design mixes were considered. The properties of reinforcing steel bars were also found out by performing tensile test in the Universal Testing Machine (UTM). Further, Carbon fiber reinforced polymer (CFRP) and glass fiber reinforced polymer (GFRP) composite were used for retrofitting of specimens. In order to evaluate the tensile strengths of CFRP and GFRP, composites coupons were made and tested following ASTM standard using UTM.

2.2 MIX DESIGN

Beam-column joint specimens were cast using design mix concrete. In order to arrive at the desired target strength, trial mix designs were carried out as per IS: 10262-1982. Ordinary Portland cement of 53 grade was used. Two grades of concretes with target strength 30 N/mm^2 and 25 N/mm^2 were used. The former was used for beam-column joint specimens with beam weak in flexure and for beam-column joint specimens with beam weak in shear, while the later was used for beam-column joint specimens with column weak in shear. The largest size of coarse aggregates used for the full size specimens was 24 mm down. The largest size of coarse aggregates used for 2/3 rd scaled specimens were

16 mm and that for the 1/3 rd scaled were 8 mm. All the aggregates used were angular and well graded. The variation in size of coarse aggregates led to slight variation in the mix proportion of the design mix for a specified target strength of concrete. Thus, three numbers of mix designs were done for target strength of 30 N/mm^2 and three more mix designs were done for target strength of 25 N/mm^2. The sand used for making concrete was conforming to zone-II as per IS: 383-2002. The details of material properties used in the mix designs are described in the next subsections.

2.2.1 Tests on Cement

OPC 53 grade cement was used for casting the specimens. The cement was tested for its standard consistency, initial setting time, specific gravity and compressive strength following relevant Bureau of Indian Standard (IS) codes. The details of test results are presented in Table 2.1. Further, compressive strength of the cement was determined as per provisions of IS: 4031(6)-1988. The average compressive strength of cement was determined. The values of compressive strength found from compression test and the standard value as per IS: 12269-1987 are shown in Table 2.2. Thus, it is evident that the cement used satisfied the compressive strength criteria of 53 grade cement.

Table 2.1 Results of tests on cement

Sl. No.	Name of test	Details of relevant code	Test result
1	Standard Consistency	IS: 4031(4)-1988.	28%
2	Initial Setting Time	IS: 4031 (5)-1988	1 hr 20 minutes
3	Final setting time	IS 4031: (5)-1988	5 hr 25 minutes
4	Specific gravity (ρ)	IS: 4031(11)-1988	3.12

Table 2.2 Compressive strength of cement

No of days	Compressive strength (MPa)	
	According to IS 12269:1987	Test results
3	27	27.31
7	37	37.36
28	53	54.3

2.2.2 Tests on Fine Aggregate

The fine aggregate (sand) was procured from a locally available source. The specific gravity of the sand was found to be 2.51 as per the provisions of IS: 2386(III)-1963. Further, the sieve analysis of sand was carried out as per IS: 2386(1)-1963. The percentage weight retained in the sieves is shown in Table 2.3. Finally, the zone to which sand sample belong was ascertained.

2.2.3 Tests on Coarse Aggregate

Three nominal sizes of well graded coarse aggregate used were 24 mm down, 16 mm down and 8 mm down for large, medium and small beam-column joint specimens respectively. The specific gravity of aggregate was found to be 2.62 as per the provisions of IS: 2386(III)-1963. The sieve analysis of aggregates was carried out as per IS: 2386(1)-1963. The result of typical sieve analysis is shown in Table 2.4 (24 mm down aggregate). The fineness modulus of aggregate was found to be 8.06.

2.2.4 Concrete Mix Design

Three numbers of concrete mix were designed for three different nominal sizes of coarse aggregates corresponding to each target strength. Thus, total six numbers of concrete mixes, with two target strengths, were considered in this study. Details of six concrete mixes designed in this study are furnished in Table 2.5

Table 2.3 Result of sieve analysis of sand

Sl.No	Sieve size	Weight retained (gm)	% Weight. retained	Cumulative % weight retained	% fine	Remark about Zone
1	4.75 mm	0	0	0	100	
2	2.36 mm	31	3.1	3.1	96.9	
3	1.18 mm	52	5.2	8.3	91.7	
4	600 μ	388	38.8	47.1	52.1	Falls in
5	300 μ	348	34.8	81.9	18.1	**Zone II**
6	150 μ	137	13.7	95.6	4.4	
7	75 μ	34	3.4	99	1	
8	Pan	10	1.0	100	0	

Table 2.4 Sieve analysis of coarse aggregate

Sl.No	Sieve size	Wt. retained (gm)	% Retained	Cumulative % retained	% Fine
1	20 mm	1401	23..35	23.35	76.65
2	10 mm	3785	63.08	86.43	13.57
3	4.75mm	730	12.17	98.6	1.4
4	2.36 mm	56	0.93	99.53	0.47
5	1.18 mm	10	0.16	99.69	0.31
6	600 μ	2	0.03	99.72	0.28
7	300 μ	2	0.03	99.75	0.25
8	150 μ	3	0.05	99.8	0.2
9	<150 μ	10	0.16	99.96	0

Table 2.5 Details of concrete mixes

Sl. No.	Target strength (N/mm^2)	Nominal size of coarse aggregates	Mix ratio	w/c	Average compressive strength (N/mm^2)
1.	30	24 mm down	1:1.85:3.82	0.59	32.0
2.	30	16 mm down	1:1.84:3.18	0.59	32.2
3.	30	8 mm down	1:1.82:2.77	0.59	31.6
4.	25	24 mm down	1:2.3:4.75	0.65	26.4
5.	25	16 mm down	1:2.26:4.0	0.65	26.7
6.	25	8 mm down	1:2.25:3.41	0.65	26.0

2.3 TESTS ON STEEL REBAR

Fe 500 steel was used predominantly as longitudinal and transverse reinforcements. However, Fe 250 steel was also used in limited number of cases. Sample rebars were tested in the UTM as per provisions of IS: 432(I)-1982 and IS: 1608-1995. The material properties of rebars as obtained from tests carried out in this study are presented in Table 2.6. Further, a typical stress-strain plot for a sample rebar is given in Fig. 2.1.

Table 2.6 Material properties of steel rebars

Sl. No	Diameter of the rebar (mm)	Yield stress (MPa)	Ultimate stress (MPa)	Young's modulus (MPa)	Elongation (%)
1	20	560	640	2×10^5	19.78
2	12	530	620	2×10^5	16.44
3	8	510	632	2×10^5	16.89
4	6	295	483	2×10^5	28.67
5	4	285	450	2×10^5	26.67
6	2	295	471	2×10^5	26.7

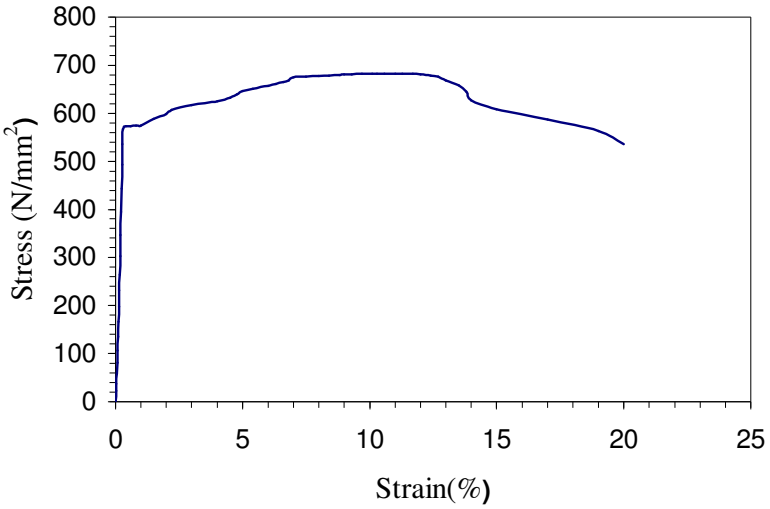

Fig 2.1 Sample stress-strain curve of 20 mm diameter Fe500 grade rebar

2.4 TESTS ON COMPOSITES

The retrofitting materials used for strengthening were procured from Fosroc Chemicals (India) Pvt. Ltd. Nitowrap 30 (base and hardener) was used as primer coat. Nitowrap 410 (base and hardener) was used as saturant i.e. resin. Woven sheets of GFRP and CFRP were used in this study. Most of the properties were adopted from the data sheet supplied by the manufacturer. The important properties of the components of adhesive materials and the FRP used are furnished in Table 2.7 and Table 2.8 respectively. Further, the most essential properties needed for the analysis of results are tensile strength and modulus of elasticity of CFRP and GFRP laminates. Therefore, tests were conducted on test coupons made as per the guide line of the standard ASTM: D 3039. Five coupons were made as per the standard recommendation for both GFRP and CFRP as shown in Fig. 2.2. Each coupon was made up of seven layers of FRP. The coupons were tested under UTM (Make: INSTRON) after seven days of maturity and the ultimate strength of specimens were found. Test arrangement of typical FRP coupon is shown in Fig. 2.3. The stress-strain plot for CFRP and GFRP coupons are shown in Fig. 2.4 and 2.5 respectively. The slopes of these graphs were reported as the values of modulus of elasticity. The

ultimate tensile strength for CFRP was found to be 630 N/mm^2 while the same for GFRP was found 315 N/mm^2. Modulus of Elasticity of CFRP and GFRP were found as 4.63×10^4 N/mm^2 and 1.167×10^4 N/mm^2 respectively.

Table 2.7 Properties of components of adhesive

Components of adhesive	Density (g/cc)	Pot life	Curing period	Flash point (°C)
Nitowrap 30	1.14	25 min. @ 27°C	7 days	25
Nitowrap 410	1.25-1.26	2 hours at 30°C	5 days at 30°C	33

Table 2.8 Properties of FRP

Name of FRP	Fibre orientation	Weight of fibre (g/m^2)	Density of fibre (g/cc)	Fibre thickness (mm)
CFRP	Unidirectional	200	1.80	0.3
GFRP	±45°	920	2.6	0.36

Fig. 2.2 Test coupons for CFRP and GFRP

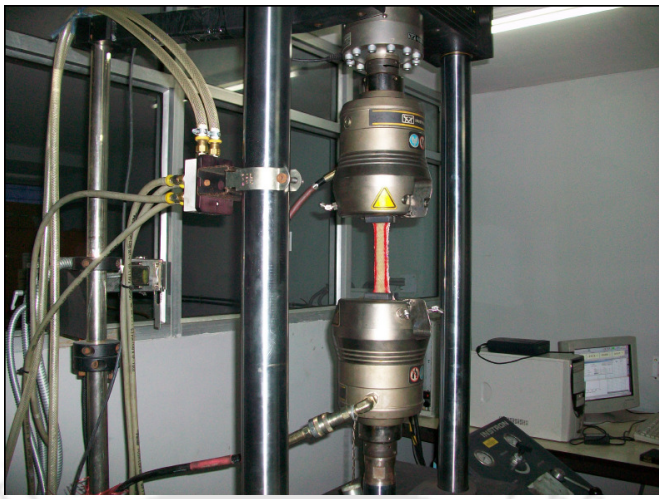

Fig. 2.3 Test arrangement of typical FRP coupon

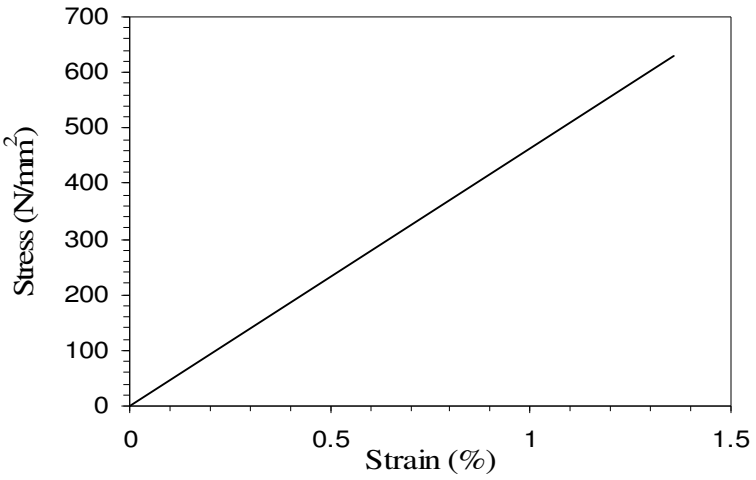

Fig. 2.4 Stress-strain plot for CFRP coupon

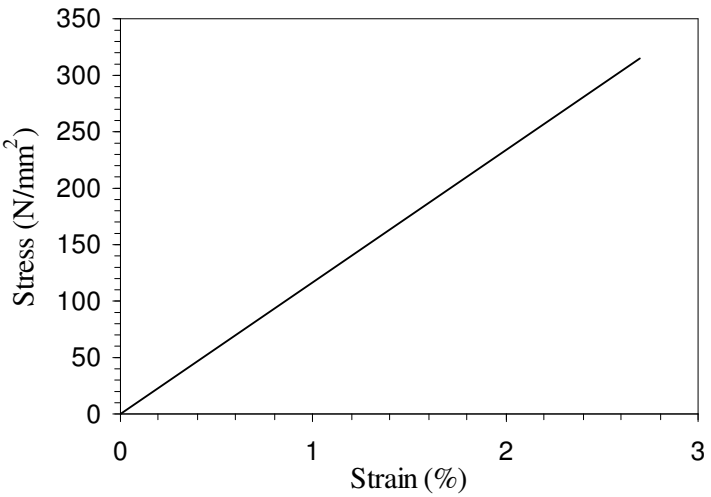

Fig. 2.5 Stress-strain plot for GFRP coupon

2.5 CONCLUDING REMARKS

In this chapter, a detailed description about the testing of all materials needed for casting and retrofitting of beam-column joint specimens have been presented. Six numbers of mix designs were carried out before casting of the RC beam-column joint specimens. Further, tests were carried out to find out the ultimate strength of retrofitting materials. An elaborate description of the beam-column joint specimens along with their casting and retrofitting process is furnished in the next chapter. Discussion about the details of test set up and instrumentation adopted is also presented in the same chapter.

CHAPTER 3

DESCRIPTION OF TEST SPECIMENS AND INSTUMENTATION

3.1 INTRODUCTION

The first experimental study on beam-column joint was conducted in United States by Hanson and Connor [1967], which served as the standard reference for subsequent investigations. Though the research on beam-column joint was in progress, yet after EI Asnam earthquake and some other devastating earthquakes, the importance of adequate performance of beam-column joint was realized globally in a better way. Lots of research work was undertaken on both RC beam-column joint and retrofitted RC beam-column joint in the past two to three decades. In the present research, tests were conducted for three typical possible deficiencies and covering three different sizes of beam-column joints. Geometrically similar scaled specimens of RC beam-column joints with different deficiencies were treated as control specimens. Same numbers of specimens as those of control specimens were also appropriately retrofitted using FRP (both CFRP and GFRP) for enhanced load carrying capacity, energy dissipation, stiffness, ductility etc. During testing of the specimens, beam was placed along vertical direction and column was placed in horizontal direction for the ease of placing and handling the specimen in the test frame. A constant axial load was applied on the column to represent gravity load during application of cyclic displacement on the beam. The axial load applied was 10% of gross capacity of the respective column. This chapter provides a detailed description of the specimens. Retrofitting process has also been described in detail. Further, description of test set-up along with details of instrumentation has also been furnished.

3.2 SELECTION OF THE FULL SCALE SPECIMEN

The deflected shape of a frame under the action of lateral loading is shown in Fig.1 (a), where the points of contraflexure lie at the mid-points of beams and columns. Further, the free body diagram of an external beam-column sub-structure assembly is shown in Fig.1 (b). It comprises of half of a column at top and bottom as well as half of a beam. It may be noted that the symmetric boundary condition should be maintained at both the ends of column for isolation of a single unit of beam-column joint. In this study, a typical full scale residential building with floor to floor height as 3.3 metres and the beam of 3.0 metres effective span was considered. The present study was concentrated on a sub-structure consisting of an external beam-column joint as shown in Fig. 1(b).

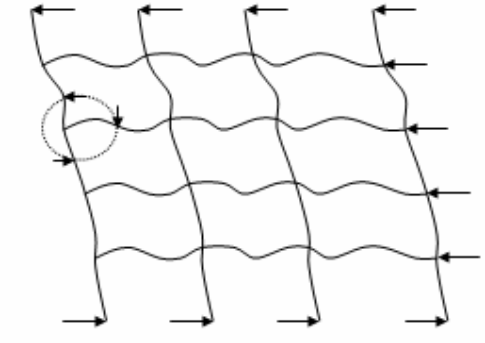

Fig.1 (a) Deflected shape of a frame under lateral loading [Paulay, 1989]

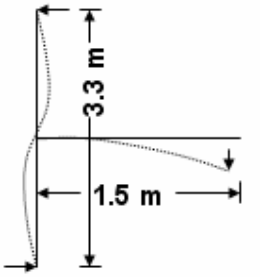

Fig.1 (b) Isolated exterior beam-column joint

3.3 DESCRIPTION OF THE SPECIMEN

In the present study, six types of specimens, namely, (a) Beam-column joint with beam weak in flexure : control, (b) Beam-column joint with beam weak in shear : control, (c) Beam-column joint with column weak in shear : control, (d) Beam-column joint with beam weak in flexure : retrofitted, (e) Beam-column joint with beam weak in shear : retrofitted and (f) Beam-column joint with column weak in shear : retrofitted, were considered. In each type, three geometrically similar specimens : full scaled, two third scaled and one third scaled sizes were considered. The naming of the specimens was done

with five alphabets, the first three alphabets cover the deficiency type, the fourth for size and the fifth for type of specimens, which can be either control or retrofitted. For example, BWFLC stands for *beam weak in flexure large control* specimen, similarly BWSMR stands for *beam weak in shear medium retrofitted* and CWSSC stands for *column weak in shear small control* specimens.

3.3.1 Beam Weak in Flexure : Control Specimen

The detailing of all the bam weak in flexure : control specimens has been shown in Fig. 3.2. The cross section of the column was chosen as 300 mm × 300 mm and that of the beam as 300 mm × 360 mm for the full scaled model. Four numbers of high strength deformed bars (Yield strength 500 : MPa) of 20 mm diameter was used as reinforcement in column and beam. Lateral ties of 12 mm diameter high strength deformed bar at 75 mm c/c spacing was used in the special confinement zone of the column as per guidelines proposed by IITK-GSDMA document [2006]. In the remaining part of the column, lateral ties of 6 mm diameter mild steel bars were used with a spacing of 150 mm c/c. In the beam, shear reinforcement of 8 mm diameter high strength deformed bar with a spacing of 75 mm c/c was used near the beam column joint for a length of 675 mm and 6 mm diameter with a spacing of 120 mm c/c was provided for the remaining part of the beam. The beam was designed as under reinforced beam following the provisions of IS: 456 [2000], IS: 1893 [1993] and IITK-GSDMA guidelines for design and detailing of buildings [2006]. The strong column-weak beam principle was adopted for the design of the beam-column joint. Moreover, the beam was idealised as a cantilever beam for arriving at the tip failure load of beam. The details design is furnished in Appendix-B. Adequate shear reinforcement was provided to avoid shear failure. Two third and one third scaled specimens were proportionately scaled down in all the three dimensions. The diameter of the reinforcing bars, development length, length of special confinement zone, cover of reinforcement etc. were also scaled down appropriately. These specimens were

cast with concrete of target cube strength of 30 N/mm^2. The detailed descriptions of all the specimens are given in Table 3.1. In the same table, the detailed about column weak in shear specimens are also given, which will be described in subsequent section.

3.3.2 Beam Weak in Shear : Control Specimen

The specimens under this category are exactly similar in all respect to that of beam weak in flexure : control specimens, except the shear reinforcement in beams. Amount of shear reinforcements were reduced to make the beam weak in shear. In BWSLC, 2-legged 6 mm diameter mild steel bars with a spacing of 600 mm c/c were provided as shear reinforcement. However, only the first two stirrups near the joint was placed with spacing of 600 mm c/c in order to maintain a pre-defined failure location and for the remaining part of the beam the spacing was reduced to 240 mm c/c. Shear reinforcement was proportionately reduced for scaled down models maintaining geometric similarity. The dimensions and reinforcement details of all the three specimens are shown in Fig. 3.3.

3.3.3 Column Weak in Shear : Control Specimen

The specimens under this category were cast by comparatively weaker grade of concrete than those used in earlier cases in order to make the column weak in shear. Concrete of target strength of 25 N/mm^2 was used for casting. The detailed description of all the specimens are given in Table 3.1. The detailed drawings for these specimens are shown in Fig.3.4. The cross section of the column was reduced than earlier cases while the cross section of beam was increased to make the beam-column joint as a strong beam-weak column joint. The supporting calculation have been furnished in Appendix-B. The main reinforcements in column were maintained similar to those of earlier cases, while same was increased in beam. Spacing for the lateral ties in the columns were increased to ensure the shear weakness of these specimens in column. In CWSLC, 2-legged 6 mm diameter mild steel bars with a spacing of 900 mm c/c were provided as lateral ties.

Table 3.1 Description of beam weak in flexure control specimen

Component of Beam-column joint	Beam				Column			
Designed Parameters	Effective Span (mm)	Section (mm×mm)	Longitudinal Reinforcement	% Tensile Reinforcement	Length (mm)	Section (mm×mm)	Longitudinal Reinforcement	% Reinforcement
BWFLC	1500	300×360	2-20ϕ-top 2-20ϕ-bottom	0.58%	3300	300×300	4-20ϕ-total	1.396%
BWFMC	1000	200×240	2-12ϕ+1-8ϕ-top 2-12ϕ+1-8ϕ-bottom	0.578%	2200	200×200	4-12ϕ+2-8ϕ-total	1.382%
BWFSC	500	100×120	1-8ϕ+2-6ϕ-top 1-8ϕ+2-6ϕ-bottom	0.65% (equivalent)	1100	100×100	2-8ϕ+4-6ϕ-total	1.57% (equivalent)
CWSLC	1500	240×450	3-20ϕ-top 3-20ϕ-bottom	0.873%	3300	240×300	4-20ϕ-total	1.745%
CWSMC	1000	160×300	3-12ϕ+1-8ϕ-top 3-12ϕ+1-8ϕ-bottom	0.812%	2200	160×200	4-12ϕ+2-8ϕ-total	1.723%
CWSSC	500	80×150	2-8ϕ-top 2-8ϕ-bottom	0.837% (equivalent)	1100	80×100	2-8ϕ+4-6ϕ-total	1.963% (equivalent)

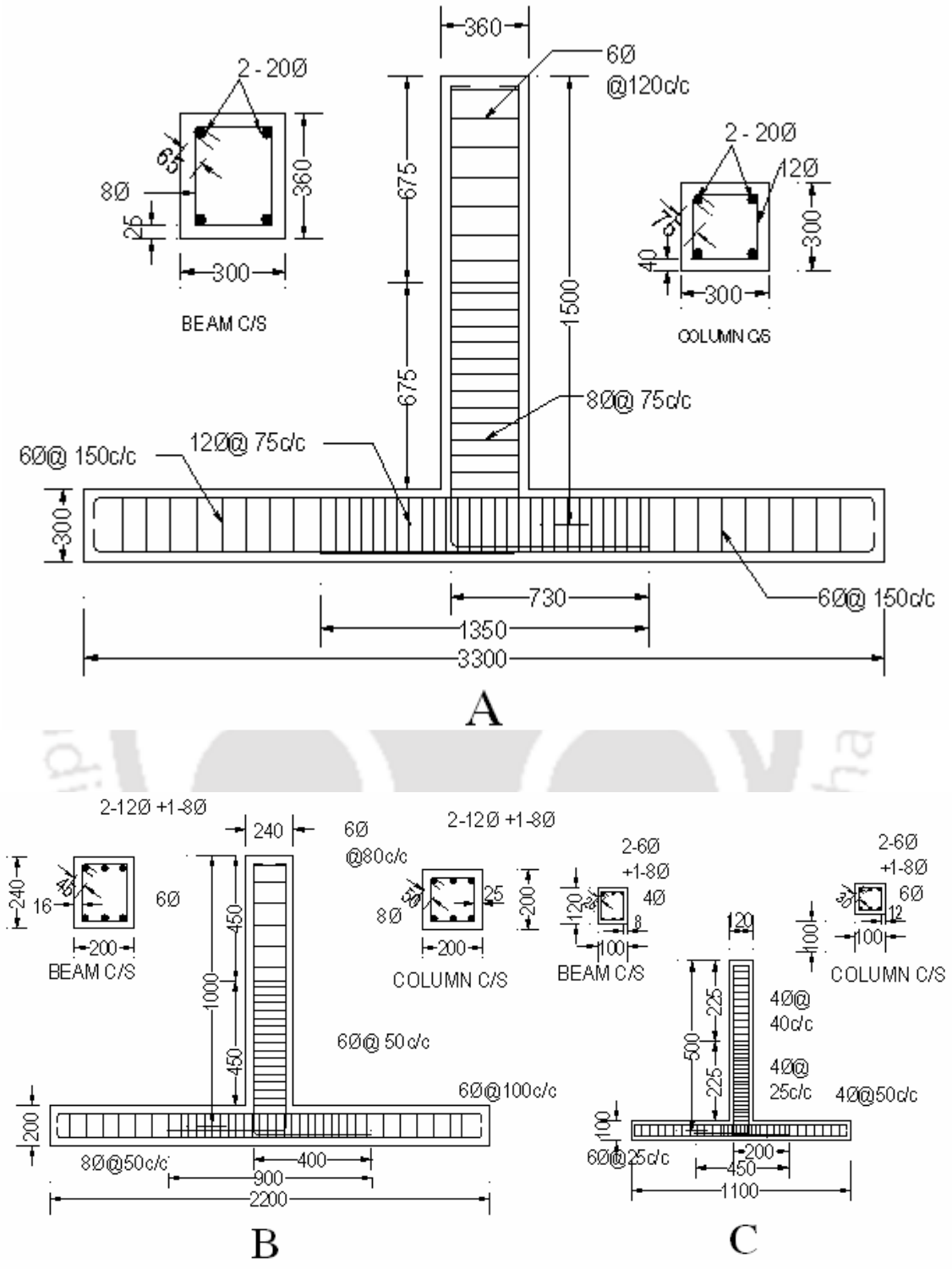

A-BWFLC; B-BWFMC; C-BWFSC

Fig. 3.2 Detailing of beam weak in flexure : control specimens

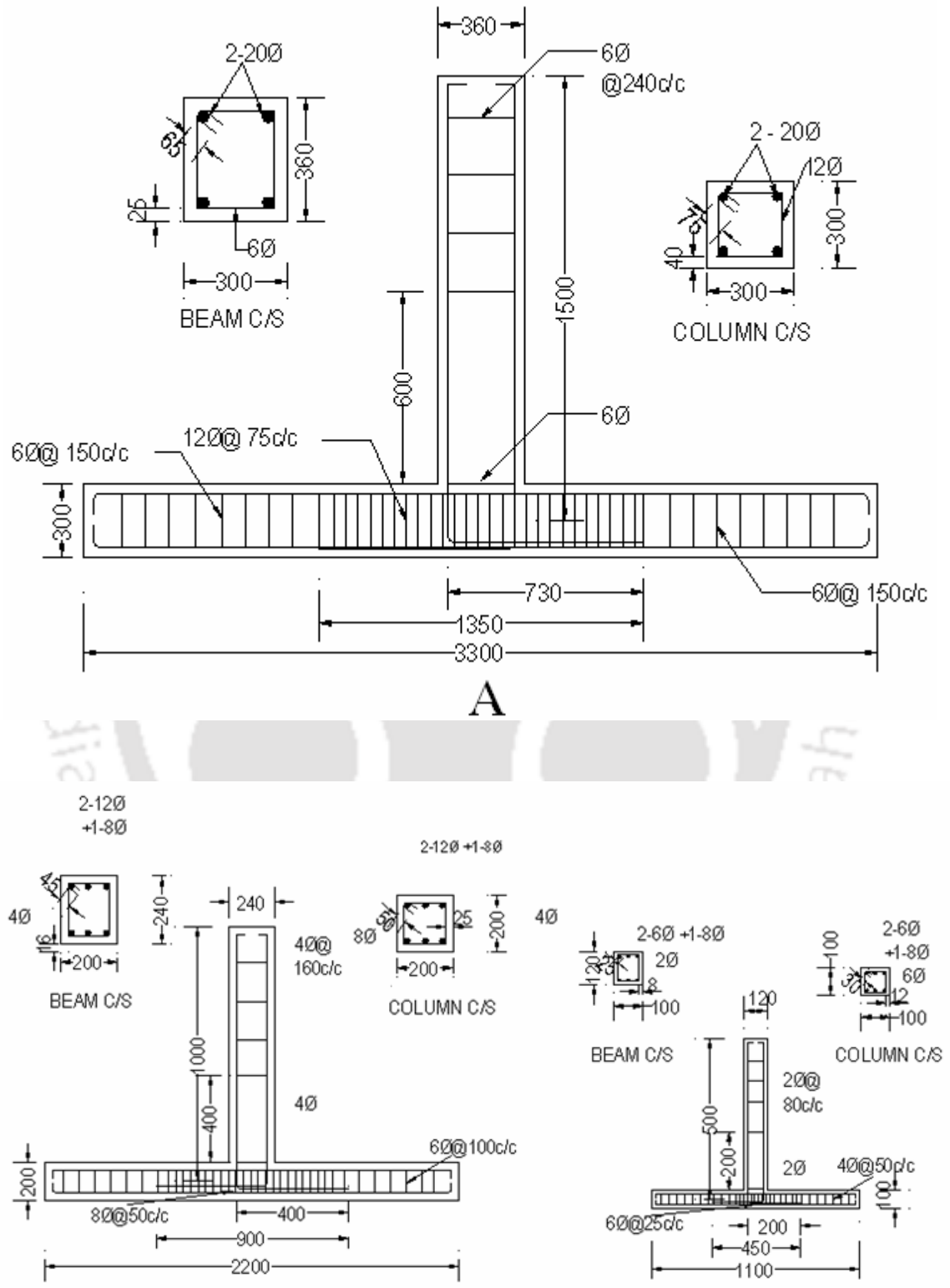

A- BWSLC; B-BWSMC; C-BWSSC

Fig. 3.3 Detailing of beam weak in shear : control specimens

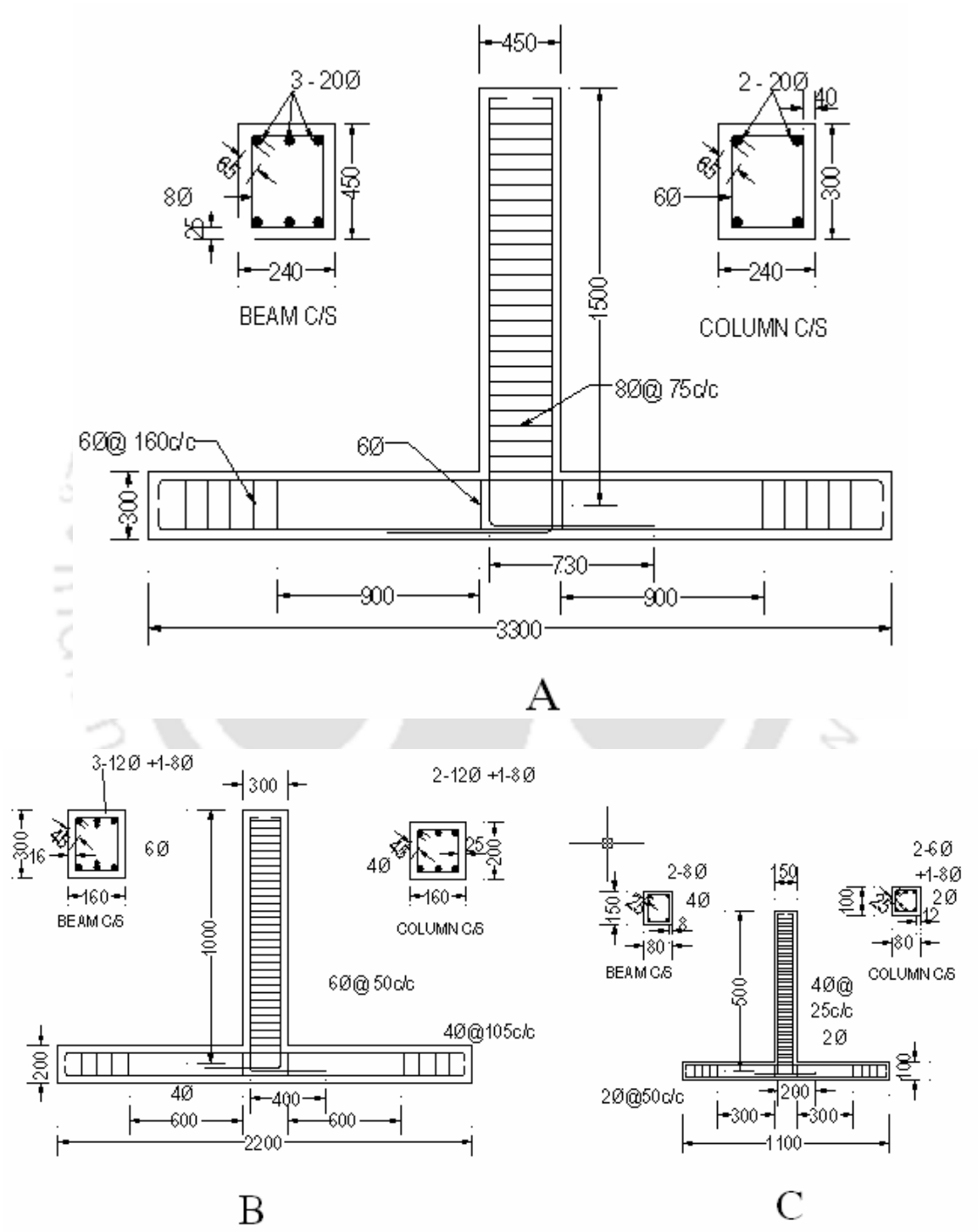

A- CWSLC; B-CWSMC; C-CWSSC

Fig. 3.4 Detailing of column weak in shear : control specimens

maintain a pre-defined failure location and the spacing was decreased for the remaining part of the column. For the full model, the cross section of the column was chosen as 240 mm × 300 mm and that of the beam as 300 mm × 450 mm. Four numbers of high strength deformed bars (Yield strength : 500 MPa) of 20 mm diameter in column and six numbers of 20 mm diameter in beam were used as reinforcement. In the beam, shear reinforcement of 8 mm diameter bars with spacing of 75 mm c/c were used over the entire span. Two third and one third scaled specimens were proportionately reduced in all the three dimensions. The diameters of the reinforcing bars were also scaled down.

3.3.4 Beam Weak in Flexure : Retrofitted Specimen

The retrofitting was carried out primarily to enhance the flexural capacity of the beam using carbon fibre reinforced polymer (CFRP). However, the increase in load carrying capacity led to the increase in shear force at any section of the beam. Thus, in order to ensure eventual flexural failure of the beam, shear retrofitting of the beam was also done using glass fibre reinforced polymer (GFRP). The joint was adequately strengthened with GFRP. It is desirable that the failure should not occur in the beam-column joint and the eventual failure should be by flexural failure of beam. This type of failure would ensure higher energy dissipation. Accordingly, the retrofitting of all the deficient members were carried out. The tailoring details for retrofitting of beam weak in flexure : retrofitted specimens are shown in Fig. 3.5. One layer of CFRP of width 300 mm was fixed over beam covering 900 mm length (marked as type A) for the specimen BWFLR. Strip of one layer of GFRP having width of 90 mm was wrapped completely around the beam with a spacing 405 mm c/c up to a length of 900 mm (marked as type B). The joint was strengthened with one layer of GFRP (marked as type C). Main objective of the present study is to explore the existence of size effect and hence geometrical similarity was strictly maintained for two scaled models during retrofitting. One layer of FRP was used in the retrofitting of the specimens of all types. Hence, the ratio of area of FRP needed for

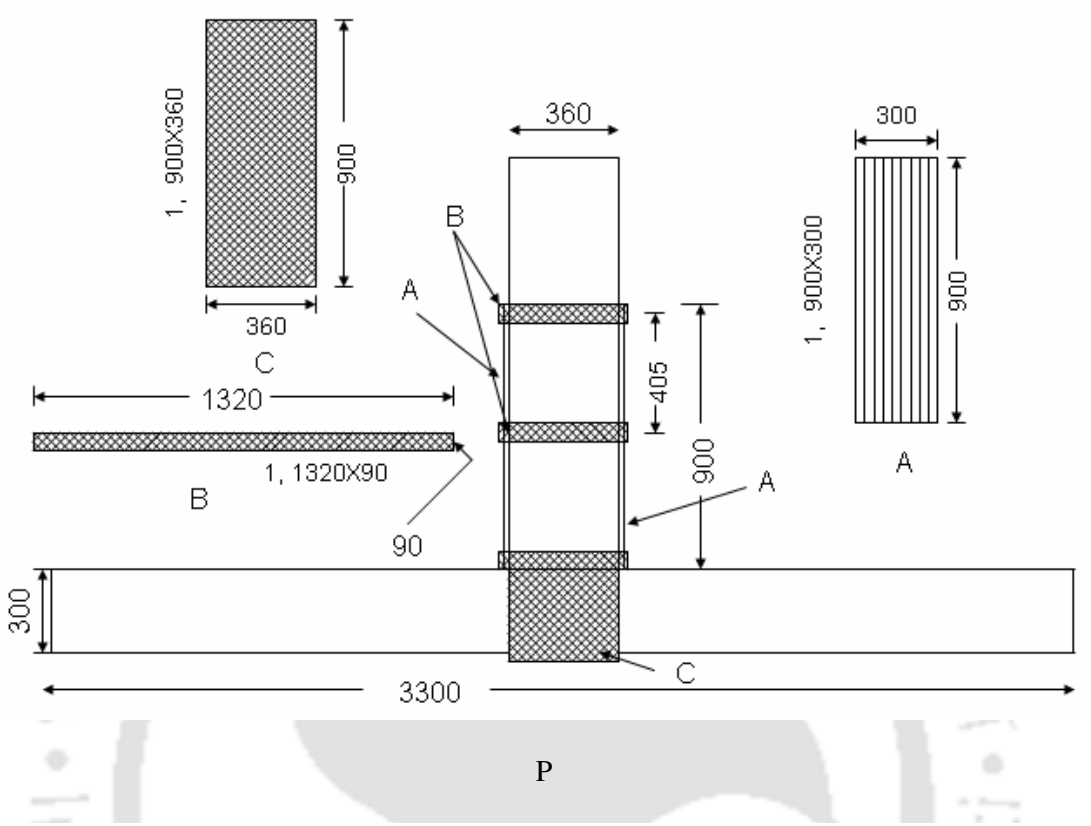

P

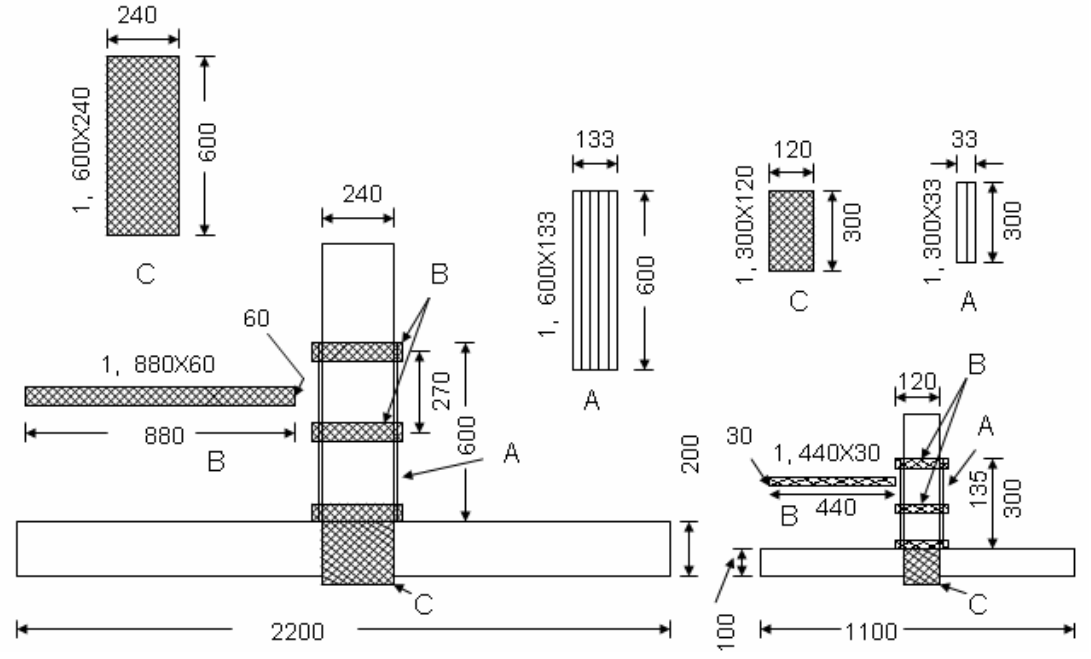

Q R

P-BWFLR specimen, Q-BWFMR specimen, R-BWFSR specimen

Fig. 3.5 Detailing of Beam weak in flexure : retrofitted specimens

scaled model were properly maintained considering geometric similitude requirement. A typical width of CFRP layer provided for full, 2/3 scaled model and 1/3 scaled model are 300 mm, 133 mm and 33 mm respectively.

3.3.5 Beam weak in Shear : Retrofitted Specimen

The specimens under this category were retrofitted so that the strengthened specimen eventually would fail in flexure which is the most preferred mode of failure. The retrofitting schedule for these specimens is furnished in Fig. 3.6. In order to strengthen the shear deficient beam weak in shear : control specimens , the retrofitting in the beam was done using GFRP. In BWSLR, strip of one layer having width of 120 mm were wrapped around the beam with a spacing 260 mm c/c up to a length 900 mm (type B). Geometric similarity was maintained for two scaled models. This scheme of retrofitting enhanced the shear capacity of the beam making it higher than the flexural capacity. Hence at this level the beam was expected to fail at the original flexural capacity of the control specimen, resulting a slight increment in the overall capacity. Further, flexural retrofitting was also carried out to achieve an appreciable increase in capacity of the specimen. The flexural retrofitting was carried with CFRP to such an extent that even after the flexural retrofitting the beam fails in flexure. Thus, it was ensured that after the flexural retrofitting, the flexural capacity of the beam remains less than the enhanced shear capacity. The flexural strengthening was carried out in beam by providing CFRP in a manner similar to that of beam weak in flexure : retrofitted specimens, as mentioned earlier (type A). The joint was also adequately strengthened with GFRP (type C). Fig. 3.6 shows strengthening configuration of beam weak in shear retrofitted specimens, which are similar to that of beam weak in flexure : retrofitted specimens except the GFRP used for shear strengthening of beam.

3.3.6 Column Weak in Shear : Retrofitted Specimen

The specimens under this category were retrofitted similar to the earlier specimens. In order to strengthen the shear deficient control specimens, the retrofitting in the column was done with GFRP. The retrofitting schedule for these specimens is furnished in Fig. 3.7. This scheme of retrofitting enhanced the shear capacity of the column. To maintain a similar trend to that of the other type of specimens, nominal flexural strengthening in the column was also carried out by CFRP. In CWSLR, three numbers of strips each with one layer of GFRP having width of 90 mm was wrapped around on both sides of the joint with spacing 360 mm c/c (type B). The flexural strengthening was carried out in column by providing CFRP. One layer of CFRP of width 240 mm was fixed on column at either side of the joint over 450 mm length for the specimen CWSLR (type A). The joint was also adequately strengthened with one layer of GFRP (type C). Geometrical similarity was strictly maintained for other two scaled down models during retrofitting.

3.4 CASTING OF THE SPECIMEN

All the constituent materials used in the design mix were tested as per relevant codes and the test results were presented in Chapter-2. The mix used for beam-column joint with beam weak in flexure and beam-column joint with beam weak in shear of target strength 30 N/mm^2, while the mix for beam-column joint with column weak in shear was of target strength 25 N/mm^2. Six different mixes were designed for two different target strengths and for three different sizes, whose details have been given in Chapter-2. The average compressive strength of collected cubes was found 30.2 N/mm^2 for beam weak in flexure and beam weak in shear specimens, while the same was found 25.8 N/mm^2 for column weak in shear specimens High yield steel deformed (HYSD) Fe 500 reinforcing steel of diameters 20 mm, 12 mm and 8 mm was mainly used, while some small quantity of Fe 250 mild steel of diameter 6 mm, 4 mm and 2 mm were used for casting. All the reinforcing steel used were tested properly, whose description have been given in the

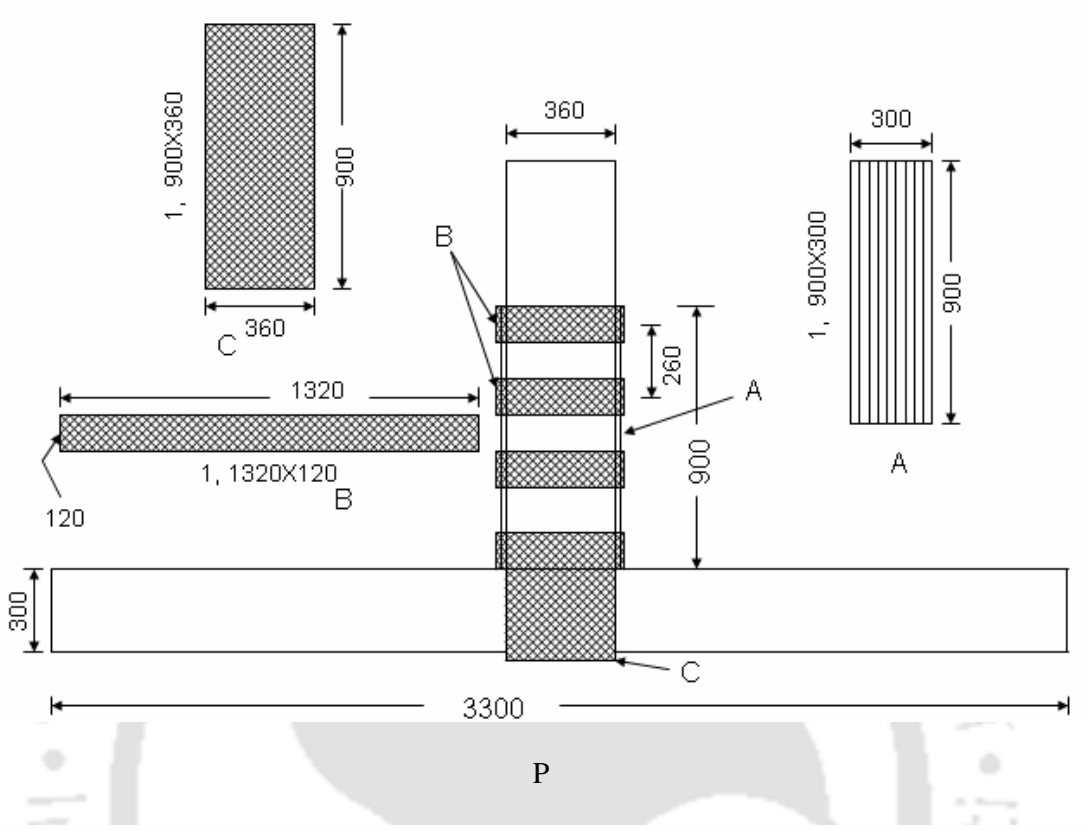

P

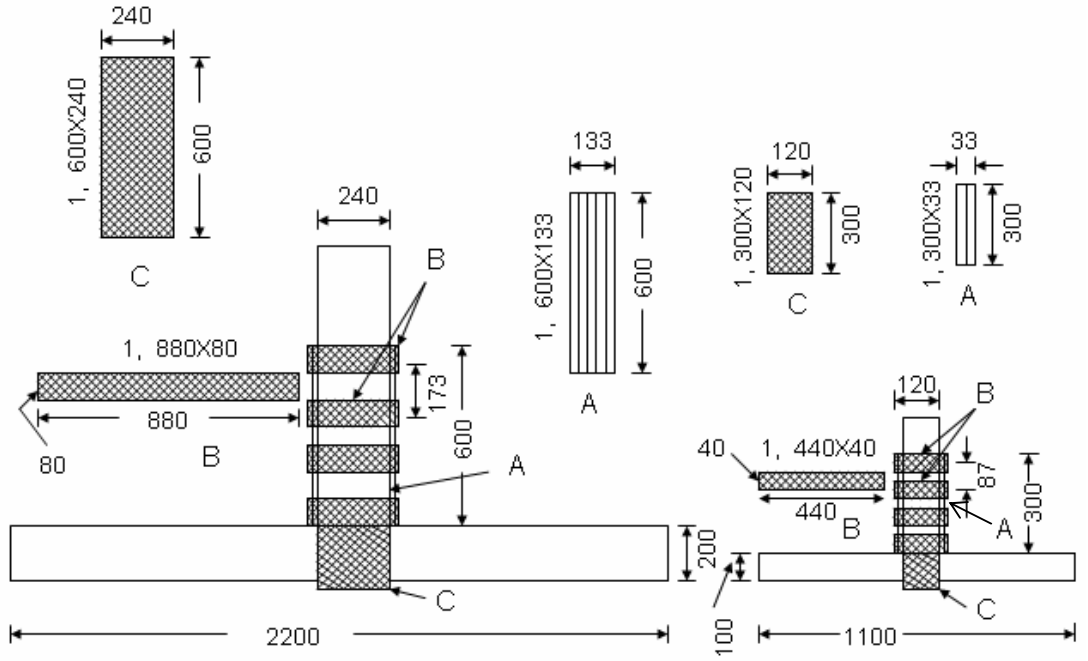

Q R

P-BWSLR specimen, Q-BWSMR specimen, R-BWSSR specimen

Fig. 3.6 Detailing of beam weak in shear : retrofitted specimens

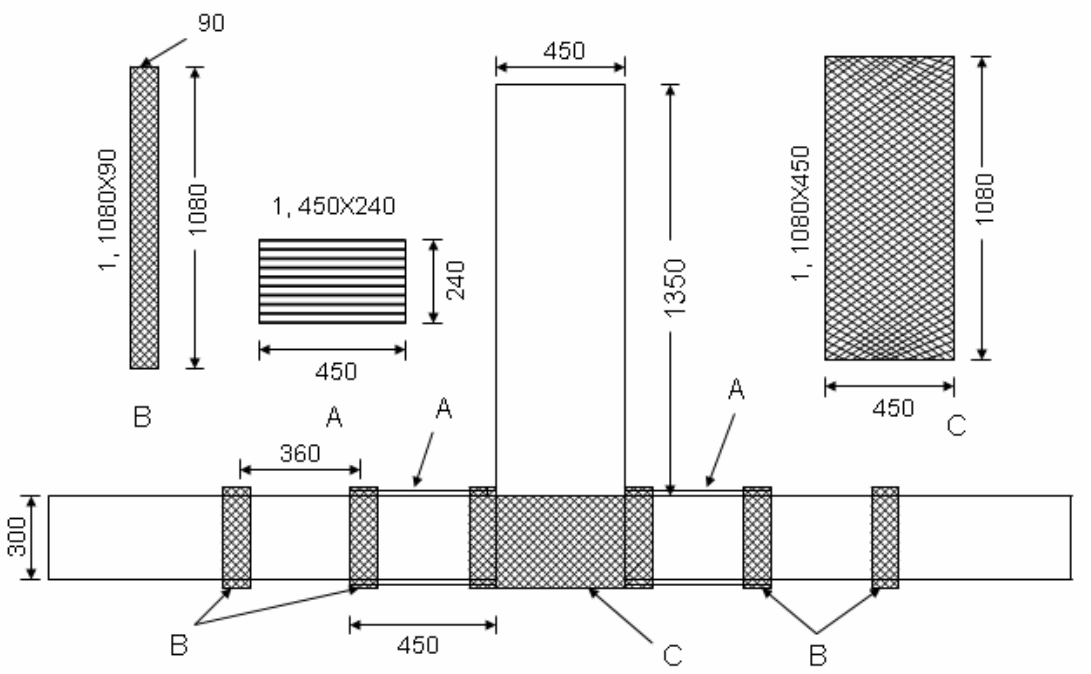

P

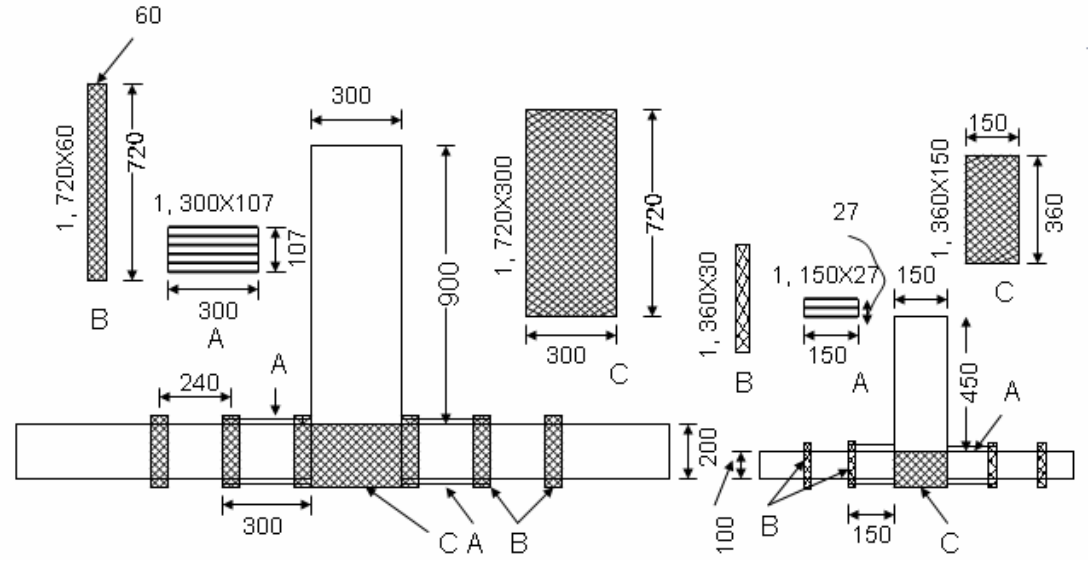

Q R

P-CWSLR specimen, Q-CWSMR specimen, R-CWSSR specimen

Fig. 3.7 Detailing of column weak in shear : retrofitted specimens

Chapter-2. Some of the typical moulds used for casting are shown in Fig. 3.8. Additional shear reinforcement was provided in the free end of the beam to take care of stress concentration due to application of the load through the actuator. A view of cast specimens in the laboratory is shown in Fig. 3.9**.**

3.5 RETROFITTING OF THE SPECIMEN

Retrofitting was done using fibre reinforced polymer sheets (GFRP and CFRP) manufactured by Fosroc Chemicals Pvt. (India) Ltd. The composite laminate coupons were tested properly as per ASTM D 3039 as described in Chapter-2. To ensure a high quality bond between the concrete and the FRP reinforcement, the retrofitting work was carried out with due caution. Various steps involved in fixing FRP over concrete surface are described in the next section.

3.5.1 Procedure for Fixing FRP

The first step of retrofitting was to make the concrete surface as polished as possible. A concrete grinding machine shown in Fig. 3.10 was used for this purpose. Care was taken to keep the wheel perfectly horizontal at the time of polishing horizontal faces, while perfect vertical alignment of the same was maintained at the time of polishing vertical faces. Further smoothening was done by rubbing the surfaces with carborundum stone and emery cloth of grain size 60. All loose materials were removed by vacuum cleaner. Grinding of the concrete was done also at the edges to make sharp corners round of radius about 25–30 mm.

The second step was to fill up all the pores and application of primer coat. These were done with Fosroc product Nitowrap 30, which comprises of two components viz. hardener and base. Both the components were mixed up in the proportion as recommended by the manufacturer and was applied over the prepared and cleaned surface up to a recommended layer thickness of 100 micron. The application was carried out

Fig. 3.8 Specimens inside the moulds

Fig. 3.9 Stack of cast specimens inside laboratory

using a brush and the primer coat was allowed to dry for about 24 hours before the application of the saturant.

The third step was placing of FRP by wet lay up process, where Nitowrap 410 was used as saturant. The base and hardener was mixed in the proportion recommended by manufacturer and was applied over the primer coat. A wet film thickness (WFT) of 250 microns was maitained. The FRP sheet was then pressed immediately after applying

saturant first by gloved hand (Fig.3.11) and then pressed with a roller made up of stainless steel to remove air bubbles. It was continuously rolled until the resin was reflected on the surface of the fabric, which was an indication of fully wetting. Extreme precaution was maintained at the time of rolling so that FRP did not bend anywhere. Rolling over the CFRP sheet was started from the centre and continued to the ends as shown in Fig. 3.12. While placing the GFRP with the fibres aligned at 45^0, it was ensured that the rolling was done along the direction of the fibres. On the top of the fabric, another layer of resin of 250 microns was applied after a minimum time lapse of 30 minutes. The specimen gained maturity after 7 days of fixing of FRP.

3.6 INSTRUMENTATION AND LOADING ARRANGENENT

The typical schematic diagram of the test set-up used is shown in Fig. 3.13. An MTS actuator of 250 kN capacity with an *A* frame was used for testing of large and medium specimens. An MTS actuator of 100 kN capacity was used with two *A* frames for testing of small specimens. The detailed description for both the cases is given in the next paragraphs.

The column was placed in horizontal position while the beam was placed in vertical position in the set-up. An axial load of 10% of gross capacity of column was applied to the column to represent gravity load. The load on column was applied by a 500 kN capacity jack, which was properly calibrated. The jack was abutting against an *A* frame, which was fabricated for the specified load carrying capacity (Fig. 3.14). To simulate support condition at both ends of the column, roller supports were fabricated by making grooves inside mild steel plates. The testing arrangement for large specimen is shown in Fig. 3.15, while the same for small specimens is shown in Fig. 3.16.

The MTS actuator is equipped with internal load cell and linear-variable differential transformer (LVDT) for measuring actuator force and displacement respectively. The LVDT is coaxially mounted within the actuator piston rod and produces an analog signal

Fig. 3.10 Surface polishing by grinding machine

Fig. 3.11 Fixing of FRP

Fig. 3.12 Rolling over FRP

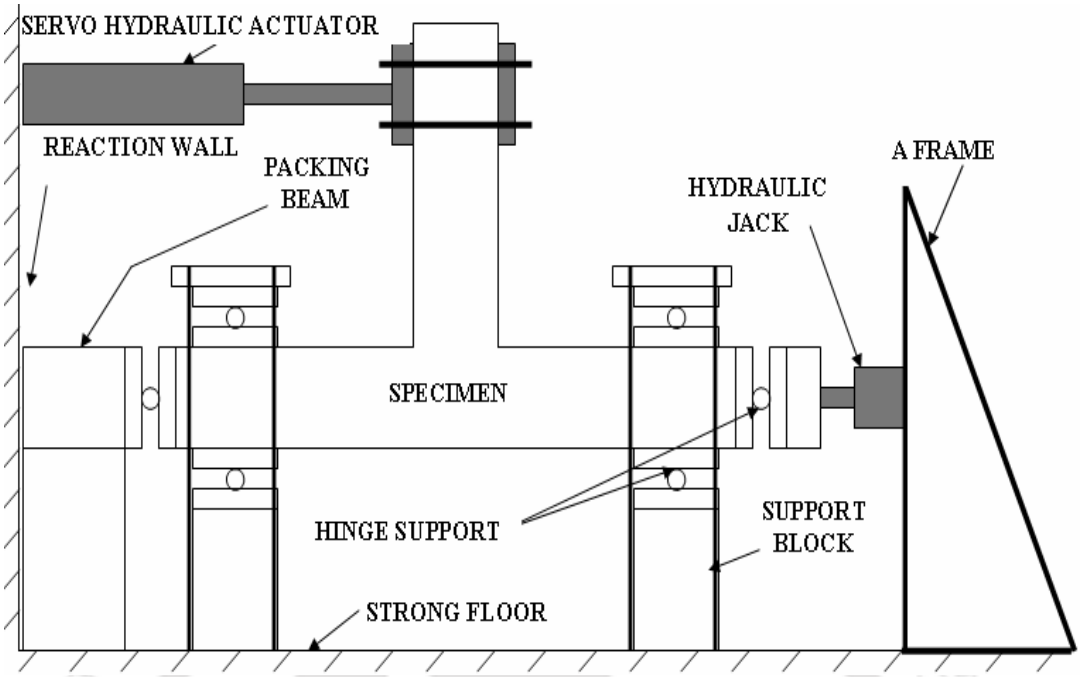

Fig. 3.13 Test set up for large and medium specimen.

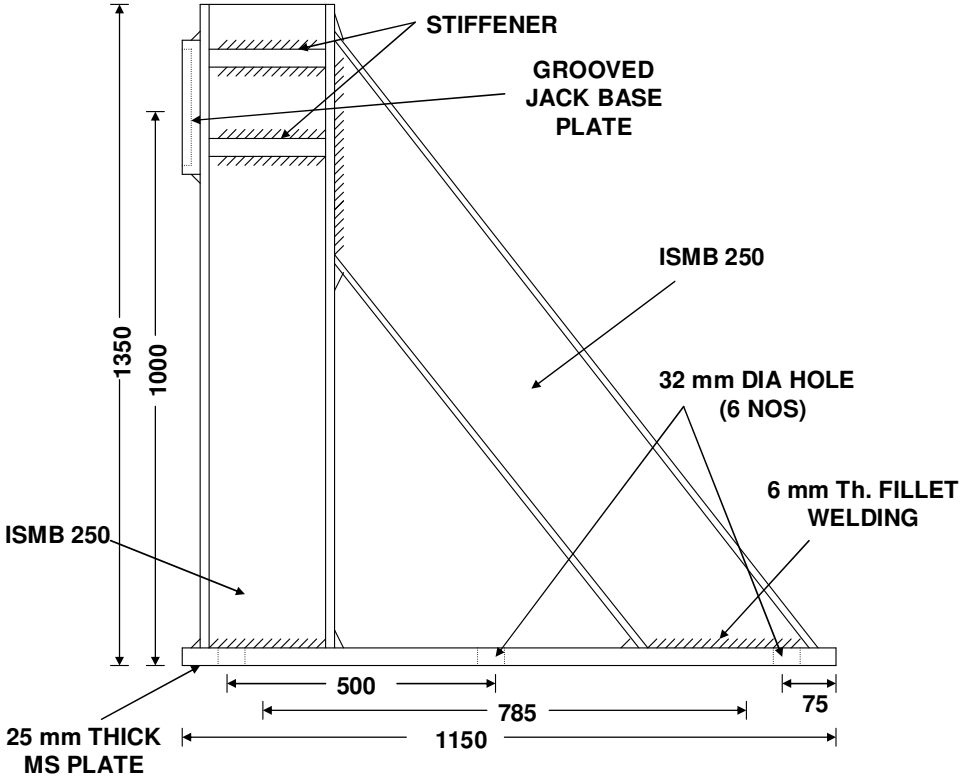

Fig. 3.14 Schematic diagram of fabricated *A* Frame

system is controlled by MTS Controller. The controller can generate prescribed dynamic displacement or force for the actuator. The actuator is of double ended and double stroke nature. Two actuators of different capacities were used in the testing. The actuator of capacity ± 250 kN (Model 244.31) was used for large and medium specimens, while the actuator of capacity ± 100 kN (Model 244.22) was used for small specimens. The double amplitude displacement is 250 mm and single amplitude it is ± 125mm for both the actuators.

Fig. 3.15 Testing arrangement for large and medium specimens

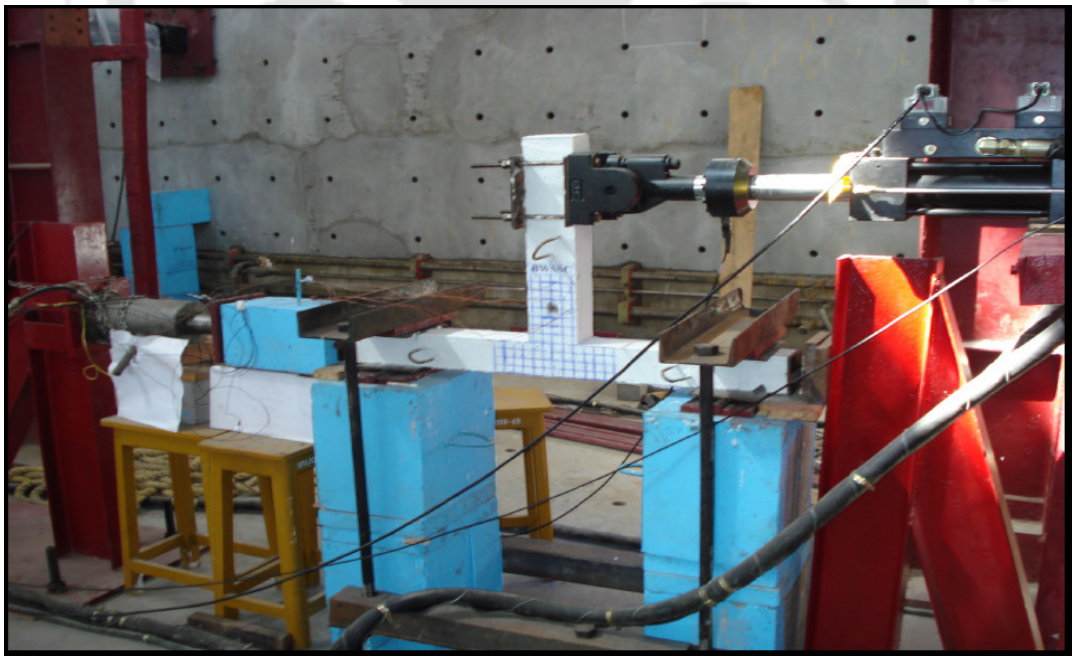

Fig. 3.16 Testing arrangement for small specimens

3.7 CONCLUDING REMARKS

In this chapter, the detailed description of control and retrofitted specimens and the testing arrangement have been presented. *A* frames of appropriate capacity were fabricated to facilitate the application of loads and keeping the specimens in proper position during testing. Roller supports were fabricated by drilling grooves inside MS plate for maintaining proper boundary conditions at all contact points of the columns during testing. Numerical analysis, using ASYS 6.0 was carried out before starting of the experiments in order to appropriately design the programme of experimental investigation. The description of numerical analysis is given in Chapter-4.

CHAPTER 4

NUMERICAL STUDIES

4.1 INTRODUCTION

This chapter presents the numerical analyses on RC beam column joints with and without retrofitting using the general purpose finite element software ANSYS 6.0. The study was carried out to simulate the behaviour of these joints subjected to monotonic loading. Nonlinear static analysis was carried out for getting prior information about the load at first crack, crack pattern, load and deflection at yielding, ultimate load etc. for all the specimens in order to appropriately plan the arrangement of experimental investigation. In the numerical study, concrete was modeled using a 3-D solid element (SOLID65), which is capable of incorporating cracking and crushing besides plastic and creep behavior. William and Warnke plasticity model was used for the concrete material failure modeling. Similarly, reinforcement bars, FRP and adhesive were also represented using appropriate finite element and material model. The various sections in this chapter discusses about various finite element and material models used to represent concrete, reinforcing steel, FRP and adhesive. Results obtained from FE analysis using ANSYS 6.0 have been compared with those obtained utilising strength criteria. The comparison shows that the results predicted by the numerical studies were slightly higher than those obtained by strength criteria. Moreover, it was also noted that the percentage gain in strength obtained by numerical analysis with respect to that by strength criteria increases as the specimen size decreases almost in all the cases. Thus, it reflects the existence of size effect on the result obtained by numerical simulation.

4.2 NONLINEAR ANALYSIS

Linear structural analysis is based on the assumption that structures undergo small deformations and the material remains elastic with linear load-displacement relationship.

The analysis is performed on the initial undeformed shape of the structure. As the applied load increases raising the stress beyond elastic limit, this assumption remains no longer valid since the deformation may cause significant changes in the structural shape. This causes a change in the stiffness matrix leading to nonlinearity in structures. The nonlinearity in an RC element is mainly of two types, viz. geometric nonlinearity and material nonlinearity. Geometric nonlinearity refers to the nonlinearity in structure or component due to the changing geometry. Geometric nonlinearity may arise due to large strain, large rotation, stress stiffening. Material nonlinearities are due to the nonlinear relationship between stress and strain implying that the stress is a nonlinear function of strain. Concrete and steel are two constituents of R.C. structures. Out of these two, concrete is much stronger in compression than in tension (tensile strength is of the order of about one tenth of the compressive strength). The tensile stress–strain relationship of concrete is almost linear up to failure, while the stress-strain relationship in compression is nonlinear from the very beginning itself. Since the concrete and steel are both highly nonlinear materials, the material nonlinearity of R.C. structure is understandably complex. The nonlinear analysis of reinforced concrete structures has become very important in recent years. It is advisable to carry out a complete progressive failure analysis of the structure up to collapse to assess all safety aspects of a structure and for finding its deformational characteristics. The development of material models for uncracked and cracked concrete for all stages of loading is particularly a challenging field in nonlinear analysis of reinforced concrete structures. Since the stiffness matrix continuously changes during application of successive loads, the analysis needs to be performed by iterative methods, like direct iteration or the Newton-Raphson method.

4.3 ELEMENT TYPES

In the present FE analysis, all the structural elements were modeled using appropriate finite element from the available element library of ANSYS. Concrete, adhesive and FRP

used were modeled by 3-D solid element. Reinforcing steel was modeled by a 3-D truss element. The next subsections discuss about all the elements used for modeling of beam-column joint.

4.3.1 SOLID65

SOLID65 was used for the 3-D modeling of concrete. The 3-D solid element is capable of cracking (in three orthogonal directions) in tension, crushing in compression, plastic deformation and creep. The element as shown in Fig. 4.1 is defined by eight nodes having three degrees of freedom at each node, namely translations in the nodal X, Y and Z directions. The most important aspect of this element is that it can treat the nonlinear material properties.

Typical shear transfer coefficients range from 0.0 to 1.0, with 0.0 representing a smooth crack (complete loss of shear transfer) and 1.0 representing a rough crack (no loss of shear transfer). When principal tensile stress at integration point exceeds the ultimate tensile strength of the concrete, the cracking sign represented by a circle appears perpendicular to the direction of the principal stress.

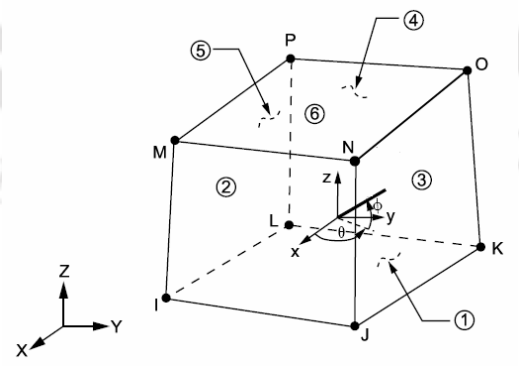

Fig. 4.1 SOLID65 Element

4.3.2 LINK8

LINK8 is a 3-D spar (or truss) element. This element as shown in Fig. 4.2 was used to model the steel in reinforced concrete. The three-dimensional spar element is a uniaxial tension-compression element with three degrees of freedom at each node, namely

translations in the nodal X, Y and Z directions. This element is capable of plastic deformation also.

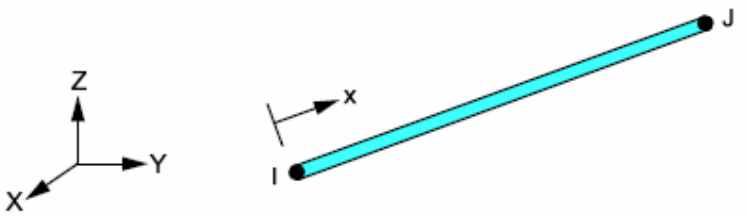

Fig. 4.2 LINK8 Element

4.3.3 SOLID45

This element was used for 3-D modeling of adhesive. The element as shown in Fig. 4.3 is defined by eight nodes having three degrees of freedom at each node, namely translations in the nodal X, Y and Z directions. The element takes into account plasticity, creep, swelling, stress stiffening, large deflection, and large strain capabilities.

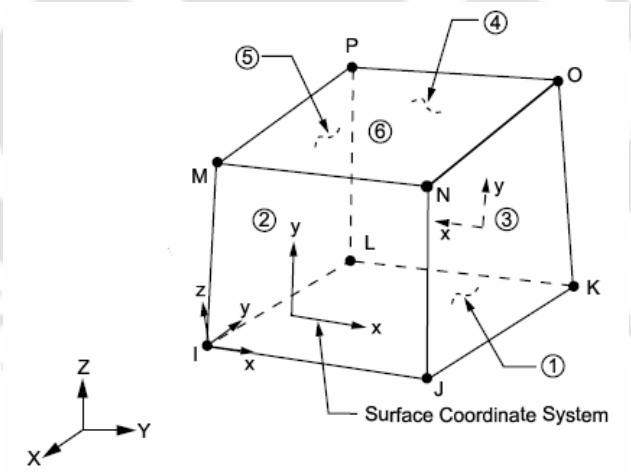

Fig. 4.3 SOLID45 Element

4.3.4 SOLID46

This element was used for 3-D modeling of fiber reinforced polymer with different layers. This is a layered version of the 8-noded SOLID45. It is designed to model layered thick shells or solids. The element allows up to 250 different material layers. Similar to other solid elements used, this element has also three degrees of freedom at each node, namely

translations in the nodal X, Y and Z directions. Fig. 4.4 shows SOLID46 element.

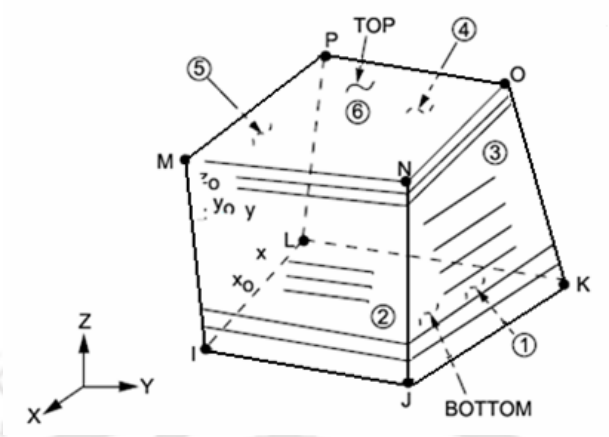

Fig. 4.4 SOLID46 Element

4.4 MATERIAL MODELLING

The material model for concrete used in the RC beam-column joint should be such that it encompasses various aspects for material nonlinearity, cracking, crushing and plasticity etc. The next subsections discusses about all the material models which were used to model beam-column joints with and without retrofitting.

4.4.1 Concrete

Concrete is a quasi-brittle material. Hence the behaviour in compression and tension are different. The tensile strength of concrete is typically 8-15 per cent of the compressive strength. A typical stress-strain curve for concrete is shown in Fig. 4.5 (Chung *et al.* 2002). The response of RC structure under load depends largely on the stress-strain relation of the materials and the stress magnitude. The stress-strain relation of concrete displays nearly linear elastic behaviour up to about 30 percent of the ultimate compressive strength. After reaching the ultimate strength, f_{cc} the diagram descends into a softening area and follows until failure takes place by crushing at an ultimate strain ε_{cu}. The descending part can be described by three coordinates *A*, *B* and *C* as shown

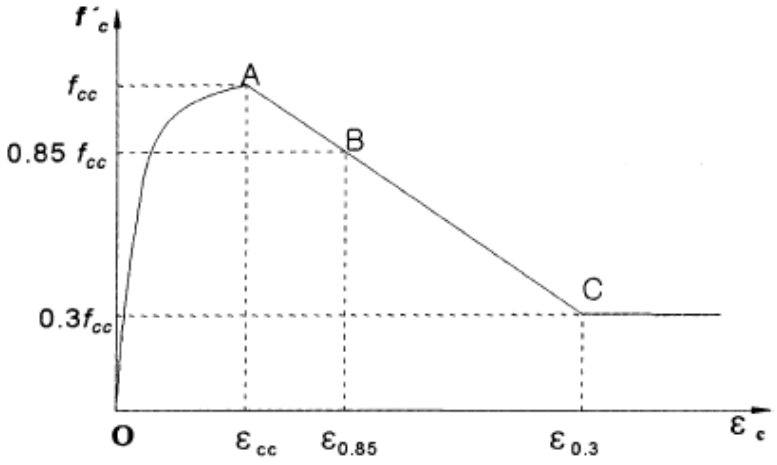

Fig. 4.5 Typical Stress–strain curve of concrete. [Chung *et al.* 2002]

in Fig. 4.5. The point A represents the peak stress f_{cc} and strain ε_{cc} . *B* corresponds to the stress and strain of 0.85 f_{cc} and $\varepsilon_{0.85}$ respectively, while *C* represents the stress and strain of 0.3 f_{cc} and $\varepsilon_{0.3}$. The co-ordinate of *C* lies at the extension line obtained by connecting the points *A* and *B*.

4.4.1.1 Multi-linear Isotropic Hardening Stress-Strain Curve

The uniaxial stress-strain behaviour of concrete was proposed by many researchers in the form of different empirical formulae. In the present numerical analysis, the uniaxial behavior of concrete was modeled by the numerical expression proposed by Desayi and Krishnan [1965] incorporating the modification proposed by Gere and Timoshenko [1997]. It is described by a piece wise linear stress-strain curve, starting at the origin with positive stress and strain values. The slope of the first segment of the curve must correspond to the elastic modulus of the material. All segments other than the first one should have slope less than elastic modulus of the material. All segments should have positive slope. The ANSYS program requires the uniaxial stress-strain relationship for concrete in compression only. The multi-linear isotropic stress-strain implementation requires that the first point (0.3 f_{cc}) of the curve be defined by the user. Stress strain properties of concrete up to failure is presented in Table 1 (Appendix A) and the

multi-linear isotropic stress-strain curve for concrete has been shown in Fig. A.1 (Appendix A).

4.4.1.2 Failure Criteria for Concrete

The concrete material model available in ANSYS is capable of predicting failure modes like cracking and crushing failure. The two input strength parameters i.e., ultimate uniaxial tensile and compressive strength are needed to define the failure surface for the concrete. The 3-D solid element (SOLID65) is capable of incorporating cracking and crushing. Further, the ability of concrete to undergo plasticity with the William and

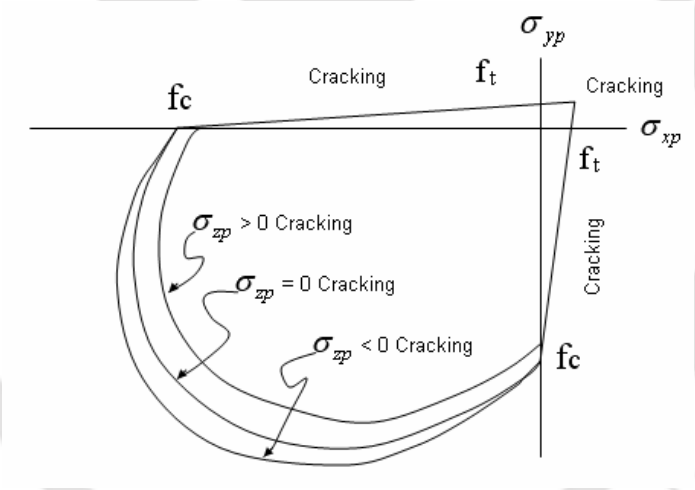

Fig. 4.6 Failure surface of concrete

Warnke [1974] failure surface besides creep behaviour had also been utilized. The presence of a crack at an integration point is represented through modification of the stress-strain relations by introducing a plane of weakness in a direction normal to the crack face. If the material at an integration point fails in uniaxial, biaxial, or triaxial compression, the material is assumed to crush at that point. In SOLID65, crushing is defined as the complete deterioration of the structural integrity of the material (e.g. material spalling). Further, crushing implies that the material strength have degraded to such an extent that the contribution to the stiffness of an element at the integration point

in question can be ignored.

A failure surface for concrete is shown in Fig. 4.6. The most significant nonzero principal stresses are in the X and Y directions, represented by σ_{xp} and σ_{yp} respectively. Three failure surfaces are shown as projections on the $\sigma_{xp} - \sigma_{yp}$ plane. The mode of failure is a function of the sign of σ_{zp} (principal stress in the Z direction). For example, if σ_{xp} and σ_{yp} are both negative (compressive) and σ_{zp} is slightly positive (tensile), cracking would be predicted in a direction perpendicular to the σ_{zp}. However, if σ_{zp} is zero or slightly negative, the material is assumed to crush [ANSYS 2003].

4.4.2 Steel Reinforcement

Unlike concrete, steel is very uniform and as such generally the specification of a simple stress-strain relation is adequate to define it numerically. Typical stress-strain curves for reinforcing steel bars used in concrete construction are obtained from standard tensile tests. Practically speaking, steel exhibits the same stress-strain curve in both compression and tension. The stress-strain relation shows a linear elastic portion at the initial stage, followed by a yield plateau until a strain hardening region is reached, in which stress again increases with strain before eventually dropping off as microscopic fracture occurs. The length of the yield plateau is dependent on the tensile strength of steel. The yield plateau of high strength, high-carbon steels is generally much shorter than relatively low-strength, low-carbon steels. Typical uniaxial stress-strain curve are as shown in Fig. 4.7 for various grades of steel.

Modulus of elasticity of steel (E_S), which corresponds to the slope of the initial linear elastic portion was adopted as $2\times10^5 \text{N/mm}^2$ as per IS-456 [2000] in the present analysis. An abrupt change in the stress-strain behaviour is observed for the material beyond the yield point. Moreover, upon unloading the material at any point beyond the yield point, a permanent deformation is introduced. This kind of behaviour can be idealized by a

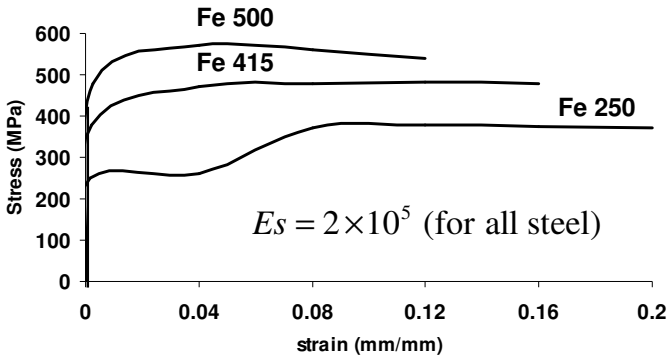

Fig. 4.7 Uniaxial stress-strain curves for steel

bilinear stress-strain relationship with two slopes, the second slope being called the tangential modulus (E_T). After reaching the yield point, the slope could be less than, equal to, or greater than zero. In the present analysis (E_T) has been assumed as $1000\ \text{N/mm}^2$. One typical idealized stress-strain curve for steel is shown in Fig. 4.8. In addition to modulus of elasticity, the value of Poisson's ratio is also provided as the input data for modeling of steel in FE analysis. This value was assumed as 0.3 in the present analysis.

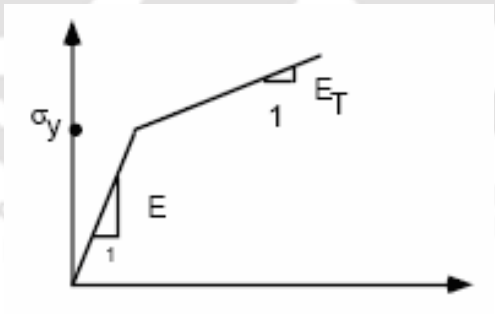

Fig. 4.8 Typical idealized stress-strain curve for steel

4.4.3 FRP Composite

FRP composite is a brittle material. The stress-strain curve is a purely straight line up to the failure strength. The various moduli which are needed for the modeling of FRP composite in FE analysis with ANSYS have been adopted from the properties of FRP

composite as shown in Table 4.1. Composites are orthotropic materials. There exist numerous strength theories for prediction of failure of orthotropic materials. These are the maximum stress theory, maximum strain theory, Tsai Hill theory and Tsai Wu theory. Tsai Hill theory [Tsai, 1966] is regarded as superior. The advantage of this theory is that it gives a single criterion for the detection of failure as compared to the other stress and strain based criterion.

Table 4.1 Properties of FRP Materials

Type of FRP	Ultimate Strength (N/mm^2)	E_x (MPa)	E_y (MPa)	E_z (MPa)	υ_{xy}	υ_{yz}	υ_{zx}	G_{xy} (MPa)	G_{yz} (Mpa)	G_{zx} (Mpa)	Fibre Orientation
CFRP	670	46300	46300	23309	0.3	0.25	0.25	16189	9713.3	9713.3	0^0
GFRP	350	11670	11670	7787.7	0.3	0.25	0.25	10385	5182.7	5182.7	$\pm 45^0$

4.5 NONLINEAR SOLUTION TECHNIQUE

In non-linear analysis, the total load applied to a finite element model is divided into a series of load increments, called load steps. At the completion of each incremental solution, the stiffness matrix of the model is adjusted to reflect nonlinear changes in structural stiffness before proceeding to the next load increment. The program ANSYS (ANSYS, 2003) uses Newton-Raphson equilibrium iterations for updating the model stiffness. Newton-Raphson equilibrium iterations provide convergence at the end of each load increment within a tolerance limit. Fig.4.9 shows the use of the Newton-Raphson approach in a single degree of freedom nonlinear analysis. Prior to each solution, the Newton-Raphson approach assesses the out-of-balance load vector, which is the difference between the restoring forces (the loads corresponding to the element stresses) and the applied loads. Subsequently, the program carries out a linear solution, using the out-of-balance loads and checks for convergence. If convergence criteria are not satisfied, the out-of-balance load vector is re-evaluated and the stiffness matrix is updated, and a new solution is obtained. This iterative procedure continues until the problem converges [ANSYS, 2003].

For the non-linear analysis, automatic time stepping in the ANSYS program predicts and controls load step sizes. Based on the previous solution history and the physics of the models, if the convergence behaviour is smooth, automatic time stepping will increase the load increment up to a selected maximum load step size. If the convergence behaviour is abrupt, automatic time stepping will bisect the load increment until it is equal to a selected converged load step.

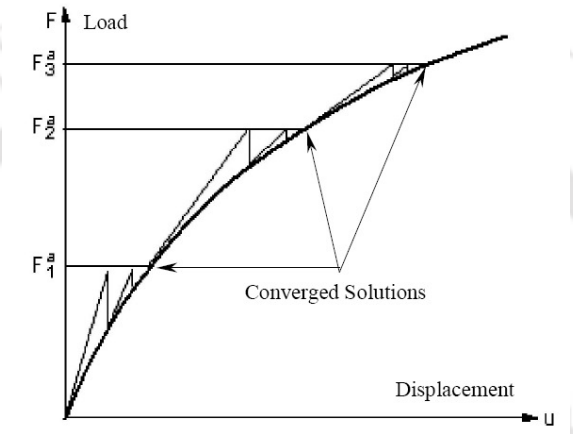

Fig. 4.9 Newton-Raphson iterative solution for typical three load increments [ANSYS, 2003]

4.6 FINITE ELEMENT ANALYSIS

The loading with the corresponding boundary conditions has been shown in Fig. 4.10. A monotonically increasing load was applied at the beam tip for carrying out static analysis. Two convergence criteria were used for the finite element analysis process namely force convergence and displacement convergence. These convergence criteria were kept to default values up to first cracking. However, after first cracking, displacement convergence was considered for the nonlinear analysis. Table 4.2 represent the convergence value used in the analysis. For the finite element analysis of beam column joint, the load corresponding to first crack, progressive cracking yielding of steel and ultimate failure load were evaluated.

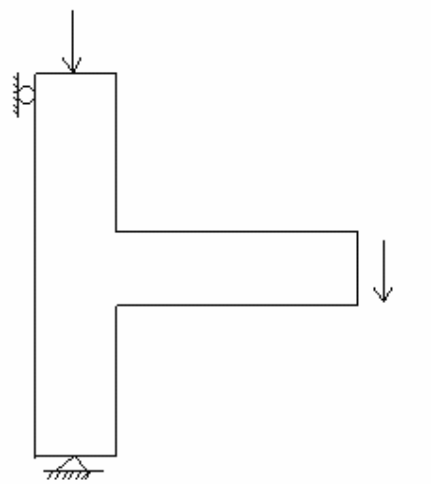

Fig. 4.10 Loading arrangement and boundary condition of the beam-column joint

Table 4.2 Convergence criteria

Level	Force	Displacement
Tolerance	0.005	0.05
Norm	L2	L2

4.7 RESULTS AND DISCUSSIONS

Some of the typical finite element models of control as well as retrofitted beam-column joint specimens are shown in Fig. 4.11 - 4.16. The nonlinear analysis was carried out in ANSYS 6.0 for all the specimens with different deficiencies and sizes along with corresponding retrofitted models. Some of the representative results obtained from the analysis is presented in Fig. 4.17 - 4.23. Fig. 4.17 shows the appearance of first flexural crack, which occurs in the beam near the beam-column joint at a load of 13800 N and displacement of about 1.4 mm at the beam tip for BWFLC. Fig. 4.18 shows the ultimate cracks at failure, which occurs in the beam as well as in the joint at a load of 75600 N for BWFLC. Fig.4.19 shows the stress contour for the same specimen. As shown in the window, "TIME" stands for the failure tip load, "DMX" for maximum deflection and

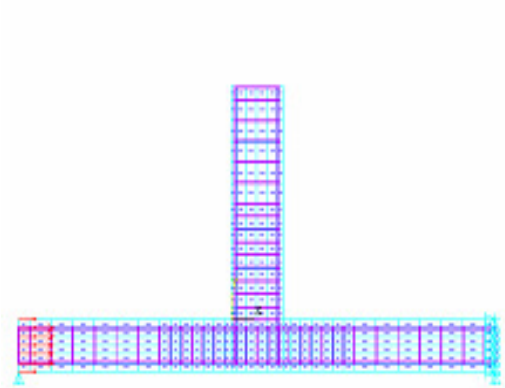

Fig.4.11 Finite element model of BWFLC

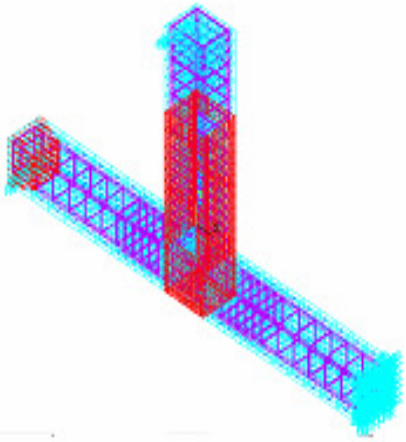

Fig.4.12 Finite element model of BWFLR

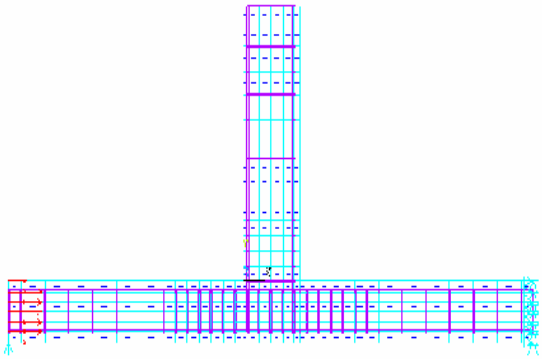

Fig.4.13 Finite element model of BWSLC

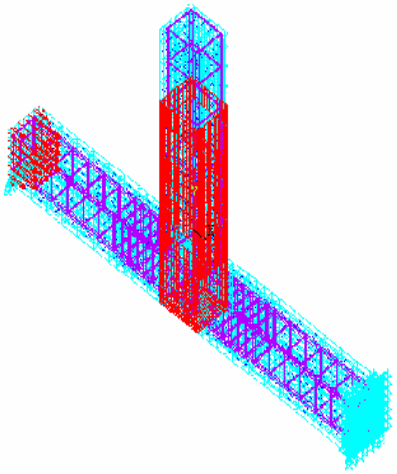

Fig.4.14 Finite element model of BWSLR

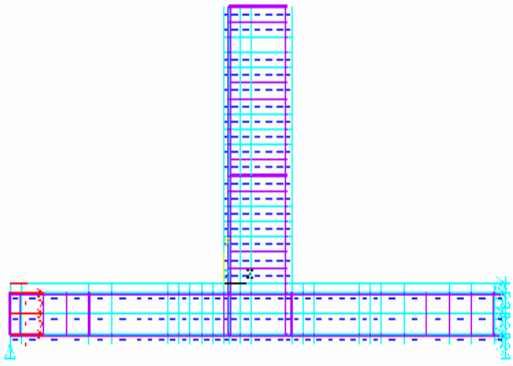

Fig.4.15 Finite element model of CWSLC

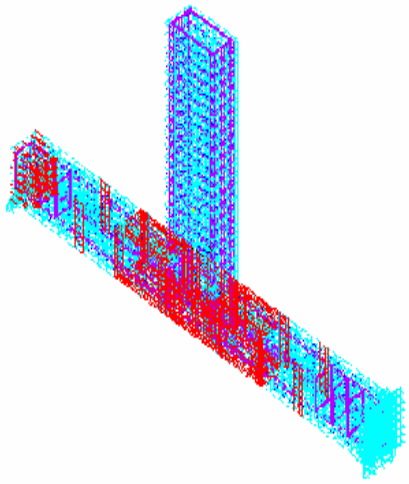

Fig.4.16 Finite element model of CWSLR

"SMN" maximum bending stress at failure. The maximum deflection for the specimen BWFLC is 16.692 mm and maximum normal stress due to bending at failure is 19.947 N/mm^2.

Fig.4.20 shows the first flexural crack for BWFLR, which occurs at a load of 15500 N. Thus, due to retrofitting, the development of first crack occurred at a higher load level in comparison to that in the corresponding control specimen. Fig. 4.21 shows the ultimate cracks of BWFLR which occurs at the ultimate load of 82000 N. Fig. 4.22 shows the plot of stress contour for BWFLR.

A typical load-displacement curve involving both control and retrofitted specimens is shown in Fig. 4.23. It can be observed that for BWFLC at a load of 13800 N, the slope of the curve changes indicating the development of first crack. After the first crack, further increase in load leads to stiffness reduction due to the development of subsequent cracks. A substantial stiffness reduction has been observed to have taken place after the load at beam tip exceeded the load corresponding to the yielding of steel. The beam tip deflection increases rapidly and the steel yielding occurs at a load of about 60000 N at a displacement of about 12.5 mm. The failure for the control specimen occurs at the load of 75600 N and at a displacement of 16.692 mm. Further, the load-displacement plot indicates that at a load of 15500 N, the slope of the curve changes indicating the development of first crack for retrofitted specimen BWFLR. The steel yielding occurs at a load of about 63000 N. The failure of the retrofitted specimen occurs at a load of 82000 N and at a displacement of 17.392 mm. Thus, it is clear that there is substantial gain in ultimate load carrying capacity due to retrofitting. The curves shown in Fig. 4.23 has been marked showing the first crack, yielding of steel and ultimate load. The failure load obtained from numerical analysis for both control and retrofitted specimens are shown in Table 4.3. In the same table, the result obtained by strength criteria is also presented for comparison. The beam-column joints with beam weak in flexure and beam weak in shear

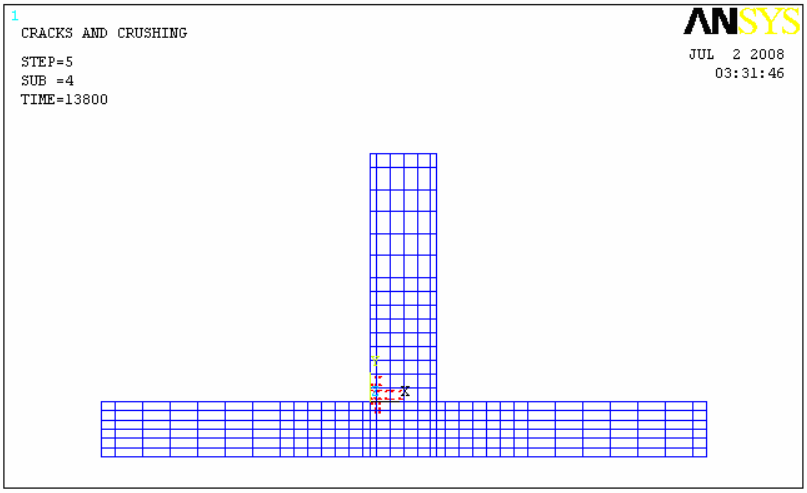

Fig. 4.17 First crack in BWFLC

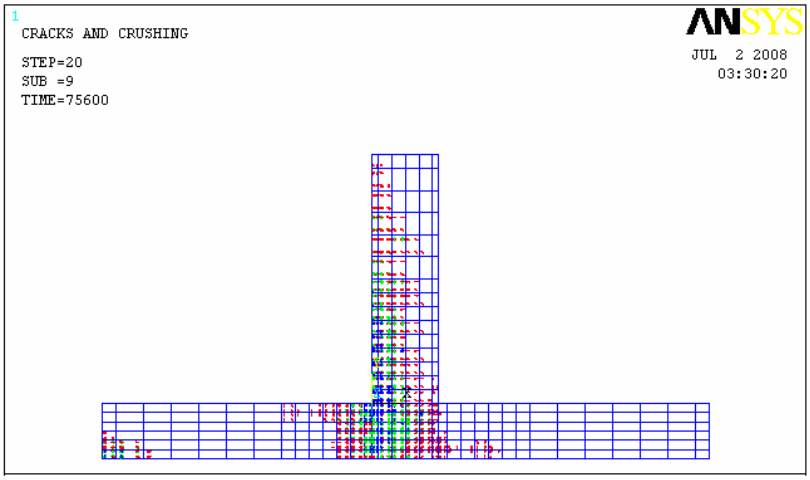

Fig. 4.18 Ultimate cracks for BWFLC

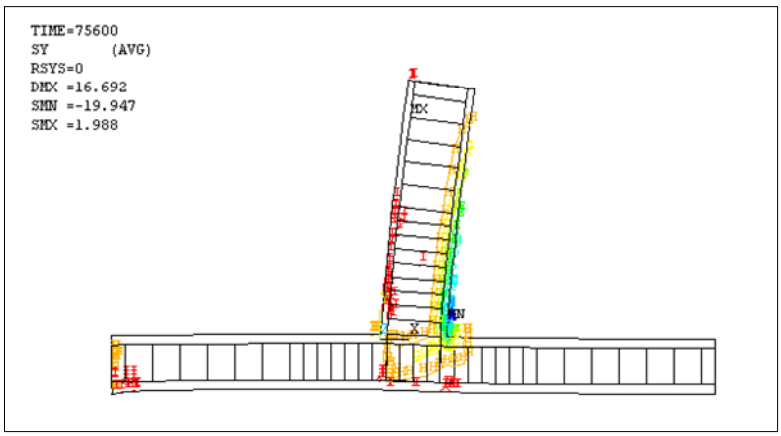

Fig. 4.19 Ultimate failure load and ultimate stresses for BWFLC

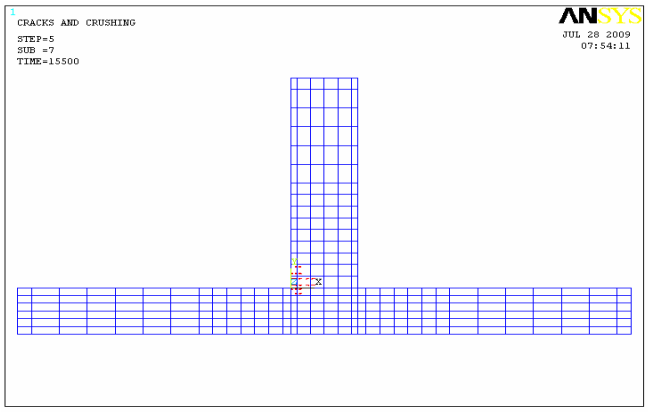

Fig. 4.20 First crack in BWFLR

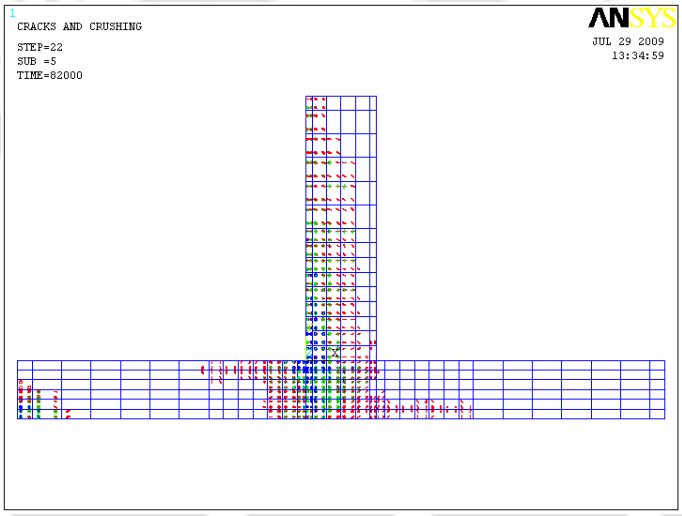

Fig. 4.21 Ultimate cracks for BWFLR

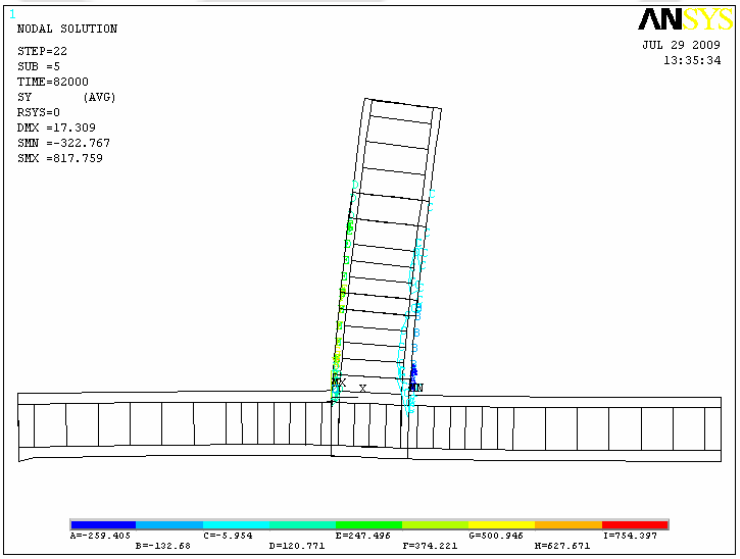

Fig. 4.22 Ultimate failure load and ultimate stresses for BWFLR

were designed as strong column-weak beam. The beam was idealised as a cantilever beam for arriving at the failure tip load of the beam. However, the same assumption was not valid for column weak in shear specimens. Hence, the calculation of load carrying capacity for such specimens was not provided in the table. The calculation for ultimate load carrying capacity for control and retrofitted specimens with strength based criteria is presented in Appendix-B. From Table 4.3 it is clear that the ultimate capacities as obtained through numerical simulations are quite close to those obtained from strength based criteria, indicating the reliability of the simulated results. In addition, it can be noted from the table that the results obtained by numerical studies were slightly higher than those obtained by strength criteria. Further, it can also be noted that the percentage gain in strength obtained from analysis using ANSYS with respect to that obtained on the basis of strength criteria increases as the specimen size decreases in all the cases considered for the study. This reflects the existence of size effect on the result obtained from analysis using ANSYS.

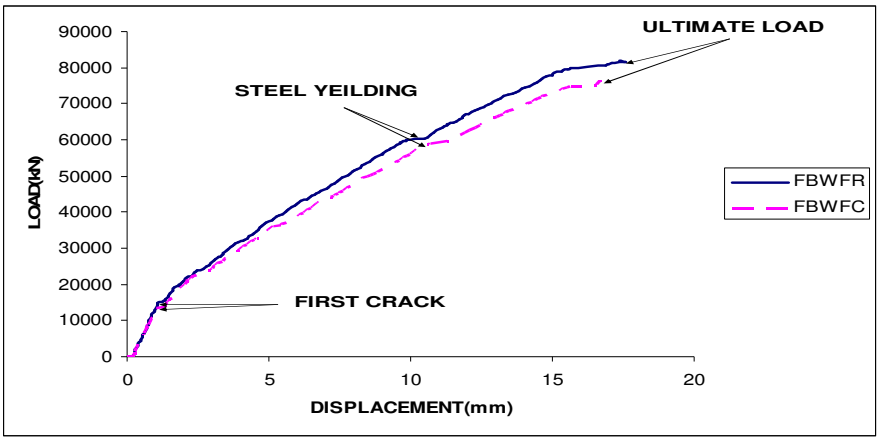

Fig. 4.23 Typical Load-Displacement Graph

Table 4.3 Ultimate load of specimens

Control specimens				Retrofitted specimens			
Name of specimen	Ultimate load by FE analysis with ANSYS (kN)	Ultimate load by strength criteria (kN)	Gain in ultimate strength by ANSYS w.r.t. strength criteria (%)	Name of specimen	Ultimate load by FE analysis with ANSYS (kN)	Ultimate load by strength criteria (kN)	Gain in ultimate strength by ANSYS w.r.t. strength criteria (%)
BWFLC	75.60	70.048	7.925994	BWFLR	82.00	82.19	-0.23117
BWFMC	35.84	31.115	15.1856	BWFMR	44.00	37.17	18.37503
BWFSC	9.45	8.045	17.46426	BWFSR	13.32	8.90	49.66292
BWSLC	73.20	66.360	10.30741	BWSLR	83.70	82.19	1.837206
BWSMC	35.84	29.630	20.95849	BWSMR	44.20	37.17	18.9131
BWSSC	9.10	7.3380	24.01199	BWSSR	13.20	8.90	48.31461
CWSLC	58.50	-----	-----	CWSLR	68.30	-----	-----
CWSMC	31.50	-----	-----	CWSMR	35.60	-----	-----
CWSSC	7.8	-----	-----	CWSSR	10.30	-----	-----

4.8 CONCLUDING REMARKS

In this chapter, the numerical simulations were carried out for all the specimens using the general purpose finite element software ANSYS 6.0. All the elements were simulated with appropriate elements from the ANSYS 6.0 library. The results obtained for ultimate failure through numerical simulation are in agreement with those obtained by theoretical calculation based on strength criteria. The important observations as obtained from numerical simulation like load at first crack, load at yielding of steel, ultimate load were used as a guideline for the experimental investigation of the specimens. The detailed discussions about experimental investigation and interpretation of results of all the tested specimens have been furnished in next three chapters.

CHAPTER 5

EXPERIMENTAL STUDY ON BEAM-COLUMN JOINTS WITH BEAM WEAK IN FLEXURE

5.1 INTRODUCTION

This chapter describes the results of experimental investigation and interpretation of experimental results on beam-column joints with beam weak in flexure specimens. Total six specimens were made. Three control and three retrofitted of three sizes, namely full size, two-third and one-third scaled models were tested. The applied cyclic displacements to the specimens were also proportionately scaled. A constant axial load of 10% of gross capacity of the respective column was applied during the application of cyclic displacement at the time of testing. The recorded data were used to draw hysteresis loop, envelope curve, variation of stiffness and energy dissipation with respect to drift angle. Comparisons of test results for control and retrofitted specimens were made in term of all the above-mentioned parameters and conclusions were drawn regarding the benefit derived out of retrofitting. Finally, bi-logarithmic plot was drawn to explore the possible existence of size effect in terms of flexural strength. Further, efforts were made to correlate specimen sizes with cumulative energy dissipated per unit volume of joint, displacement ductility and flexural stress.

5.2 DISPLACEMENT HISTORY OF SPECIMENS

Cyclic displacement was applied to all the specimens with the help of hydraulic dynamic actuators. The typical displacement histories applied to specimens of three different sizes are shown in Fig. 5.1. Displacement controlled load with a frequency of 0.025Hz was applied to the test specimens. Three cycles of specific amplitude consisting of a push and a pull segment were repeated before the next increment in displacement was made. The first amplitude applied in full scaled models was ± 1.4 mm. This displacement level corresponds to appearance of first crack as per result of numerical analysis. This was

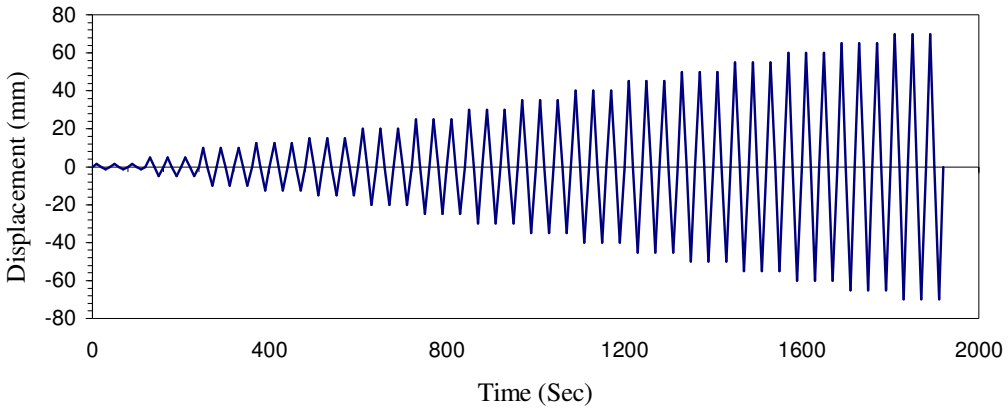

(a)

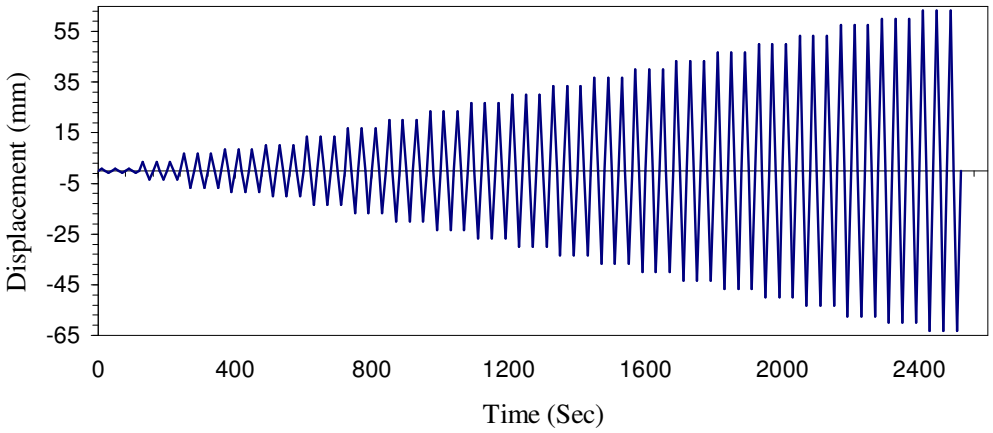

(b)

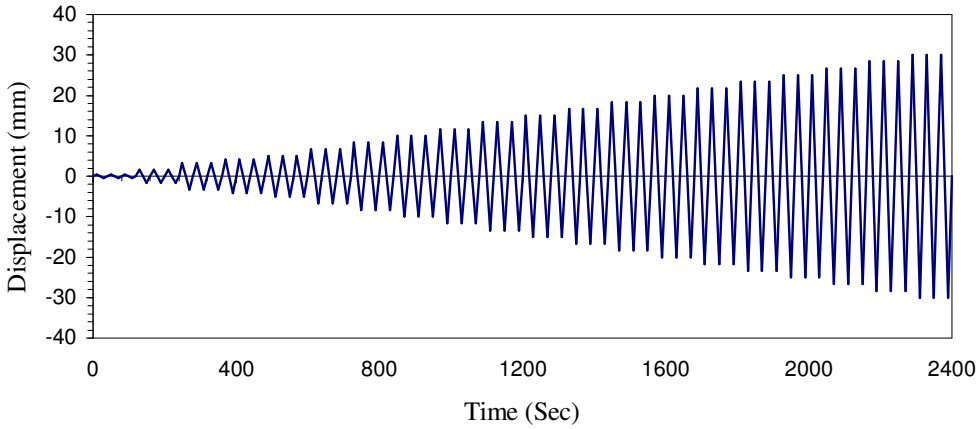

(c)

Fig. 5.1 Typical displacement history for: (a) full scaled, (b) two-third scaled (c) one-third scaled specimen

followed by displacement amplitude of ±5 mm, ±10 mm, ±12.5 mm ±15 mm and there after displacement amplitude increment of 5 mm was applied. Based on the prediction of numerical analysis the amplitude of 12.5 mm was chosen because at this displacement level yielding of steel was expected. Amplitude of the displacement histories were scaled down for two-third and one-third models. The typical displacement histories for scaled down specimens are shown in Fig. 5.1 (b) and (c). These displacements histories were applied for the retrofitted specimens also. However, control specimens were subjected to slightly less final displacement level as the failure occurred earlier compared to those of the retrofitted specimens.

5.3 TESTING OF LARGE SPECIMENS

The displacement history as shown in Fig. 5.1 (a) was applied to these specimens by a servo hydraulic dynamic actuator (MTS make) of capacity ±250 kN with maximum displacement amplitude of ±125 mm. The experiment was stopped for control specimen at a stage when the load came down in the range of 65-70% of the ultimate load carrying capacity. Similarly, the experiment on retrofitted specimen was also stopped at about the same magnitude of load at which experiment was stopped for control specimen.

5.3.1 Large Control Specimen

The test arrangement of large control specimen is shown in Fig. 5.2. A close view of the damaged area at the failure state of the specimen is shown in Fig. 5.3. The hysteretic response obtained by plotting the test data is presented in Fig. 5.4. Some of the important observations made during testing and analysis of the hysteresis loop are presented here.

The first flexural crack appeared in the beam part, very close to the beam-column joint at displacement amplitude of ±5mm. More cracks started to develop in the beam including the joint region as the amplitude was increased. It is observed from the hysteresis loop of Fig. 5.4 that the specimen attains the maximum load of 72.57 kN in the pull direction at

22nd cycle at a displacement of 30 mm. Similarly, the maximum load of 74.51 kN in the push direction is observed at 25th cycle at a displacement of 35 mm. The width of the first developed crack became wider to a considerable extent at ±40 mm amplitude. Spalling of concrete also started in the beam as well as in the joint region at this amplitude. Large pieces of concrete started spalling out with further widening of cracks at displacement amplitude of ±50 mm. Further, plastic hinge at the joint region got developed followed by the rotation of the beam-column joint. The experiment was stopped at displacement amplitude of ±65 mm at which the load came down to the desired level. The averages of peak loads in the push and pull direction in the first cycle

Fig. 5.2 BWFLC specimen at the starting of experiment

Fig. 5.3 BWFLC specimen at the end of testing

of each amplitude were calculated. The maximum load as obtained by such averaging was considered as Ultimate load carrying capacity of the specimen and it was found to be 73.285 kN for BWFLC specimen.

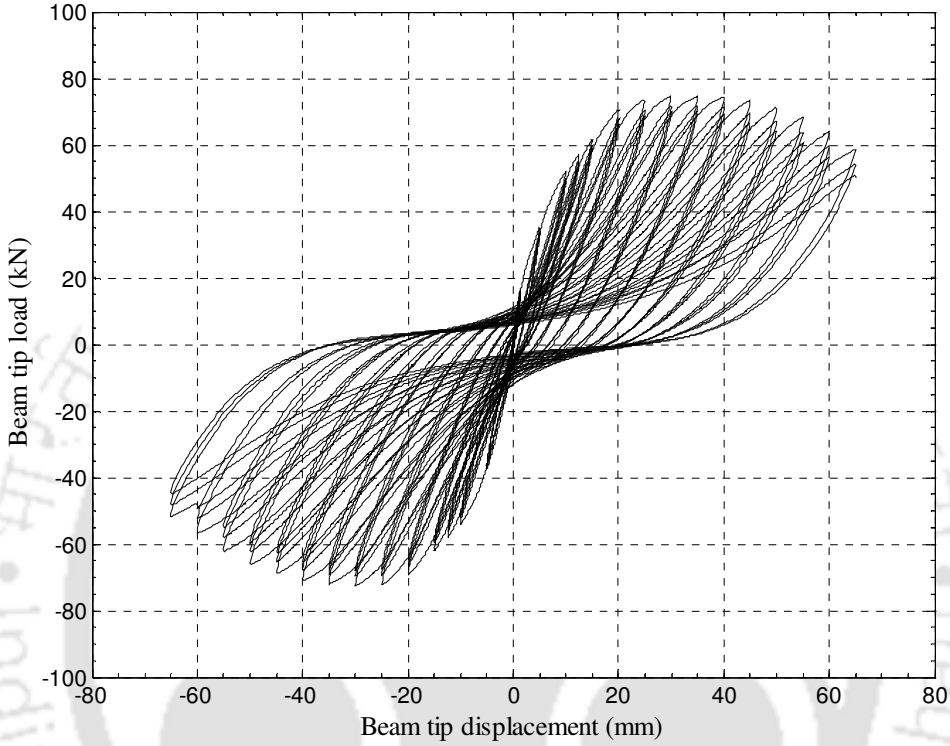

Fig. 5.4 Hysteretic response of BWFLC specimen

5.3.2 Large Retrofitted Specimen

This specimen was tested in an identical condition to that of control specimen. Fig. 5.5-5.7 show some of the important photographs at three different stages of the experiment. The hysteretic response obtained by plotting the test data is shown in Fig. 5.8.

The first rupture of GFRP sheet appeared in the beam-column joint marked *A* Fig.5.7 at a displacement amplitude of ± 10 mm. The first visible crack appeared in the concrete of the beam at a location between first strip of GFRP (in beam) and GFRP sheet provided at the joint at displacement amplitude of ± 15 mm. It is observed from Fig. 5.8 that the specimen attains the maximum load of 83.96 kN in the push direction at a displacement amplitude of 25 mm in 19th cycle. In the same cycle it reaches to maximum load of 70.37 kN in the pull direction also. It was noted that crack appeared in the column also at

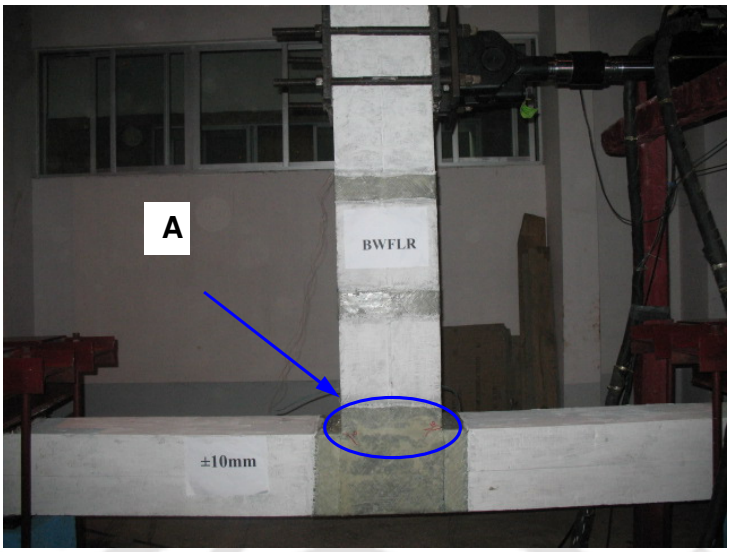

Fig. 5.5 Appearance of rupture in GFRP sheet at joint in BWFLR specimen

Fig. 5.6 Delimitation of FRP sheets near joint region in BWFLR specimen

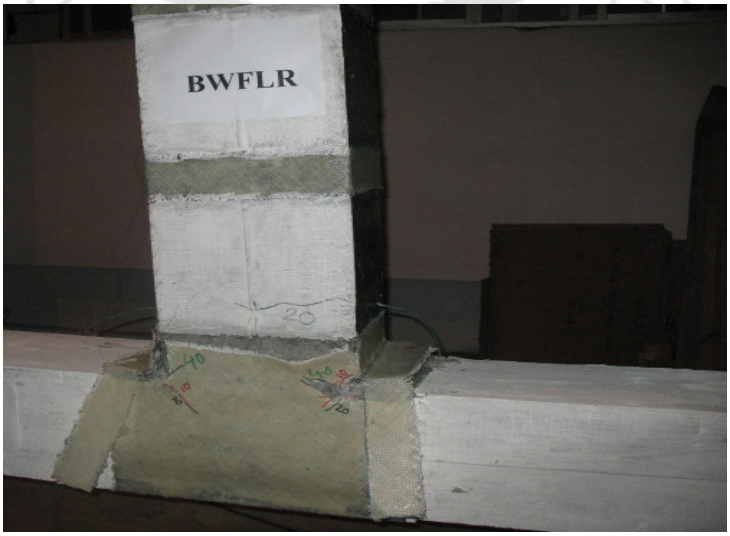

Fig. 5.7 BWFLR specimen at the end of test

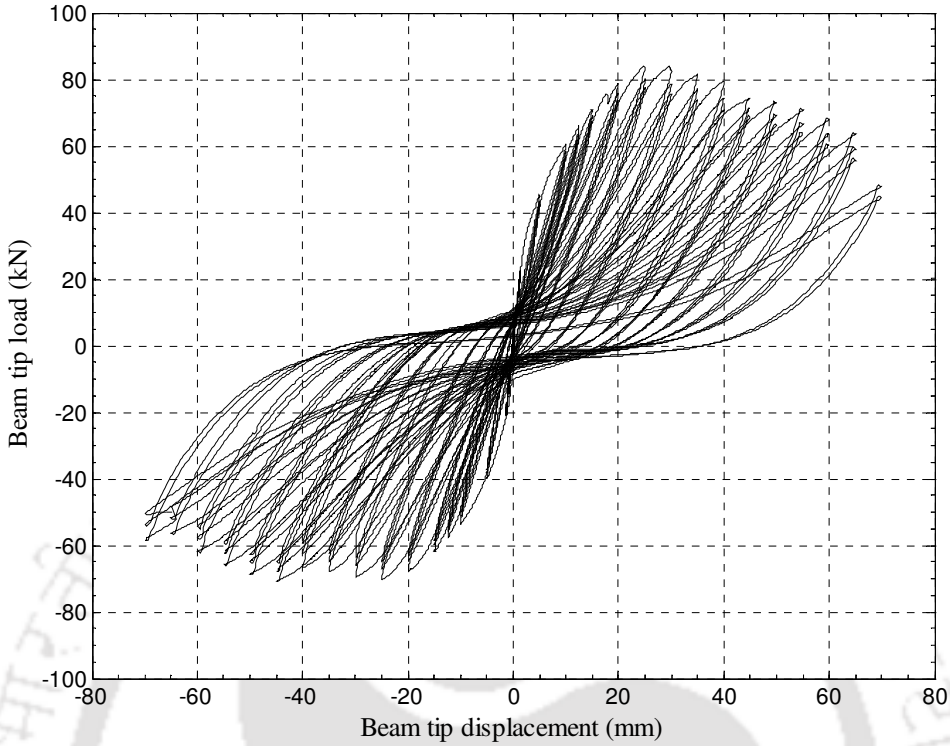

Fig. 5.8 Hysteretic response of BWFLR specimen

±40 mm amplitude. Spalling of concrete started with a loud sound at a displacement amplitude of ±45 mm. The sound was mainly due to the sudden rupture and delamination of GFRP as shown in Fig. 5.6. The rupture in GFRP sheet got widened to a considerable extent at ±50 mm amplitude. The GFRP sheet in the joint region got separated into distinct two pieces at ±65 mm displacement amplitude. Further, the beam started to rotate about the beam-column joint due to the development of plastic hinge in the vicinity of the joint region. The GFRP was intact without any breakage and delamination at the exterior face of the beam-column joint. There was no sign of distress in the GFRP sheet in the exterior face of the joint even up to the end of the test at a displacement of ±70 mm amplitude. The specimen at the end of testing is shown in Fig. 5.7. The ultimate load carrying capacity of BWFLR specimen was found to be 77.165 kN.

5.3.3 Comparison of Test Results of Control and Retrofitted Large Specimens

The hysteresis loops presented in Fig. 5.4 and 5.8 show that the load is the highest in its first cycle out of three cycles for a particular displacement amplitude. Therefore, peak values of the load corresponding to first cycle for each of the displacement amplitude were used to plot envelope curve. The envelope curve of hysteresis loop for control as well as retrofitted specimen is shown in Fig. 5.9. It can be observed that the envelope curve for the retrofitted specimen shows little improvement in ultimate load carrying capacity in the push direction, though in the pull direction the same is almost similar. The percentage gain in ultimate load carrying capacity due to retrofitting was found to be 5.18%. The envelope curves reflect nonlinear behaviour of the tested beam-column joints. The secant stiffness corresponding to a specified displacement was considered as stiffness of the assemblage. The procedure for calculation of stiffness is shown in Fig. 5.10. Two points A and A′ in positive and negative direction of the envelope curve for a particular amplitude are joined by a straight line. The straight line so obtained by joining both the points is a secant to the envelope curve. The slope of this straight line is the stiffness (K) of the joint assemblage corresponding to the particular amplitude and this is calculated by the following expression recommended by Naeim and Kelly [1999]:

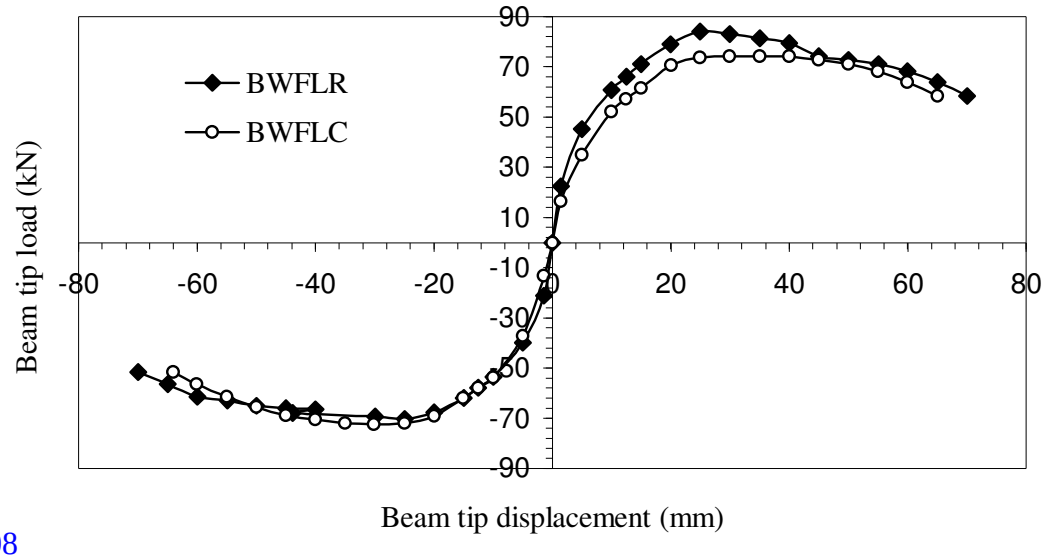

Fig. 5.9 Envelopes of hysteresis loops for BWFLC and BWFLR specimens

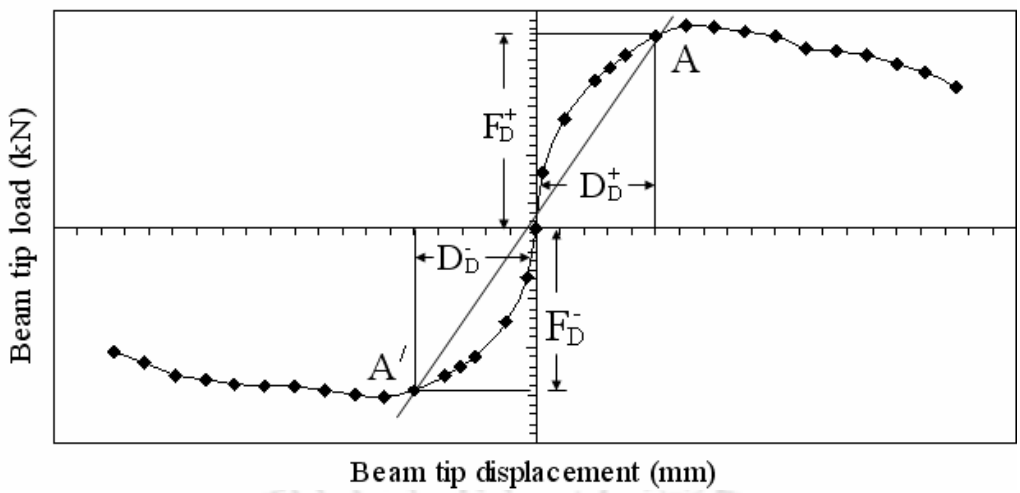

Fig. 5.10 Determination of secant stiffness from envelope curve

$$K = \frac{F_D^+ - F_D^-}{D_D^+ - D_D^-} \tag{5.1}$$

Where D_D^+ and D_D^- in Eq. 5.1 are the *X* co-ordinates of A and A′ respectively, F_D^+ and F_D^- are the corresponding *Y* co-ordinates in envelope curve (Fig. 5.10).

Drift angle is defined as the ratio of beam tip displacement to the length of the beam. Drift obtained by horizontally displacing the beam ends are equivalent to the inter storey drift angle of a frame structure subjected to lateral loads. The stiffness was plotted against the drift angle in Fig. 5.11. The stiffness of BWFLR specimen is more than that of BWFLC specimen corresponding to any drift angle at the initial stage of the curve. However, stiffness in both the cases are almost same after rupture or failure of FRP. The initial stiffness for retrofitted specimen corresponding to the first applied amplitude of ± 1.4 mm (drift angle 0.103%) is 15.72 kN/mm, while that for control specimen is 10.68 kN/mm. Thus, the gain in initial stiffness was found to be 47.2% due to retrofitting for the case under study. Strengthening by FRP contributed to increase in the moment of inertia of the beam, which was the reason for gain in initial stiffness. At the second amplitude of ± 5 mm (drift angle of 0.37%) the stiffness of control specimen got reduced by 32.5%. At the same drift angle, the reduction in stiffness for retrofitted specimen was found to be 46%. Thus, the retrofitted specimen showed faster degradation of stiffness at the initial

stage.

The ability of a structural element to resist an earthquake depends to a large extent on its capacity to dissipate the energy. The area of hysteresis loop is a measure of the energy dissipated. The cumulative energy dissipated at a particular amplitude was calculated by summing up the energy dissipated in all the preceding cycles including that amplitude. The plot of energy dissipation versus drift angle for control and retrofitted specimens are shown in Fig. 5.12. The figure shows that cumulative energy dissipated by retrofitted specimen is higher than that of control specimen at every drift angle. The gain in cumulative energy dissipation at failure stage due to retrofitting is 26.03%. The increase in stiffness attracted more load at any drift angle for the retrofitted specimen in comparison to that of control specimen. Thus, the total area enclosed by the plot of beam tip load versus beam tip displacement was more for retrofitted specimen than that of control specimen. This was the reason for gain in cumulative energy dissipation due to retrofitting and hence the retrofitted structure has the better capability to resist an earthquake.

5.4 TESTING OF MEDIUM SPECIMENS

A displacement controlled loading cycle shown in Fig. 5.1(b) was applied to these specimens by a servo hydraulic dynamic actuator of capacity ± 250 kN. The experiment was stopped when percentage reduction of load of similar order as that in the case of large specimen was attained.

5.4.1 Testing of Medium Control Specimen

Testing arrangement of this specimen is shown in Fig. 5.13. The condition of the specimen at end of testing is shown in Fig. 5.14. The hysteretic response obtained by plotting the test data is shown in Fig. 5.15. Some of the important observations made during testing and analysis of the hysteresis loop are stated here. There was no crack

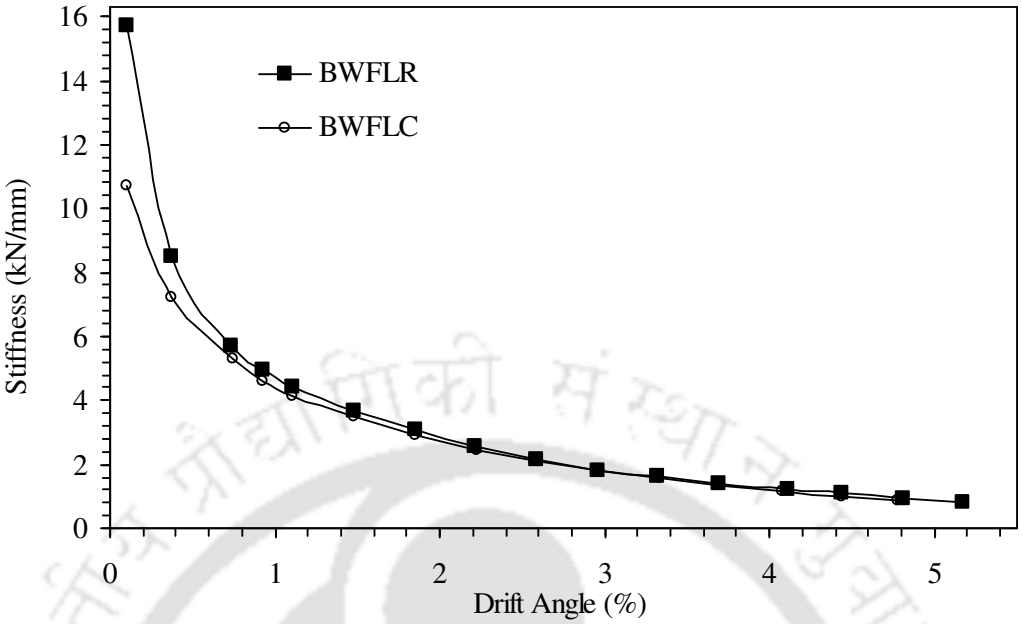

Fig. 5.11 Stiffness versus drift angle plot for BWFLC and BWFLR specimens

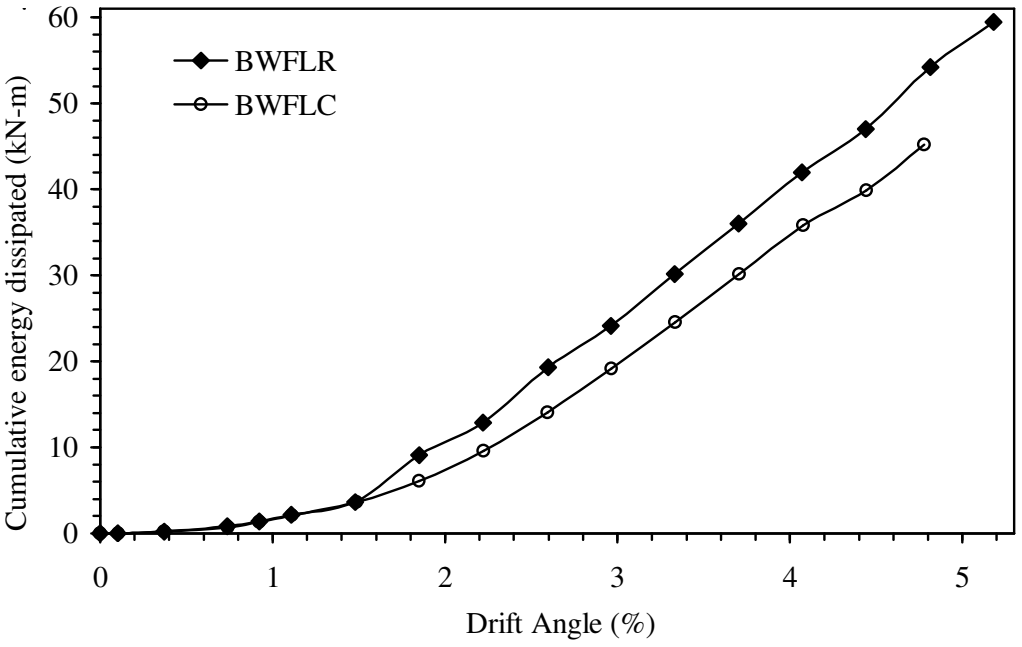

Fig. 5.12 Cumulative energy dissipated by BWFLC and BWFLR specimens

observed up to the applied displacement amplitude of ±3.33 mm. As soon as the next amplitude of ±6.67 mm was applied, the first flexural crack was observed in the beam part. Just after the appearance of the first crack, 2nd and 3rd crack also appeared at the

junction of the joint in the consecutive cycles of the same amplitude. All these developed cracks are shown in Fig. 5.13. The load reached to the maximum value of 34.78 kN in the push direction at 19th cycle at a displacement of 16.67 mm. In the same displacement amplitude, opening of crack started and gradually continued from one end of the joint to the other end. The load attained the maximum value of 31.18 kN in the pull direction at 28th cycle at a displacement of 26.67 mm. The cracks started to get widened at this amplitude of displacement. Spalling of concrete was also observed. The opening and closing of cracks became distinct and many cracks started to become wider at amplitude ±30 mm. Cracks appeared in the column face of beam-column joint at ±53.33 mm amplitude and the experiment was finally stopped. The ultimate load carrying capacity of

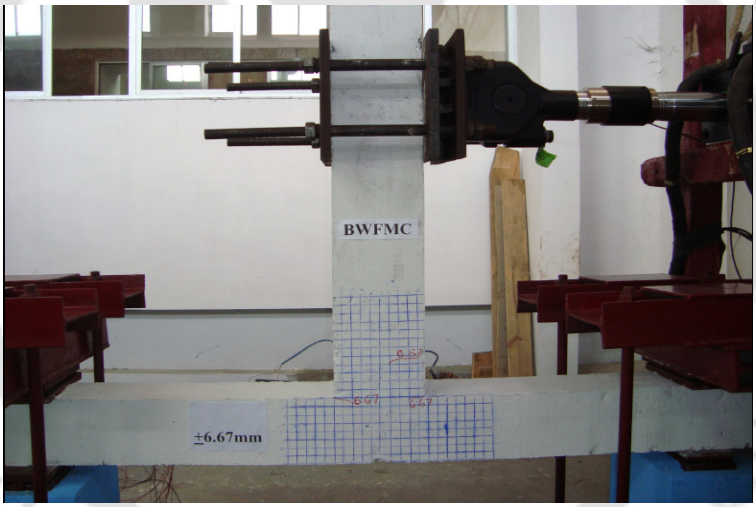

Fig. 5.13 Appearance of first cracks in BWFMC specimen

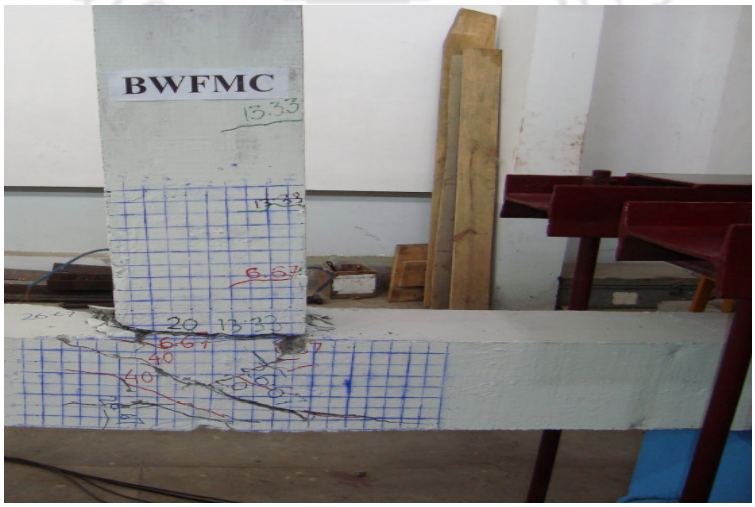

Fig. 5.14 BWFMC specimen at the end of the test

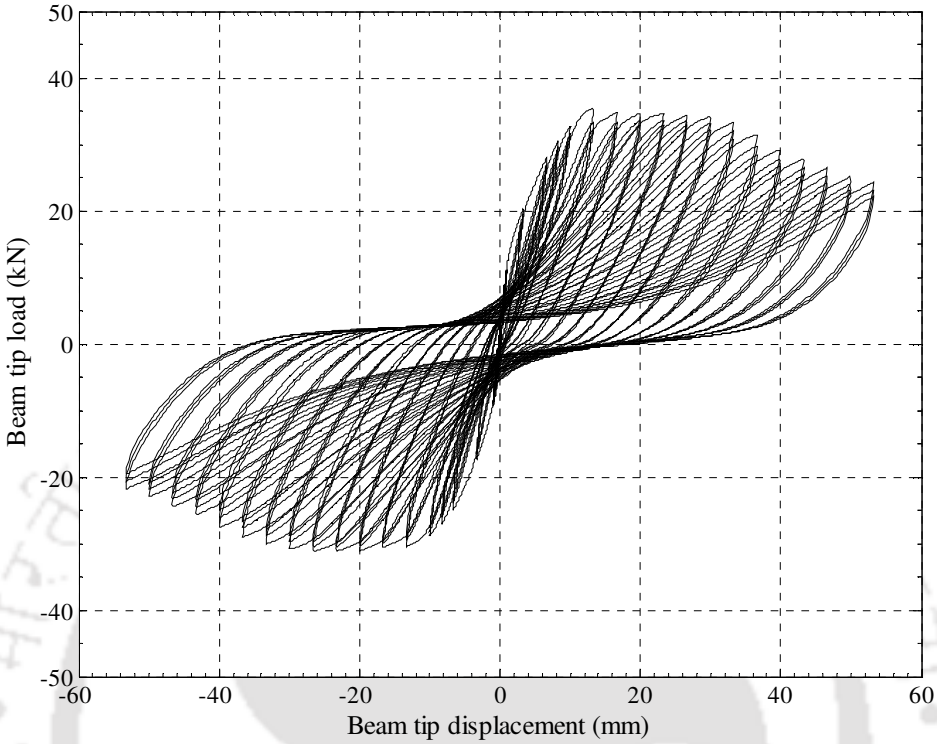

Fig. 5.15 Hysteretic response of BWFMC specimen

the BWFMC specimen was found to be 32.91 kN.

5.5.2 Medium Retrofitted Specimen

This specimen was tested an in identical condition to that of control specimen. Some of the photographs at different stages of testing are shown in Fig. 5.16-5.18. The hysteretic response obtained by plotting the test data is shown in Fig. 5.19. The following important observations were made during testing and analysis of the hysteresis loop.

The first visible crack appeared in the beam in zone *A* marked in Fig, 5.16 (where there was no FRP provided) at ± 6.67 mm amplitude. At the same amplitude, three more cracks appeared (Fig. 5.16) in the beam. The load reached to 42.02 kN at 19^{th} cycle at a displacement of ± 13.33 mm, which was maximum in the push direction and in the same cycle it also reached to maximum load of 39.79 kN in the pull direction. Rupture in GFRP

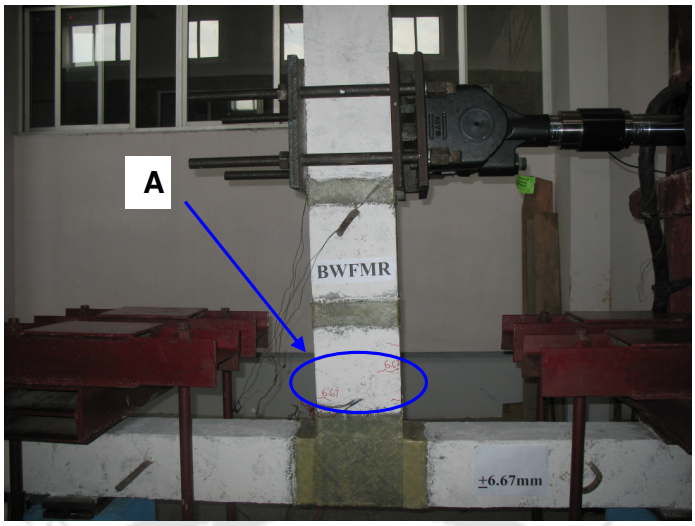

Fig. 5.16 Appearance of first flexural crack in BWFMR specimen

Fig. 5.17 Appearance of rupture in GFRP sheet for BWFMR specimen

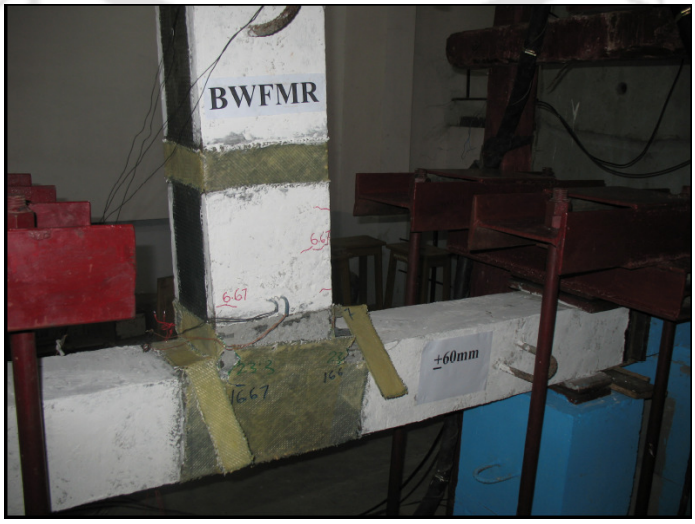

Fig. 5.18 BWFMR specimen at the end of the test

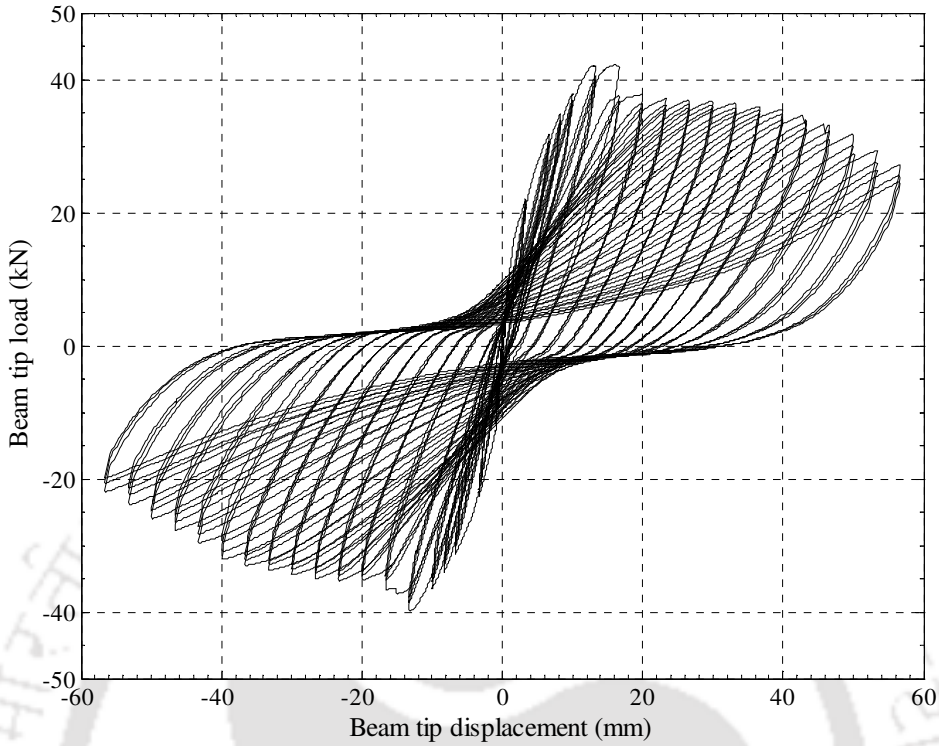

Fig. 5.19 Hysteretic response of BWFMR specimen

sheet appeared just at the contact point of beam with joint at displacement amplitude of ± 16.67 mm. In further cycles of the same amplitude, GFRP sheets from beam delaminated with total opening. GFRP sheet in column started delamination with visibility of cracks in the concrete at ± 26.67 mm amplitude in a location below the GFRP sheet. Further delamination of GFRP sheet was noticed in the beam at ± 30 mm amplitude. A noticeable crack appeared in one side of column beyond the joint, which was not reinforced with FRP at ± 40 mm amplitude. Spalling of concrete started followed by isolation of first strip of GFRP provided in the beam from one side with a loud sound at ± 46.67 mm amplitude. The beam started to rotate at ± 50 mm amplitude due to probable formation of plastic hinge. Major portion of GFRP sheet at the joint got disconnected with a loud sound at ± 56.67 mm amplitude. Finally, the experiment was stopped noting the degradation in loading. The ultimate load carrying capacity of BWFMR specimen was found as 40.92 kN.

5.4.3 Comparison of Test Results of Control and Retrofitted Medium Specimens

Envelopes of hysteresis loops for control as well as retrofitted specimen is shown in Fig. 5.20. It can be observed that the envelope curve of hysteresis loop for the retrofitted specimen shows higher load carrying capacity than the control specimen both in the push and pull direction. The percentage gain in ultimate load carrying capacity due to retrofitting was 20.6%. The plot of stiffness for BWFMC and BWFMR specimens is shown in Fig. 5.21. The stiffness of BWFLR specimen is more than that of BWFLC specimen corresponding to any drift at the initial stage of the curve. The initial stiffness of the retrofitted specimen is 11.58 kN/mm, while that of control specimen it is 10.84 kN/mm. Thus, the gain in initial stiffness is 6.82% due to retrofitting. The stiffness of control specimen got reduced by 47.9% at drift angle of 0.37%, which corresponds to the second amplitude of displacement. The reduction in stiffness for retrofitted specimen was found to be 42.2% at the same drift angle. Thus, the degradation rate of stiffness is almost same for both the specimens up to the drift angle of 0.37%. However, in the rest part of the curve, retrofitted specimen reflects faster degradation.

The plot of cumulative energy dissipation for control and retrofitted specimens is shown in Fig. 5.22. The figure shows that the cumulative energy dissipated by retrofitted specimen is higher than that of control specimen at every drift angle. The gain in energy dissipation due to retrofitting is 28.16% at failure stage.

5.5 TESTING OF SMALL SPECIMENS

The displacement history shown in Fig. 5.1(c) was applied to these specimens by a servo hydraulic dynamic actuator of capacity ± 100 kN with maximum displacement amplitude of ± 125 mm. The experiment was stopped for control specimen when the load came down to the extent of 65-70% of the ultimate load carrying capacity of the specimen. Similarly, the experiment on retrofitted specimen was also stopped at about the same magnitude of load at which experiment was stopped for control specimen.

5.5.1 Small Control Specimen

The testing arrangement of this specimen is shown in Fig. 5.23. The hysteresis loop obtained by plotting the test data is shown in Fig. 5.25. The following observations were made during testing and analysis of the hysteresis loop.

The first flexural crack was observed in the beam near the junction of the joint at displacement amplitude of ± 3.33 mm. The second crack appeared in the beam-column joint at amplitude of ± 5 mm. The load reached to the maximum value of 8.269 kN in the

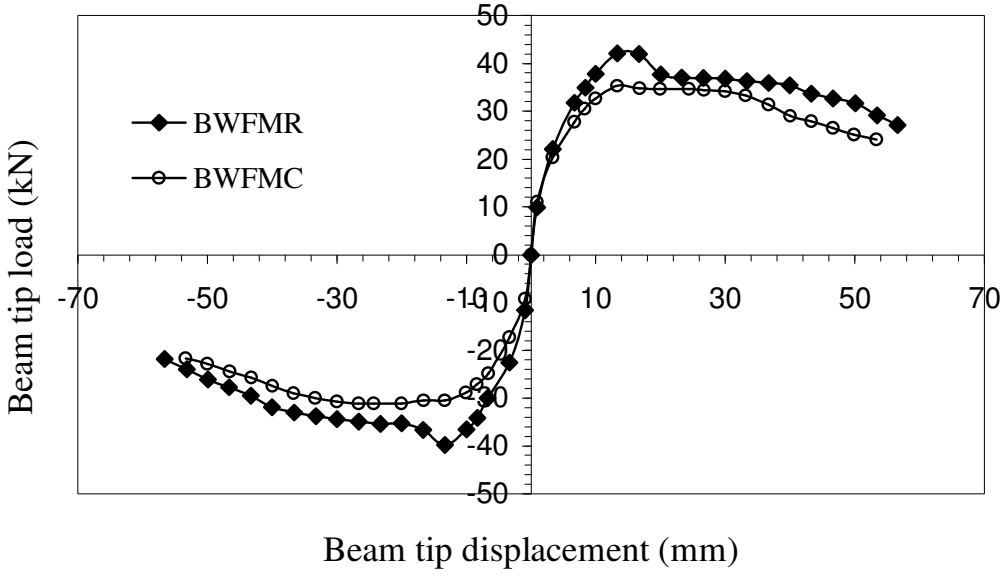

Fig. 5.20 Envelopes of hysteresis loops for BWFMC and BWFMR specimens

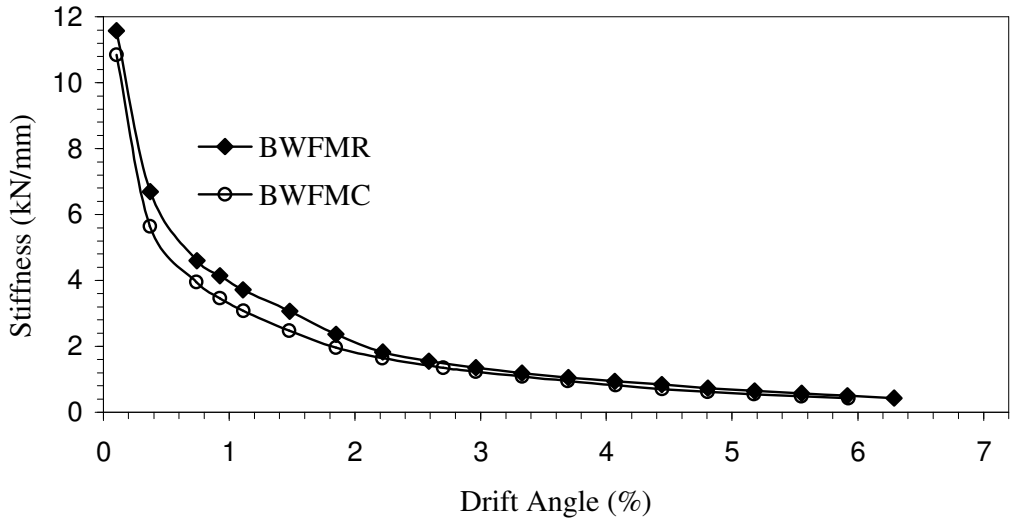

Fig. 5.21 Stiffness versus drift angle plot for BWFMC and BWFMR specimens

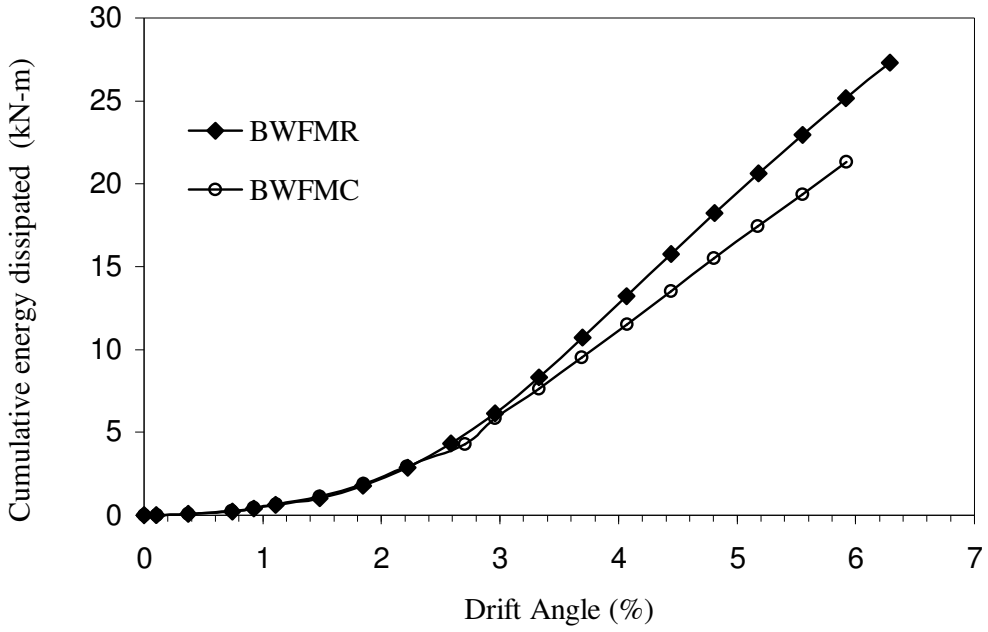

Fig. 5.22 Cumulative energy dissipated by BWFMC and BWFMR specimens

push direction at 22nd cycle at a displacement of 10 mm. Similarly, the load reached to the maximum value of 9.579 kN in the pull direction at 28th cycle at a displacement of 13.33 mm. A piece of concrete got separated from the right side of the joint at ± 16.67 mm amplitude and immediately a big crack got developed near that portion. The beam could be observed to rotate at the beam-column joint due to the development of plastic hinge in the joint region at amplitude of ± 20 mm. More spalling of concrete started at ± 23.33 mm displacement amplitude. Finally, at displacement amplitude of ± 28.33 mm, the experiment was stopped noting the degradation in loading (Fig. 5.24). The ultimate load carrying capacity of the BWFSC specimen was found to be 8.83 kN.

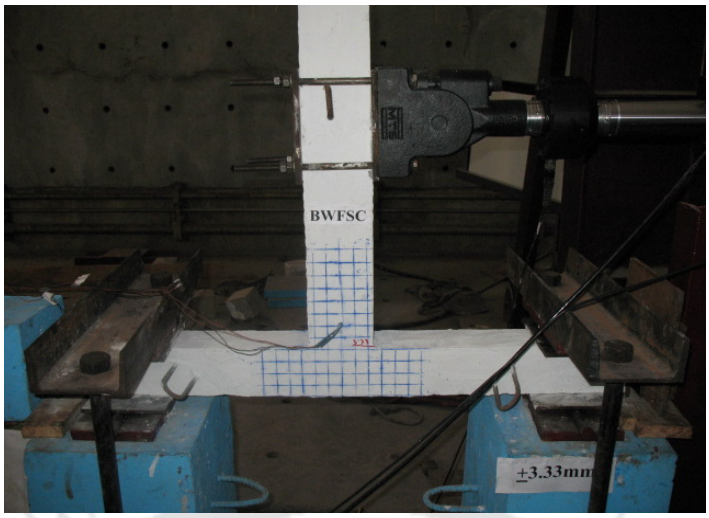

Fig. 5.23 First flexural crack in BWFSC specimen

Fig. 5.24 BWFSC specimen at the end of the test

5.5.2 Small Retrofitted Specimen

This specimen was tested in a similar manner to that of control specimen. Fig. 5.26 shows the testing arrangement and Fig. 5.27 shows the specimen at the end of test. The hysteretic response obtained by plotting the test data is shown in Fig. 5.28. The following important observations were made during testing and analysis of the hysteresis loop.

The first visible crack appeared in the beam at ± 10.0 mm amplitude. The load reached to the maximum value of 10.87 kN in the pull direction at 28th cycle at a displacement of 13.33 mm. The load also reached to maximum load of 11.0 kN in the push direction at 31st cycle at a displacement of 15 mm. Rupture in GFRP sheet in beam-column joint

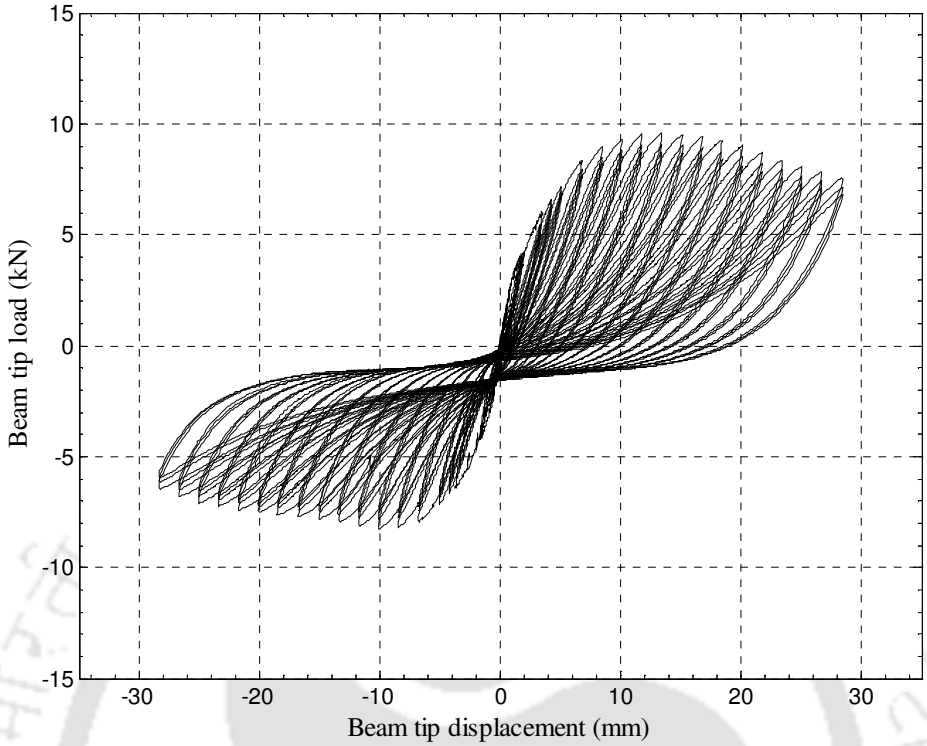

Fig. 5.25 Hysteretic response of BWFSC specimen

appeared just at the contact point of beam with joint at displacement amplitude of ± 21.67 mm. In further cycles of the same amplitude, GFRP strips from beam delaminated with total opening. A crack appeared in the column at a location marked *B* in Fig. 5.27 at ± 30.0 mm amplitude. The beam was observed to rotate at the beam-column joint due to development of plastic hinge in the vicinity of the joint region. At this level the experiment was finally stopped. The ultimate load carrying capacity of BWFSR specimen was found to be 10.915 kN.

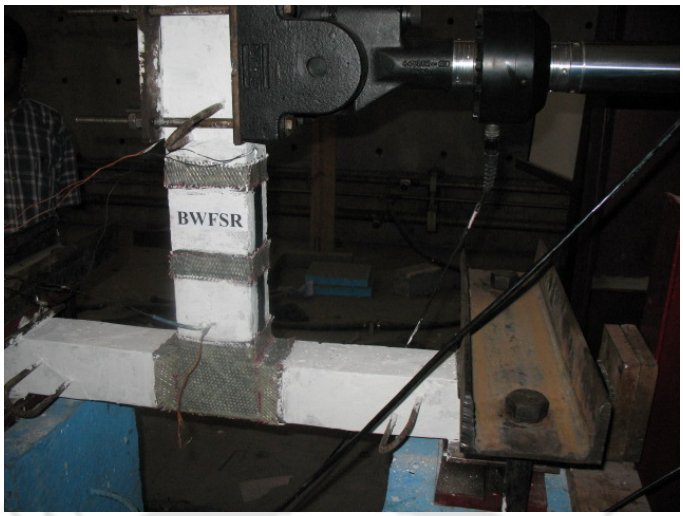

Fig. 5.26 Testing arrangement of BWFSR specimen

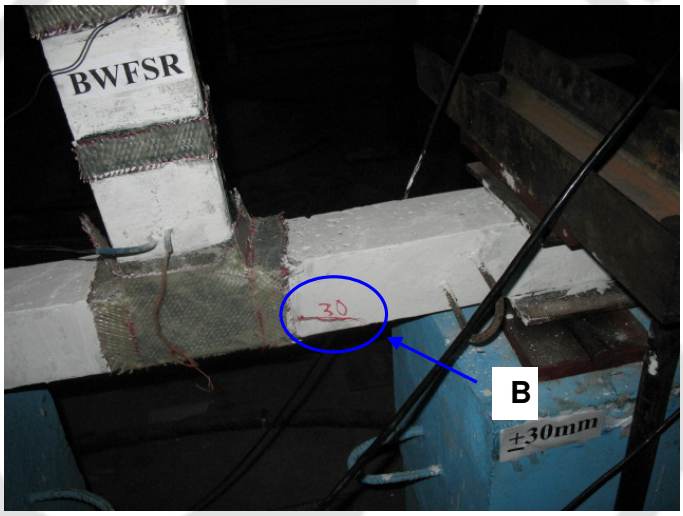

Fig. 5.27 BWFSR specimen at the end of the test

5.5.3 Comparison of Test Results of Control and Retrofitted Small Specimen

The envelope curve of hysteresis loops for control as well as retrofitted specimen is shown in Fig. 5.29. It can be observed in the envelope curve that the retrofitted specimen shows higher load carrying capacity than that of the control specimen both in the push and pull direction. The percentage gain in ultimate load carrying capacity due to retrofitting was found as 23.6%.

The variation of stiffness for BWFSC and BWFSR specimens is shown in Fig. 5.30. The stiffness of BWFSR specimen is more than that of BWFSC specimen, except the last part of the curve. The initial stiffness for retrofitted specimen is 5.22 kN/mm, while that of

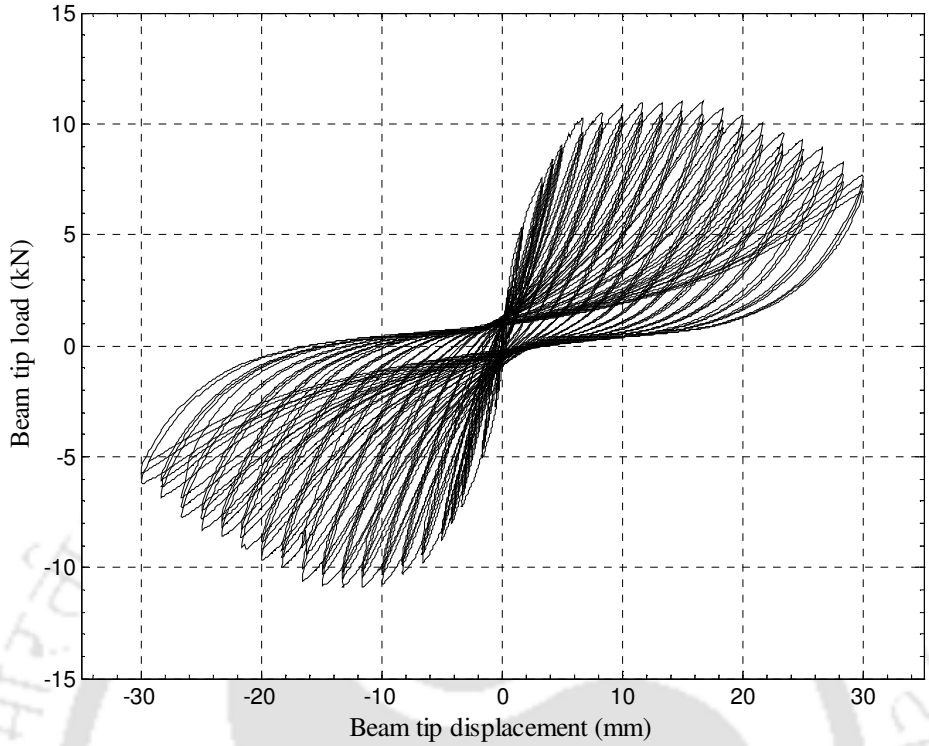

Fig. 5.28 Hysteretic response of BWFSR specimen

control specimen is 3.98 kN/mm. Therefore, the gain in initial stiffness is 31.15% due to retrofitting. At the drift angle of 0.37%, the stiffness of control specimen got reduced by 35.9%. At the same drift angle, the reduction in stiffness for retrofitted specimen was found to be 40.6%. Thus, the retrofitted specimen showed faster degradation of stiffness.

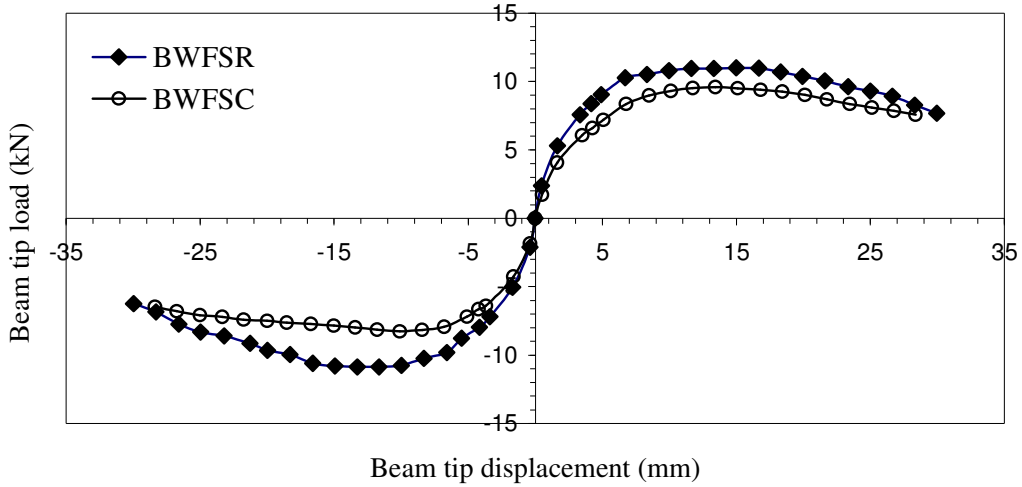

Fig. 5.29 Envelopes of hysteretic loops for BWFSC and BWFSR specimens

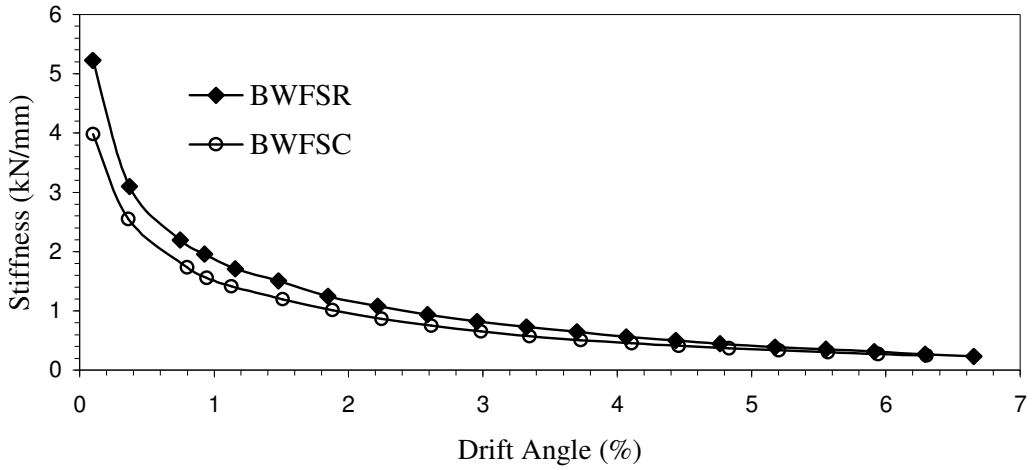

Fig. 5.30 Stiffness versus drift angle plot for BWFSC and BWFSR specimens

Fig. 5.31 shows the cumulative energy dissipation curve for control and retrofitted specimens. The figure shows that the cumulative energy dissipated by retrofitted specimen is higher than that of control specimen at every drift angle. The gain in energy dissipation due to retrofitting is 33.08% at failure stage .

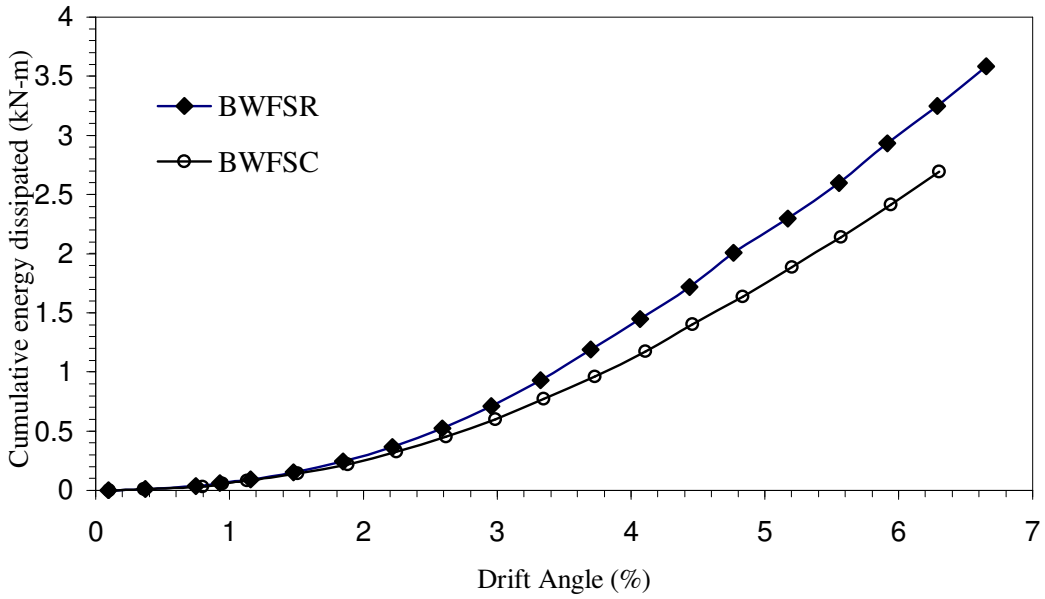

Fig. 5.31 Cumulative energy dissipated by BWFSC and BWFSR specimens

5.6 INTERPRETATION OF RESULTS TO EXPLORE THE EXISTANCE OF SIZE EFFECT

The results obtained by testing the specimens were used to draw bi-logarithmic plot to explore the possibility of existence of size effect for both control and retrofitted specimens. Further, the percentage gain in ultimate load carrying capacity due to retrofitting was correlated with size of the specimens. Similarly, the enhancement in displacement ductility was also correlated with size of the tested specimen. To compare the energy dissipation of specimens having different sizes of beam-column joints, a parameter *energy dissipation per unit volume of joint* (e_N) was introduced. The volume which is common to both beam and column in a sub-assemblage is considered as the volume of a joint. Variation of this parameter e_N was correlated with the size of the specimen at different drift angles. Both retrofitted as well as control specimen were considered for this plotting. Finally, the variation of relative deflection versus stress were also correlated with size of the specimens.

5.6.1 Bi-logarithmic Plot

The failure mode of both control and retrofitted specimens under consideration in this chapter was in flexure. Hence, ultimate bending stress denoted by σ_{N_U} for all the specimens were calculated. The calculation of bending stress is presented in Appendix-C. Using σ_{N_U} , bi-logarithmic plots were drawn for both control and retrofitted specimens. For the purpose of statistical regression of data, the size effect law proposed by Bazˇant [Bazˇant and Planas, 1998] was used. This law can be expressed as

$$\sigma_{N_U} = \frac{Bf_t'}{\sqrt{1 + D/D_0}} \tag{5.1}$$

The unknown constants B and D_0 were determined by statistical regression analysis. The value of tensile strength of concrete, f_t' was adopted as $2.504\ \text{N/mm}^2$, which was

calculated as per IS: 456 [2000]. A linear regression was achieved by Eq. (5.1) as follows:

Squaring Eq. 5.1 and rearranging we get

$$\left(\frac{f_t'}{\sigma_{N_U}}\right)^2 = \frac{D}{D_0 B^2} + \frac{1}{B^2} \tag{5.2}$$

This equation is in the form :

$$Y = AX + C \tag{5.3}$$

Where,

$$Y = \left(\frac{f_t'}{\sigma_{N_U}}\right)^2 \text{ and } X = D \tag{5.4}$$

$$A = \frac{1}{D_0 B^2},\ C = \frac{1}{B^2} \tag{5.5}$$

The values of A and C thus obtained was substituted in Eq. (5.5) to find the value of D_0 and B as $D_0 = \frac{C}{A}$ and $B = \frac{1}{\sqrt{C}}$.

The calculated value of bending stress and other parameters necessary to carry out regression analysis and to draw bi-logarithmic plot for both control as well as retrofitted cases are furnished in the Table 5.1. The typical result of regression analysis for control specimens is shown in Fig. 5.32. From this figure, the value of B and D_0 were found to be 6.25 and 1280 respectively. Using these values, the bi-logarithmic plot was drawn with Log (D/D_0) in the X axis and $Log(\sigma_{N_U} / Bf_t')$ in the Y axis as shown in Fig. 5.33. It is observed from the plot that it follows a horizontal line at the initial part, indicating no size effect. The curve approaches a straight line with slope of about -1/2 towards the end. In the intermediate zone there is a smooth curved transitional part. Thus, it can be concluded that the plot shows presence of size effect in accordance with Bazˇant's size effect law. Similarly, the value of B and D_0 was found as 9.2 and 236 respectively for retrofitted specimens. The bi-logarithmic plot for retrofitted specimens is shown in Fig. 5.34. This plot also shows presence of significant size effect and follows Bazˇant's size effect law.

Table 5.1 Parameters for bi-logarithmic plotting

Type of specimen	Name of specimen	Bending stress, σ_{N_U} (N/mm^2)	Depth of specimen, D (mm)	$\left(\frac{f_t'}{\sigma_{N_U}}\right)^2$	Log (D/Do)	$Log(\sigma_{N_U} / Bf_t')$
Control	BWFSC	15.017	120	0.027804	-1.02803	-0.01793
	BWFMC	14.530	240	0.029699	-0.72700	-0.03225
	BWFLC	13.970	360	0.032127	-0.55091	-0.04932
Retrofitted	BWFSR	18.510	120	0.018300	-0.29373	-0.09502
	BWFMR	17.510	240	0.020450	0.00729	-0.11914
	BWFLR	14.670	360	0.029135	0.18339	-0.19599

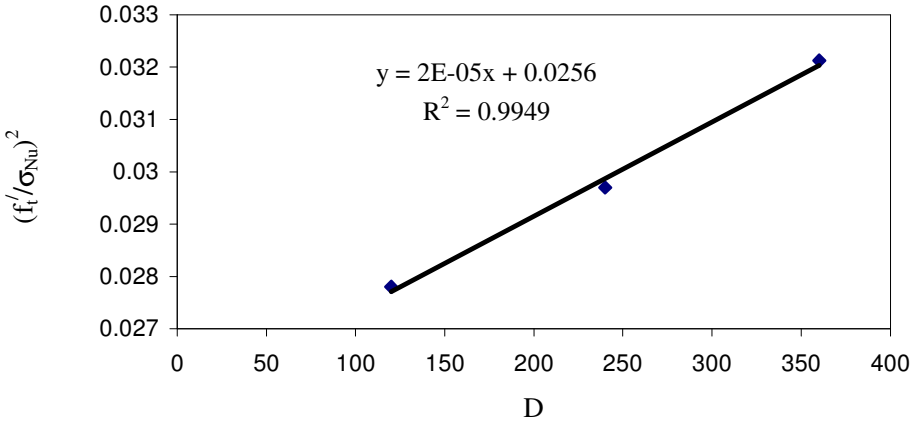

Fig. 5.32 Typical regression plot for control specimens

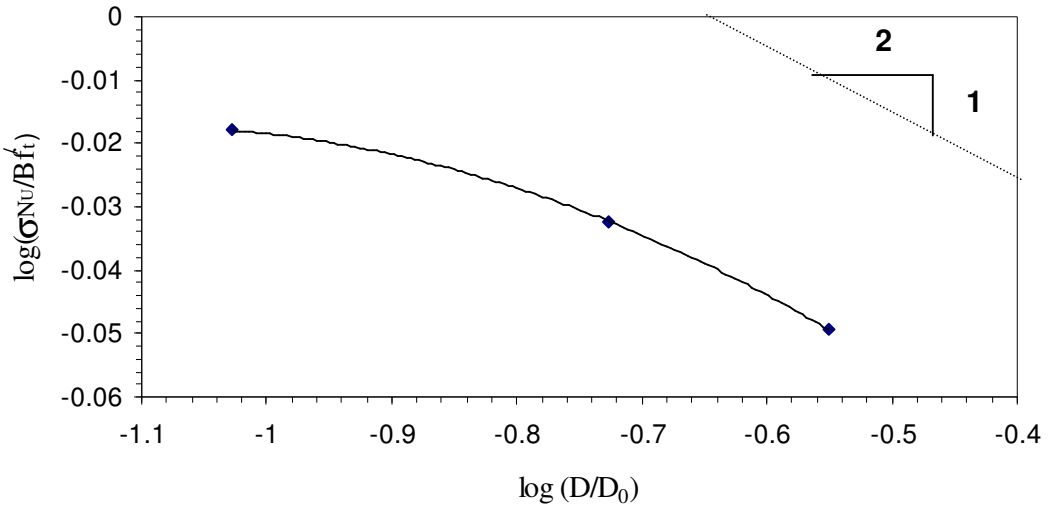

Fig. 5.33 Bi-logarithmic plot for beam weak in flexure : control specimens

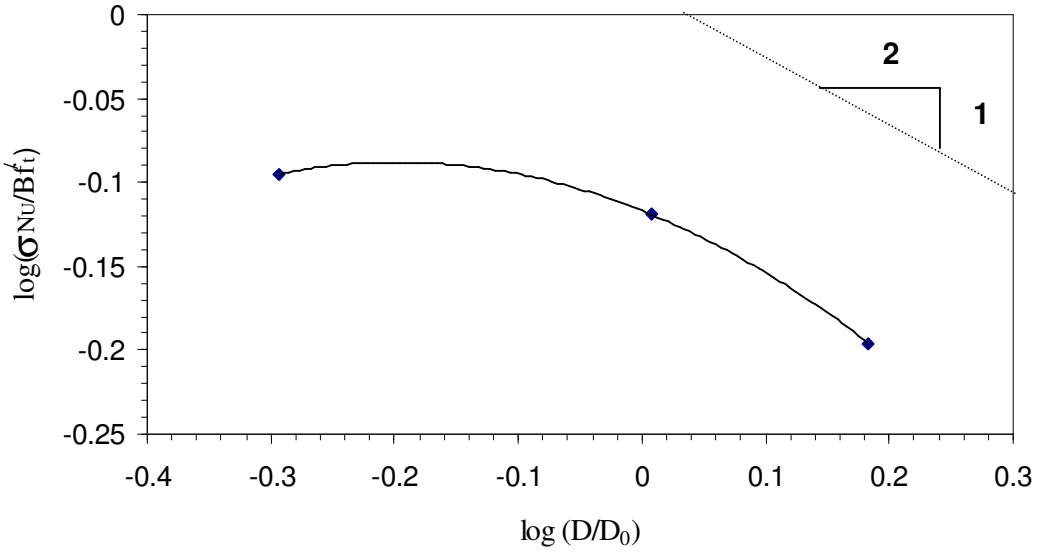

Fig. 5.34 Bi-logarithmic plot for beam weak in flexure : retrofitted specimens

Further, the slope of the bi-logarithmic plot towards the end of the curve for control specimens is found less in comparison to that of retrofitted specimens. The slope of the bi-logarithmic plot for retrofitted specimens is found very close to -1/2. Thus, the observed size effect is more pronounced in case of retrofitted specimens than control specimens.

5.6.2 Size Effect on Gain in Ultimate Strength due to Retrofitting

The average of maximum load in push and pull direction recorded in first cycle of each amplitude of displacements was calculated. The maximum of all the average values of load was designated as the ultimate load carrying capacity of a specimen. The percentage gain in ultimate load carrying capacity of retrofitted specimens with respect to control specimen for all sizes was calculated. The variation of this gain is presented in Fig. 5.35. It is observed that this parameter vary from 5.1% for large specimen to 23.6% for small specimen. This clearly indicates that the gain in strength increases as the specimen size decreases supporting the size effect principle.

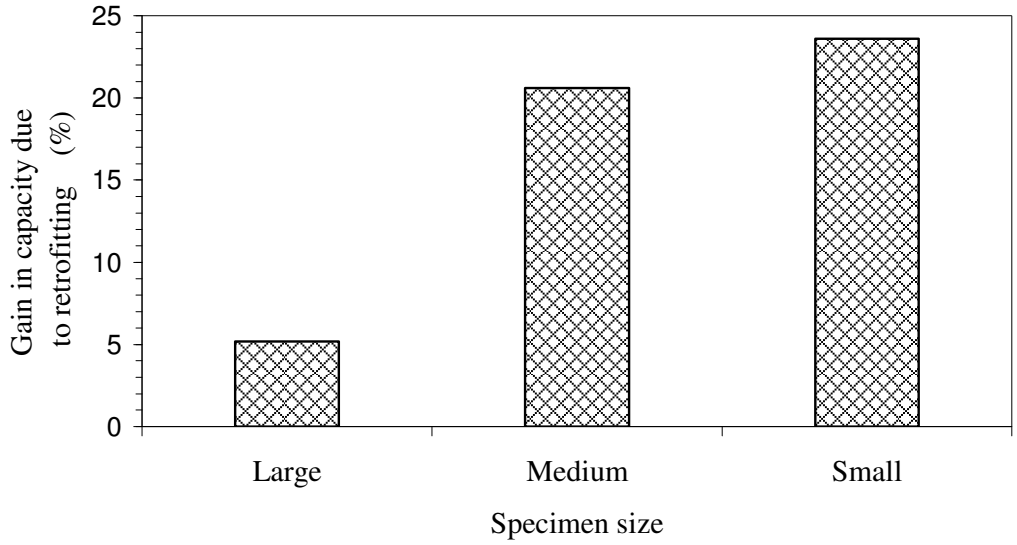

Fig. 5.35 Plot of percentage gain in ultimate load carrying capacity due to retrofitting

5.6.3 Size Effect on Displacement Ductility of Specimens

The displacement ductility for all the specimens was calculated from the respective envelope curve as per the procedure proposed by Shannag *et al.* [2005], which is explained in Fig. 5.36. As shown in the figure, the yield displacement was calculated as the point of intersection between two straight lines drawn in the envelope curve. The first line was obtained by joining the origin and 50% of ultimate load capacity point on positive and negative sides of the envelope curve, while the second line was obtained by

drawing a horizontal line through the 80% of ultimate load capacity point on either side. The average value of yield displacement obtained from both positive and negative direction was calculated. In the figure, *dy1* and *dy2* represent the yield displacement in positive and negative direction on the envelope curve respectively. Horizontal lines drawn through the 80% of ultimate load capacity point on positive and negative side intersect the envelope curve at far end at points *B1* and *B2*. The average of abscissae of these two points (denoted by *dm1* and *dm2* in figure) was taken as maximum displacement. The displacement ductility was calculated as the ratio of maximum displacement to the yield displacement.

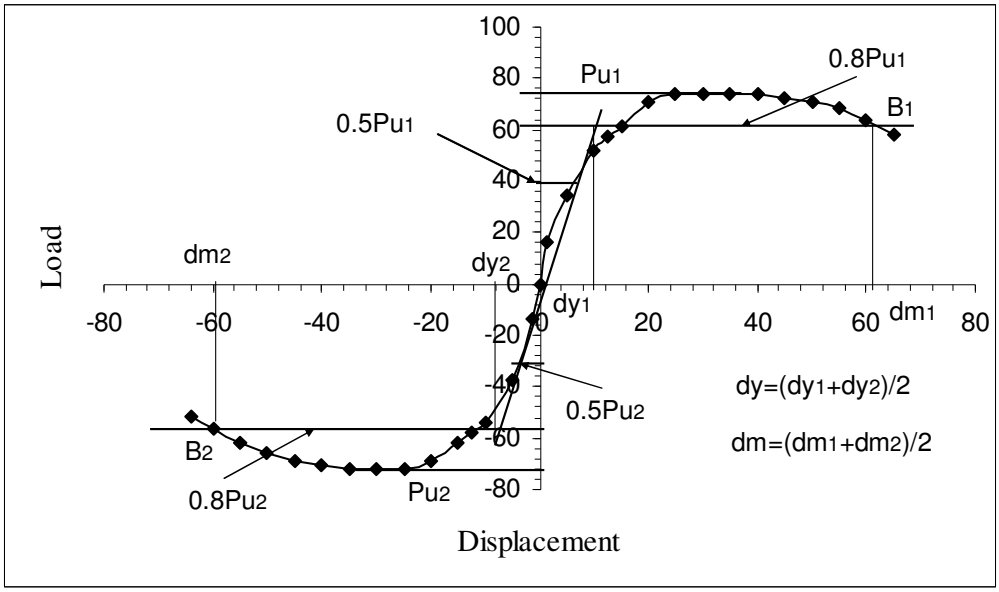

Fig. 5.36 Typical calculation procedure for ductility

The displacement ductility of the control as well as retrofitted specimen is shown in Fig. 5.37. It can be concluded from the figure that the displacement ductility increases marginally as the specimen size decreases for both control as well as retrofitted specimens. Displacement ductility varies from 8.71 to 9.75 for the control specimens. Large specimen has the least value and small specimen has the largest value. Further, it

can also be noted from the figure that the ductility gets enhanced due to retrofitting for the specimens of all sizes. Displacement ductility varies from 10.67 to 11.81 for the retrofitted specimens and trend to the variation is similar to that of control specimens. Thus, it can be concluded that the displacement ductility also follows the principle of size effect.

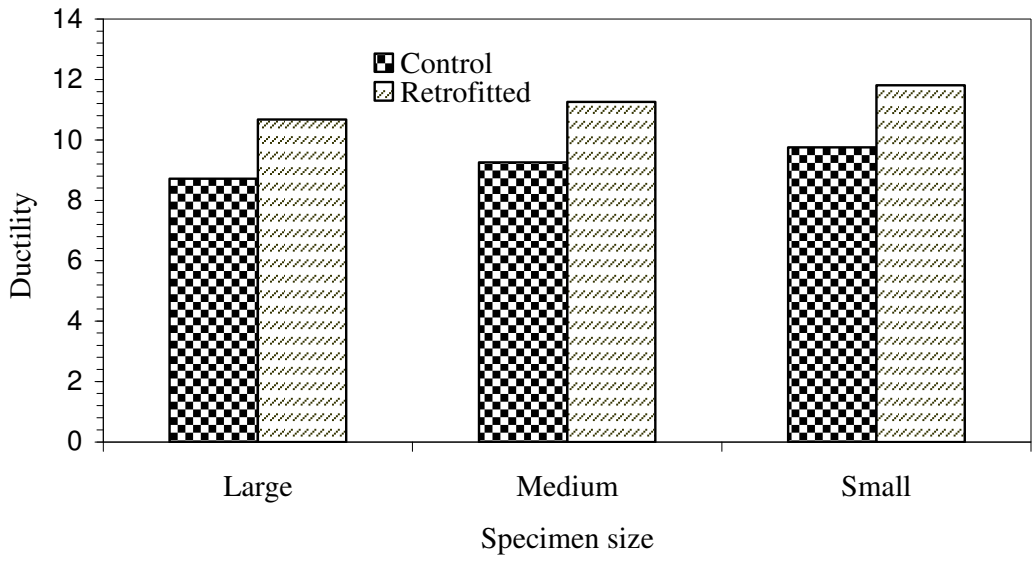

Fig. 5.37 Displacement Ductility of control and retrofitted specimens

5.6.4 Size Effect on Energy Dissipated Per Unit Volume of Joint Region

The variation of cumulative energy dissipated per unit volume of the joint, e_N for all the specimens were plotted with respect to drift angle. The plot for control specimens is shown in Fig. 5.38. The same for retrofitted specimens is shown in Fig. 5.39. It can be clearly observed that the uppermost curve is for the smallest specimen and lowermost curve for large specimen in both the cases. Thus, the energy dissipation per unit volume of joint increases as the specimen size decreases. This establishes the fact that the *energy dissipated per unit volume of join region* is dependant on specimen size.

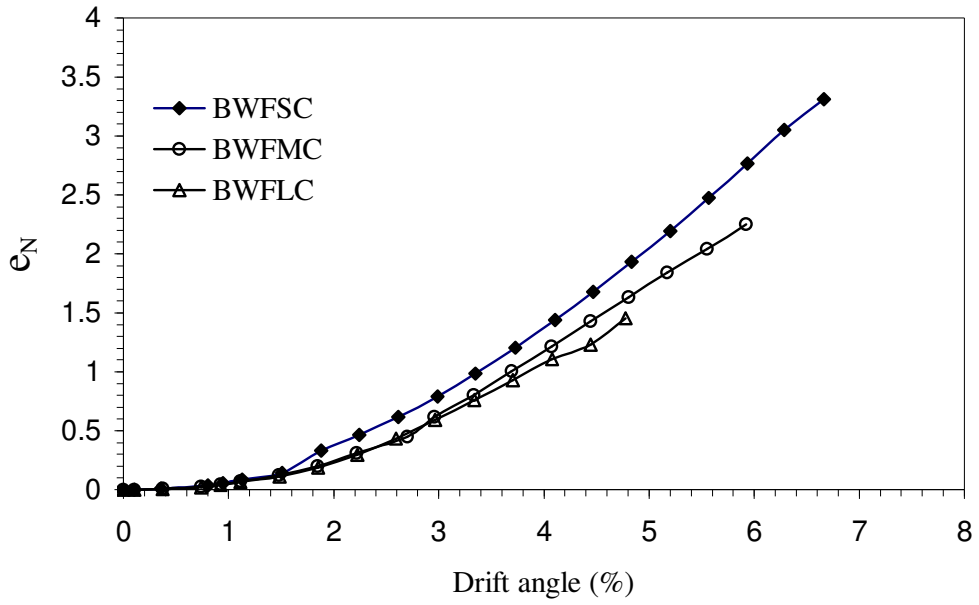

Fig. 5.38 Cumulative energy dissipated per unit volume of joint for control specimens

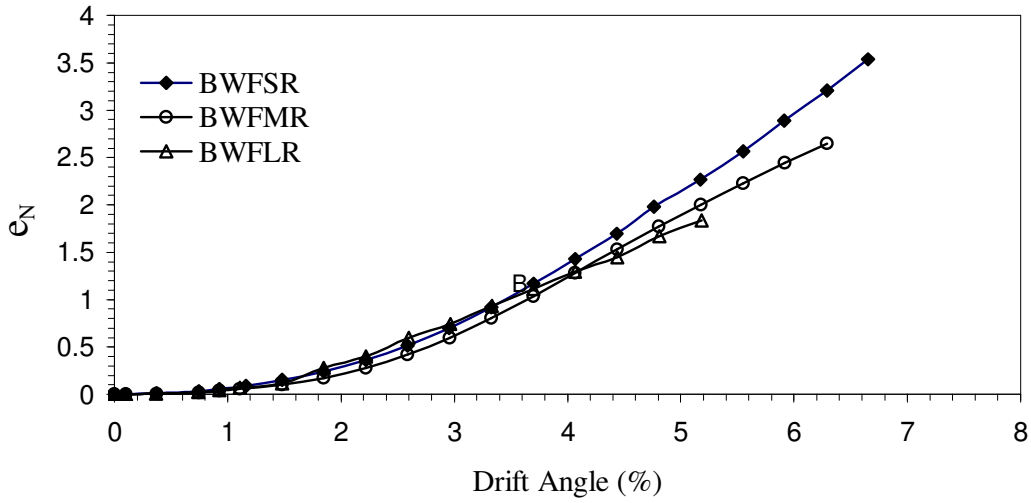

Fig. 5.39 Cumulative energy dissipated per unit volume of joint for retrofitted specimens

5.6.4 Size Effect on Variation of Stress Versus Relative Deflection

The relative deflection for different scaled models were calculated as the ratio of actual deflection to the scale of the model. Peak value of the load of each displacement cycle was used to calculate the bending stresses. The evaluated relative deflection and stresses were plotted for control and retrofitted specimens in Fig. 5.40 and Fig. 5.41 respectively. The plot for small specimen shows highest stresses at every level of relative deflection, while the least for large specimen in both the cases. Therefore, the principle of size effect is evidenced by these plots also.

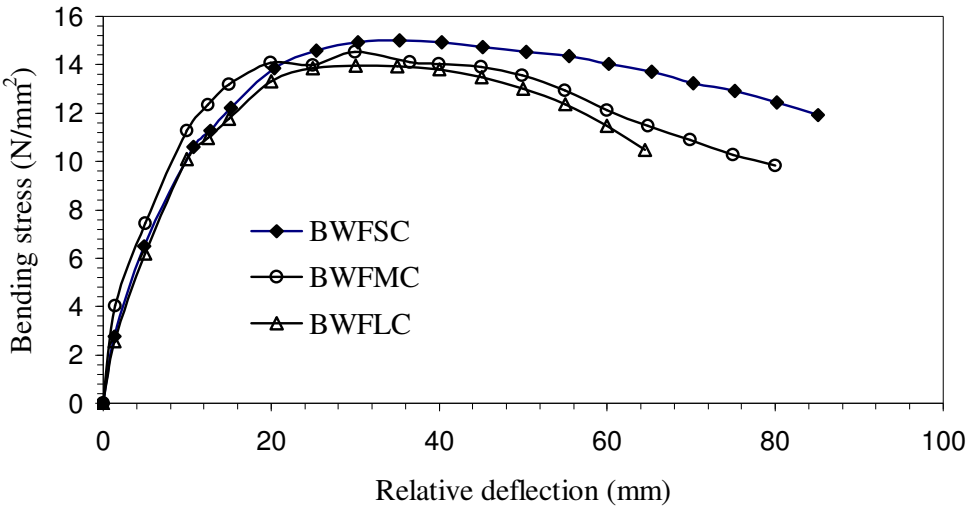

Fig. 5.40 Bending stress versus relative deflection plot for control specimen

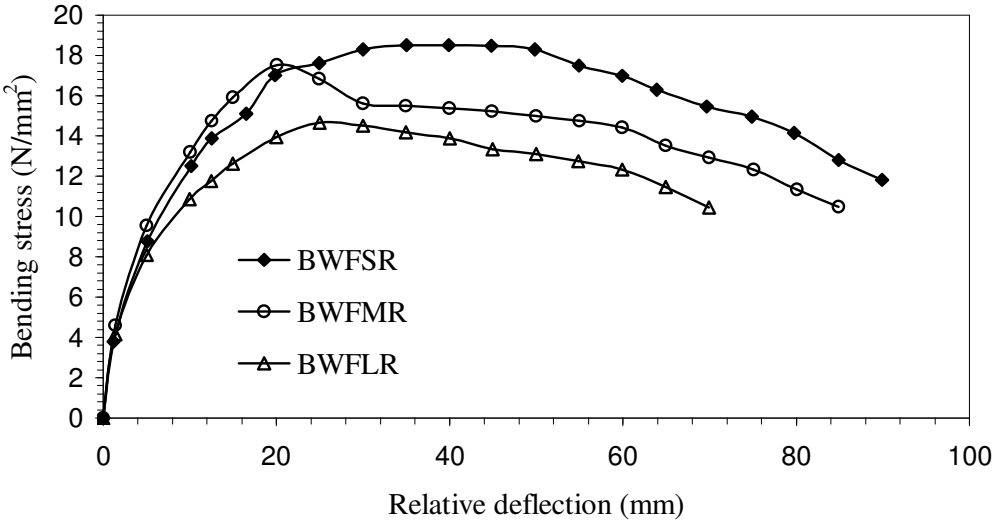

Fig. 5.41 Bending stress versus relative deflection plot for retrofitted specimen

5.7 CONCLUDING REMARKS

In this chapter, the experimental results of beam column joints with beam weak in flexure specimens were analysed and interpreted to examine the existence of size effect in various parameters. Results were used for drawing bi-logarithmic plot to observe variation of ductility, cumulative energy dissipation per unit volume of joint with respect to drift angle and variation of stress with relative deflection. It was observed that the bi-logarithmic plot for both control and retrofitted specimens substantiate the size effect law proposed by Baz˘ant. The displacement ductility for both control and retrofitted specimens increased with the decrease in size of specimens. Further, it was noted that the cumulative energy per unit volume of the joint at every drift angle for small specimen was the maximum and it decreased as the specimen size increased. This was an indication for existence of size effect. The variation of flexural stress with respect to relative deflection also agrees with the size effect principle.

The analysis of results reveals that there was remarkable improvement in ultimate load carrying capacity, energy dissipation, initial stiffness and ductility due to retrofitting of all the specimens studied. It was also noted that the enhancement in all these parameters substantiated the size effect principle. The next two chapters describe about other two types of deficient and retrofitted joints.

CHAPTER 6

EXPERIMENTAL STUDY ON BEAM-COLUMN JOINTS WITH BEAM WEAK IN SHEAR

6.1 INTRODUCTION

This chapter describes the results of experimental investigation and interpretation of those experimental results on beam-column joint with beam weak in shear specimens. Six number of beam-column joint specimens with beam weak in shear were tested in a similar way as that for the joints with beam weak in flexure. The applied displacement history has been described in chapter 5. The recorded data were used to draw hysteresis loop, envelope curve, variation of stiffness and energy dissipation with respect to drift angle. Results of control and retrofitted specimens were compared in term of all these above mentioned parameters and conclusions were drawn regarding the benefit derived out of retrofitting. Bi-logarithmic plots were drawn to explore the possibility of size effect in terms of strength. Specimen sizes were correlated with cumulative energy dissipated per unit volume of joint, displacement ductility and stresses.

6.2 TESTING OF LARGE SPECIMENS

The displacement history as described in Fig. 5(a) was applied to these specimens through a servo hydraulic dynamic actuator of loading capacity ± 250 kN and maximum displacement capacity of ± 125 mm. The experiment was stopped for control specimen at a stage when the load came down in the range of 65-70% of the ultimate load carrying capacity. Similarly, the experiment on retrofitted specimen was also stopped at about the same magnitude of load at which experiment was stopped for control specimen.

6.2.1 Large Control Specimen

The close view of the joint region of this specimen with some initial cracks developed during testing is shown in Fig. 6.1. The specimen at the end of the test is shown in

Fig. 6.2. The hysteretic response obtained by plotting the test data is shown in Fig. 6.3. Some of the important observations made during testing and analysis of the hysteresis loop are stated here. The first visible crack appeared in the beam part at displacement amplitude of ± 5 mm. More cracks started to develop in the beam and the joint region as the displacement amplitude was increased. These cracks are shown in Fig.6.1. It is observed from the hysteresis loop shown in Fig. 6.3 that the load reached to the maximum of 72.37 kN in the push direction at 19th cycle at a displacement of 25 mm. Similarly, the load reached to the maximum of 67.65 kN in the pull direction at 22nd cycle at a displacement of 30 mm. The first crack got widened and spalling of concrete started in

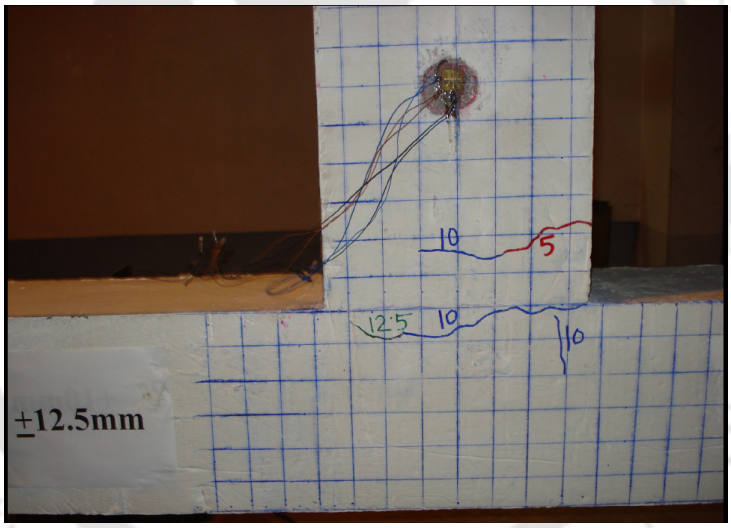

Fig.6.1 Initial cracks in BWSLC specimen at displacement amplitude of 12.5 mm

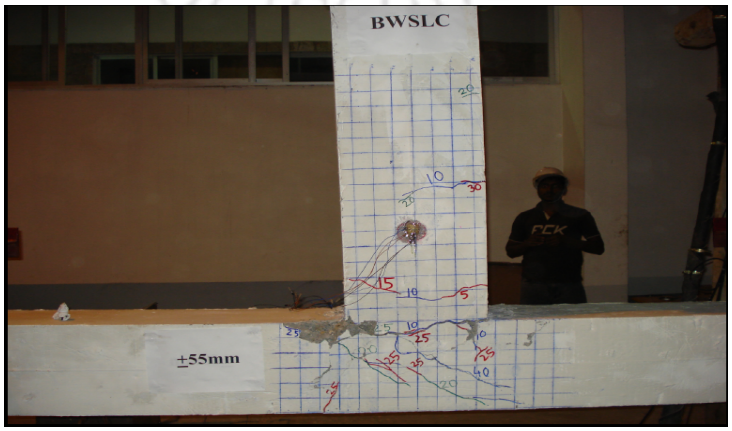

Fig. 6.2 BWSLC specimen at the end of test

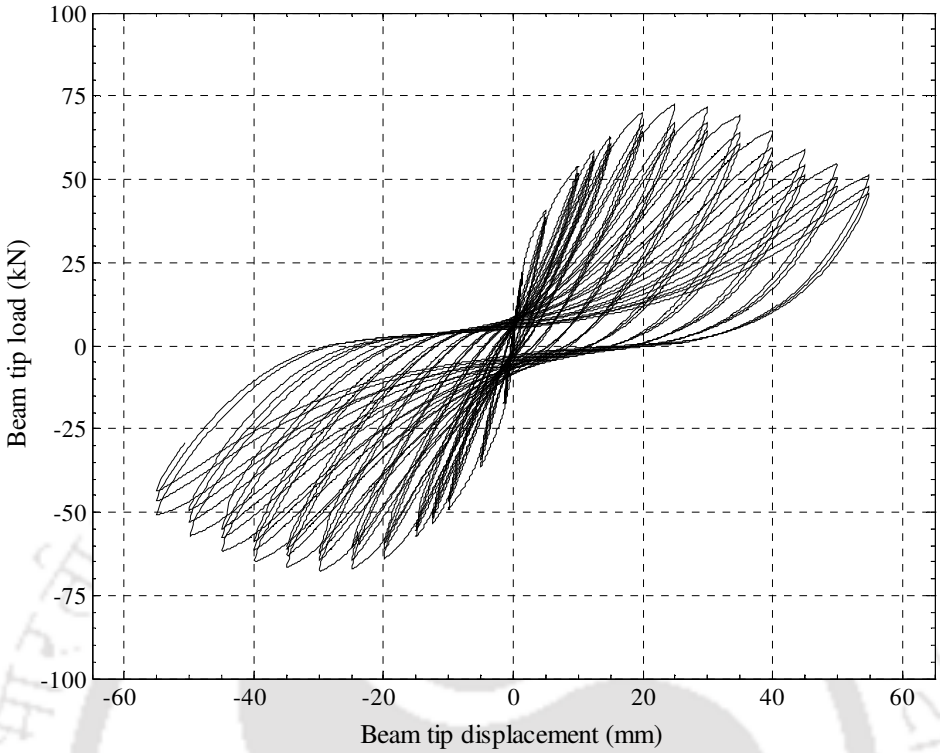

Fig.6.3 Hysteretic response of BWSLC specimen

the joint at ±35 mm displacement amplitude. Spalling of more concrete was observed from the joint region at displacement amplitude of ± 40 mm. The crack width became sufficiently wider at ±45 mm amplitude. The joint started to behave like a hinge and closing and opening of crack became distinct causing the failure of the specimen at ± 55 mm displacement amplitude. The ultimate load carrying capacity of BWSLC specimen was found to be 69.635 kN.

6.2.2 Large Retrofitted Specimen

This specimen was tested in a manner similar to that of the control specimen. The first rupture in GFRP sheet occurred at displacement amplitude of ±15 mm, followed by appearance of first visible crack in the beam in zone *A* shown in Fig. 6.4. The hysteresis loop obtained by plotting the test data is shown in Fig. 6.6. From the hysteresis loop it is observed that the specimen attained the maximum load of 88.927 kN in the push direction at 19th cycle at a displacement amplitude of 25 mm. In the same cycle it also reached to

the maximum load of 71.14 kN in the pull direction. The rupture in GFRP sheet in the joint propagated from one end to the other end of the joint at the same displacement amplitude. A crack appeared in the column in zone *B* shown in the Fig. 6.7 at ±40 mm displacement amplitude. Spalling of concrete started with a loud sound at ±45 mm displacement amplitude. The sound was created due to the delamination of CFRP sheet from one side of the column. The rupture in GFRP sheet got widened at displacement amplitude of ±50 mm. More cracks appeared in the joint at ±60 mm amplitude and the experiment was stopped noting the degradation in loading. The specimen at the end of the

Fig. 6.4 Appearance of first rupture in BWSLR specimen at ± 15 mm amplitude

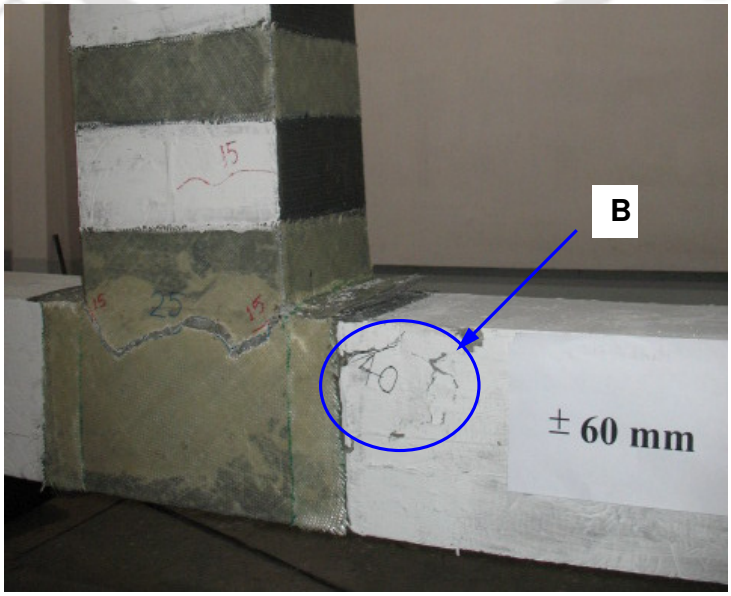

Fig. 6.5 BWSLR specimen at the end of test

test is shown in Fig. 6.5. The ultimate load carrying capacity of BWSLR specimen was found to be 78.12 kN.

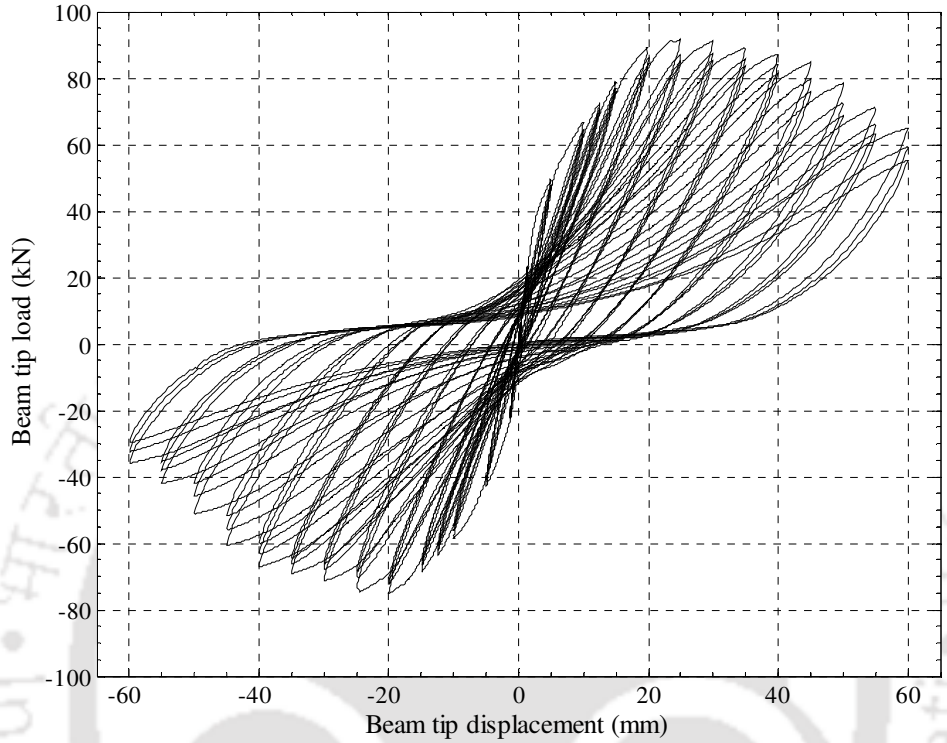

Fig. 6.6 Hysteretic response of BWSLR specimen

6.2.3 Comparison of Test Results of Control and Retrofitted Large Specimen

The envelope curves of hysteresis loops for control as well as retrofitted specimens are shown in Fig. 6.7. It can be observed that the retrofitted specimen shows significant improvement in load carrying capacity both in the push and pull direction in comparison to that for the control specimen for every displacement level in the envelope curve. The percentage gain in ultimate load carrying capacity due to retrofitting was found to be 12.18%.

The variation of stiffness with respect to drift angle for BWSLC and BWSLR specimens is shown in Fig. 6.8. It can be observed that the stiffness of BWSLR specimen is more than that of BWSLC specimen corresponding to any drift angle. The initial stiffness for retrofitted specimen was found as 16.29 kN/mm, while that for control specimen was

13.98 kN/mm. Thus, the gain in initial stiffness was found to be 16.31% for the case under study due to retrofitting.

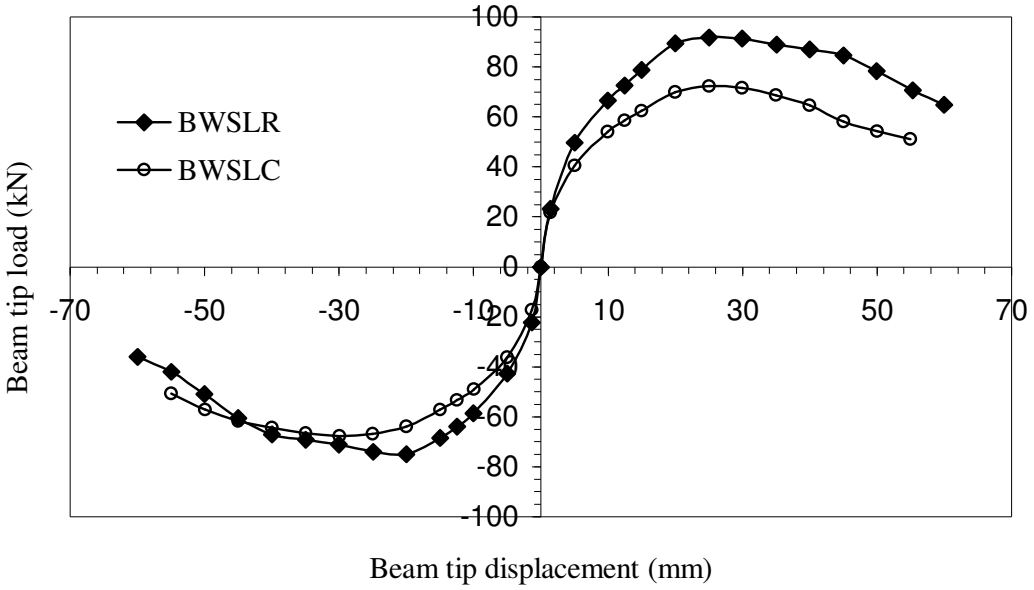

Fig. 6.7 Envelope of hysteresis loops for BWSLC and BWSLR specimens

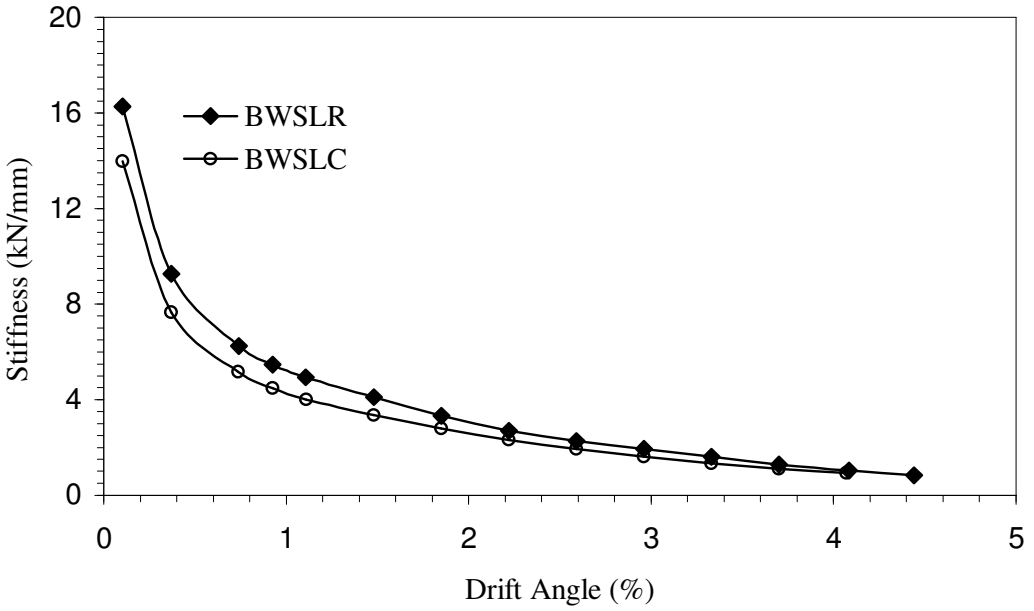

Fig. 6.8 Stiffness versus drift angle plot for BWSLC and BWSLR specimens

Fig. 6.9 shows the variation of cumulative energy dissipation with drift angle for control and retrofitted specimens. The figure shows that the energy dissipated by retrofitted specimen is higher than that of control specimen corresponding to every drift angle. The gain in energy dissipation due to retrofitting is 55.96% at the failure stage of the specimen.

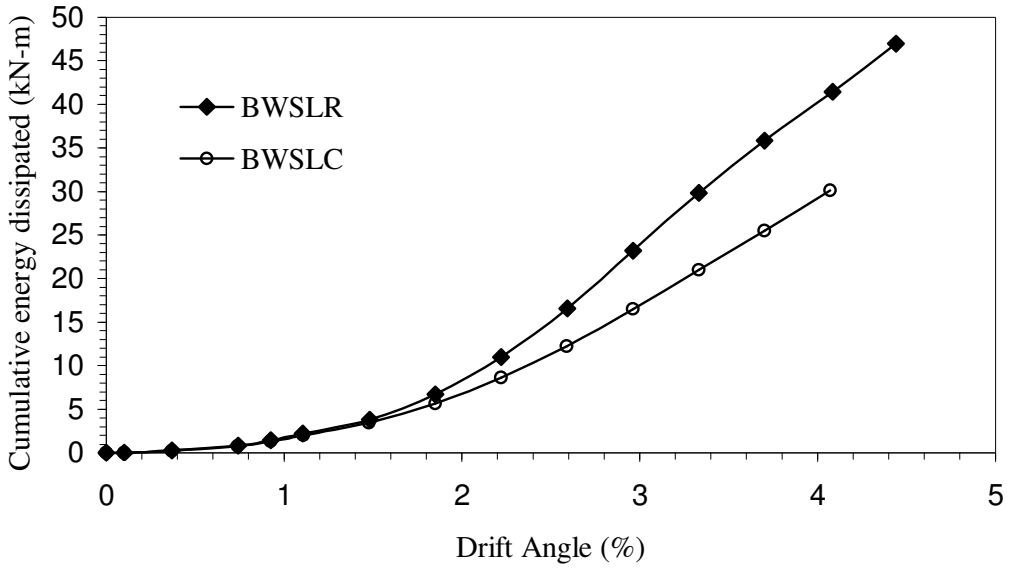

Fig. 6.9 Cumulative energy dissipated by BWSLC and BWSLR specimens

6.3 TESTING OF MEDIUM SPECIMENS

A displacement controlled loading cycle described in section 5.2 was applied to these specimens by a servo hydraulic dynamic actuator of capacity ± 250 kN. The experiment was stopped when percentage reduction of load of similar order as that in the case of large specimen was attained.

6.3.1 Medium Control Specimen

Testing arrangement along with the first crack of this specimen is shown in Fig. 6.10. A close view of the joint region at the end of the test is shown in Fig. 6.11. The hysteretic response obtained by plotting the test data is shown in Fig. 6.12. Some of the important

observations made during testing and analysis of the hysteresis loop are stated here. The first visible crack appeared in the beam very near the junction of beam-column joint (Fig. 6.10) at amplitude of ±3.33 mm. The maximum load 34.08 kN was recorded in the pull direction in 19th cycle at displacement amplitude of ±6.67 mm. The earlier developed cracks started to get widened along with appearance of new ones at ±16.67 mm amplitude. Maximum load of 35.01 kN was observed in the push direction in 25th cycle at a displacement amplitude of 23.33 mm. Two typical diagonal long cracks appeared in the joint region. Widening and propagation of these cracks was observed with increase of displacement amplitude. Spalling of concrete was also started at this amplitude. Formation of plastic hinge was noted at ±33.33 mm displacement amplitude. A crack

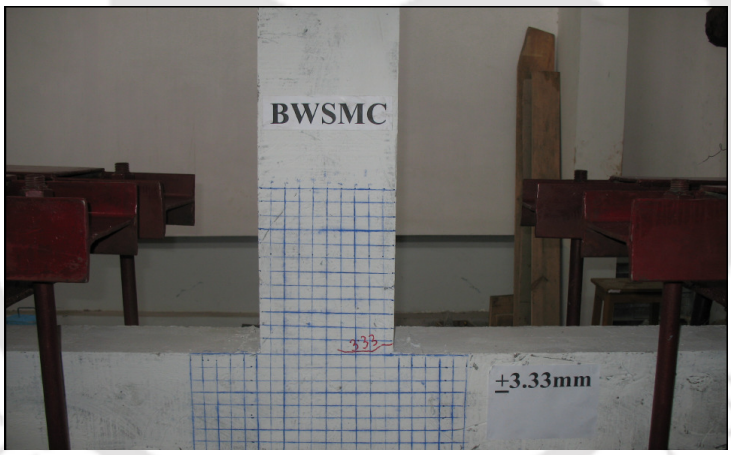

Fig. 6.10 Appearance of first cracks in BWSMC specimen

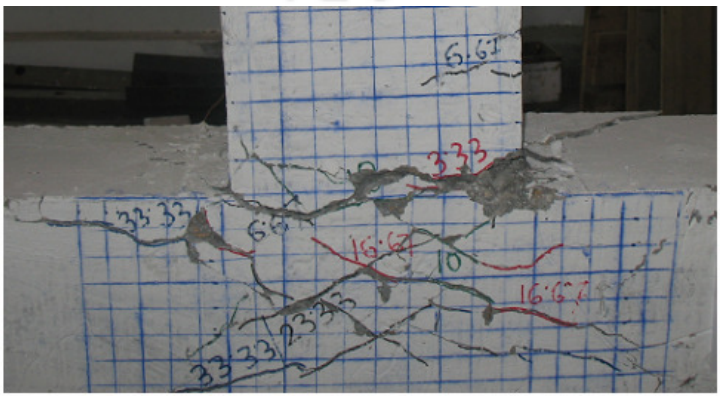

Fig. 6.11 BWSMC specimen at the end of testing

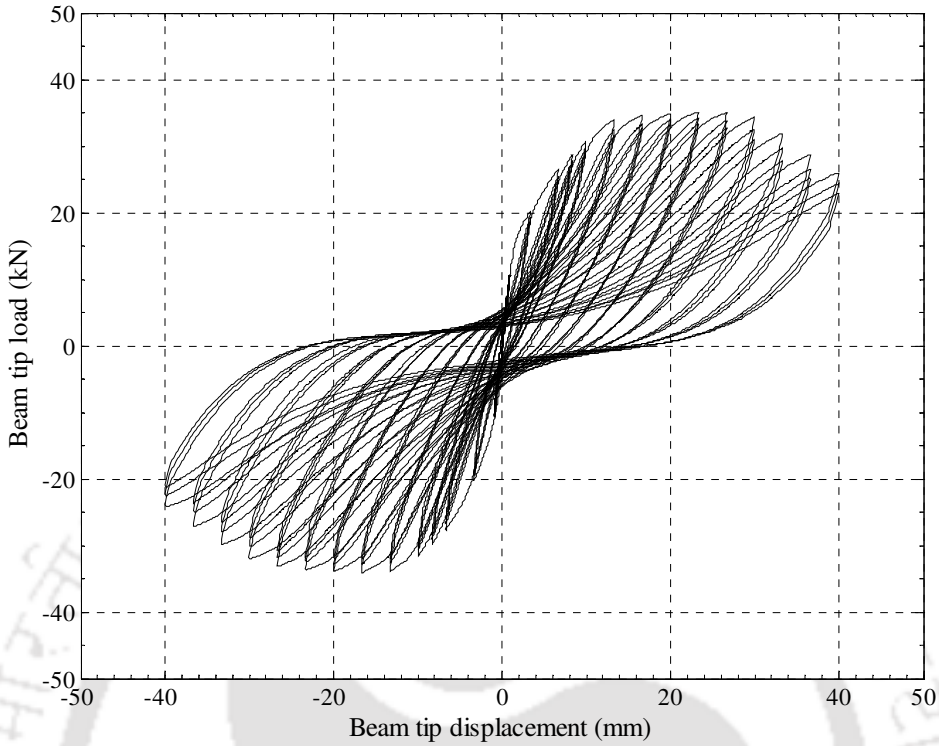

Fig. 6.12 Hysteretic response of BWSMC specimen

appeared at the exterior face of the beam-column joint making the specimen unstable at ± 40 mm displacement amplitude and subsequently the experiment was stopped. The ultimate load carrying capacity of BWSMC specimen was found to be 34.055 kN.

6.3.2 Retrofitted Specimen

This specimen was tested in a manner similar to that of control specimen. Fig. 6.13 shows the appearance of first visible crack. The initiation of rupture in GFRP sheet at the column face of the beam is shown in Fig. 6.14. Damaged specimen at the end of the test is shown in Fig. 6.15. The hysteretic response obtained by plotting the test data is shown in Fig. 6.16. Some of the important observations made during testing and analysis of the hysteresis loop are presented in this section.

The first visible crack was observed at ± 3.33 mm amplitude in the beam near the joint region is shown in zone *A* of Fig. 6.13. The maximum load of 38.24 kN was reached in

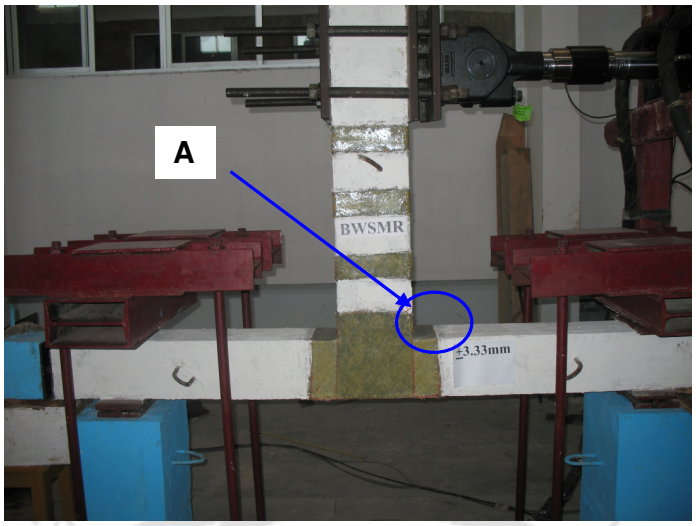

Fig. 6.13 Appearance of first visible crack in BWSMR specimen

Fig. 6.14 Appearance of rupture in GFRP of BWSMR specimen

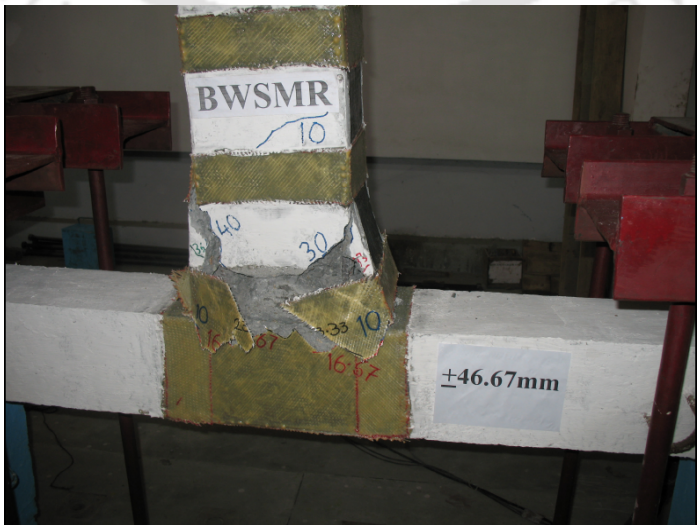

Fig. 6.15 BWSMR specimen at the end of test

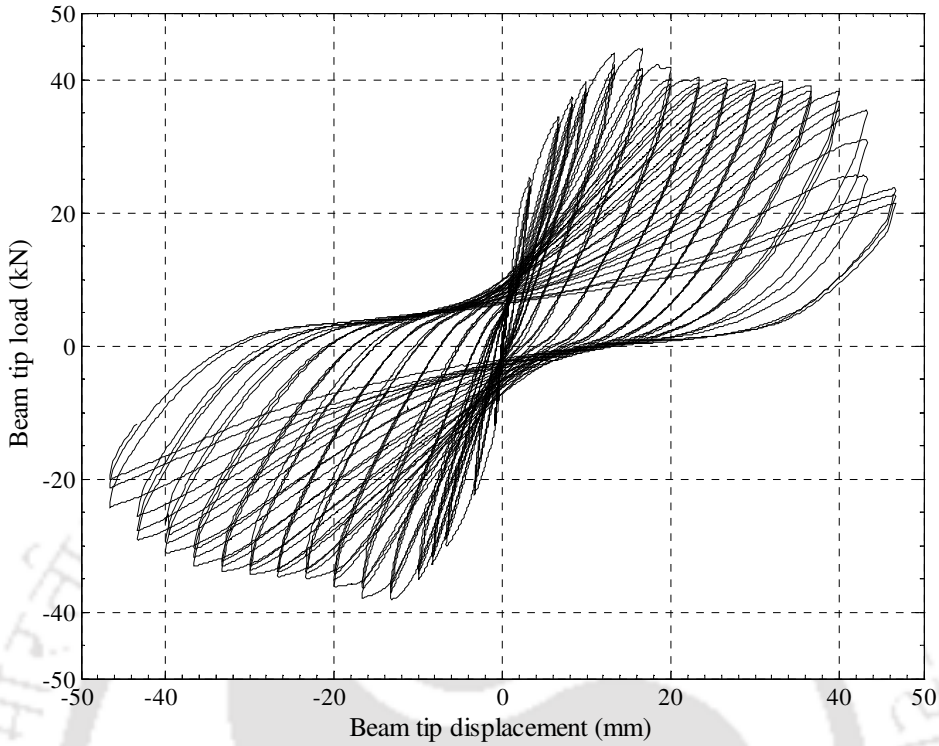

Fig. 6.16 Hysteretic response of BWSMR specimen

the pull direction at 16th cycle at displacement of 13.33 mm. The maximum load recorded in the push direction was 44.56 kN at amplitude of 16.67 mm during 19th cycle. The rupture in GFRP sheet in the joint region started to propagate further at the same amplitude of ± 16.67 mm. The whole GFRP sheet covering the joint got splitted into two parts at ± 23.33 mm amplitude. Spalling of concrete started along with formation of new cracks on increasing displacement amplitude. Delamination of the first strip of GFRP sheet provided in beam started with a loud sound at ± 40 mm amplitude. The cracks got widened to a considerable extent at ± 43.33 mm amplitude. The first strip of GFRP sheet provided in the beam for shear strengthening got splitted into two pieces and finally delaminated almost totally from the beam at ± 46.67 mm amplitude. The ultimate load carrying capacity of BWSMR specimen was found to be 41.25 kN.

6.3.3 Comparison of Test Results of Control and Retrofitted Medium Specimen

The envelope curves of hysteresis loops for control as well as retrofitted specimen are shown in Fig. 6.17. It is observed that the load carrying capacity of retrofitted specimen is higher than that of the control specimen in both the push and pull direction. The percentage gain in ultimate load carrying capacity due to retrofitting was found to be 21.13%.

The variation of stiffness with drift angle for BWSMC and BWSMR specimens have been plotted in Fig. 6.18. It can be observed that the stiffness of retrofitted specimen is more than that of control specimen corresponding to any drift angle. The initial stiffness for retrofitted specimen is 13.58 kN/mm, while the same for control specimen it is 11.46 kN/mm. Thus, the gain in initial stiffness is 18.5% due to retrofitting. Fig. 6.19 shows the cumulative energy dissipation curve for control and retrofitted specimens. It is clear that the energy dissipated by retrofitted specimen is higher than that of control specimen. The gain in energy dissipation due to retrofitting at failure stage is 95.7%.

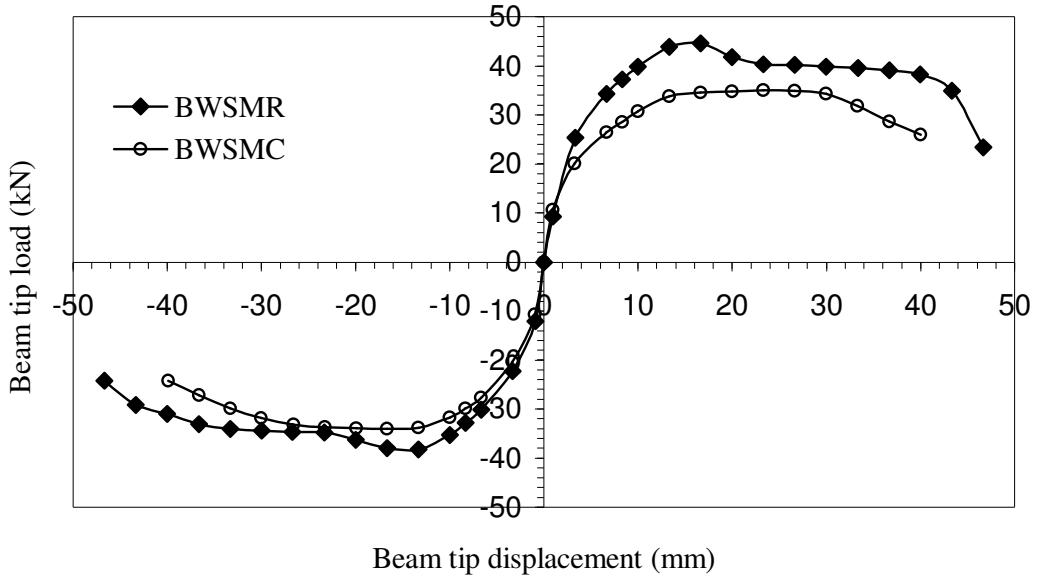

Fig. 6.17 Envelope of hysteresis loops for BWSMC and BWSMR specimens

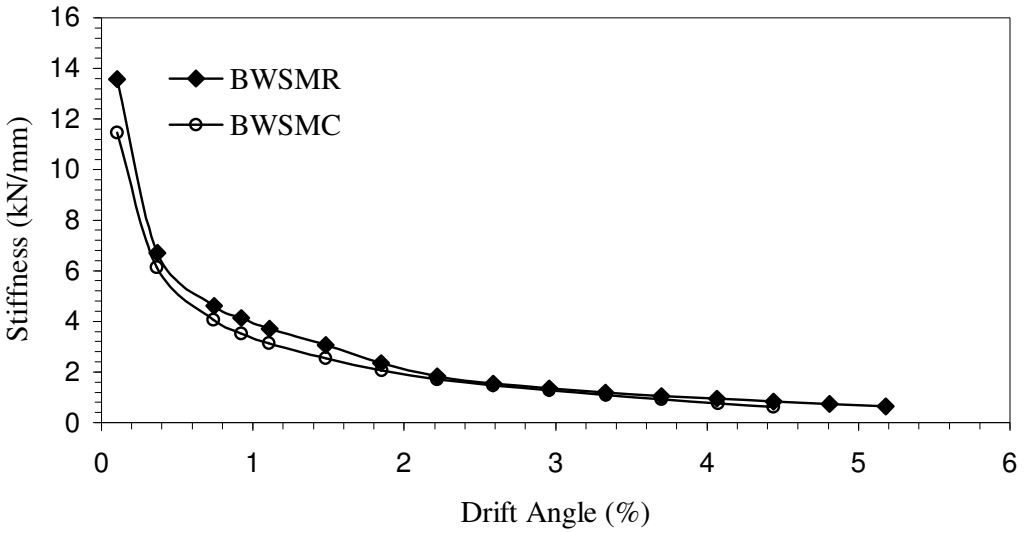

Fig. 6.18 Stiffness versus drift angle plot for BWSMC and BWSMR specimens

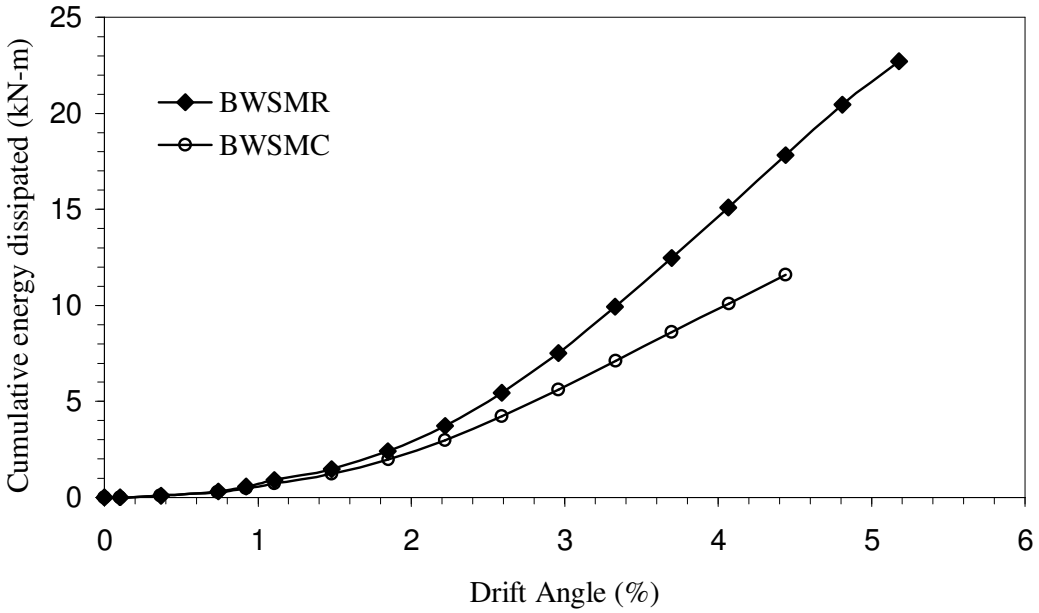

Fig.6.19 Cumulative energy dissipated by BWSMC and BWSMR specimens

6.4 TESTING OF SMALL SPECIMENS

The displacement history described in section 5.2 was applied to these specimens by a servo hydraulic dynamic actuator of capacity ±100 kN and maximum displacement capacity of ±125 mm. The experiment was stopped for control specimen when the load came down to the extent of 65-70% of the ultimate load carrying capacity of the

specimen. Similarly, the experiment on retrofitted specimen was also stopped at about the same magnitude of load at which experiment was stopped for control specimen.

6.4.1 Small Control Specimen

The testing arrangement of this specimen is shown in Fig. 6.20. At the end of testing the condition of the specimen is shown in Fig. 6.21. The hysteretic response obtained by plotting the test data is presented in Fig. 6.22. The following observations were made during testing and by analysing the hysteresis loop. The first crack was observed in the beam near the column face at amplitude of ± 3.33 mm. The load reached to the maximum value of 8.961 kN in the push direction at 19^{th} cycle at a displacement of 8.33 mm. The

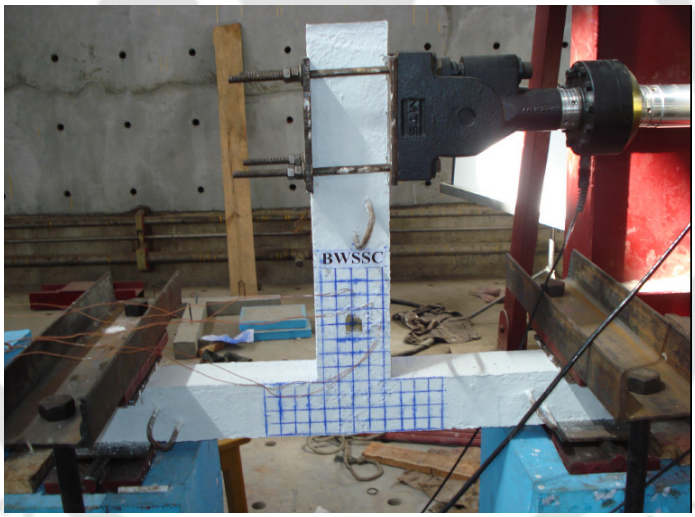

Fig.6.20 Testing set up for BWSSC specimen

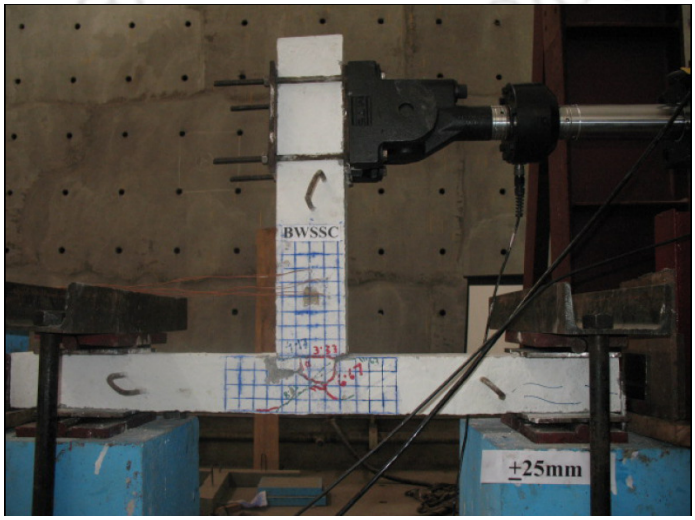

Fig. 6.21 BWSSC specimen at the end of test

first developed crack became wider at the same amplitude of ± 8.33 mm. The load reached to maximum value of 10.54 kN in the pull direction at 25th cycle at a displacement of 11.67 mm. Spalling of concrete noticed at ± 13.33 mm amplitude. A big piece of concrete spalled down from beam close to column face at ± 18.33 mm amplitude. Significant cyclic rotation of the beam was observed near column face due to the formation of plastic hinge at amplitude of ± 20 mm. Finally, the experiment was stopped noting the desired degradation in loading at displacement of ± 25 mm. The ultimate load carrying capacity of BWSSC specimen was found to be 10.018 kN.

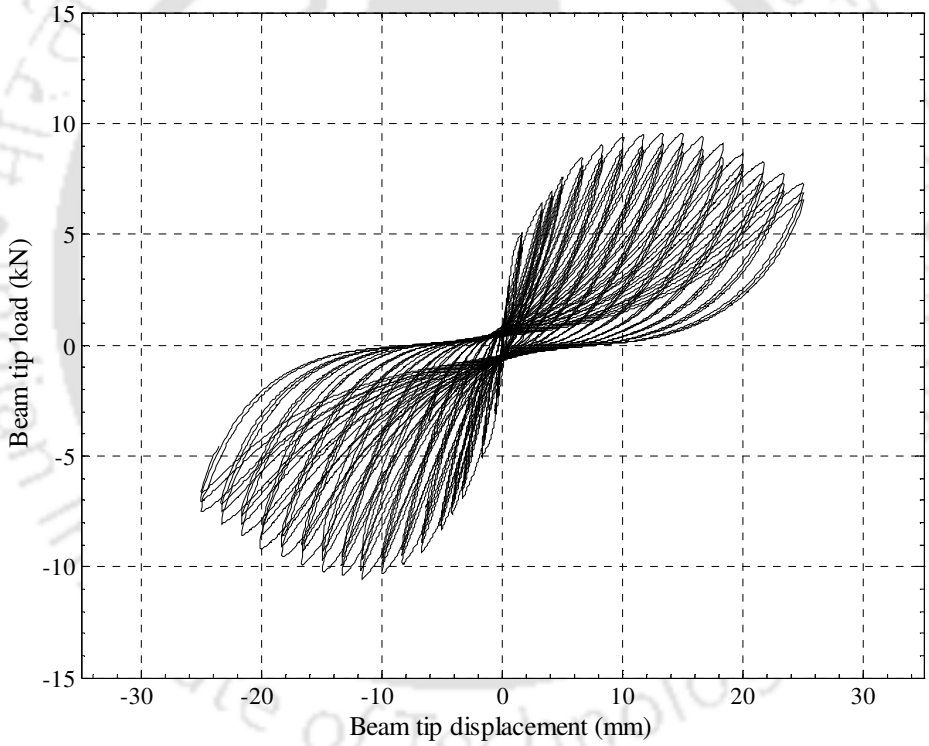

Fig. 6.22 Hysteretic response of BWSSC specimen

6.4.2 Small Retrofitted Specimen

This specimen was tested in an identical manner to that of control specimen. Fig. 6.23 shows the appearance of first crack in this specimen at displacement amplitude of ± 6.67 mm. The specimen at the end of test is shown in Fig. 6.24. The hysteretic response is shown in Fig. 6.25. The observations which were made during testing and analysis of the

hysteresis loop are presented in this section. The load reached to the maximum value of 13.83 kN in the pull direction at 22nd cycle at a displacement of 10.0 mm. Further, the load reached maximum value of 11.97 kN in the push direction at 25th cycle at displacement of 11.67 mm and simultaneously debonding of GFRP sheets from the joint with loud sound was noticed. The debonding touched the other end of the joint by gradual expansion at ± 13.33 mm amplitude. Delamination of CFRP sheet started at the displacement amplitude of ± 28.33 mm. Substantial cyclic rotation of beam was observed near column face due to the possible formation of plastic hinge at ± 30 mm displacement amplitude and noting the degradation of load the experiment was stopped.

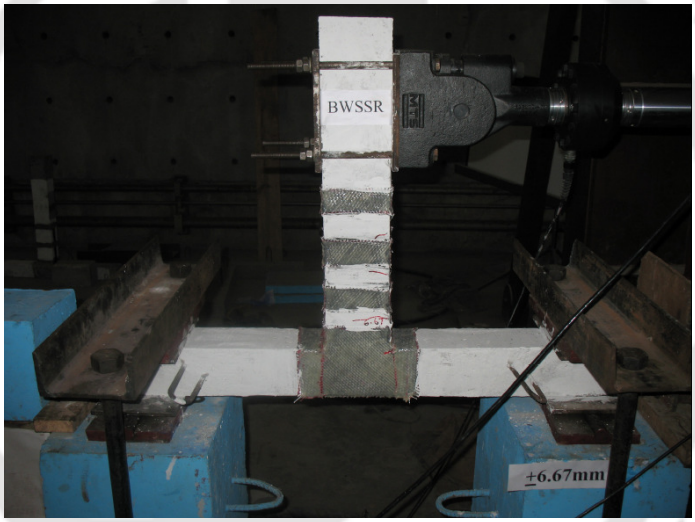

Fig.6.23 Appearance of first crack in BWSSR specimen

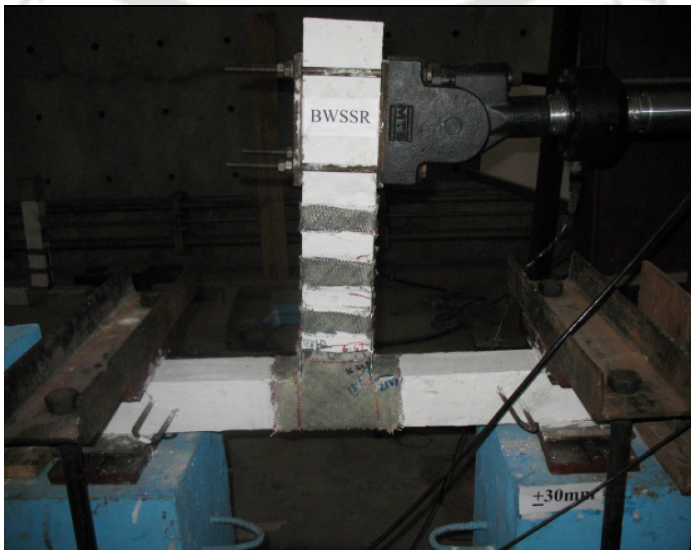

Fig. 6.24 BWSSR specimen at the end of test

The ultimate load carrying capacity of BWSSR specimen was found to be 12.715 kN.

6.4.3 Comparison of Test Results of Control and Retrofitted Small Specimen

The envelope curve of control and retrofitted specimen is shown in Fig. 6.26. It is observed that the envelope curve for the retrofitted specimen shows higher load carrying capacity than that of the control specimen in both the push and pull direction. The

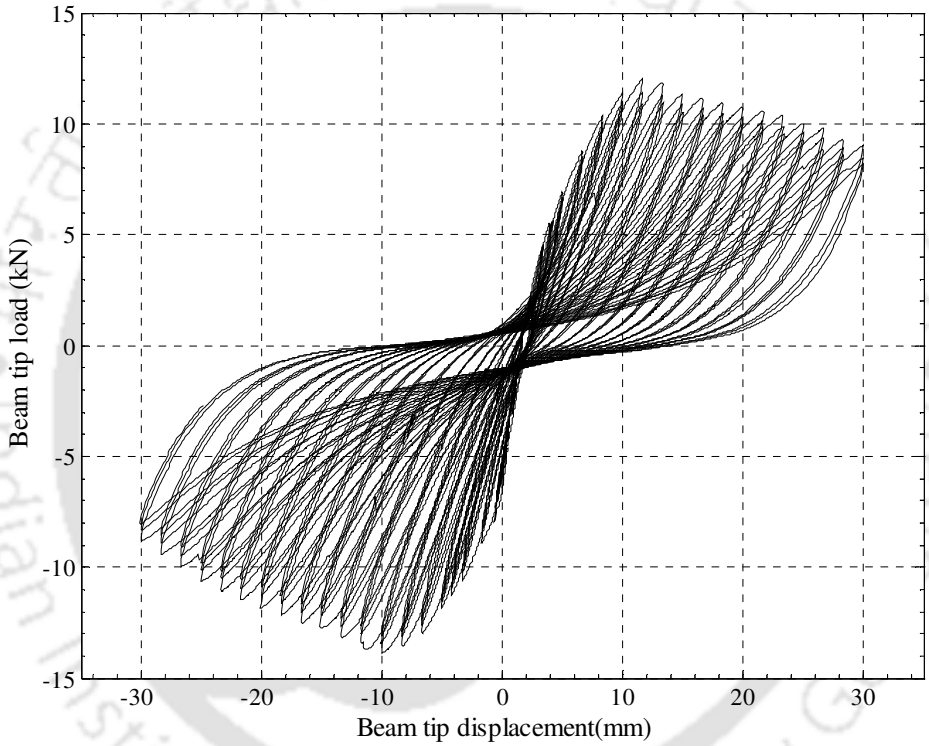

Fig.6.25 Hysteretic response of BWSSR specimen

percentage gain in ultimate load carrying capacity due to retrofitting was found as 26.91%. The variation of stiffness for BWSSC and BWSSR speimens is shown in Fig. 6.27. The stiffness of BWFSR specimen is more than that of the BWFSC specimen. The initial stiffness for retrofitted specimen is 8.251 kN/mm, while that of control specimen is 5.175 kN/mm. Therefore, the gain in initial stiffness is 59.43% due to retrofitting. Fig. 6.28 shows the energy dissipation curve for control and retrofitted specimens. This figure shows that the energy dissipated by retrofitted specimen is higher than that of control specimen at every drift angle. The gain in energy dissipation due to retrofitting is

97.7% at the ultimate drift angle.

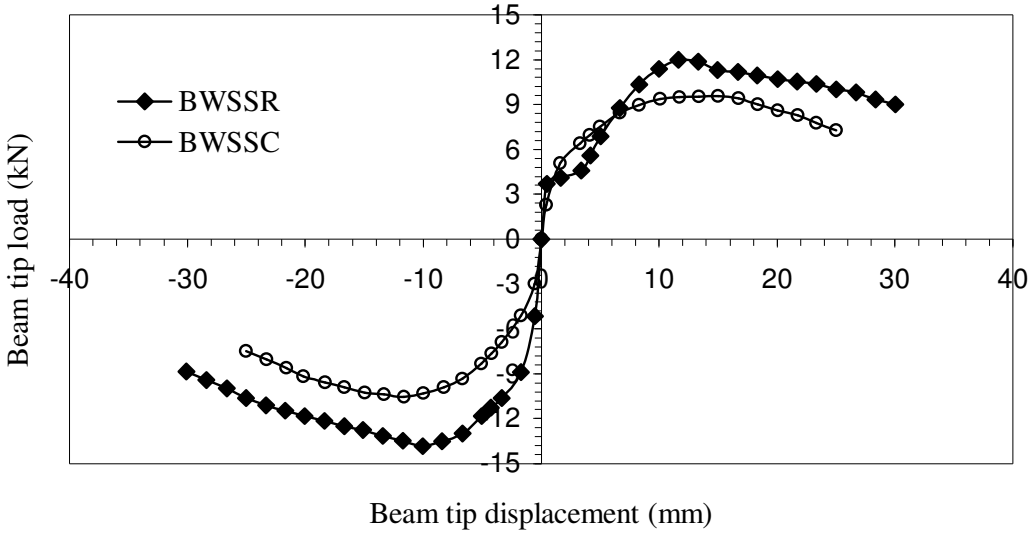

Fig. 6.26 Envelope of hysteretic loops for BWSSC and BWSSR

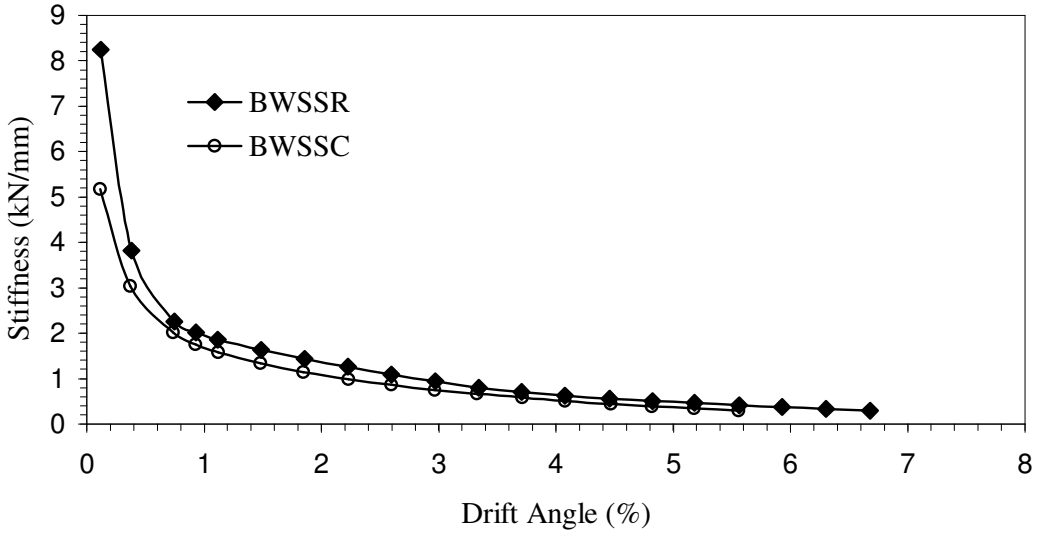

Fig. 6.27 Stiffness versus drift angle plot for BWSSC and BWSSR specimens

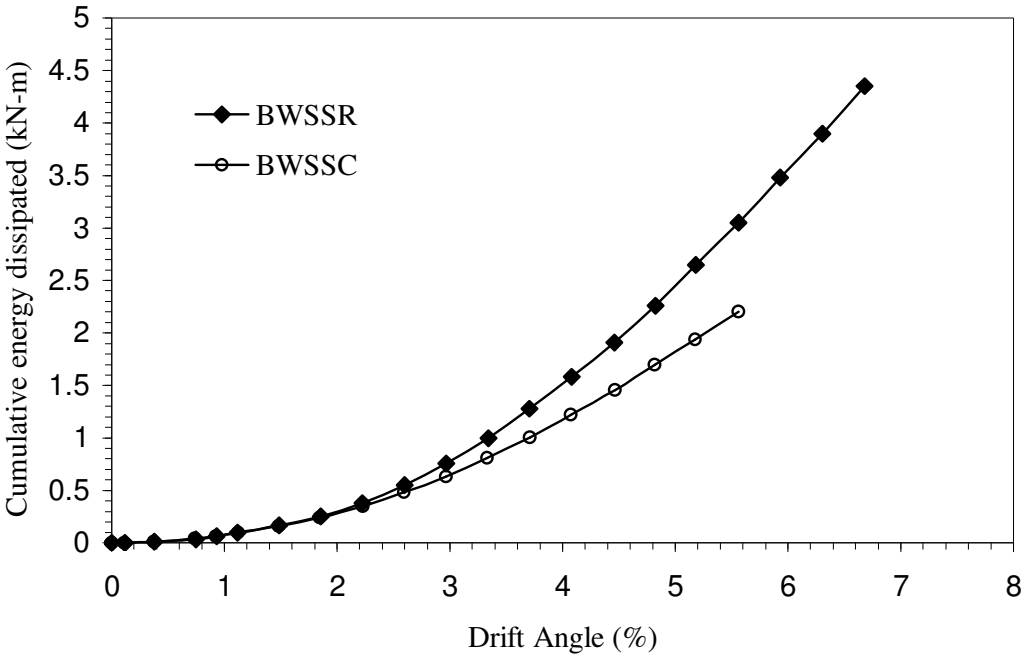

Fig. 6.28 Energy dissipation of BWSSC and BWSSR specimens

6.5 INTERPRETATION OF RESULTS TO EXPLORE THE EXISTANCE OF SIZE EFFECT

The results obtained by testing the specimens were used to draw bi-logarithmic plot in order to explore the possibility of existence of size effect. Further, the percentage gain in ultimate load carrying capacity, stiffness and energy dissipation due to retrofitting were correlated with size of specimens. Finally, specimen sizes were correlated with displacement ductility, energy dissipation per unit volume of the beam-column joint and variation of stress with relative deflection of the control as well as retrofitted specimens.

6.5.1 Bi-logarithmic Plot

Ultimate shear stress σ_{N_U} was calculated for the control specimens as the failure mode of the specimens was in shear. Ultimate bending stress was calculated for retrofitted specimens as the failure mode in this case was in flexure. The calculation of both type of stresses are furnished in Appendix-C.

The stress and calculation of other parameters necessary to carry out regression analysis and to draw bi-logarithmic plot for the both control as well as retrofitted cases are furnished in Table 6.1. Regression analysis was carried out to determine B and D_0. Finally, bi-logarithmic plots for the control and retrofitted specimens were drawn as shown in Fig. 6.29-6.30. It is observed that both the plots show presence of size effect and substantiate Bazˇant's size effect law. Further, the slope of the bi-logarithmic plot towards the end of the curve for control specimens is found less in comparison to that of retrofitted specimens. The slope of the bi-logarithmic plot for retrofitted specimens is found very close to -1/2. Thus, the observed size effect is more pronounced in case of retrofitted specimens than control specimens.

Table 6.1 Parameters for bi-logarithmic plot

Type of specimen	Name of specimen	Stress, σ_{N_U} (N/mm^2)	Depth of specimen, D (mm)	$\left(\frac{f_t'}{\sigma_{N_U}}\right)^2$	Log (D/Do)	$Log(\sigma_{N_U}/Bf_t')$
Control	BWSSC	1.250	120	4.01281	-0.30719	-0.08348
	BWSMC	1.110	240	5.088886	-0.00616	-0.13507
	BWSLC	0.967	360	6.705261	0.169928	-0.19496
Retrofitted	BWSSR	21.558	120	0.013491	0.234083	-0.21975
	BWSMR	19.025	240	0.017323	0.535113	-0.27404
	BWSLR	14.523	360	0.029727	0.711204	-0.39131

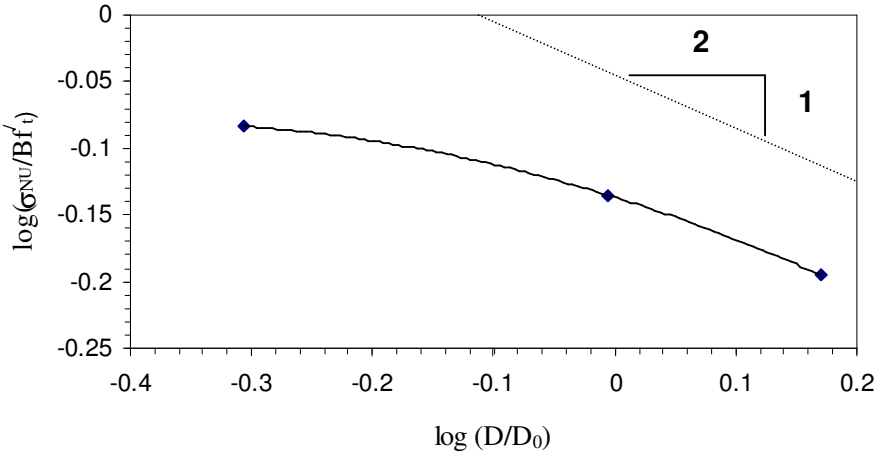

Fig. 6.29 Bi-logarithmic plot for beam weak in shear : control specimens

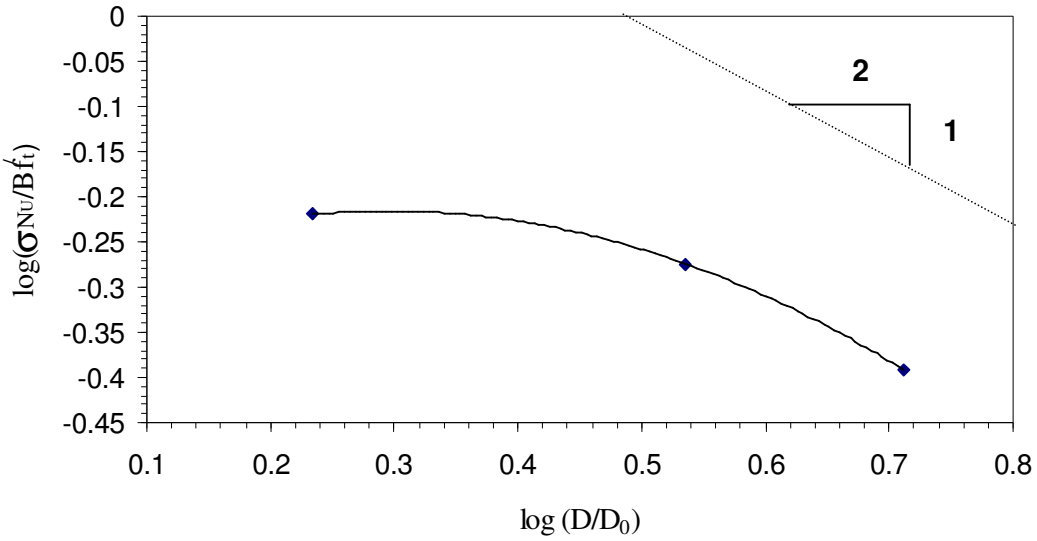

Fig. 6.30 Bi-logarithmic plot for beam weak in shear : retrofitted specimens

6.5.2 Size Effect on Gain in Ultimate Load Carrying capacity, Stiffness and Energy Dissipation on Retrofitting

The percentage gain in ultimate load carrying capacity of retrofitted specimens with respect to control specimen for different sizes were calculated and presented in Fig. 6.31. The figure shows that the gain in ultimate load carrying capacity is the largest for small specimen and vice versa. Similarly, percentage gain in initial stiffness and energy dissipation due to retrofitting are plotted in Fig 6.32 and Fig. 6.33 respectively. It can be observed that, these figures also follow the same trend as that of Fig. 6.31. Thus it can be concluded that gain in ultimate load carrying capacity, initial stiffness and energy dissipation increases as the specimen size decreases supporting the size effect principle.

6.5.3 Size Effect on Displacement Ductility of Specimens

The displacement ductility of the control as well as retrofitted specimen is shown in Fig. 6.34. It is noted that the displacement ductility increases as the specimen size decreases for both control as well as retrofitted specimens. Displacement ductility varies from 6.85 to 10.89 for the control specimens with the least value for large specimen and the highest

value for small specimen. In addition, it can also be noted from the figure that the ductility gets enhanced due to retrofitting irrespective to size of the specimens.

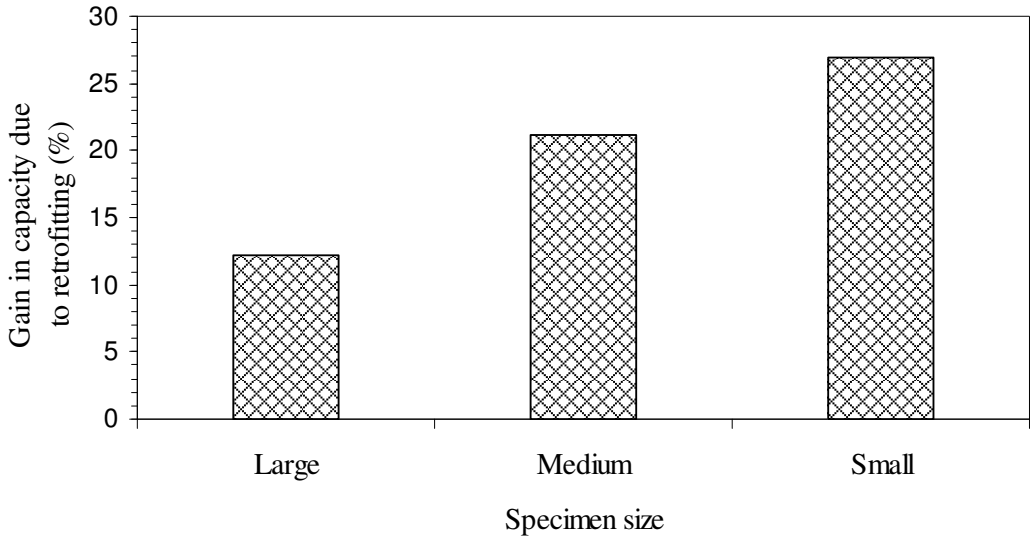

Fig. 6.31 Percentage gain in ultimate load carrying capacity due to retrofitting

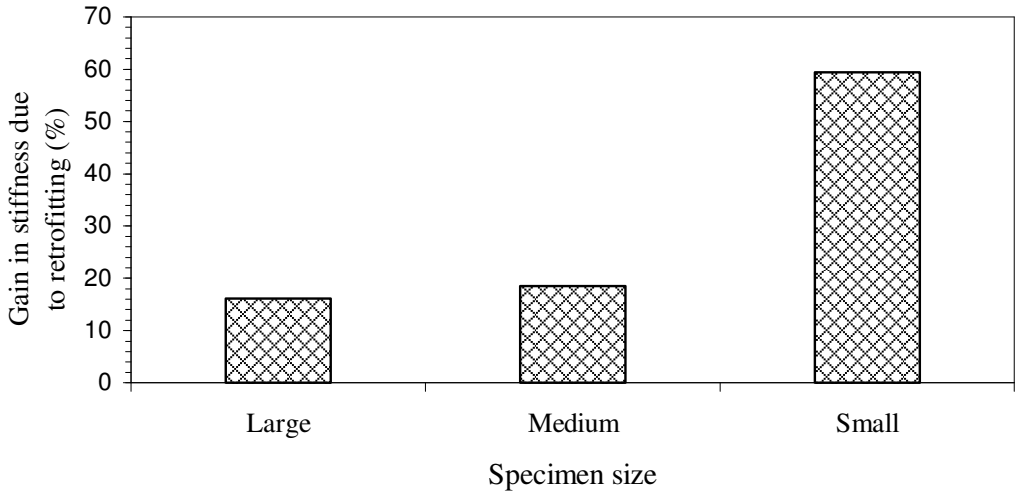

Fig. 6.32 Percentage gain in initial stiffness due to retrofitting

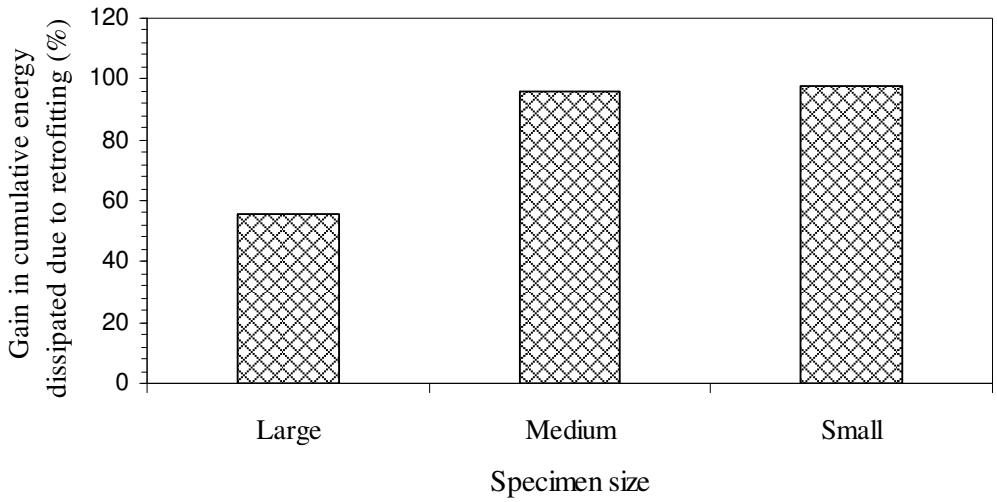

Fig. 6.33 Percentage gain in energy dissipation due to retrofitting

Displacement ductility varies from 8.33 to 14 for the retrofitted specimens with the least value for large specimen and the largest value for small specimen. Further, the increase in displacement ductility varies from 21.6% to 28.5% due to retrofitting Thus, it can be concluded that the displacement ductility follows the principle of size effect for both control as well as retrofitted specimens. In addition, the gain in displacement ductility due to retrofitting also follows the same trend.

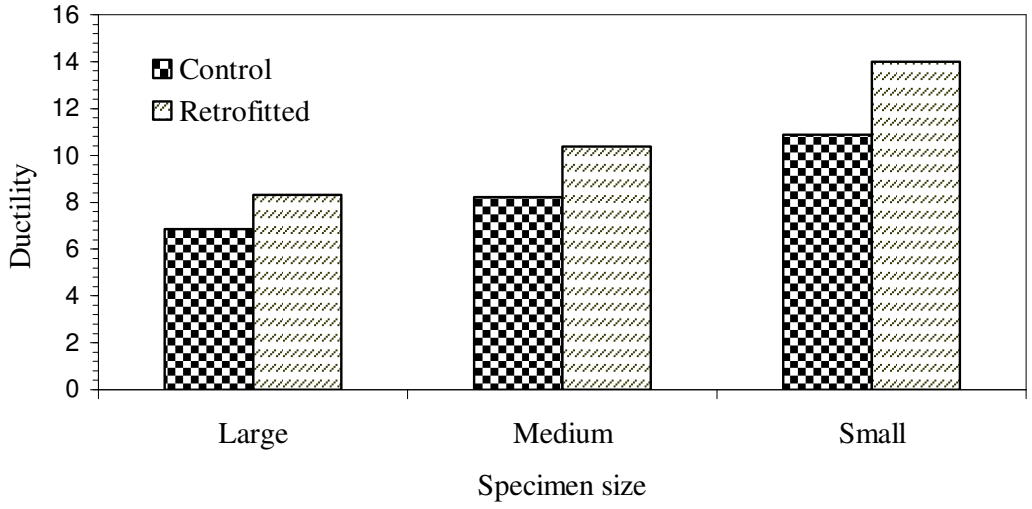

Fig. 6.34 Ductility of control and retrofitted specimens

6.5.4 Size Effect on Energy Dissipated Per Unit Volume of Joint

The cumulative energy dissipated per unit volume of the joint, e_N for all the specimens were plotted with respect to drift angle. Fig. 6.35 shows the plot for control specimens, while Fig. 6.36 shows the same for retrofitted specimens. It can be clearly observed that in both the cases, the uppermost curve is for the smallest specimen and lowermost curve for largest specimen. This proves that during cyclic loading, the energy dissipated per unit volume of joint by smaller specimen is more than larger specimen. This is an indication for the existence of size effect.

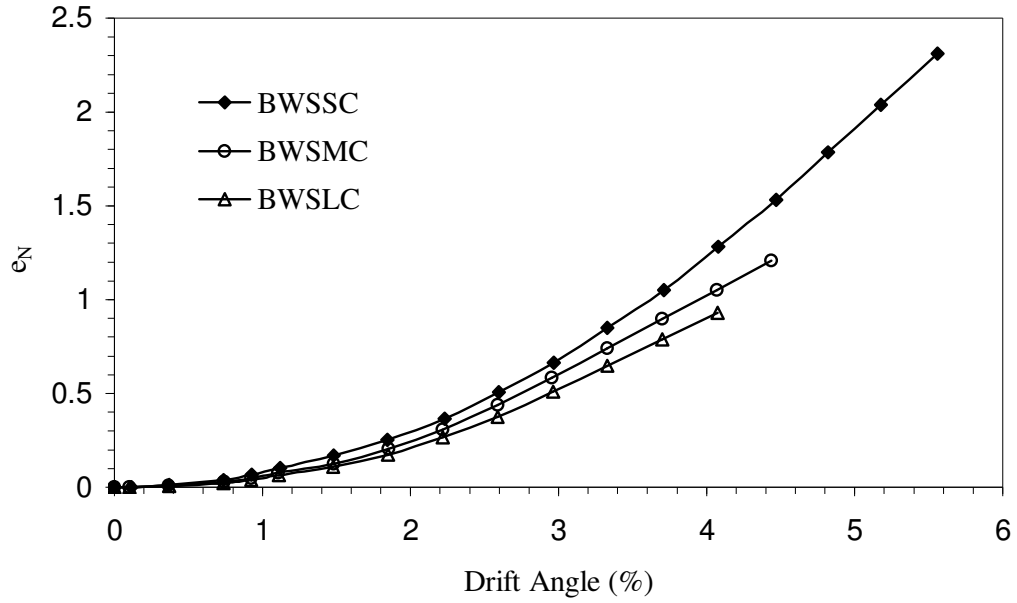

Fig.6.35 Cumulative energy dissipated per unit volume of joint for control specimens

6.5.5 Size Effect on Variation of Stress versus Relative Deflection

The relative deflection and stresses were calculated and the variation of stress with relative deflection was plotted for both control and retrofitted specimens (Fig.6.37 and Fig.6.38). Shear stress was calculated for control specimens, while bending stress was calculated for retrofitted specimens. It is observed that stress are highest for the smallest specimen and lowest for the largest specimen corresponding to any level of relative

deflection level for both the cases. This confirms the existence of size effect.

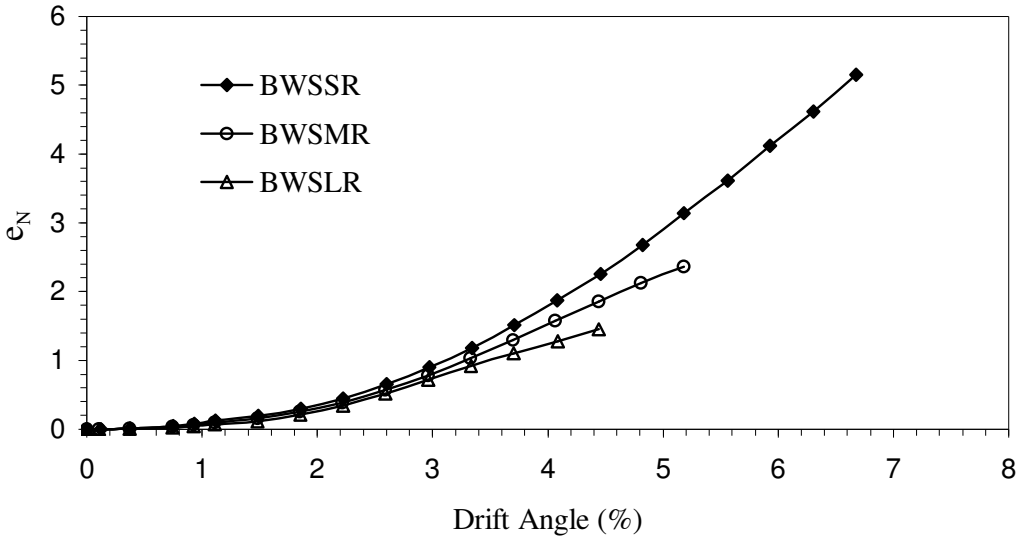

Fig. 6.36 Cumulative energy dissipated per unit volume of joint for retrofitted specimens

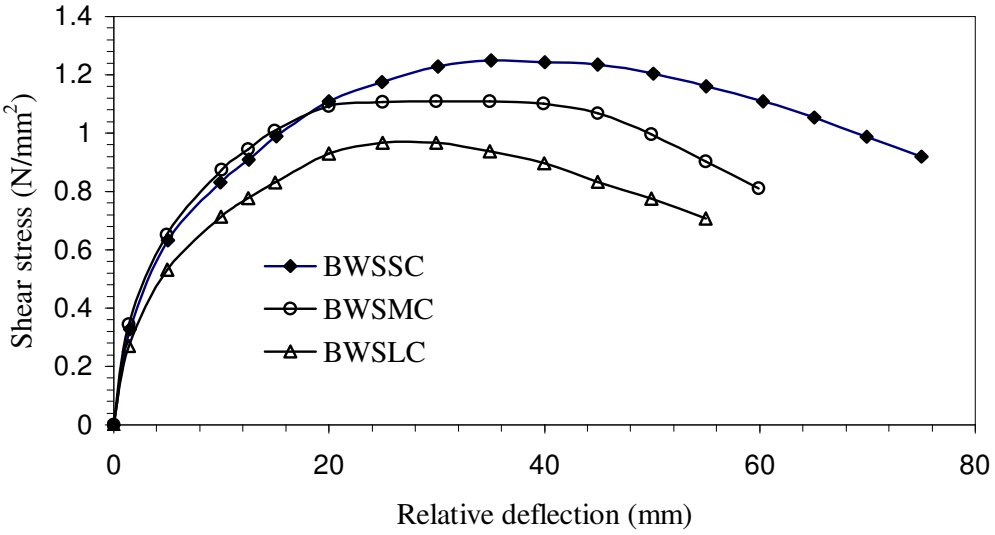

Fig.6.37 Variation of shear stress with relative deflection for control specimens

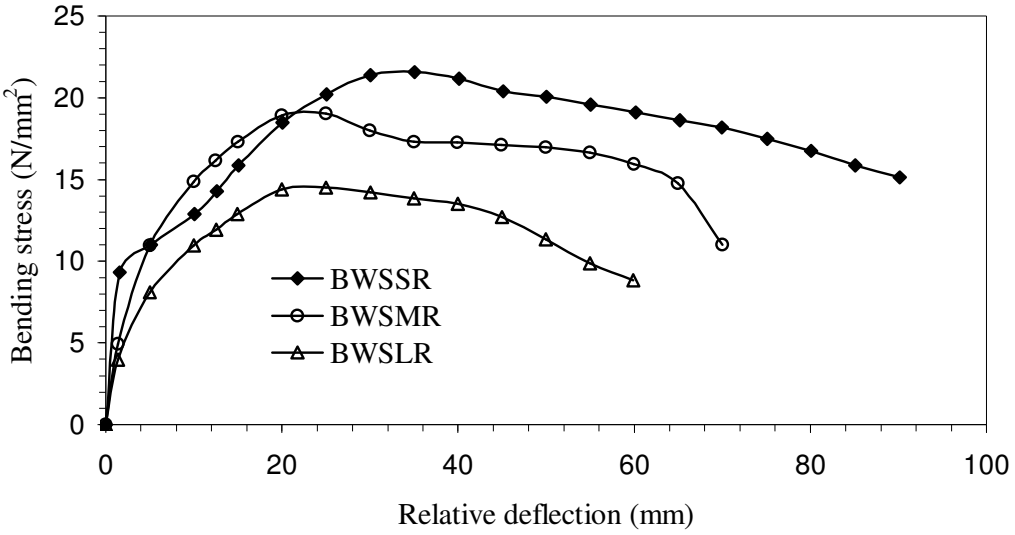

Fig. 6.38 Variation of bending stress with relative deflection for retrofitted specimens

6.6 CONCLUDING REMARKS

In this chapter, the experimental results of beam column joints with beam weak in shear specimens were analysed and interpreted for various parameters. Bi-logarithmic variation, variation of ductility with respect to drift angle, cumulative energy dissipation per unit volume of joint and variation of stress with relative deflection were plotted to observe the influence of size effect. It was observed that the bi-logarithmic plot for both control and retrofitted specimens followed the size effect law proposed by Baz˘ant. However, the size effect was more pronounced for retrofitted specimens than control specimen in the bi-logarithmic plotting. Further, the displacement ductility for both control and retrofitted specimens increased with the decrease in size of specimens. Further, it was noted that the cumulative energy per unit volume of the joint at every drift angle for small specimen was the maximum and it decreased as the specimen size increased. This was an indication for existence of size effect. The variation of shear stress with respect to relative deflection in case of control specimen as well as variation of bending stress in case of retrofitted specimens also supported the size effect principle.

The analysis of results reflects that there was notable improvement in ultimate load carrying capacity, energy dissipation, initial stiffness and ductility due to retrofitting of all the specimens studied. It was also noted that the enhancement due to strengthening in all these parameters followed the size effect principle. The next chapter describes about testing and analysis results of beam-column joints with column weak in shear specimens.

CHAPTER 7

EXPERIMENTAL STUDY ON BEAM-COLUMN JOINTS WITH COLUMN WEAK IN SHEAR

7.1 INTRODUCTION

This chapter describes the experimental result of beam-column joint specimens with column in shear. Similar to earlier two cases, six specimens were tested under this category also. The experimental data were plotted to construct hystersis loop, envelope curve, variation of stiffness, energy dissipation etc. Results of control and retrofitted specimens of various sizes were compared in term of all these above mentioned parameters and conclusions were drawn about benefit derived due to retrofitting. Finally, bi-logarithmic plots were drawn to explore the possibility of size effect in term of shear strength. At the end, specimen sizes were correlated with cumulative energy dissipated per unit volume of joint, stress, ultimate load carrying capacity etc.

7.2 TESTING OF LARGE SPECIMENS

The displacement history which has been shown in Fig. 5.1(a) was applied to these specimens by a servo hydraulic dynamic actuator of capacity ± 250 kN with maximum displacement amplitude of ± 125 mm. The experiment was stopped for control specimen at a stage when the load came down in the range of 65-70% of the ultimate load carrying capacity. Similarly, the experiment on retrofitted specimen was also stopped at about the same magnitude of load at which experiment was stopped for control specimen.

7.2.1 Large Control Specimen

The testing arrangement of this specimen is shown in Fig. 7.1. The appearance of initial cracks and the cracks at the end of the test are shown in Fig. 7.2 and 7.3 respectively. The hysteretic response obtained by plotting the test data is shown in Fig. 7.4. Some of the

important observations made during testing and those by analysing the hysteresis loop are presented here.

The first visible crack appeared in the beam- column joint at a displacement amplitude of ±5mm as shown in Fig. 7.2. More cracks started to develop in the column and the joint region as the amplitude was increased. It is observed from the hysteresis loop of Fig. 7.4 that the load reached to the maximum value of 56.17 kN in the push direction at 16^{th} cycle at displacement amplitude of 20 mm. Further, the load also reached the maximum value of 51.4 kN in the pull direction in the same cycle. The developed crack gradually propagated in the column from the joint on further increase in displacement. The crack reached the weakest shear zone in the column at the displacement amplitude of ±20 mm. The crack in the joint region became wider to a considerable extent and spalling of concrete started in the joint region at ±30 mm displacement amplitude. The propagated cracks in zones away from joints got further widened followed by spalling of concrete at column region and the testing was stopped at displacement amplitude of ±40 mm at which the load came down to the desired level. The ultimate load carrying capacity of CWSLC specimen was found to be 53.78 kN.

7.2.2 Large Retrofitted Specimen

This specimen was tested in a manner similar to that of control specimen. The testing arrangement is shown in Fig.7.5. The first visible crack appeared both in beam and column marked *A* in Fig. 7.6 at the first cycle of the deflection amplitude ±10 mm. Slight debonding of the GFRP sheet in joint region was also observed during the next cycles of ±10 mm amplitude. The view of the specimen at the end of testing is shown in Fig.7.7. The hysteretic response obtained by plotting the test data is shown in Fig. 7.8. It can be noted from the hysteresis loop that the specimen attained the maximum load of 64.57 kN in the push direction at 10^{th} cycle at a displacement of 12.5 mm. The load reached

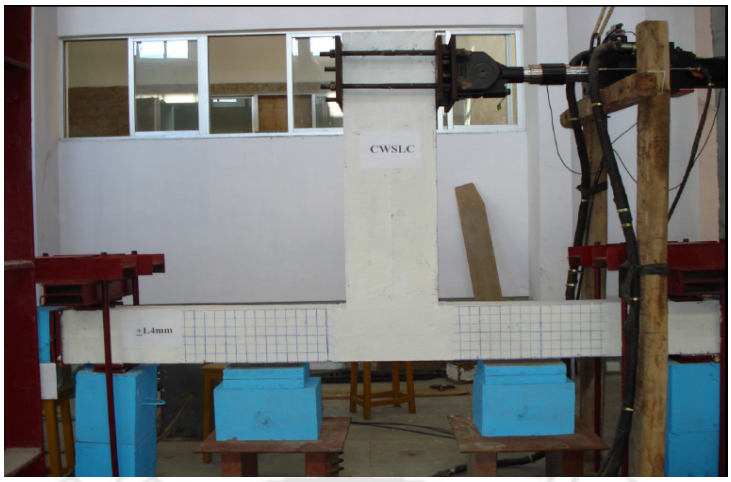

Fig.7.1 Testing arrangement of CWSLC specimen

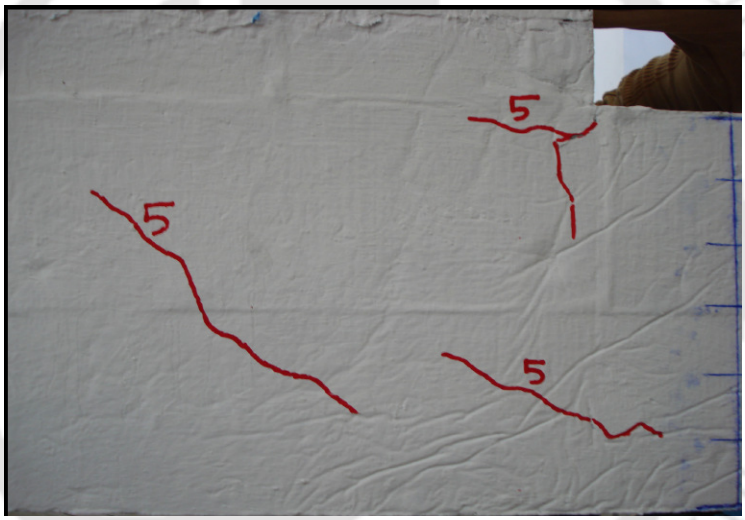

Fig.7.2 Appearance of first crack in CWSLC specimen

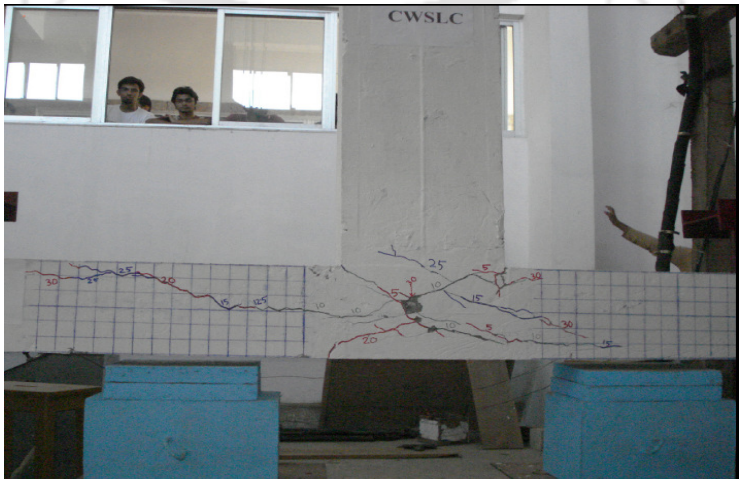

Fig. 7.3 CWSLC specimen at the end of testing

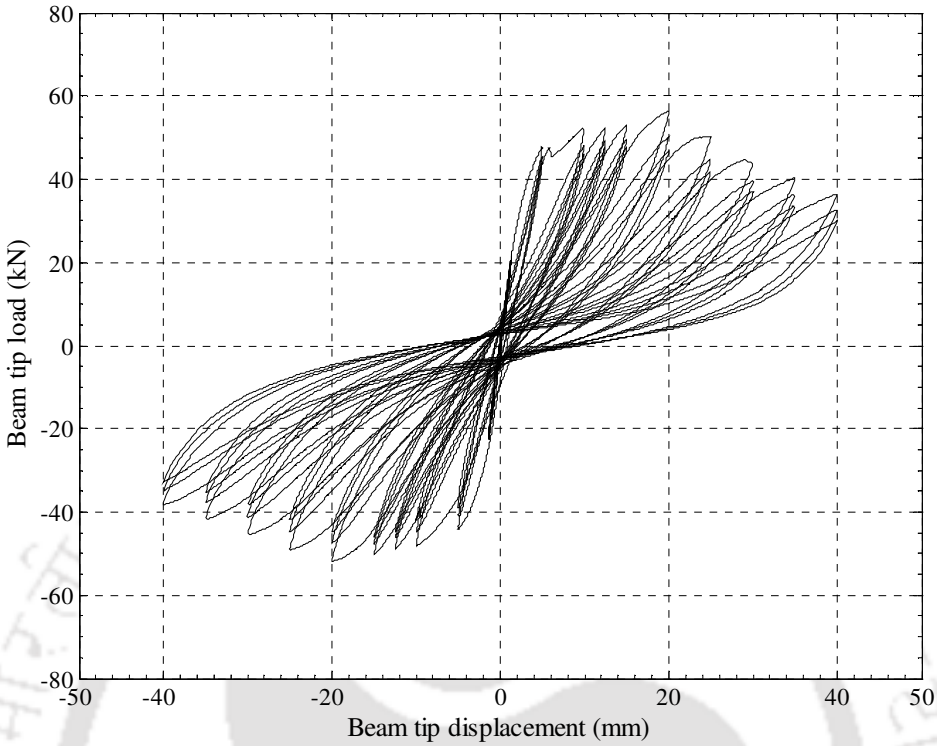

Fig.7.4. Hysteretic response of CWSLC specimen

to the maximum value of 63.09 kN in the pull direction in the 16th cycle corresponding to displacement of 20 mm. During that instant, more debonding of GFRP sheet was observed at the joint. First rupture on GFRP sheet appeared in column in this amplitude of ± 20 mm. The rupture in GFRP sheet at the joint propagated and reached from one end to the other end at ±25 mm amplitude. Crack was also observed on column beyond the strengthened zone. Delamination of CFRP sheet appeared in the column on either side at ±30 mm displacement amplitude. Spalling of concrete near the first GFRP shear strip in column was observed at ±40 mm displacement amplitude. The experiment was stopped at ±45 mm amplitude observing the reduction in load. The ultimate load carrying capacity of CWSLR specimen was found to be 64.06 kN.

7.2.3 Comparison of Test Results of Control and Retrofitted Large Specimen

The envelope curves of hysteresis loops for control as well as retrofitted specimen are shown in Fig. 7.9. It can be observed that the envelope curve for the retrofitted specimen

Fig. 7.5 Testing arrangement of CWSLR specimen

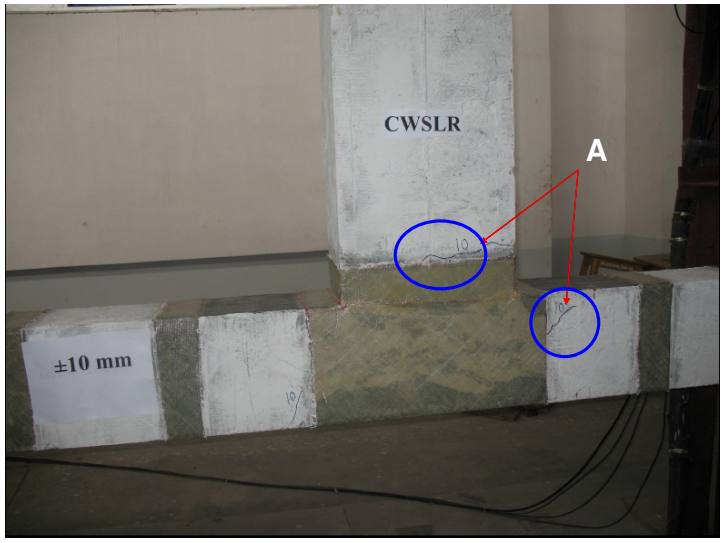

Fig.7.6 Appearance of first visible crack in CWSLR specimen

Fig. 7.7 CWSLR specimen at the end of testing

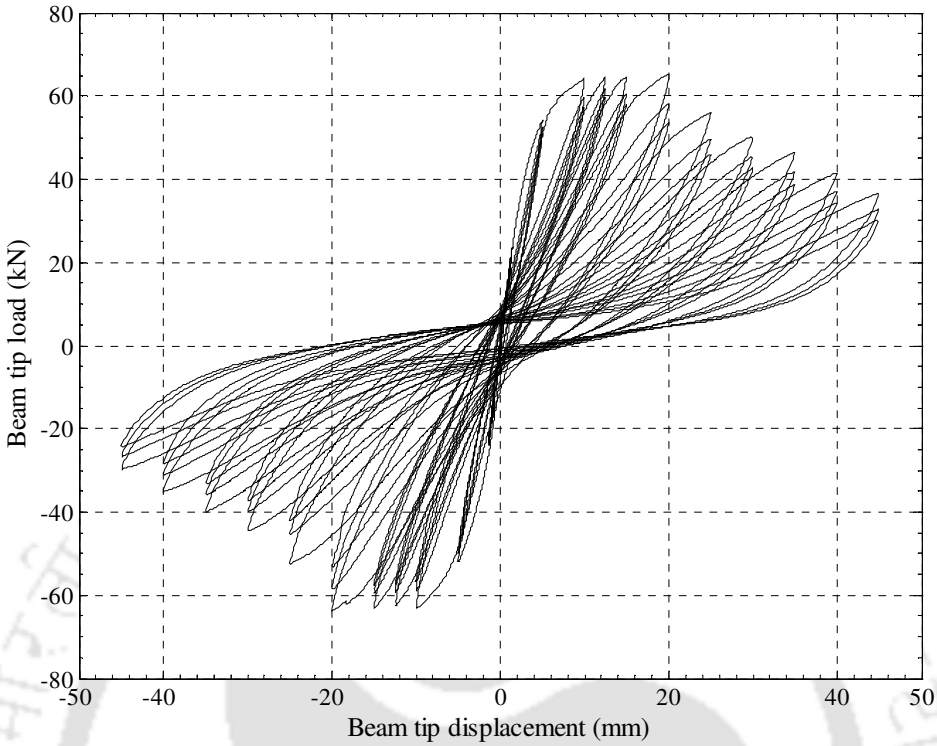

Fig.7.8 Hysteretic response of CWSLR specimen

shows significant improvement in load carrying capacity both in the push and pull direction. The percentage gain in ultimate load carrying capacity due to retrofitting was found as 19.10%.

The variation of stiffness with respect to drift angle for CWSLC and CWSLR specimens is shown in Fig.7.10. It can be observed that the stiffness of CWSLR specimen is generally more than that of CWSLC specimen corresponding to any particular drift angle. However, the initial stiffness for both the specimens are nearly same i.e. there is no significant improvement in initial stiffness due to retrofitting. The reason for such observation may be attributed to the fact that the retrofitting for this case was done only in column and not in beam. At the initial application of loading at the tip of the beam when the magnitude of applied load was low, the load was mainly resisted by the beam alone without transferring much load on the column. Since the beam portion was not strengthened, there was no visible improvement in the magnitude of initial stiffness. However, when displacement level was increased, column also participated to share

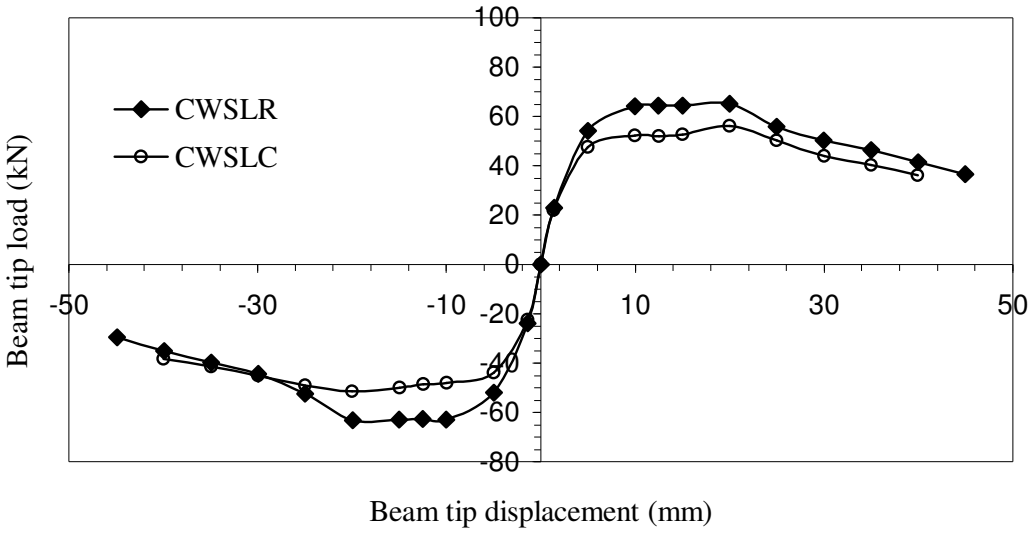

Fig. 7.9 Envelope curve for hysteresis loops of CWSLC and CWSLR specimens

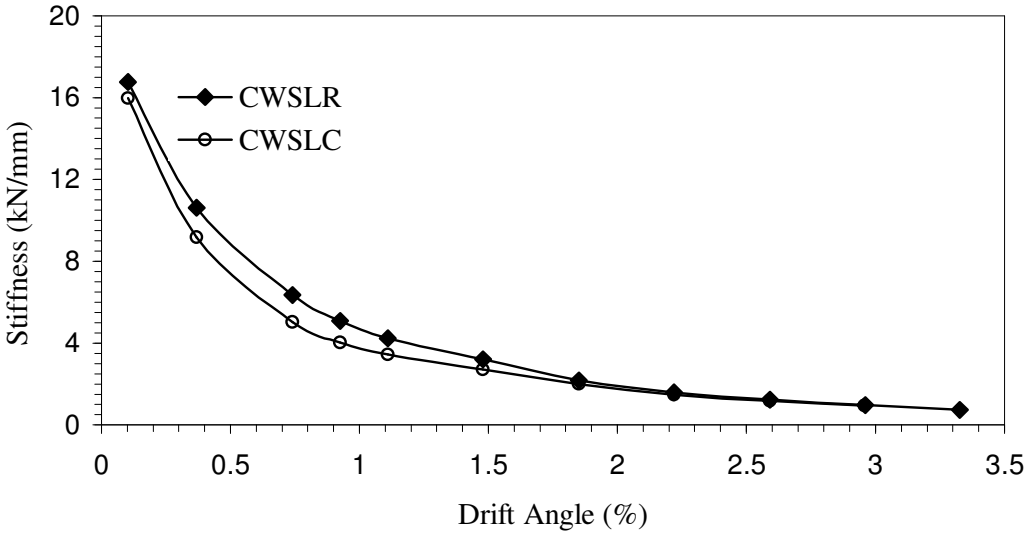

Fig. 7.10 Stiffness versus drift angle plot for CWSLC and CWSLR specimens

the applied load. Since the column was strengthened, hence significant improvement in stiffness could be noticed at subsequent stages of loading.

Fig. 7.11 shows the variation of energy dissipation with respect to drift angle for control and retrofitted specimens. The figure shows that the cumulative energy dissipated by retrofitted specimen is higher than that of control specimen at every drift angle. The gain in energy dissipation due to retrofitting is observed to be 69.57% corresponding to the

ultimate drift level.

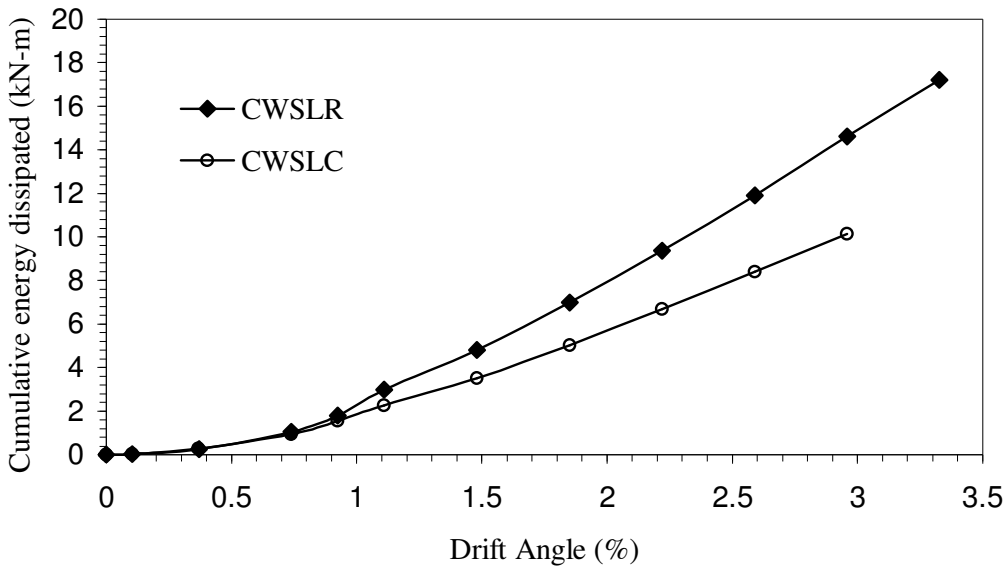

Fig. 7.11 Cumulative energy dissipated by CWSLC and CWSLR specimens

7.3 TESTING OF MEDIUM SPECIMENS

The displacement history as depicted by Fig. 5.1 (b) was applied to these specimens by a servo hydraulic dynamic actuator of capacity ±250 kN and maximum displacement capacity of ± 125 mm. The experiment was stopped when percentage reduction of load of similar order as that in the case of large specimen was attained.

7.3.1 Medium Control Specimen

Testing arrangement of this specimen is shown in Fig.7.12. The view of the specimen at the end of testing is shown in Fig. 7.13. The hysteresis loop obtained by plotting the test data is shown in Fig. 7.14. Some of the important observations made during testing and those by analysing the hysteresis loop are presented here briefly. The first crack appeared in the junction point of beam and column at amplitude of ± 3.33 mm (Fig. 7.12). The load reached the maximum level of 34.14 kN in the push direction in the 7th cycle at an amplitude of ± 6.67 mm. At the same amplitude, cracks appeared in column on either

side of the joint. The already developed cracks propagated towards the end of column at ± 10 mm amplitude. Maximum load of 34.09 kN was observed in the pull direction in 16th cycle at a displacement of 13.33 mm. In the subsequent cycles of this amplitude, the crack extended up to the location of the first lateral tie provided in column. Development of a major crack was noticed at ± 16.67 mm displacement amplitude. Spalling of

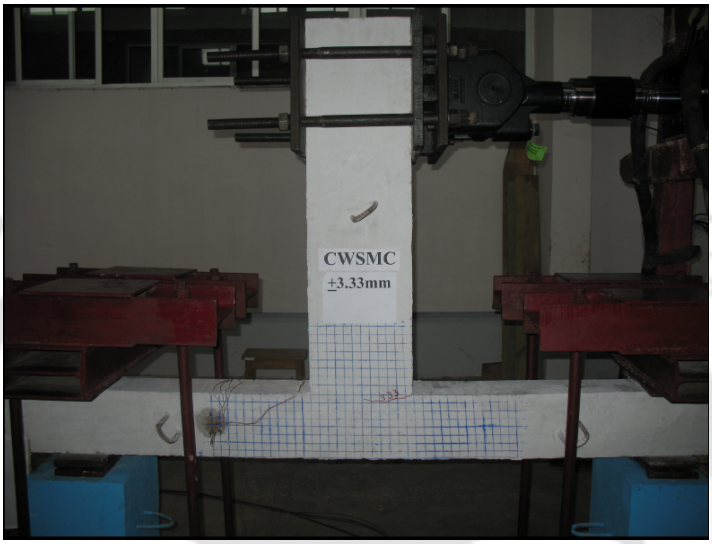

Fig. 7.12 Appearance of first cracks in CWSMC specimen

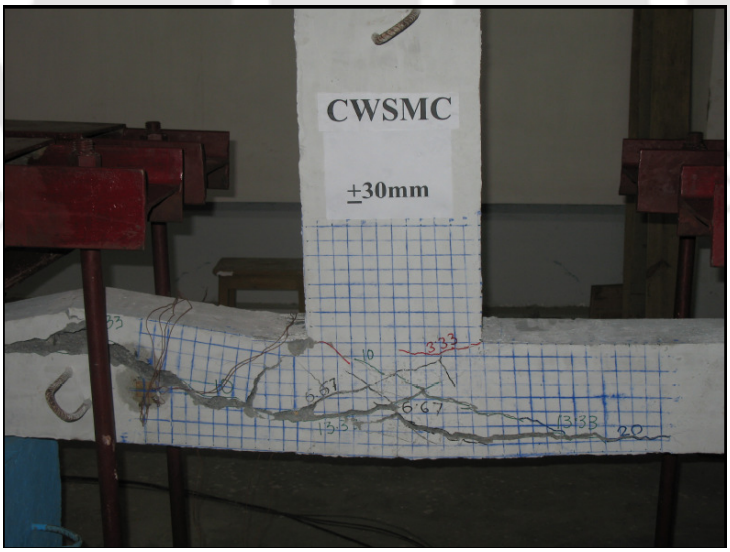

Fig. 7.13 CWSMC specimen at the end of testing

concrete started at ± 20 mm displacement amplitude. The shear reinforcement provided in one of the side of column started to fail with a loud noise at ± 26.67 mm amplitude. The experiment was stopped at ± 30 mm displacement amplitude. The ultimate load

carrying capacity of CWSMC specimen was found to be 32.76 kN.

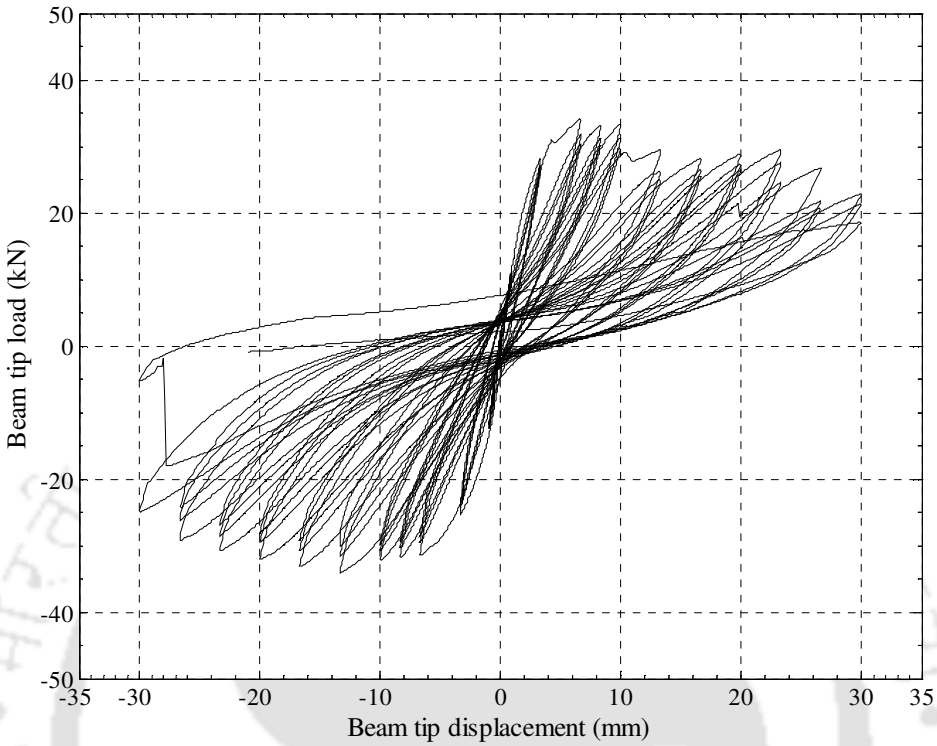

Fig.7.14 Hysteretic response of CWSMC specimen

7.3.2 Medium Retrofitted Specimen

This specimen was tested in a similar manner to that of control specimen. Fig. 7.15 shows the appearance of first visible crack, which occurred in the beam at a displacement amplitude of ± 6.67 mm. Fig.7.16 shows the appearance of rupture in GFRP sheet at the column face of the beam, which occurred at ± 10 mm amplitude. Further cracks were observed in the beam at the subsequent cycles of the same amplitude of ± 10 mm. Fig. 7.17 shows the view of the specimen at the end of testing. The hysteresis loop obtained by plotting the test result is shown in Fig. 7.18. The delamianation of GFRP sheet started at the joint region at ± 13.33 mm amplitude. The load reached the maximum value of 45.64 kN in the push direction at 19th cycle at a displacement of ± 16.67. In the same cycle, large crack appeared in the column. The load attained the highest value of 35.89 kN in the pull direction at 22nd cycle at a displacement of ± 20 mm. The rupture in GFRP sheet got further widened and finally got separated into two distinct pieces at ± 23.33 mm

Fig. 7.15Appearance of first visible crack in CWSMR specimen

Fig. 7.16 Appearance of rupture in GFRP in CWSMR specimen

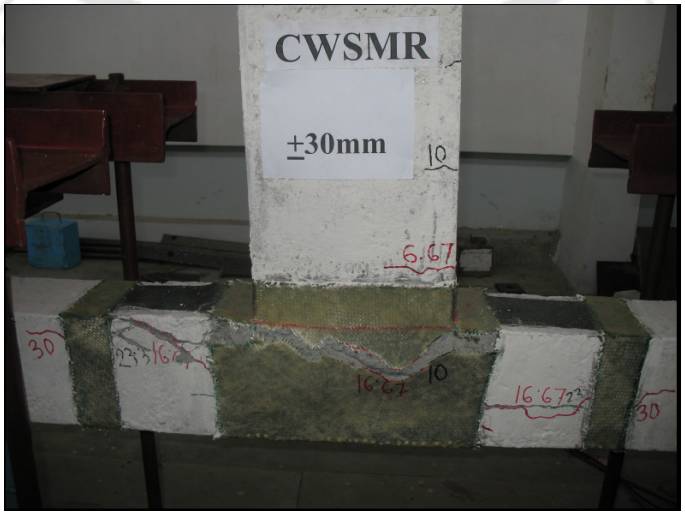

Fig. 7.17 CWSMR specimen at the end of testing

amplitude. Spalling of concrete started. The load carrying capacity of the specimen came down to desired level at displacement amplitude of ± 30 mm and the experiment was stopped. The ultimate load carrying capacity of CWSMR specimen was found to be 42.36 kN.

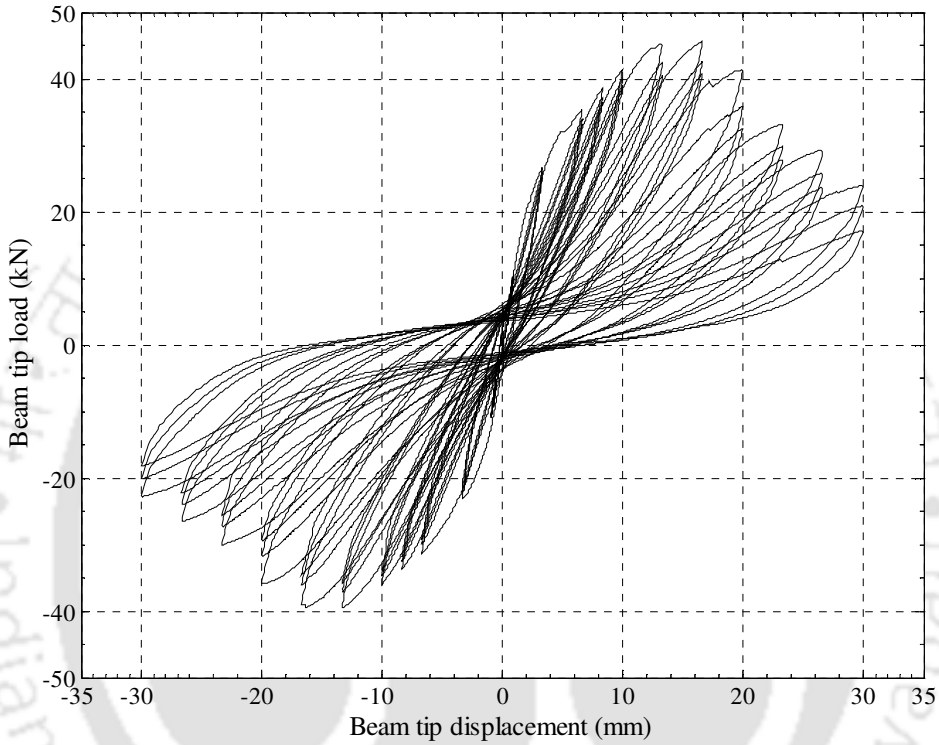

Fig. 7.18 Hysteretic response of CWSMR specimen

7.3.3 Comparison of Test Results of Control and Retrofitted Medium Specimen

The envelope curves of hysteresis loop for control as well as retrofitted specimen are shown in Fig. 7.19. It can be observed that the retrofitted specimen shows appreciable increase in load carrying capacity both in push and pull directions. The percentage gain in ultimate load carrying capacity due to retrofitting was calculated as 29.30%.

The variation of stiffness for CWSMC and CWSMR specimens are shown in Fig. 7.20. It can be concluded that the stiffness of retrofitted specimen is slightly improved than that of control specimen though at the initial phase there is hardly any improvement. Fig. 7.21 shows the energy dissipation curve for control and retrofitted specimens. It is clear that the energy dissipated by retrofitted specimen is higher than that of control specimen at

different drift angles. The maximum gain in energy dissipation due to retrofitting is 28.11%.

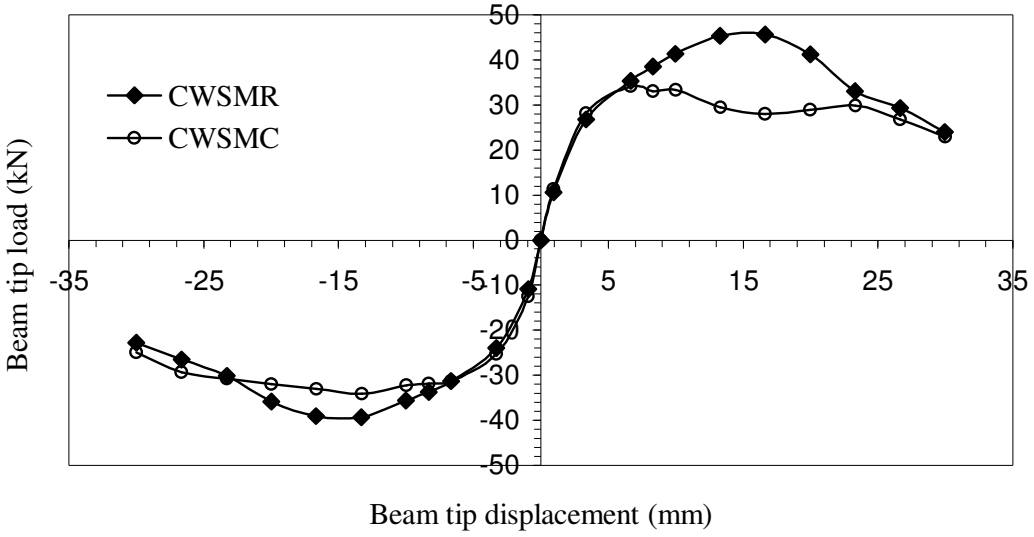

Fig. 7.19 Envelopes of hysteresis loops for CWSMC and CWSMR specimens

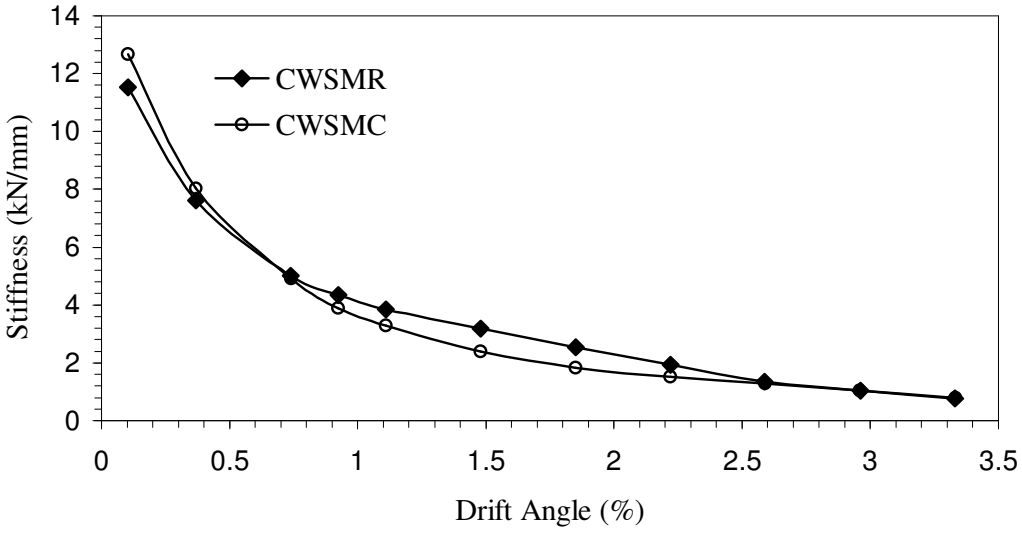

Fig. 7.20 Stiffness versus drift angle plot for CWSMC and CWSMR specimens

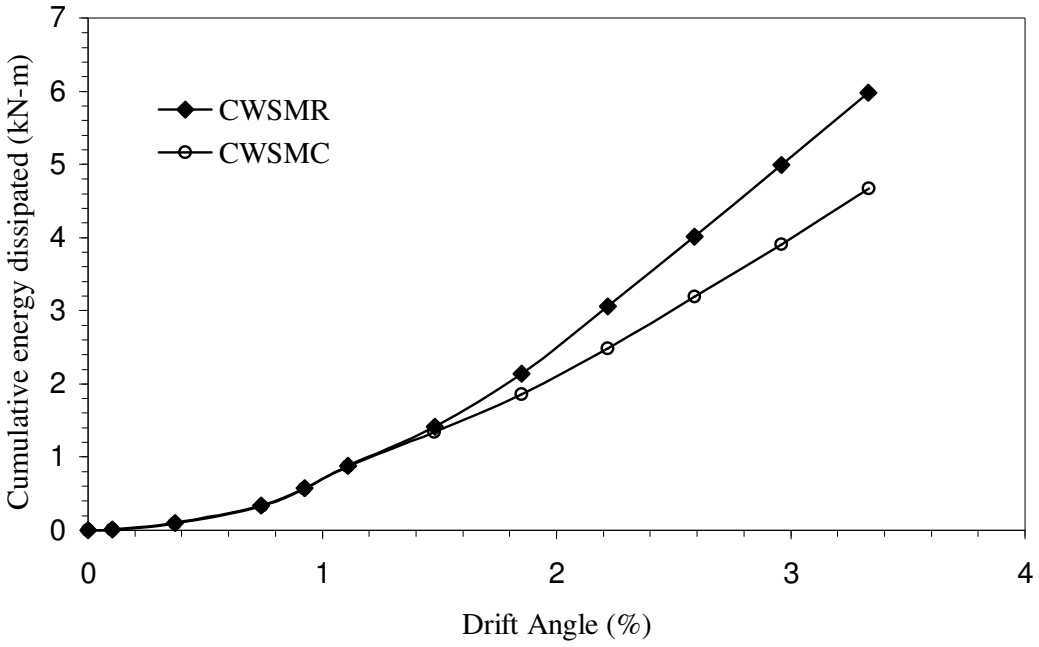

Fig.7.21 Cumulative energy dissipated by CWSMC and CWSMR specimens

7.4 TESTING OF SMALL SPECIMENS

The displacement history as defined in Fig. 5.1 (c) was applied to these specimens by a servo hydraulic dynamic actuator of capacity ±100 kN and maximum displacement capacity of ±125 mm. The experiment was stopped when the load came down to the same extent of percentage as that in the case of large specimen.

7.4.1 Small Control Specimen

The views of this specimen during testing are shown in Fig.7.22 and 7.23. The hysteretic response obtained by plotting the test data is presented in Fig. 7.24. The first visible crack was observed in the beam-column joint region at displacement amplitude of ±3.33 mm. More cracks appeared in the joint region at ±5 mm displacement amplitude. The load reached the maximum value of 9.224 kN in the push direction and 8.064 kN in the pull direction at 16th cycle at a displacement of 8.33 mm. Spalling of concrete started at displacement amplitude of ± 15 mm. The experiment was finally stopped at ± 16.33 mm. It was noted that till the end of the test, no crack was observed in the beam portion.

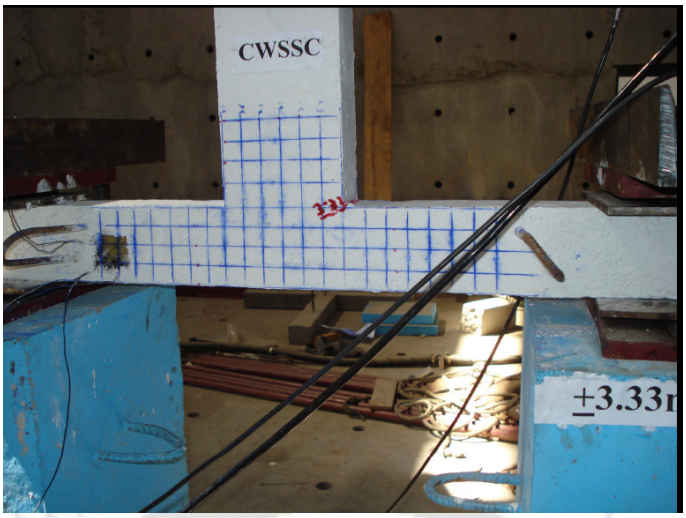

Fig. 7.22 Appearance of first crack in CWSSC specimen

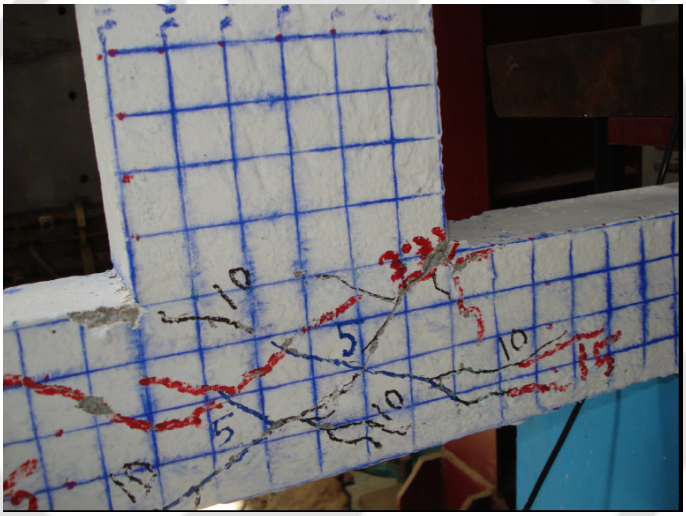

Fig. 7.23 CWSSC specimen at the end of testing

The ultimate load carrying capacity of CWSSC specimen was found to be 8.635 kN.

7.4.2 Small Retrofitted Specimen

This specimen was tested in a manner similar to that of the control specimen. Fig. 7.25 shows the appearance of first visible crack in this specimen, which occurred at displacement amplitude of ± 8.33 mm. Rupture in GFRP sheet at the junction of beam-column joint was also observed at that instant. The experiment was stopped at amplitude of ± 16.67 mm and the specimen at the end of testing is shown in Fig.7.26. The hysteretic response is shown in Fig. 7.27. The load reached the highest value of 11.28 kN in the

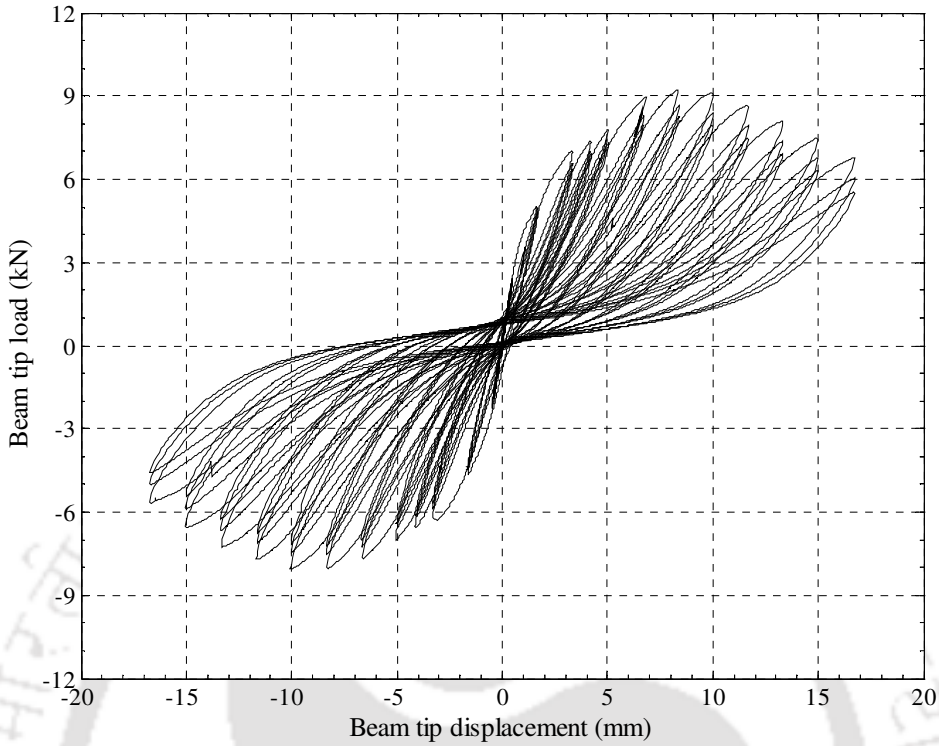

Fig. 7.24 Hysteretic response of CWSSC specimen

push direction at 19th cycle at a displacement of 10 mm. It also reached to the highest value of 11.62 kN in the pull direction in the same cycle. Diagonal cracks appeared in the junction of the beam-column joint with a loud sound at ± 13.33 mm amplitude. More rupture of GFRP sheet took place with a loud sound at ± 15 mm amplitude. Pieces of concrete started to get separated from the specimen at displacement amplitude of ± 16.67 mm. This led to the decline in the load carrying capacity to the desired extent and finally the test was stopped. The ultimate load carrying capacity of CWSSR specimen was found to be 11.45 kN.

7.4.3 Comparison of Test Results of Control and Retrofitted Small Specimen

The envelope curves of hysteresis loops for control as well as retrofitted specimen are shown in Fig. 7.28. It can be observed that retrofitted specimen shows higher load carrying capacity than that of the control specimen both in push and pull directions. The percentage gain in ultimate load carrying capacity due to retrofitting was calculated as

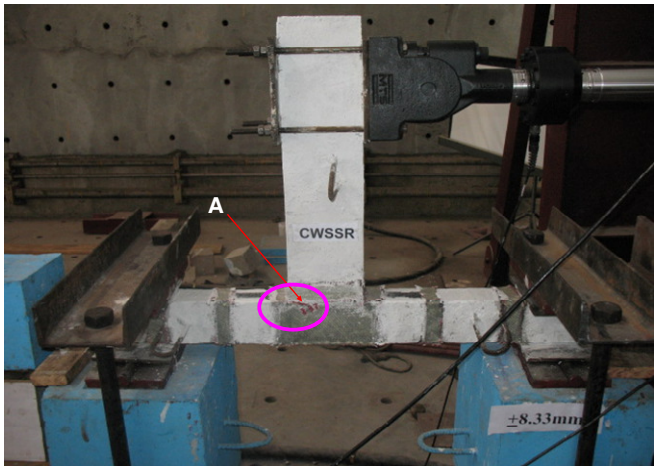

Fig.7.25 Appearance of first visible crack in CWSSR specimen

Fig. 7.26 CWSSR specimen at the end of testing

32.56%. The variation of stiffness for CWSSC and CWSSR specimens is presented in Fig. 7.29. The stiffness of CWSSR specimen is more than that of CWSSC specimen throughout the curve, though the initial stiffness remains almost same. Fig. 7.30 shows the energy dissipation curve for control and retrofitted specimens. The Figure shows that the energy dissipated by retrofitted specimen is higher than that of control specimen at every drift angle. The maximum gain in energy dissipation due to retrofitting is 27.6% till the end of experimental investigation.

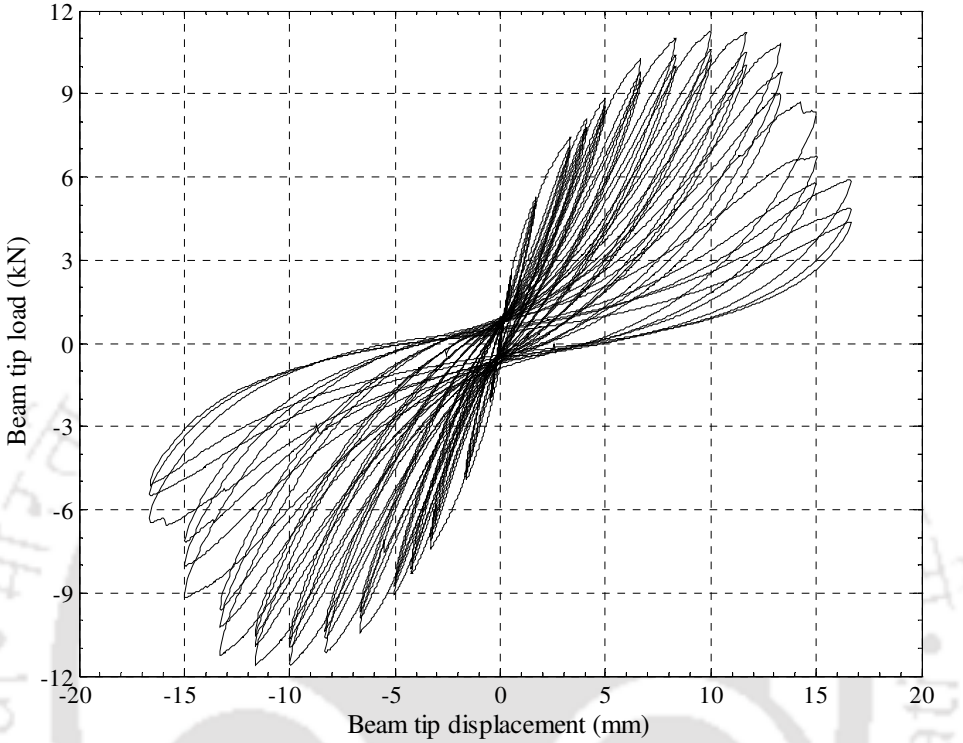

Fig.7.27 Hysteretic response of CWSSR specimen

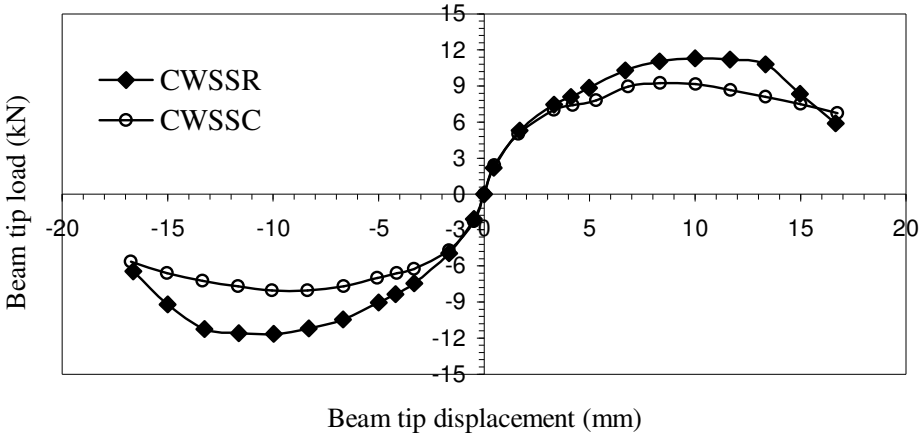

Fig. 7.28 Envelopes of hysteresis loops of CWSSC and CWSSR specimens

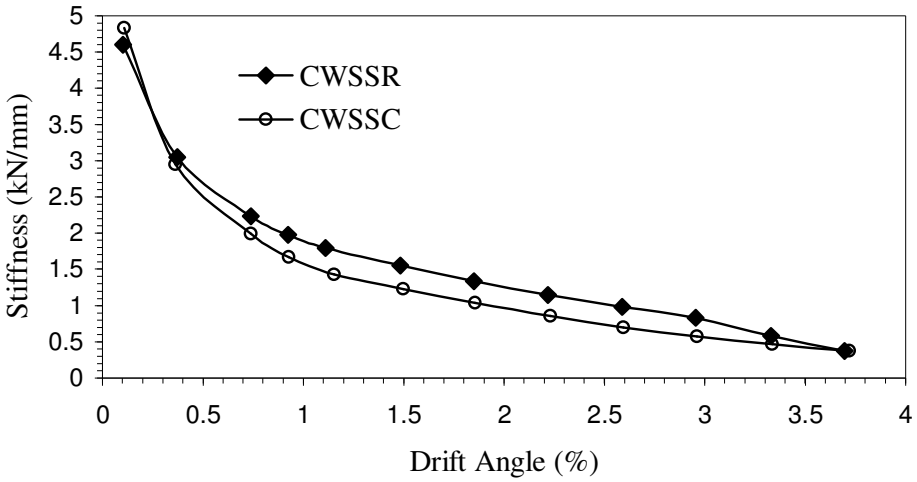

Fig. 7.29 Stiffness versus drift angle plot for CWSSC and CWSSR specimens

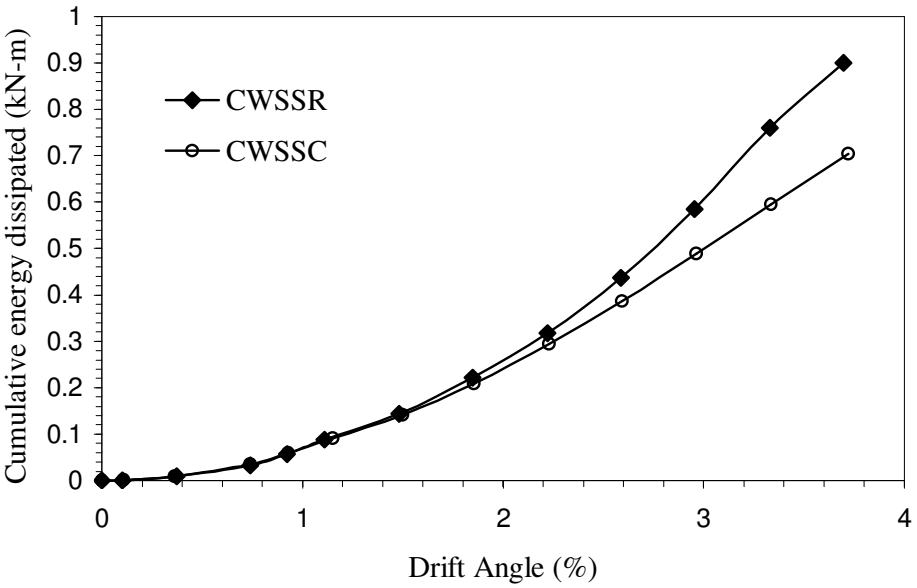

Fig. 7.30 Energy dissipation of CWSSC and CWSSR specimens

7.5 INTERPRETATION OF RESULTS TO EXPLORE THE EXISTANCE OF SIZE EFFECT

The results obtained by testing the specimens were used to draw bi-logarithmic plot. In addition, the percentage gain in ultimate load carrying capacity and energy dissipation due to retrofitting were correlated with size of specimens. Finally, specimen sizes were correlated of with energy dissipation per unit volume of the beam-column joint and variation of stresses versus relative deflection of the control as well as retrofitted specimens.

7.5.1 Bi-logarithmic Plot

The specimens failed in shear and hence shear stress was calculated in all the cases. The calculation of shear stress is shown in Appendix-C. The calculated shear stress and other parameters necessary for drawing of regression and bi-logarithmic plot are shown in the Table 7.1. Regression analysis was carried out to find B and D_0 and finally the bi-logarithmic plot was drawn as shown in Fig. 7.31 and 7.32. These graphs show presence of size effect and support Bazˇant's size effect law similar to other cases. However, the calculated slope towards the end of both the curves was found steeper than the slope prescribed by Bazˇant's size effect law.

Table 7.1 Parameters for bi-logarithmic plot

Type of specimen	Name of specimen	Shear stress, σ_{N_U} (N/mm^2)	Depth of specimen, D (mm)	$\left(\frac{f_t'}{\sigma_{N_U}}\right)^2$	Log (D/Do)	$Log(\sigma_{N_U}/Bf_t')$
control	CWSSC	0.662	100	11.96616	0.243668	-0.24227
	CWSMC	0.628	200	13.29694	0.544698	-0.26517
	CWSLC	0.458	300	25.0000	0.720789	-0.40226
Retrofitted	CWSSR	0.878	100	6.80271	-0.0593	-0.15512
	CWSMR	0.811	200	7.973138	0.241732	-0.1896
	CWSLR	0.545	300	12.60525	0.417823	-0.28906

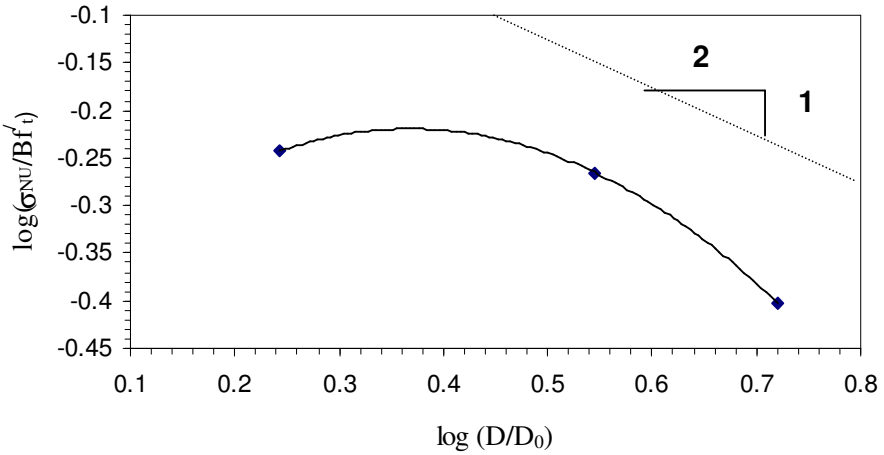

Fig. 7.31 Bi-logarithmic plot for column weak in shear : control specimens

7.5.2 Size Effect on Gain in Ultimate Load Carrying Capacity on Retrofitting

The percentage gain in ultimate load carrying capacity of retrofitted specimens with respect to control specimen for all sizes were calculated and presented in Fig. 7.33. The figure shows that the gain in ultimate load carrying capacity for the smallest specimen is largest (32.6%), while for the largest specimen it is least (19.1%). Thus, the gain in ultimate load carrying capacity due to retrofitting supports the size effect principle. Further, it was noted that there was considerable gain in energy dissipation due to retrofitting ranging from 27.6% to 69.57%.

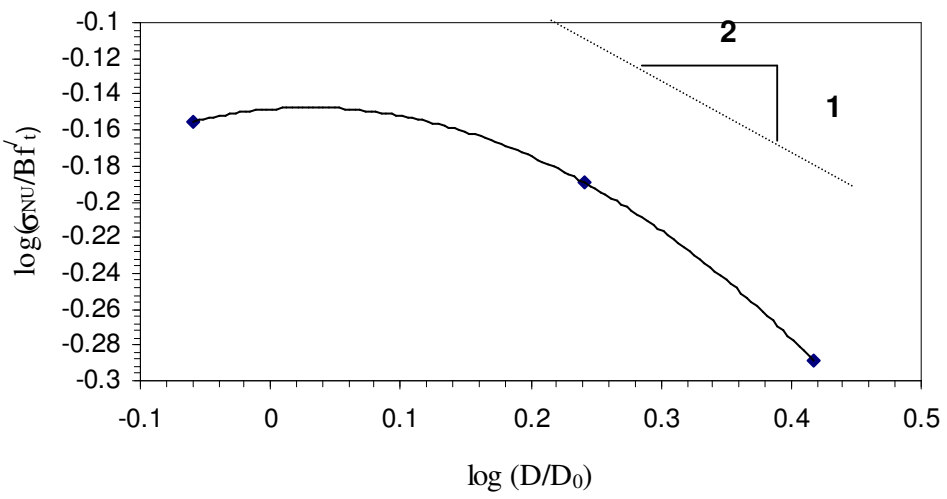

Fig. 7.32 Bi-logarithmic plot for column weak in shear : retrofitted specimens

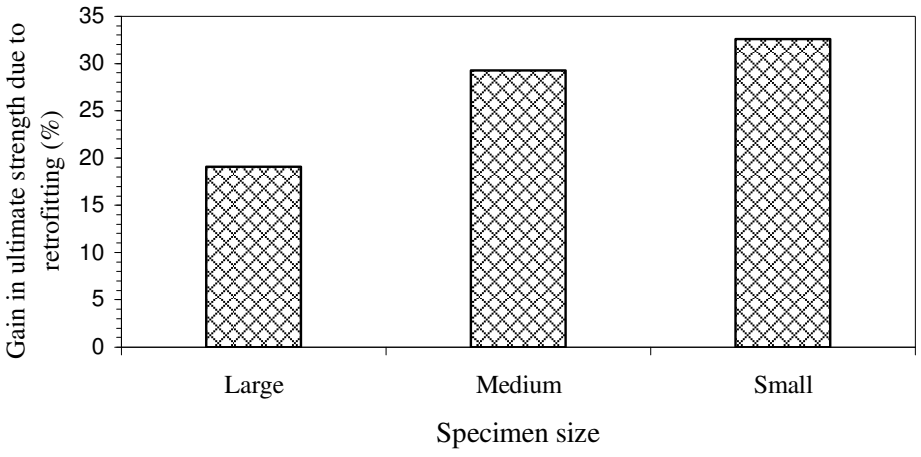

Fig.7.33 Percentage gain in ultimate load carrying capacity due to retrofitting

7.5.3 Size Effect on Energy Dissipated per Unit Volume of Joint

The cumulative energy dissipated per unit volume of the joint, e_N for all the specimens were plotted with respect to drift angle. Fig. 7.34 shows the plot for control specimens, while Fig. 7.35 shows the same for retrofitted specimens. It can be clearly observed that in both the figures the Cumulative energy dissipated per unit volume of joint of is the highest for the smallest specimen and vice versa. Thus, it can be concluded that the

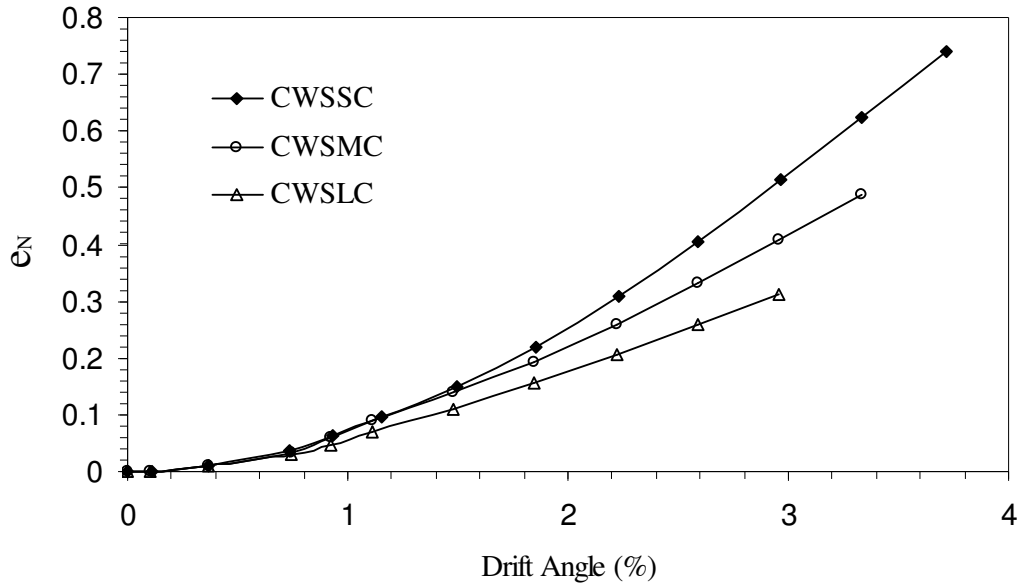

Fig.7.34 Cumulative energy dissipated per unit volume of joint for control specimens

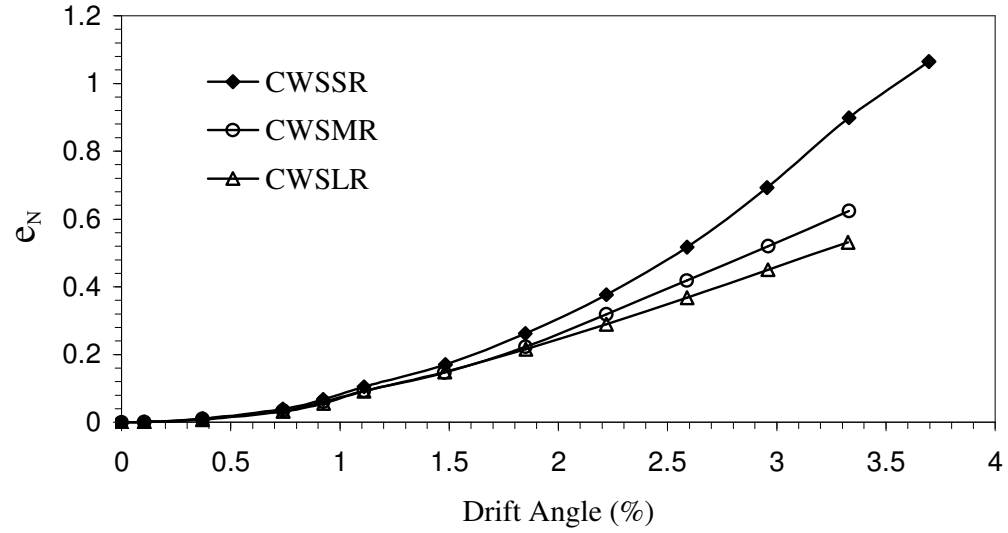

Fig.7.35 Cumulative energy dissipated per unit volume of joint for retrofitted specimens

cumulative energy dissipated per unit volume of the joint increases as the size of the specimen decreases, which is a clear indication of size effect.

7.5.4 Size Effect on Variation of Stress versus Relative Deflection

The variation of shears stress with relative deflection were plotted for both control and retrofitted specimens in Fig.7.36 and Fig.7.37 respectively. The plot for small specimen shows highest stresses at every level of relative deflection while least for large specimen in both the cases. Thus it substantiates the size effect principle.

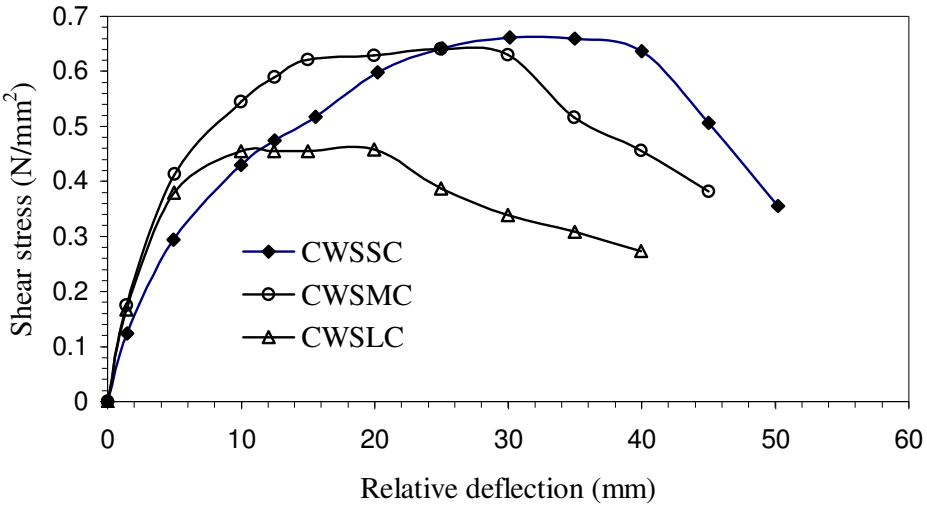

Fig.7.36 Shear stress versus relative deflection for control specimens

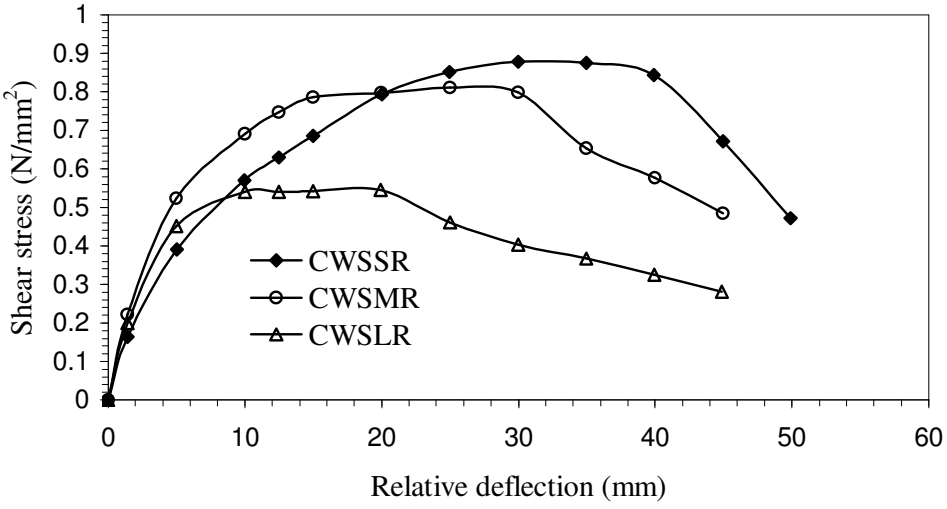

Fig. 7.37 Shear stress versus relative deflection for retrofitted specimens

7.6 CONCLUDING REMARKS

In this chapter the result of beam column joint for column weak in shear specimens were interpreted for various parameters. Similar to the earlier cases, it was observed that the bi-logarithmic plot for both control and retrofitted specimens followed the size effect law proposed by Bazˇant. However, slope of the curves towards the end was found steeper than the slope prescribed by Bazˇant's size effect law. Further, it was noted that the cumulative energy per unit volume of the joint at every drift angle for small specimen was the maximum and it decreased as the specimen size increased. This was an indication for existence of size effect. The variation of shear stress with respect to relative deflection also supported the size effect principle. The gain in ultimate load carrying capacity due to retrofitting also corroborated the size effect phenomena. The summary of the whole experimental investigation and overall conclusion is presented in chapter-8.

CHAPTER 8

SUMMARY AND CONCLUSIONS

8.1 SUMMARY

In the present study, the performances of beam-column joints with three possible deficiencies and subjected to cyclic loading were evaluated and documented in terms of load carrying capacity, displacement ductility, energy dissipation etc. The joints were retrofitted using CFRP and GFRP sheet for reddressal of the specific deficiencies in the three cases considered in the present study. Total six types of specimens were considered, namely (a) Beam-column joint with beam weak in flexure : control (b) Beam-column joint with beam weak in shear : control (c) Beam-column joint with column weak in shear : control (d) Beam-column joint with beam weak in flexure : retrofitted (e) Beam-column joint with beam weak in shear : retrofitted and (f) Beam-column joint with column weak in shear : retrofitted. Three geometrically similar specimens of full scale, two-third scale and one-third scale sizes were considered in each type of deficient beam-column joint. Thus, total eighteen specimens were tested covering control specimens with three different deficiencies and their retrofitted specimens with three different sizes in each category of specimens. The design of control specimens of beam weak in flexure were done following provisions of the relevant design codes, while all the provisions of code were not followed for the specimens of other two types in order to attain a predefined deficiency. The specimens were retrofitted to enhance load carrying capacity, energy dissipation, ductility etc. The design of retrofitted specimens were carried out following guidelines in some published literatures. Two-third and one-third sized specimens were proportionately scaled down in all the three dimensions. The diameter of the reinforcing bars, development length, length of special confinement zone, cover of reinforcement etc. were also scaled down appropriately. Prior to the experiments, numerical studies were carried out using the general purpose finite element software

ANSYS 6.0. Nonlinear static analyses were carried out for getting prior information about load at first crack, load and deflection at yielding, crack pattern, ultimate load etc. of all the specimens in order to appropriately design the arrangement of experimental investigation. The experimental set-up needed for the testing of different sizes of beam-column joints were developed.

Displacement controlled loading system with a frequency of 0.025Hz was applied to the specimens by servo hydraulic dynamic actuators (MTS make). The ultimate load carrying capacity of all the eighteen specimens as obtained by experimental investigation is furnished in Appendix-D (Table D.1). In the same table, the available results of ultimate load carrying capacity found by strength based criteria and by numerical simulation are also presented for comparison. The beam-column joints with beam weak in flexure and beam weak in shear were designed as strong column-weak beam. The beam was idealised as a cantilever beam for arriving at the failure tip load of the beam. However, the same assumption was not valid for column weak in shear specimens. Hence, the calculation of load carrying capacity for such specimens were not carried out in the present study. However, it can be observed that the available results obtained by different methods are in good agreement. Further, it was noted that as the specimen size decreased, the difference between result obtained by experimental investigation and strength based criteria became more prominent. The same was also true for result obtained by FE analysis with ANSYS 6.0. This is an indication of existence of size effect as manifested by results of both experimental as well as numerical investigation using ANSYS 6.0. It is interesting to note that the result obtained by experimental investigation was closer to the result obtained through numerical simulation by ANSYS 6.0 in comparison to the result obtained by strength based criteria.

However, it may be noted that the deflection at first crack recorded experimentally did not match properly with those observed from numerical simulation using ANSYS. For example, the first visible crack in beam weak in flexure large control specimen appeared

at 5.0 mm displacement during experiment, while the same was observed as 1.4 mm as per numerical simulation. The reason may be attributed to the fact that perhaps very minor crack got developed at 1.4 mm, which could not be noticed by naked eye.

The results obtained by testing the specimens were used for the bi-logarithmic plotting to explore the possibility of existence of size effect. For the purpose of statistical regression of data, the size effect law proposed by Bazˇant was used. Different plots were drawn for control and retrofitted specimens in each of the cases. In all the cases, it was found that these graphs followed the well established size effect law proposed by Bazˇant.

It is observed from the bi-logarithmic plots of all the control specimens that the slope of the curve at the end of the LEFM zone is the least for beam weak in flexure : control specimens and highest for column weak in shear : control specimens. Thus, as the specimen exhibits more and more brittle mode till failure, the size effect also become more pronounced. Further, the slope of the curve for beam weak in flexure : retrofitted and beam weak in shear : retrofitted specimens are more or less same and are lesser than that of column weak in shear : retrofitted specimens. Thus, similar trend as before has also been observed for retrofitted specimens that the size effect get more and more prominent as the specimen become more and more brittle.

In all the three cases of deficient beam-column joints, there were considerable gain in ultimate load carrying capacity due to retrofitting. The overall gain in ultimate load carrying capacity due to retrofitting for all the three cases of beam-column joints tested is presented in Appendix-D (Fig. D.1). The percentage gain in ultimate load carrying capacity varied from 5.18% to 32.56% for the specimens studied. The least gain is for beam weak in flexure large specimen and the highest gain is for column weak in shear small specimen.

Moreover, it was found that the percentage gain in ultimate load carrying capacity due to retrofitting decreased with increase in specimen size in all the cases studied. Thus, it supported the existence of size effect in the retrofitted beam-column joints.

The percentage gain in energy dissipation of all specimens due to retrofitting were also appreciable and varied from 26.03% to 97.7%. The gain in energy dissipation coroborrated size effect principle in majority of the cases studied. To compare the energy dissipation of specimens having different sizes of beam-column joints, a parameter viz. energy dissipation per unit volume of joint region, e_N was introduced. This parameter was correlated with the size of the specimen at different drift angles and accordingly variation of e_N versus drift angle were plotted for different sizes of specimens. Both retrofitted as well as control specimen were considered. It was observed from these plots that the size effect principle was valid i.e. energy dissipation per unit volume of the joint (e_N) decreased with increase in size of specimen. This proved that the energy dissipated per unit volume of joint by smaller specimen is more than larger specimen during cyclic loading. This is an indication for the existence of size effect.

There was a substantial gain in initial stiffness for both beam weak in flexure as well as beam weak in shear specimens due to retrofitting and it vary from 6.82% to 59.43% following the principle of size effect. However, the result of beam-column joint with column weak in shear did not reflect any gain in initial stiffness.

Further, displacement ductility of the control as well as retrofitted specimens were correlated with size of specimens. It was observed that the displacement ductility follows principle of size effect in majority of the cases studied. Finally, the variation of stress versus relative deflection were also studied for different sizes of the specimens and the existence of size effect was observed.

8.2 MAJOR CONCLUSIONS

Based on the experimental studies carried out for all the six categories of beam-column joints, the following conclusions were drawn –

- The bi-logarithmic plots of stresses for both control and retrofitted specimens followed closely the size effect law proposed by Bazˇant in all the cases studied.
- The gain in ultimate load carrying capacity due to retrofitting increased with decrease in size of the specimens corroborates the existence of size effect for all the cases studied.
- There was remarkable enhancement in cumulative energy dissipation for all specimens due to retrofitting. The gain in energy dissipation followed size effect principle in most of the cases studied.
- The cumulative energy per unit volume of the joint at every drift angle indicated the existence of size effect. This established that the energy dissipation per unit volume of joint increased as the specimen size decreased.
- In general, there was considerable gain in initial stiffness due to retrofitting supporting the existence of size effect. However, in beam-column joint with column weak in shear there was no change in initial stiffness due to retrofitting.
- The displacement ductility followed the principle of size effect in most of the cases studied.
- The variation of stresses with respect to relative deflection showed the existence of size effect for all the cases studied in this test programme.
- The ultimate load carrying capacity obtained for control and retrofitted specimens by numerical simulation through ANSYS also supported the existence of size effect when studied under monotonic loading.
- Finally, the experimental programme carried in this study established that the size effect is more pronounced in case of brittle mode of failure.

8.3 SCOPE FOR FUTURE WORK

Additional work may be undertaken in the following areas:

- Three different sizes of specimens were considered in the present study. The prohibitive cost of material and manpower primarily limited the number of such specimens. However, larger number of specimens may be attempted for better acceptability of results.
- The damaged specimens can be rehabilitated and a similar study can be performed on size effect of rehabilitated specimens.
- Numerical analysis may be carried out by introducing appropriate model for all constituent materials concrete to reflect the behaviour under cyclic loading.

REFERRENCES

Abdel-Fattah B, Wight JK (1987). Study of Moving Beam Plastic Hinging Zones for Earthquake-Resistant Design of R/C Buildings. ACI Structural Journal, 31-39.

ACI 318 (2005)__Building Code Requirements for Structural concrete.

ACI 352R-02 (2002)__Recommendations for design of beam-column-joints in monolithic reinforced concrete structures, American Concrete Institute, ACI- ASCE, Committee 352, Detroit.

Agarwal P, Shrikhande M (2007). Earthquake resistant design of structures. Prentice Hall of India Private Limited, New Delhi.

Alcocer M, Jirsa JO (1993). Strength of Reinforced Concrete Frame Connections Rehabilitated by Jacketing. ACI Structural Journal, 249-261.

Anania L, Badala A, Failla G (2005). Increasing the flexural performance of RC beams strengthened with CFRP materials. Construction and Building Materials, Elsevier, 19, 55–61.

An W, Saadatmanesh H, Ehsani M R (1991). RC Beams Strengthened with FRP Plates. II:Analysis and Parametric Study. Journal of Structural Engineering, 117(11), 3434-3455.

Anil A (2006). Improving shear capacity of RC T-beams using CFRP Composites subjected to cyclic load. Cement &Concrete Composites, Elsevier, 28,638-649.

ANSYS, Inc. Theory Reference (2003). ANSYS release

Antonopoulos CP, Triantafillou TC (2002). Analysis of FRP-Strengthened RC Beam-Column Joints. Journal of Composites for Construction, 6(1), 41- 51.

Antonopoulos CP, Triantafillou TC (2003). Experimental investigation of FRP-strengthened RC beam-column joint. Journal of composites for construction, ASCE 7(1), 39-49.

Arya C, Clarke JL, Kay EA, O'Regan PD (2002). TR 55: Design guideline for strengthening concrete structures using fibre composite materials: a review. Elsevier, Engineering structures, 24, 889-900.

Bakir PG, Boduroglu HM (2002). A New Design Equation for Predicting the Joint Shear Strength of Monotonically Loaded Exterior Beam-Column Joints. Engineering Structures, 24(8), 1105-1117.

Bazˇant ZP (1984). Size effect in blunt fracture: Concrete, rock, metal. J Engrg Mech ASCE, 110(4):518–535.

Bazˇant ZP, Pfeiffer PA (1986). Shear fracture tests of concrete. Mater. Struct, 19,111-121.

Bazˇant ZP, Pfeiffer PA (1987). Determination of fracture energy from size effect and brittleness number. ACI Mater. J, 84(6), 463-480.

Bazˇant ZP, Planas J (1998). Fracture and size effect in concrete and other quasibrittle materials, CRC Press, Boca Raton: Fla,

Bazˇant ZP (1999). Size effect on structural strength: a review. Archive of applied mechanics, Springer-verlag, 69, 703-725.

Beres A, EI-Borgi, White RN, Gergely P (1992). Experimental results of repaired and retrofitted beam-column joint tests in lightly reinforced concrete frame buildings. Technical report NCEER-92-0025, SUNNY/Buffalo.

Biddah A, Ghobarah A, Aziz TS (1997). Upgrading of Nonductile Reinforced Concrete Frame Connections. Journal of Structural Engineering, 123(8), 1001-1010.

Bindiganavile V, Banthia N (2006). Size effects and the dynamic response of plain concrete. Journal of Materials in Civil Engineering, ASCE , 18(4), 485-491.

Bonacci J, Pantazopoulou S (1995). Parametric Investigation of Joint Mechanics. ACI Structural Journal, 90(1), 61-71.

Bullock RE (1974). Strength ratios of composite materials in flexure and intension. J Compos Mater, 8, 200-206.

Camponeschi ET, Gillespie JW, Wilkins DJ (1993). Kink-band failure analysis of thick composites in compression. Journal of Compo- site Materials, 27, 471-490.

Chaallal O, Nollet MJ. Perraton D. Strengthening of reinforced concrete with externally bonded fibber-reinforced-plastic plates. Design guideline for shear and flexure. Canadian journal of civil engineering, 1998; 25(4):692-704.

Chung HS, Yang KH, Lee YH, Eun HC (2002). Stress–strain curve of laterally confined concrete. Elsevier, Engineering Structures, 24, 1153–1163.

Chutarat N, Aboutaha RS. (2003). Cyclic Response of Exterior Reinforced Concrete Beam-Column Joints Reinforced with Headed Bars-Experimental Investigation. ACI Structural Journal, 100(2), 259-264.

Coc V, Sener S (2009). Size effect in normal- and high-strength concrete with different notches under the axial load. J of materials in civil Engineering, ASCE, 21(9), 433-445

Corazao M, Durrani AJ (1989). Repair and strengthening of beam-to-column connections subjected to earthquake loading. Technical report NCEER-89-0013, SUNNY/Buffalo.

Daniel IM, Hsiao HM (1999). Is there a thickness effect on compressive strength of unnotched composite laminates ? International Journal of fracture mechanics, 95, 143-158.

Durrani AJ, Wight JK (1985). Behaviour of interior beam-to-column connections under earthquake-type loading. ACI Journal proceedings, 82(3), 343-349.

El-Amoury T, Ghobarah A (2002). Seismic Rehabilitation of Beam-Column Joint Using GFRP Sheets. Engineering Structures, 24(11), 1397-1407.

El-Mihilmy MT, Tedesco JW (2000). Analysis of Reinforced Concrete Beams Strengthened with FRP Laminates. Journal of Structural Engineering, 126(6), 684-691.

Elfahal MM, Krauthammer T, Ohno T, Beppu M, Mindess S (2005). Size effect of normal strength concrete cylinder subjected to axial impact. International journal of impact engineering, 31,461-481.

Ehsani MR, Alameddine F (1991). Design Recommendations for Type 2 High-Strength Reinforced Concrete Connections. ACI Structural Journal, 277-291.

Filiatrault A, Lebrun I (1996). Seismic Rehabilitation of Reinforced Concrete Joints by Epoxy Pressure Injection Technique. ACI special publication SP160, 73-92.

French CW, Thorp GT, Tsai W. (1990). Epoxy Repair Techniques for Moderate Earthquake Damage. ACI Structural Journal, 87(4), 416,424.

Gadve S, Mukherjee A, Malhotra SN (2009). Corrosion of steel reinforcements embedded in FRP wrapped concrete. J of Construction and building materials, Elsevier 23, 153-161.

Gergely J, Pantelides CP, Reaveley LD (2000). Shear Strengthening of RCT-Joints Using CFRP Composites. Journal of Composites for Construction, 4(2), 56-64.

Ghobarah A, Aziz TS, Biddah A (1997). Rehabilitation of Reinforced Concrete Frame Connections Using Corrugated Steel Jacketing. ACI Structural Journal, 94(3), 283-294.

Ghobarah A, Said A (2002). Shear Strengthening of Beam-Column Joints. Engineering Structures, 24(7), 881-888.

Ghobarah A, El-Amoury T (2005). Seismic Rehabilitation of Deficient Exterior Concrete Frame Joints. ASCE, Journal of composites for construction, 9(5),408-416.

Granata PJ, Parvin A (2001). An Experimental Study on Kevlar Strengthening of Beam-Column Connections. Composite Structures, 53(2), 163-171.

Gurvich MR, Pipes RB (1995). Strength size effect of laminated composites. Composites Science and Technology, 55, 93-105.

Hanson NW, Connor HW (1967). Seismic resistance of reinforced concrete beam-column Joints. Journal of Structural Division, 93, 533-560.

Hakuto S, Park R, Tanaka H (2000). Seismic Load Tests on Interior and Exterior Beam-Column Joints with Substandard Reinforcing Details. ACI Structural Journal, 97(1), 11-25.

He W, Yu YF, Liew KM (2008). A fracture energy based constitutive model for the analysis of reinforced concrete structures under cyclic loading. Comput. Methods Appl. Mech. Engrg. Elsevier, 197, 4745-4762.

Hitchon JW, Phillips DC (1978). The effect of specimen size on the strength of CFRP. Composites, 9, 119-124.

IS 383 (2002). Indian Standard Specification for Coarse and Fine Aggregates from natural sources for Concrete. Bureau of Indian Standard, New Delhi.

IS 432 (1982). Specification for mild steel and medium tensile steel wire for concrete reinforcement. Bureau of Indian Standard, New Delhi.

IS 456 (2000). Plain and Reinforced concrete- Code of Practice. Bureau of Indian Standard, New Delhi.

IS 1608 (1995). Mechanical testing of metals- Tensile Testing. Bureau of Indian Standard, New Delhi.

IS 1893 (1984). Criteria for earthquake resistant design of structures. Bureau of Indian Standard, New Delhi.

IS 1893 (I) (2002). Criteria for Earthquake Resistant Design of Structures- Part 1 : General Provisions and buildings. Bureau of Indian Standard, New Delhi.

IS 2386: Part 1 (1963). Methods of Test for Aggregates for Concrete- Part 1: Particle Size and Shape. Bureau of Indian Standard, New Delhi.

IS 2386: Part 3 (1963). Methods of Test for Aggregates for Concrete- Part 3: Specific gravity, Density, Voids, Absorption and Bulking. Bureau of Indian Standard, New Delhi.

IS 4031: Part 4 (1988). Methods of physical tests for hydraulic cement: Part 4 Determination of consistency of standard cement paste. Bureau of Indian Standard, New Delhi.

IS 4031: Part 5 (1988). Methods of physical tests for hydraulic cement: Part 5 Determination of Initial and Final setting time. Bureau of Indian Standard, New Delhi.

IS 4031: Part 6 (1988). Methods of physical tests for hydraulic cement: Part 6 Determination of compressive strength of hydraulic cement (other than masonry cement). Bureau of Indian Standard, New Delhi.

IS 4031: Part 11 (1988). Methods of physical tests for hydraulic cement: Part 11 Determination of Density. Bureau of Indian Standard, New Delhi.

IS 10262 (1982). Recommended guidelines for concrete mix designs. Bureau of Indian Standard, New Delhi.

IS 12269 (1987). Specification for 53 grade ordinary Portland cement. Bureau of Indian Standard, New Delhi.

IS 13920 (1993). Ductile Detailing of Reinforced Concrete Structures subjected to Seismic Forces- Code of Practice. Bureau of Indian Standard, New Delhi.

Issa CA, Debs P (2007). Experimental study of epoxy repairing of cracks in concrete. Construction and Building Materials , Elsevier, 21, 157-163.

Jackson KE (1992). Scaling effects in the flexural response and failure of composite beams. AIAA Journal, 30, 2099-2105.

Jackson KE, Kellas S, Morton J (1992). Scale effect in response of failure of composite laminates. Journal of composite materials, SAGE journal online, 26(18), 2674-2705.

Jain SK, Murty CVR (2006) Proposed draft provision and commentary on ductile detailing of RC structures subjected to seismic forces. Document No. :: IITK-GSDMA-EQ11-V-3.0 :: IITK-GSDMA-EQ16-V2.0.

Jeng YS, Shah SP (1985). A fracture toughness criteria for concrete. Engg. Fract mechanics. 21(50), 1055-1069.

Jones MR (1999). Mechanics of composite materials. Philadelphia, Taylor & Francis publishers.

Joshi MK, Murty CVR, Jaisingh MP (2005). Cyclic behaviour of precast RC connections. The Indian concrete journal, November 2005, 43-50.

Karayannis CG, Chalioris CE, Sideris KK (1998). Effectiveness of RC beam-column connection repair using epoxy resin injections. Journal of earthquake engineering, 2(2), 217-240.

Kwak HG, Fillippou F (1990). Finite Element Analysis of Reinforced Concrete Structures under Monotonic Loads. UCB/SEMM-90/14, Dept. of Civil Engineering, University of California, Berkeley, California.

Laxmi GA, Dutta A, Deb SK (2008). Numerical studies of strengthening of beam column under cyclic excitation using FRP composites. J of structural Engg, SERC (India); 35(1) ,59-65.

Leung C, Chen Z, Lee S, Ng M, Xu M,Tang J (2007). Effect of Size on the Failure of Geometrically Similar Concrete Beams Strengthened in Shear with FRP Strips. Journal of composites for construction, ASCE, 11(5), 487-496.

Li J, Bakoss SL, Samali B, Ye L (1999). Reinforcement of Concrete Beam-Column Connections with Hybrid FRP Sheet. Composite Structures, 47(1-4), 805-812.

Li B, Chua HYG (2009). Seismic performance of strengthened reinforced concrete beam-column joints using FRP composites. J of structural engineering, ASCE, 135(10), 1177-1190.

Mahini SS, Ronagh HR (2010). Strength and ductility of FRP web-bonded RC beams for the assessment of retrofitted beam-column joints. Composite Structures, 92(6), 1325-1332

Malek AM, Saadatmanesh H, Ehsani MR (1998). Prediction of Failure Load of R/C Beams Strengthened with FRP Plate Due to Stress Concentration at the Plate End. ACI Structural Journal, 95(1), 142-152.

Megget LM, Park R (1971). Reinforced Concrete Exterior Beam-Column Joints Under Seismic Loading. New Zealand Engineering, 26(11), 341-353.

Meier U, Deuring M, Meier H, Schwegler G (1993). CFRP bonded sheets, Fibre-Reinforced-Plastic (FRP) Reinforcement for Concrete Structures: Properties and Applications, edited by A. Nanni, Elsevier Science, Amsterdam, The Netherlands.

Mirza MS, Labonte LRS, McCutcheon JO (1972). Size effect in model concrete mixes. Paper presented in ASCE National Convention, Cleveland, April.

Mosallam AS (2000). Strength and Ductility of Reinforced Concrete Moment Frame Connections Strengthened with Quasi-Isotropic Laminates. Composites Part B-Engineering, 31(6-7), 481-497.

Mukherjee A, Joshi M (2005). FRPC reinforced concrete beam-column joints under cyclic excitation. Composite structures, 70:185-199.

Murty CVR, Rai DC, Bajpai KK, Jain SK (2003). Effectiveness of reinforcement details in exterior reinforced concrete beam-column joints for earthquake resistance. ACI structural journal, 100 (2), 149-156.

Naeim F, Kelly JM (1999). Design of seismic isolated structures from theory to practice. John willey & sons, inc.

Nie J, Bai Y, Cai CS (2008). New connection system for confined concrete columns and beams. I: experimental study. J of structural engineering, ASCE, 134(12), 1787-1799.

Pantelides CP, Gergely J, Reaveley LD, Volnyy VA (1999). Retrofit of RC Bridge Pier with CFRP Advanced Composites. Journal of Structural Engineering, 125(10), 1094-1099.

Pantazopoulou S, Bonacci J (1992). Consideration of Questions about Beam-Column Joints. ACI Structural Journal, 89(1), 27-36.

Paulay T, Park R, Priestley MJN (1978). Reinforced Concrete Beam- Column Joints under Seismic Actions. ACI Journal(NO.75-60), 585-593.

Paulay T (1989). Equilibrium Criteria for Reinforced-Concrete Beam-Column Joints. ACI Structural Journal, 86(6), 635-643.

Paulay T, Priestley MJN (1992). Seismic design of reinforced concrete and masonry buildings, John Wiley & Sons, INC.

Prabin A, Granata P (2000). Investigation on the size effect of fibre composites at concrete joints. Composite part B, 31, 499-509.

Prabin A, Granata P (2001). Investigation on the size effect of fibre composites at concrete joints. Composite part B ;31:499-509.

Rios RD, Riera JD (2004). Size effect in the analysis of reinforced concrete structures. Engineering structures 2004, 26, 1115-1125.

Reeder JR (1995). Stitching vs a toughened matrix: compression strength effects. Journal of composite materials, 29, 2464-2487.

Saadatmanesh, H, Ehsani MR (1991). Fibre Composite Plates Can Strengthen Beams. Concrete International, 65-71.

Saadatmanesh H, Malek AM (1998). Design Guidelines for Flexural Strengthening of RC Beams with FRP Plates. Journal of Composites for Construction, 2(4), 158-164.

Sabnis GM, Mirza MS (1979). Size effects in model concretes? ASCE, Journal of structural division, 105(ST6), 1007-1020.

Scarpas A, Paulay T. (1981). "The Inelastic Behaviour of Earthquake Resistant Reinforced Concrete Exterior Beam-Column Joints." Department of Civil Engineering, University of Canterbury, Christchurch New Zealand.

Shannag MJ, Abu-Dyya N, Abu-Farsakh G (2005). Lateral load response of high performance fibre reinforced concrete beam-column joints. Construction and building materials, Elsevier, 19, 500-508.

Shash AA (2005). Repair of concrete beams- a case study. Construction and Building Materials, Elsevier , 19, 75-79.

Scribner CF, Wight JK (1980). Strength decay in R/C beams under load Reversals. Journal of structural Division, Proceedings of the American Society of Civil Engineers, 106(ST4), 861-876.

Sener S, Bazˇant ZP, Becq-Giraudon E (1999). Size effect on failure of bond splices of steel bars in concrete beams. J structural Engrg, ASCE, 125(6), 653-660.

Sener S, Begimgil M, Belgin C (2002). Size effect on failure of concrete beam with and without fibre. J of materials in civil Engrg, ASCE, 14(5), 436-440.

Sener S, Barr BIG, Abusiaf HF (2004). Size effect in axially loaded reinforced column." J structural Engrg, ASCE, 130(4):662-670.

Sing SB (2008). Strength of CFRP stirrups: experimental and analytical study, The Indian concrete journal, August 2008, 11-17.

Structural analysis guide, ANSYS release 5.6. 1999.

Teng JG, Chen JF, Smith ST, Lam L (2002). FRP-Strengthened RC Structures. John Wiley & Sons, Ltd.

Triantafillou TC, Plevris N. (1992). Strengthening of RC beams with Epoxy- Bonded Fibre-Composite Materials. Materials and Structures, 25(148), 201- 211.

Tsai SW (1966). Strength theories of filamentary structures, in fundamental aspects of fibre reinforced plastic composites. Conference proceedings, RT Schwartz and HS Schwartz (Editors), Dayton, 24-26 May, Willey interscience, New York, 1968, 3-11.

Uma SR, Prasad AM (2006). Seismic behaviour of beam column joints in reinforced concrete moment resisting frames. Document No. :: IITK-GSDMA-EQ31-V1.0, Final Report :: A - Earthquake Codes , IITK-GSDMA Project on Building Codes.

Vollum RL. (1998). Design and Analysis of Reinforced Concrete Beam-Column Joints. Ph.D., Imperial College, London.

Yen JYR, Chien HK (2010). Steel plates rehabilitated RC beam-column joints subjected to vertical cyclic loads. Journal of Construction and Building Materials, Elsevier, 24(3), 332-339.

Walsh PF (1972). Fracture of plain concrete. Indian concrete journal. 46(11), 469-470 and 476.

Wisnom MR (1991). The effect of specimen size on flexural unidirectional carbon fibre-epoxy. Composite structures, 18, 47-63.

Wisnom MR, Atkinson JA (1997). Reduction in tensile and flexural strength of unidirectional glass fibre-epoxy with increasing specimen size. Composite Structures, 38, 405-412.

Will GT, Uzumeri SM, Sinha, SK (1972). Application of the Finite Element Method to the Analysis of Reinforced Concrete Beam-Column Joints. Specialty of Conference on Finite Element Method in Civil Engineering, Canada, 745-766.

William KJ, Warnke EP (1974). Constitutive models for the triaxial behaviour of concrete. International Association of Bridge and structural Engineers seminar on Concrete structures subjected to triaxial stresses, Paper III-I, Bergamo, Italy May 17-19;1-30.

LIST OF PUBLICATIONS FROM THESIS

Conference Proceedings (International)

1. A. M. Choudhury, A. Dutta and S.K. Deb. Comparative study of full scale beam-column joints under cyclic loading. Proc. of 3rd International Earthquake Symposium, Bangladesh Dhaka, March 5-6, 2010. pp 205-213.
2. A. M. Choudhury, A. Dutta and S.K. Deb. Study on size effect of retrofitted beam column joint with beam weak in flexure. 35th International conference on our world in concrete and structures. Singapore, 25-28th august, 2010. (Accepted)

Conference Proceedings (National)

3. A. M. Choudhury, S.K. Deb and A. Dutta. Experimental verification of a full scale beam-column joint under cyclic loading. National seminar on earthquake hazard disaster management of north eastern states of India. NIT Silchar, India, 18-20th October, 2008, pp 183-194.

Journal (National)

4. A.M.Choudhury, P.Poluraju, A.Dutta and S.K.Deb. Effective retrofitting of plain concrete elements using externally bonded fibre reinforced polymer. Communicated (Indian concrete journal).

Journal (International)

5. S.S.Reddy, A.M.Choudhury, A.Dutta and S.K.Deb. Studies on size effect of RC and retrofitted beam-column joints using numerical approach. J. of Earthquakes and Structures. (About to communicate).
6. A. M. Choudhury, A. Dutta and S.K. Deb. Study on size effect of RC beam-column joints under cyclic loading. J. of materials in civil engineering. (About to communicate)
7. A. M. Choudhury, A. Dutta and S.K. Deb. Study on size effect of retrofitted RC beam-column joints under cyclic loading. J. of composite for construction. (About to communicate).

APPENDIX A

MULTILINEAR STRESS-STRAIN CURVE OF CONCRETE

The uniaxial behavior of concrete was modeled by the numerical expression proposed by Desayi and Krishnan [1965] incorporating the modification proposed by Gere and Timoshenko [1997]. Equations A.1 and A.2 were proposed by Desayi and Krishnan, while Eq. A.3 was proposed by Gere and Timoshenko. These Equations are presented below :

$$f = \frac{E_C \in}{1 + \left(\frac{\in}{\in_O}\right)^2} \qquad (A.1)$$

$$\in_O = \frac{2 f_{ck}}{E_c} \qquad (A.2)$$

$$E_c = \frac{f}{\in} \qquad (A.3)$$

where,

f : Stress at any strain level

$\in$: Strain at the corresponding stress and

$\in_o$: Strain at the ultimate compressive strength f_{ck}

Compressive strength of concrete was adopted as 30 N/mm^2. Considering 0.67 as factor for consideration of size effect [IS: 456-2000], the maximum compressive strength of concrete was obtained as 20 N/mm^2. The maximum strain in concrete in bending was taken as 0.0035. The stress corresponding to the first point of the stress-strain curve was adopted as 6.67 N/mm^2, which was 30% of the maximum compressive strength of the concrete. From origin up to the first point, the variation of stress-strain was assumed as linear so that it follows Hooke's Law. Additional Points on stress-strain curve were obtained by using Eq. (A.1-A.3). Some of the sample points are furnished in the Table A.1. The piecewise linear stress-strain plot is presented in Fig. A.1

Table A.1 Data points of Multi-linear isotropic stress-strain curve for concrete

Points	1	2	3	4	5	6
Stress (N/mm^2)	6.67	10.36	17.03	19.69	20	20
Strain (mm/mm)	0.0002982	0.0005	0.001	0.0015	0.002	0.0035

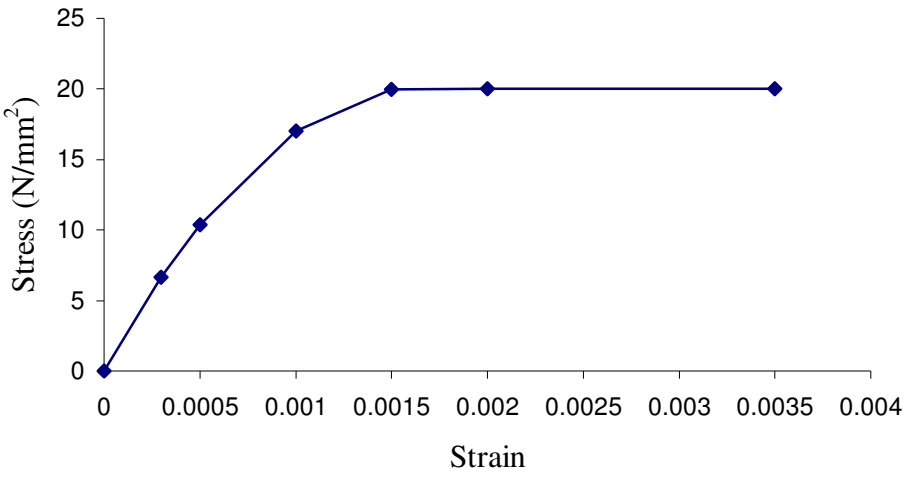

Fig. A.1 Multi-linear isotropic stress-strain curve for concrete

APPENDIX-B

ANALYSIS AND DESIGN OF THE SPECIMENS

B1. ANALYSIS AND DESIGN OF BEAM-COLUMN JOINT WITH BEAM WEAK IN FLEXURE SPECIMENS

Full scaled specimen (BWFLC)

Analysis of beam

Analysis of beam was done after removing material factor of safety of concrete and steel.

Calculation of neutral axis depth

The equilibrium equation for a doubly reinforced RC beam is given by

$$C_{uc} + C_{us} = T_u \qquad \text{(B1)}$$

Where,

C_{uc} = Resultant compressive force in concrete,

C_{us} = Resultant compressive force in the compressive steel,

T_u =Resultant tensile force in tension steel,

x =Neutral axis depth.

$$C_{uc} = 0.36 \times 1.5 \times f_{ck} \times b \times x$$

$$= 0.54 \times 30 \times 300 \times x$$

$$= 4860 \times x \text{ N}$$

$$C_{us} = \in_{s1} \times E_s$$

Where $\in_{s1}$ is strain in compressive steel (Ref. Fig B1) and E_s is modulus of elasticity of steel

$$C_{us} = 2 \times 10^5 \times 0.0035 \times \frac{x-35}{x} \times 628.32$$

$$= 439824 \times \frac{x-35}{x} \text{ N}$$

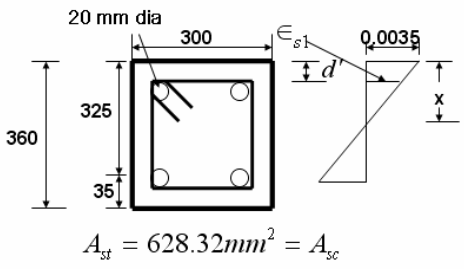

Fig. B1 Strain diagram of beam

$T_u = f_y \times A_{st}$

$= 500 \times 628.32$

$= 314160$ N

Substituting values in eqn. (B1)

$$4860x+439824\frac{x\text{-}35}{x}=314160$$

Solving for x (Depth of Neutral axis),

x=44.8 mm

Corresponding stress developed in compressive steel

$f_{S1}=153.152$ N/mm^2

Moment carrying capacity of beam,

$M_u = C_{uc}\times$(d-0.42$\times x$)+$C_{us}\times(d - d')$, (d' =effective cover)

M_u=4860×44.8×(325-.42×44.8)+153.125×628.32×(325-35)

M_u=66.665×10^6+27.9×10^6

$M_u = 94.565\times10^6$ N-mm

$M_u = 94.565$ kN-m.

As the beam-column joint is a strong column-weak beam joint (proved in subsequent section), so assuming the beam as fixed like a cantilever (Fig. B2)

Ultimate Load carrying capacity of beam,

$P_u = M_u / L$

P_u=94.565/1.35

P_u=70.048 kN.

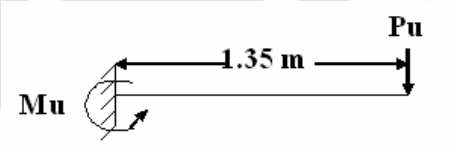

Fig. B2 F.B.D. diagram of Force and moment

Design of shear reinforcement in beam

Percentage of tensile reinforcement provided, $p_t = 0.58\%$

Corresponding shear stress can be obtained by interpolation for M30 and $p_t = 0.58\%$

% of steel	Design shear strength of concrete
0.5	0.50
0.75	0.59

$\tau_c = 0.529$N/mm^2 (from IS:456-2000, Table 19)

Shear resisted by concrete:-

$V_c = \tau_c bd$

=0.529×300×325

=51.57 kN<70.048 kN

Hence shear design is required.

Shear to be resited by steel,

$V_{us} = V_u - V_c$

=70.048-51.57

=18.43kN

using 2- legged 6mm dia mild steel bars

A_{sv}=2×28.27=56.54 mm^2

$V_{us} = f_y \times A_{sv} \times d / S_v$

18430=250×56.54×325/S_v

S_v=249 mm

As per Clause 6.3.5 of IS:13920-1993,

The spacing should not exceed $d/2$, i.e.325/2=162.5 in any part of beam.

Minimum shear reinforcement as per Clause 26.5.1.6 of IS:456-2000 is given

$S_v = A_{sv} \times f_y / (0.4b)$

=56.54×250/(0.4×300)

=120mm

spacing of links over a length of 2d at end of beam as per clause 6.3.5 of IS:13920-1993 shall be least of

1. d/4=325/4=81.25 mm
2. 8 times the diameter of smallest bar = 8×20 =160mm

Provide 2-legged 8 mm dia stirrups ties @ 75mm c/c up to 2d (i.e., 650) and then 2 -legged 6 mm diameter stirrups @ 120mm c/c for remaining length of beam.

Design of Column

$T_u = f_y \times A_{st}$

=500×628.32

=314160N

$$C_{uc} = 0.54 \times f_{ck} \times b \times x$$
$$= 0.54 \times 30 \times 300 \times x$$
$$= 4860x \text{ N}$$

$$C_{us} = 0.0035 \times 2 \times 10^5 \times 628.32 \times (x - 50)/x$$
$$= 439824 \times (x - 50)/x \text{ N}$$

Axial load applied on Column,

$$P_u = 0.1 \times f_{ck} \times A_g$$
$$= 0.1 \times 0.8 \times 30 \times 300 \times 300$$
$$= 216 \text{kN}$$

Eqilibrium Eq. is

$$C_{uc} + C_{us} - T_u = P_u$$
$$4860x + 439824 \times (x - 50)/x) - 314160 = 216000$$

solving this Eq.

$$x = 77.2\text{mm}.$$

$$f_{s1} = 0.0035 \times 2 \times 10^5 \times (77.2 - 50)/77.2$$
$$= 246.63 \text{ N/mm}^2$$

Moment carrying capacity of column:-

$$\text{M.R} = 4860 \times 77.2 \times (250\text{-}0.42 \times 77.2) + 628.32 \times 246.63 \times (250\text{-}50)$$
$$= 81.63 \times 10^6 + 30.99 \times 10^6$$
$$= 112.62\text{kN-m}.$$

Design of shear reinforcement in column:-

$P_t = 0.698\%$

Permissible shear stress = 0.57 N/mm^2

$$\delta = 1 + \left(\left(216 \times 10^3 \times 3\right) \Big/ \left(300 \times 300 \times 20\right) \right)$$
$$= 1.24 < 1.5 \text{ (Clause 40.2.2:IS 456:2000)}$$

$\tau_c = 1.24 \times 0.57 = 0.7068$ N/mm^2

Effective depth of column=300-40-(20/2)=250 mm

Shear resisted by concrete:-

$V_c = \tau_c bd$

=0.7068×300×250

=53.01 kN

Shear force due to possible plastic hinge formation in the longitudinal beam:-

$V_u = M_u{}^{br} / h_{st}$

=94.565/3.3

=28.65 kN < V_c

Hence concrete of column alone is capable of resisting the shear force. However, nominal shear design is provided as per the following clauses.

Design of lateral ties:-

Clause 7.4.1 of IS: 13920 states the special confinement should extend up to l_0 given by

a. least lateral dimension (i.e.300mm)

b. $(1/6)^{th}$ of clear span (i.e. (3300-360)/6 =490mm)

c. 450mm

Adopt 495 mm from joint on either side of column.

For special confinement zone, try 12 mm diameter bars,

βc= 300-2 ×40+2×12=244<300

Here, $\beta c = hc$ = 244

$A_g = 9 \times 10^4$ mm^2

$A_k = (300 - 2\times 40 + 2\times 12)^2 = 59536$ mm^2

$A_{sh} = 0.18 \times S \times h \times f_{ck} \times ((A_g / A_k) - 1) / f_y$

$113.09 = 0.18 \times S \times 244 \times 30 \times 0.5117/500$

S= 83 mm

Provide 2-legged 12 mm dia lateral ties @ 75mm c/c up to 495mm from the joint and beyond that, provide 2-legged 6 mm diameter @ 150mm c/c (i.e.300/2) (Clause 7.3.3, IS: 13920-1993)

Design of Joint

Check for strong column-weak beam condition

$$\sum M_C / \sum M_B = (112.62 + 112.62)/94.565$$

$$= 2.38 > 1.1(\text{As per IS : 1920})$$

$$> 1.2(\text{As per ACI 318})$$

Hence, the joint satisfies the criteria of strong column-weak beam condition.

$$V_{col} = V_u = 28.65 \text{ kN}$$

Force developed in bars provided at the top of beam

$$T_1 = 1.25 \times A_{st} \times fy$$
$$= 1.25 \times 628.32 \times 415$$
$$= 325.941 \text{ kN}$$

$$V_{joint} = T_1 - V_{col}$$
$$= 325.941 - 28.65$$
$$= 297.29 \text{ kN}$$

Check for joint shear strength

$$b_c \le (b_b + b_c)/2$$
$$b_j \le b_b + h$$
$$b_c = 300 ; b_b = 300 ; h = 300$$
$$b_j \le \frac{300 + 300}{2} \le 300$$

$$b_j \le 300 + 300 \le 600$$

Hence $b_j = 300$

Effective area of joint resisting shear

$$A_c = b_j \times h$$

$$= 300 \times 300 = 90000 \text{ mm}^2$$

Shear strength of joint

$$= 1.0\sqrt{f_{ck} \times A_c} \qquad \text{(Clause 8.2.1 ; IS 13920:1993)}$$

$$= 402.49 \text{ kN} > 297.29 \text{ kN}.$$

Hence OK.

The design calculations are similar for two-third and one third scaled beam-column joints.

B2. ANALYSIS AND DESIGN OF BEAM-COLUMN JOINT WITH BEAM WEAK IN SHEAR SPECIMENS

Full scaled specimen (BWSLC)

The cross section and longitudinal reinforcement of beam under this category of beam-column joint was maintained same as that of earlier case. However, the shear reinforcement was reduced to make the beam weak in shear.

$V_c = 51.57$ kN (As calculated earlier)

To make the beam weak in shear, provide 2 –legged 6mm dia stirrups @ 600mm c/c.

Shear resisted by steel,

$$V_{us} = \frac{\left(f_y \times A_{sv} \times d\right)}{S_v}$$

$$V_{us} = \frac{\left(483 \times 2 \times 28.26 \times 325\right)}{600}$$

$$V_{us} = 14.79k\text{N}.$$

Total shear resisted by the section of beam,

$$V_u = V_{us} + V_c$$
$$= 51.57 + 14.79$$
$$= 66.36\text{kN} < 70.048\,\text{kN}$$

Hence, the beam is weak in shear.

However, to keep a predefined failure location and to ensure that the failure does not occur near tip of the beam, only the first stirrup near the joint is maintained at a spacing of 600 mm c/c and for the rest part spacing is decreased to 240mm c/c. The design calculations are similar for two-third and one third scale beam-column joints.

B3. ANALYSIS AND DESIGN OF BEAM-COLUMN JOINT WITH COLUMN WEAK IN SHEAR SPECIMENS

Full scaled specimen (CWSLC)

The cross section of the column was adopted 300 mm×240 mm and cross section of beam was adopted 450 mm×300 mm.

Analysis of Beam

Analysis has been done after removing factor of safety for concrete and steel.

The equilibrium Eq. is

$C_{uc} + C_{us} = T_u$

Where

C_{uc} = Resultant compressive force in concrete,

C_{us} = Resultant compressive force in the compressive steel,

T_u =Resultant tensile force in tension steel,

x =Neutral axis depth.

C_{uc}=0.36×1.5×f_{ck} ×b×x

=0.54×25×240×x

=3240×x N

C_{us}=2×10^5×0.0035×972.48×(x-35)/x

=659736×(x-35)/x N

T_u=f_y × A_{st}

=942.48×628.32

=471.24 kN

Substituting the values in equilibrium Eq., the depth of neutral axix is found

x=60.20 mm

Moment carrying capacity of beam:-

M_u=C_{uc}×(d-0.42×x)+C_{us}×(d - d')

=3240×60.20×(415-.42×60.20)+293×942.48×(415-35)

=76.01×10^6+104.93×10^6

=180.94×10^6 N-mm

=180.94 kN-m.

Ultimate Load carrying capacity of beam

$P_u = M_u / L$

=180.94/1.35

=134.029kN.

Design of Shear Reinforcement in Beam

Percentage of tensile reinforcement provided, $p_t = 0.873\%$

Corresponding shear stress can be obtained by interpolation for M25 and $p_t = 0.873\%$

% of steel	Design shear strength of concrete
0.75	0.54
1.00	0.60

$\tau_c = 0.569\,\text{N/mm}^2$ (IS:456-2000, Table 19)

Shear resisted by concrete:-

$V_c = \tau_c bd$

$= 0.569 \times 240 \times 415$

$= 56.67$ kN<134.029 kN

Hence shear design is required.

Shear to be resited by steel,

$V_s = V_u - V_c$

=134.029-56.67

=78.27kN

using 2-legged 8 mm dia stirrups

A_{sv}=2×50.26=100.54mm^2

$V_s = f_y \times A_{sv} \times d / S_v$

78270=500×100.54×415/S_v

S_v = 265mm

However, as per Codal provision near the beam column joint, it should not exceed d/4 =(415/4)=103.75mm.

Provide 2-legged 8 stirrups @ 75mm *c*/c throughout the beam.

Analysis of Column

$T_u = f_y \times A_{st}$

=500×628.32

=314160 N

$C_{uc} = 0.54 \times f_{ck} \times b \times x$

$=0.54 \times 25 \times 240 \times x$

$=3240x$ N

$$C_{us} = 0.0035 \times 2 \times 10^5 \times 628.32 \times (x - 50)/x$$
$$= 439824 \times (x - 50)/x \text{ N}$$

Axial load applied on Column

$$P_U = 0.1 \times A_g \times f_{ck}$$
$$= 0.1 \times 0.8 \times 25 \times 240 \times 300$$
$$= 144 \text{ kN}$$

Depth of neutral axis x is calculated by the following equilibrium Eq.

$$C_{uc} + C_{us} - T_u = P_u$$

and was found as

x=80.78 mm.

$$f_{S1} = 0.0035 \times 2 \times 10^5 \times (80.78 - 50)/80.78$$
$$= 226.72 \text{ N/mm}^2$$

Moment carrying capacity of column

$$\text{M.R} = 3240 \times 80.78 \times (250 - .42 \times 80.78) + 226 \times 628.32 \times (250 - 50)$$
$$= 56.55 \times 10^6 + 33.51 \times 10^6$$
$$= 90.067 \text{ kN-m.}$$

Check for strong column-weak beam condition of the joint

$$\sum \text{M}_\text{C} / \sum \text{M}_\text{B} = (90.067 + 90.067)/180.94$$
$$= 0.99 < 1.1$$

Therefore, it is a weak column-strong beam joint [IS: 13920]

Since, it is a weak column-strong beam joint, hence the assumption of cantilever beam is no more valid unlike beam-column joint with beam weak in flexure specimens. Thus, the calculation of the ultimate load carrying capacity of the specimen has not been done. Moreover, lesser shear reinforcement than codal provision were provided in column to make the specimen shear deficient in column. In CWSLC, 2-legged 6 mm diameter mild steel bars with a spacing of 900 mm c/c were provided as lateral ties.

B4. ANALYSIS AND DESIGN OF BEAM-COLUMN JOINT WITH BEAM WEAK IN FLEXURE RETROFITTED SPECIMENS

Material Properties of CFRP:-

Thickness of one layer of composite = 0.5mm

Out of this, thickness of CFRP=0.3mm

Thickness of CFRP sheet=0.3mm

Tensile strength of CFRP=630 N/mm^2

Modulus of elasticity of CFRP composite=4.63 $\times 10^4$ N/mm^2

Therefore, Ultimate strain=0.0136

Material Properties of GFRP:-

Tensile strength of GFRP = 315 N/mm^2

Modulus of elasticity = 1.167 $\times 10^4$ N/mm^2

Thickness of CFRP sheet=0.36 mm

Design of CFRP for flexural strengthening:-

Providing one layer of CFRP

Analysis of beam:-

The following calculations have been done as per guidelines proposed by Amoury and Ghobarah [2002] and Teng *et al.*(2003).

Taking tensile strain as negave and compressive strain as positive (Teng *et al.*, 2003)

$$\in_{s1} = \frac{x - d'}{x} \times \in_c$$

$$\in_{s2} = -\frac{h - x - d'}{x} \times \in_c$$

$$\in_{frp} = -\frac{h - x}{x} \times \in_c$$

(Ref. to Fig. B3)

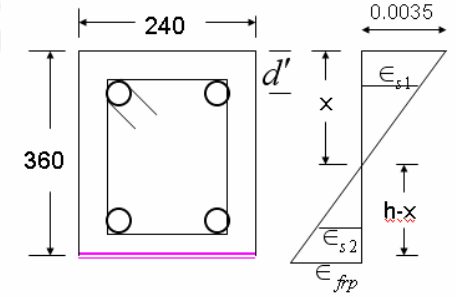

Fig. B3 Strain diagram

Calculation of neutral axis depth (x):-

$$C_c + C_{cs} + T_s + T_{frp} = 0 \qquad \text{(B2)}$$

(Ref. to Fig. B4)
Where

$$C_{uc} = 0.36 \times 1.5 \times f_{ck} \times b \times x$$
$$= 0.54 \times 30 \times 300 \times x$$
$$= 4860 \times x \; N$$

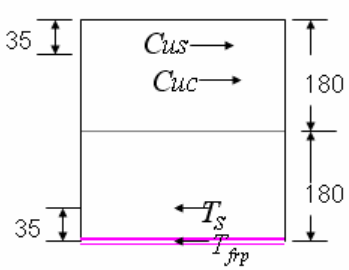

Fig. B4 F.B.D. of forces

$$C_{us} = 2 \times 10^5 \times 0.0035 \times 628.32 \times (x-35) \div x$$
$$= 439824 \times (x-35) \div x \; N$$

$$T_s = -1.25 \times f_y \times A_{st}$$
$$= -1.25 \times 500 \times 628.32$$
$$= -392700 \; N$$

$$T_{frp} = -300 \times 0.3 \times 630 \quad \text{(Assuming FRP is yielding)}$$
$$= -56700 \; N$$

Substituting the values in Eq. B2 and solving, the depth of N.A.

x = 49.63 mm

Compressive stress developed in compressive steel

$$f_{sc} = E_s \times \in_{s1}$$
$$= 206.35 \; N/mm^2 < 500$$

Hence steel is not yielding

$\in_{frp} = 0.02188 > 0.0136$, hence FRP is yielding

Ultimate moment of resistance of the section

$$M_u = C_{uc} \times (D/2 - 0.42x_u) + C_{us} \times (D/2 - d') + T_s \times (D/2 - d') + T_{frp} \times D/2$$

where D= overall depth

$$M_u = 4860 \times 49.63 \times (180 - 0.42 \times 49.63) + 682.32 \times 206.35 \times (180 - 35)$$
$$+ 314.16 \times 10^3 \times (180 - 35) + 56.7 \times 10^3 \times 180$$

$$M_u = 110.96 \; kN\text{-}m$$

Ultimate load carrying capacity:

$$P_u = M_u / L$$
$$P_u = 110.96/1.35$$
$$P_u = 82.19 kN$$

For calculating the length up to which FRP fixing is needed, similar triangle concept from BM diagram is used. FRP is fixed on the portion where BM is more than the BM of control beam

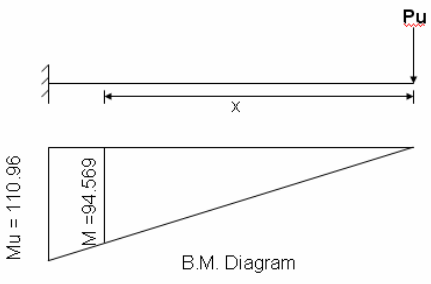

Fig. B5 Variation of B.M.

From Fig. B5,

$x = 0.85 \times 1.35$

$= 1.15$ m

Therefore, length up to which FRP fixing is needed

=1.35-1.15

=0.35 m.

However, keep a sufficient length for avoiding debonding

Provide a length of 900 mm so that a round figure can be obtained for scaled down models.

Design of GFRP strips for shear strengthening:-

Shear force on the beam

= 82.19 kN

Providing 90 mm wide strips of GFRP @ 270 mm c/c

Shear contributed by GFRP as per the formula proposed by Chaallal *et al.* [1998]

$$V_{frp} = \phi_{frp} \times A_{frp} \times f_{frp} \frac{(\sin\beta + \cos\beta)d}{s_{frp}} \quad \text{(B3)}$$

Where,

f_{frp} is tensile strength of FRP

ϕ_{frp} = 0.8, the material reduction factor of FRP

A_{frp} = Area of cross section of FRP strips

β = Angle of fibre orientation of FRP strips

d = Effective depth of beam

s_{frp} = Spacing of FRP strips

Substiting the values

$$V_{frp} = 0.8 \times 90 \times 0.36 \times 315 \times \frac{(\sin 45^0 + \cos 45^0) \times 325}{270}$$

=138 kN > 82.19 kN

Therefore, the beam fails in flexure.

Moment capacity of column needed = (1.1x110.66)/2

=60.86 kN-m<112.62 kN-m.

Hence column doesn't require any retrofitting.

Shear on column =110.66/3.3

=33.53<78.59 kN

Hence shear retrofitting for column is also not required.

Shear strengthening of joint:-

Horizontal Shear force acting on the joint,

$V_j = 1.25 \times A_{st} \times f_y + A_{frp} \times f_{frp} - V_{col}$ [Amoury and Ghobarah, 2002]

$= 1.25 \times 628.32 \times 500 + (2 \times 300 \times 0.30) \times 630 - (110.96 \times 10^6 / 3.3 \times 10^3)$

$= (392.7 + 108 - 30.67) \times 10^3$ N

$= 470.03$ kN

Total shear capacity of the joint

$V_{jh} = V_{uc} + V_{us} + V_{frp}$

$V_{uc} = 300 \times 300 \times 0.7068 = 63.61$ kN

$Vus = (f_y \times A_{st} \times d) / s_v$

$= (500 \times 2 \times \pi / 4 \times 12^2 \times 250) / 75$

$= 376.9 kN$

Equating V_j and V_{jh} and solving for V_{frp}

$V_{frp} = 29.49$ kN

The equation developed by Triantafillou [1998] and supported by Teng *et al.*[2003]

$V_{frp} = 0.9 \times \rho_{frp} \times E_{frp} \times \varepsilon_{frp} \times b_w \times d \times (1 + \cot\beta) \times \sin\beta / \gamma_{frp}$

Removing Factor of safety and substituting $\rho_{frp} = 2t_{frp} / b_w$

$V_{frp} = 0.9 \times 2 \times E_{frp} \times \varepsilon_{frp} \times t_{frp} \times d \times (1 + \cot\beta) \times \sin\beta$

where $\beta = 45^o$ and $E_{frp} \times \varepsilon_{frp} = f_{frp}$

$\Rightarrow V_{frp} = 1.8 \times f_{frp} \times A_{frp} \times (1 + \cot\beta) \times \sin\beta$

$\Rightarrow 29490 = 1.8 \times 2293 \times \cos 45^o \times (1 + \cot 45^o) \times \sin 45^o \times A_{frp}$

$\Rightarrow A_{frp} = 7.16 \text{ mm}^2$

Area of one wrap of GFRP= $300 \times 0.36 \times 2 = 259.2 \text{ mm}^2 > 7.16 \text{ mm}^2$

Hence one wrap is of GFRP is O.K.

The design calculations are similar for two-third and one third scale beam-column joints.

B5. ANALYSIS AND DESIGN OF BEAM-COLUMN JOINT WITH BEAM WEAK IN SHEAR RETROFITTED SPECIMENS

The beams of these joints were strengthened in shear by GFRP. The proposed width of GFRP strips for BWSLC is 120 mm @ 260 mm c/c.

Shear contributed by these shear strips is calculated by using Eq. B3 and found as

$V_{frp} = 184$ kN.

The beam is also retrofitted by CFRP for flexural strengthening with one layer of CFRP in an exactly identical manner to that of beam weak in flexure retrofitted specimens. Thus after retrofitting, the flexural capacity of the beam is same as earlier case.

Therefore, Flexural load carrying capacity of beam

=82.19 kN $< V_{frp}$ (=184).

Thus, after both shear and flexural retrofitting, the beam remain weak in flexure and its ultimate load carrying capacity is 82.19 kN. Similar calculation was done for scaled models.

APPENDIX-C
CALCULATION OF ULTIMATE STRESSES

C.1 CALCULATION OF ULTIMATE STRESSES FOR BEAM WEAK IN FLEXURE SPECIMENS

C.1.1 Beam weak in flexure : control specimens

The failure mode of these specimens were in flexure and hence bending stress was calculated for this type of specimens.

Bazˇant and Planas [1998] proposed the expression for nominal bending stress as follows :

$$\sigma_{N_U} = C_N \frac{P}{(bD)} \qquad \text{C.1}$$

where,

C_N = Coefficient introduced for convenience

P = Applied load and

(bD) = Area of the cross section

For a cantilever beam C_N was calculated as

$$C_N = 6S/h \qquad \text{C.2}$$

where,

S = Span of the beam and

h = Depth of the beam.

Large Specimen (BWFLC)

In the present calculation, area of steel was converted to equivalent area in term of concrete to arrive at the equivalent area of cross section of the beam.

Equivalent area of the section,

$$A = b \times D + (m_1 - 1)(A_{sc} + A_{St}) \qquad C.3$$

where, A_{sc} and A_{St} are the area of steel provided in the compression and tension side of the beam respectively.

m_1 is the modular ratio = E_s/E_c

Modulus of elasticity of Concrete, E_c = 22360 N/mm^2

Modulus of elasticity of Steel, E_s=200000 N/mm^2

Hence, $m_1 = E_s/E_c = 8.94$

Using Eq. C.2,

$$C_N = 6 \times \frac{1350}{360}$$
$$= 22.5$$

Using Eq. C.3, gross area was found

$$A = 117.97 \times 10^3 \text{ mm}^2$$

P = 73.285 kN (As obtained experimentally)

Substituting the values of P, C_N and bD (=A) in Eq. C.1, the ultimate nominal bending stress was found as

σ_{N_U} = 13.97 N/mm^2.

Similarly, σ_{N_U} for medium and small specimen were calculated as 14.53 N/mm^2 and 15.017 N/mm^2 respectively.

C.1.2 Beam weak in flexure : retrofitted specimens

The failure mode of these specimens were also in flexure and hence bending stress was calculated for this type of specimens. Area of steel and area of CFRP were converted to equivalent areas in term of concrete to arrive at the gross area of cross section.

Thus, equivalent area may be written as

$$A = b \times D + (m_1 - 1)(A_{sc} + A_{St}) + m_2 \times A_{frp} \qquad C.4$$

where, A_{frp} is the area of CFRP provided in the section and m_2 is the modular ratio, given by

$$m_2 = \frac{E_{frp}}{Ec}$$

Modulus of elasticity of FRP, E_{frp} = 46300 N/mm^2

Hence, $m_2 = \frac{E_{frp}}{Ec} = 2.07$

Large specimen (BWFLR)

Substituting the values of all the terms in Eq. C.4 for large specimen, equivalent area was found as :

$A = 118.34 \times 10^3$ mm^2

P = 77.165 kN (As obtained experimentally) and C_N is same as earlier case = 22.5

Substituting all the values nominal bending stress were found as σ_{N_U} = 14.67 N/mm^2.

Similarly, σ_{N_U} for medium and small specimen were found as 17.51 N/mm^2 and 18.51 N/mm^2 respectively.

C.2 CALCULATION OF ULTIMATE STRESSES FOR BEAM WEAK IN SHEAR SPECIMENS

C.2.1 Beam weak in shear : control specimens

The failure mode of these specimens were in shear and hence shear stress was calculated for this type of specimens.

Large specimen (BWSLC)

Baz˘ant and Planas [1998] proposed the expression for maximum shear stress similar to Eq. (C.1) as follows :

$$\sigma_{N_U} = C_N \frac{P}{(bD)}$$

where, P is the load, (bD) is the area of cross section of the beam and C_N is the coefficient.

For a cantilever beam, C_N was calculated as equal to 1.5

The shear reinforcement provided in this category of beam was very less, and hence the contribution of steel was neglected for arriving at the equivalent area of the section used in Eq.C.1.

P = 69.635 kN (As obtained experimentally)

Substituting the value of P, C_N and (bD) in Eq. (C.1), Ultimate shear stress

$$\sigma_{N_U} = 1.5 \times \frac{69.635 \times 10^3}{(300 \times 360)}$$
$$= 0.967 \text{ N/mm}^2$$

Similarly, for medium and small specimens the shear stress σ_{N_U} were found as 1.164 N/mm^2 and 1.125 N/mm^2 respectively.

C.2.2 Beam weak in shear : retrofitted specimens

The failure mode of these specimens were in bending and hence bending stress was calculated for this type of specimens.

Large specimen (BWSLR)

The equivalent area of the section is same as that of BWFLR specimen.

i.e. $A = 118.34 \times 10^3$ mm^2

The value of C_N is also same as in the case of BWFLR.

P = 78.12 ken (As obtained experimentally)

Substituting the values in Eq. C.1, the ultimate nominal bending stress was found as

σ_{N_U} = 14.523 N/mm^2

Similarly, σ_{N_U} for medium and small specimens were found as 19.025 N/mm^2 and 21.558 N/mm^2 respectively.

C.3 CALCULATION OF ULTIMATE STRESSES FOR COLUMN WEAK IN SHEAR SPECIMENS

C.3.1 Column weak in shear : control specimens

The failure mode of these specimens were in shear, and hence shear stress was calculated for this type of specimens.

Ref. to Fig. C-1, the equilibrium equation for the forces may be written as

$$S \times h = P \times l \qquad \text{(C.5)}$$

where,

S = Shear forces transmitted on column corresponding to the applied load P on the beam tip.

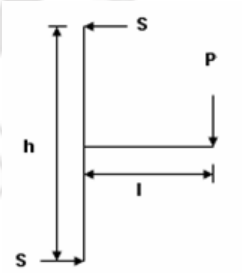

Fig. C-1 F.B.D. of forces

l, Span of the beam = 1350 mm (For large specimen)

h, Height of column = 3300 mm (For large specimen)

Large specimen (CWSLC)

The shear reinforcement provided in this category of columns were very less, and hence the contribution of steel was neglected for arriving at the equivalent area of the section.

Substituting the value of ultimate load carrying capacity P as found experimentally in Eq. C.5, we get

$S \times 3.3 = 53.78 \times 1.35$

$\Rightarrow S = 22.00$ kN.

Maximum shear stress is given by

$$\sigma_{N_U} = 1.5 \times \frac{S}{A}$$
$$= 1.5 \times \frac{22.00 \times 10^3}{(300 \times 240)}$$
$$= 0.458 \text{ N/mm}^2$$

Similarly, for medium and small specimens the shear stress σ_{N_U} were found as 0.628 N/mm^2 and 0.662 N/mm^2 respectively.

C.3.2 Column weak in shear : retrofitted specimens

The failure mode of these specimens were also in shear, and hence shear stress was calculated as earlier. Further, since the contribution of GFRP was very less, equivalent area of cross section of the column was calculated disregarding the same.

Large specimen (CWSLR)

The ultimate load carrying capacity was P found to be 64.06 kN. Substituting the value of load P in Eq. C.5

$S \times 3.3 = 64.06 \times 1.35$

$\Rightarrow S = 26.2$ kN.

Maximum shear stress is given by

$$\sigma_{N_U} = 1.5 \times \frac{S}{A}$$
$$= 1.5 \times \frac{26.2 \times 10^3}{(300 \times 240)}$$
$$= 0.545 \text{ N/mm}^2$$

Similarly, σ_{N_U} was found as 0.811 N/mm^2 and 0.878 N/mm^2 for medium and small specimens respectively.

APPENDIX-D

Table D.1 Ultimate load carrying capacity of specimens

Control specimens				Retrofitted specimens			
Name of specimen	**Ultimate load by Experimental investigation (kN)**	**Ultimate load by FE analysis with ANSYS (kN)**	**Ultimate load by strength criteria (kN)**	**Name of specimen**	**Ultimate load by Experimental investigation (kN)**	**Ultimate load by FE analysis with ANSYS (kN)**	**Ultimate load by strength criteria (kN)**
BWFLC	73.285	75.6	70.048	BWFLR	77.165	82	82.19
BWFMC	32.91	35.84	31.115	BWFMR	40.92	44	37.17
BWFSC	8.83	9.45	8.045	BWFSR	10.915	13.32	8.9
BWSLC	69.635	73.2	66.36	BWSLR	78.12	83.7	82.19
BWSMC	34.055	35.84	29.63	BWSMR	41.25	44.2	37.17
BWSSC	10.018	9.1	7.338	BWSSR	12.715	13.2	8.9
CWSLC	53.78	58.5	-----	CWSLR	64.06	68.3	-----
CWSMC	32.76	31.5	-----	CWSMR	42.36	35.6	-----
CWSSC	8.635	7.8	-----	CWSSR	11.45	10.3	-----

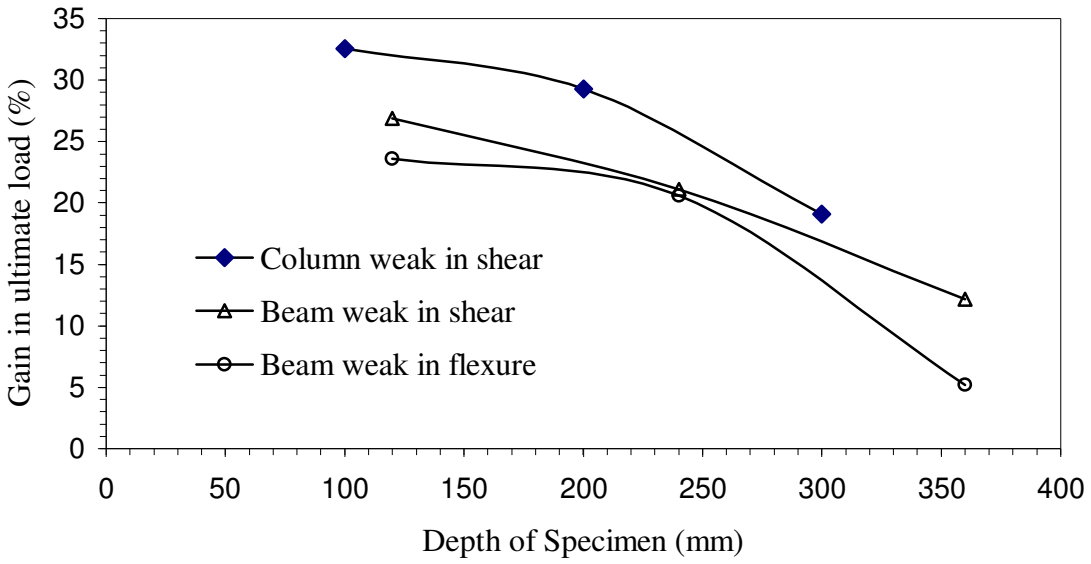

Fig. D.1 Percentage gain in ultimate load carrying capacity of different specimens due to retrofitting